UNIVERSITÀ DEGLI STUDI DI MESSINA

Dipartimento di Scienze Matematiche, Scienze Fisiche e Scienze della Terra

Ph. D. Thesis in Physics, XXXVI cycle (FIS/03)

Cavity QED: unconventional phenomena and new perspectives on quantum technologies

Alberto Mercurio

Supervisor:
Prof. Salvatore Savasta

Ph.D. Coordinator:
Prof. Vincenza Crupi

Co-supervisor:
Dr. Vincenzo Macrì

ACADEMIC YEAR 2022/2023

Riconoscimenti

Ringrazio inoltre prof. Roberto Stassi e prof. Alessandro Ridolfo, con i quali spero di continuare a collaborare in futuro.

Continuo con il ringraziare tutti i collaboratori con cui ho avuto a che fare in questi anni. Ringrazio prof. Vincenzo Savona, Fabrizio Minganti e Luca Gravina per la loro magnifica ospitalità all'EPFL di Losanna. Con voi è sempre molto stimolante vivere il mondo della ricerca. Ringrazio anche Marco Scigliuzzo, prof. Pasquale Scarlino e David Schlegel.

Ringrazio prof. Franco Nori per tutte e collabolazioni che abbiamo avuto e che spero continueremo a fare. Grazie anche per la magnifica ospitalità offerta al RIKEN in Giappone. Ringrazio prof. Marco Polini, Marcello Andolina, Francesco Pellegrino. Ringrazio anche prof. Marco Affronte, Alberto Ghirri e Claudio Bonizzoni. Ringrazio inoltre prof. Rosario Lo Franco per la calorosa ospitalità nella città di Palermo e Carlos Sánchez Muñoz per la fantastica collaborazione che abbiamo avuto e per i bei momenti trascorsi insieme. Ringrazio anche prof. Adam Miranowicz e Simone De Liberato. Ringrazio l'Army Research Office (ARO) (Grant No. W911NF-19-1-0065)

Seppur fuori dal mondo della fisica, ringrazio il mondo della danza. Ringrazio tutti i miei allievi, che tra un passo e l'altro scappava sempre qualche discorso sulle stelle e sull'universo. Ringrazio Berta e Desy, amici da una vita, per essermi sempre vicini e farmi passare sempre magnifici momenti. Ringrazio il piccolo Lorenzo per riempirmi sempre il cuore di gioia.

Ringrazio ovviamente la mia famiglia. Partendo da mia madre Santina, senza la quale non avrei mai intrapreso la strada della fisica. Ringrazio mio padre Antonio (Totò) per essere stato la scintilla che ha acceso la mia passione per la tecnologia e per avermi fatto scoprire quanto è bello sporcarsi le mani nel lavoro. Ringrazio mia sorella Federica per essere stata la prima persona a credere in me, dalla danza alla fisica. Ringrazio mio cognato osteopata Aurelio per tutti i magnifici momenti passati insieme e per tutte le volte che mi hai fatto passare i dolori. Non posso non ringraziare Eros. Non importa a che ora torno a casa, trovo sempre la sua coda scodinzolare per la gioia di rivedermi.

Ringrazio Angela e Gaetano, per tutte le volte che mi ospitano a casa e tutte le volte che mi chiamano professore, anche se non lo sono ancora. Ma fa sempre piacere illudersi.

Infine ringrazio Roberta, alla quale dedico questa tesi. Non basterebbe un libro per ringraziarti per tutto quello che fai per me. Grazie per tutte le volte che mi hai supportato, dalla danza alla fisica, facendomi sentire sempre importante. Grazie anche per tutte le volte che mi hai sopportato. Come adesso, che io sto scrivendo questa dedica alle due di notte e tu sei in camera con me che dormi (o provi a farlo), nonostante il frastuono della tastiera meccanica. Eh amore mio, quanto mi sopporti. Sappi che sei una persona speciale, e che ti amo tanto.

Acknowledgments

I had three exceptional years, in which I have met exceptional people and to whom I would like to be able to express my gratitude. I start by thanking my supervisor, Prof. Salvatore Savasta, a man as brilliant as he is crazy. A person with whom you can really discuss anything, and who always listens to every idea proposed.

I canàt help but thank my co-supervisor, Vincenzo Macrì. Thank you for teaching me so much, from physics to life. Sometimes you indirectly remind me of something I often forget, that it is not so important to know everything, but it is important to have passion and curiosity.

I thank all my colleagues at the university, starting with my Ph.D. and fellow adventurer Fabio Mauceri. We spent hours and hours of discussions about concepts and calculations we didn't understand, that made us grow a lot. I thank all my other Ph.D. and Master colleagues: Enrico Russo, Daniele Lamberto, Samuel Napoli, Paola Mantineo, Elisa Bonaccorso, Andrea Ciccolo, Andrea Zappalà, Mariangela Ruggeri, Chiara Ammendola, Fabio Risitano, Giorgio Foti, and Chiara Tripodi; with whom I shared wonderful lunches, outings, and coffees often accompanied by interesting discussions.

I thank Prof. Omar Di Stefano, a man of so much goodness and sympathy. Returning teenagers with you is so easy, which is just a

Acknowledgments

professor, even though I am not yet one. But it is always a pleasure to delude oneself.

Finally, I thank Roberta, to whom I dedicate this thesis. A book would not be enough to thank you for all you do for me. Thank you for all the times you supported me, from dance to physics, always making me feel important. Thank you also for all the times you put up with me. Like now, that I am writing this dedication at two in the morning and you are in the room with me sleeping (or trying to), despite the noise of the mechanical keyboard. Oh my love, how much you put up with me. Know that you are a special person, and that I love you so much.

A Roberta,

*che dà sempre un motivo
alle mie giornate.*

Abstract

Light can interact with matter in a variety of ways. When the electromagnetic field is confined in a cavity, larger light-matter coupling strengths can be achieved, which opens the possibility to discover unconventional phenomena that are usually impossible to observe. When the coupling strength is comparable to the frequency of the electromagnetic field, the so-called ultrastrong coupling (USC) regime is reached. In this regime, the rotating wave approximation (RWA) is no longer valid, and the interaction between light and matter must be treated in a non-perturbative way. Moreover, the number of total particles is no longer conserved, meaning that several processes (or virtual transitions behind them) can create particles (or virtual particles) from the vacuum. Nevertheless, in this regime, several theoretical issues arise. For example, the number of photons in the ground state acquires a non-negligible value, which means that, in principle, the cavity can emit photons even in the lowest energy state, which is unphysical. A breakdown of gauge invariance also occurs, suggesting that the standard approach must be treated properly. Furthermore, the standard way to describe open quantum systems in Markovian baths must be revised, since the subsystems in this regime are strongly correlated.

In this Thesis, we explore the context of light-matter interaction,

showing how these issues can be interpreted and fixed. We start by defining the basics of light-matter interaction. Starting from a Lagrangian approach, we derive the most two common gauges in cavity QED: the Coulomb gauge and the multipolar gauge (also known as dipole gauge in the case of a constant vector potential). We then pass in the Hamiltonian framework, deriving a full quantum treatment of light-matter interaction.

Compared to the quantum harmonic oscillator, which has a linear energy spectrum, matter systems usually present non-linear energy spectra. Thus, a truncation of the Hilbert space to the lowest energy levels can simplify the treatment of the system, leading to the quantum Rabi model in the case of a two-level atom in interaction with a single-mode cavity field. However, this truncation process leads to the breakdown of gauge invariance. Specifically, the Coulomb gauge reproduces different results concerning those in the dipole gauge or even in the non-truncated system Hamiltonian. We show that this breakdown is due to the non-locality that the matter potential acquires when performing the projection into the lowest energy states. To overcome this issue, the correct Coulomb gauge can be obtained through a generalized minimal coupling replacement, which is introduced after the truncation and not before.

The dipole gauge, however, is not always well defined. Indeed, in this frame, the minimal coupling replacement is performed in the photonic part of the Hamiltonian rather than in the matter part. Thus, the conjugate momentum of the vector potential is different from the standard one and contains the polarization vector of the matter system. Everything related to the electric field must be redefined in this gauge because the electric field is no longer the conjugate momentum of the vector potential. This includes photodetection, the interaction with an external environment, pure dephasing effects, and photon condensation.

In this Thesis, we will focus on all these topics. First, we will show how to define the photodetection. Specifically, following Glauber's theory, it is defined as the product of the negative and positive frequency parts of the electric field. In the absence of any interaction with

the matter, the negative and positive frequency parts correspond to the creation and destruction operator, respectively. However, when the interaction becomes relevant, this is no longer true. Moreover, we will derive a generalized master equation, which, compared to the standard one, is derived with a minimal amount of assumptions: the Born and Markov approximations. Using the standard master equation in the USC regime leads to a finite number of photons at the steady state, even at zero temperature, and with the correct photodetection operators. We then apply this solid approach to an incoherent pumping process, showing how thermal excitations of the atom can be detected from an emission spectrum of the electromagnetic field. We apply this framework also to coherent pumping, showing the peculiar effect of spontaneous scattering of Raman photons without vibrational degrees of freedom. As mentioned above, this process can be observed only when the number of particles is not conserved (i.e., the USC regime). We then study the effect of pure dephasing in the USC regime, showing a gauge-invariant treatment of this process, demonstrating also here that the standard approach is no longer valid when the light-matter coupling strength is comparable to the frequency of the electromagnetic field. Finally, we study the phenomenon of photon condensation (or superradiant phase transition), where the ground state acquires a macroscopic number of coherent photons. We prove that this phenomenon can not be achieved in the absence of a magnetic field, showing that previous works that claim the existence of this phenomenon used gauge-dependent approaches.

List of Publications

[1] F. Mauceri, A. Mercurio, S. Savasta, and O. Di Stefano, "Ultrastrong coupling of a qubit with a nonlinear optical resonator", Phys. Rev. A **105**, 023719 (2022).

[2] A. Mercurio, V. Macrì, C. Gustin, S. Hughes, S. Savasta, and F. Nori, "Regimes of cavity QED under incoherent excitation: From weak to deep strong coupling", Phys. Rev. Res. **4**, 023048 (2022).

[3] G. Andolina, F. Pellegrino, A. Mercurio, O. Di Stefano, M. Polini, and S. Savasta, "A non-perturbative no-go theorem for photon condensation in approximate models", The European Physical Journal Plus **137**, 1 (2022).

[4] V. Macrì, A. Mercurio, F. Nori, S. Savasta, and C. Sánchez Muñoz, "Spontaneous Scattering of Raman Photons from Cavity-QED Systems in the Ultrastrong Coupling Regime", Phys. Rev. Lett. **129**, 273602 (2022).

[5] A. Mercurio, S. Abo, F. Mauceri, E. Russo, V. Macrì, A. Miranowicz, S. Savasta, and O. Di Stefano, "Pure Dephasing of Light-Matter Systems in the Ultrastrong and Deep-Strong Coupling Regimes", Phys. Rev. Lett. **130**, 123601 (2023).

[6] E. Russo, A. Mercurio, F. Mauceri, R. Lo Franco, F. Nori, S. Savasta, and V. Macrì, "Optomechanical two-photon hopping", Phys. Rev. Res. **5**, 013221 (2023).

[7] A. Ghirri, C. Bonizzoni, M. Maksutoglu, A. Mercurio, O. Di Stefano, S. Savasta, and M. Affronte, "Ultrastrong Magnon-Photon Coupling Achieved by Magnetic Films in Contact with Superconducting Resonators", Phys. Rev. Appl. **20**, 024039 (2023).

Under Review

[8] A. Mercurio, S. De Liberato, F. Nori, S. Savasta, and R. Stassi, "Flying atom back-reaction and mechanically generated photons from vacuum", arXiv preprint arXiv:2209.10419, https://doi.org/10.48550/arXiv.2209.10419 (2022).

[9] A. Mercurio, G. M. Andolina, F. Pellegrino, O. Di Stefano, P. Jarillo-Herrero, C. Felser, F. H. Koppens, S. Savasta, and M. Polini, "Photon condensation, Van Vleck paramagnetism, and chiral cavities", arXiv preprint arXiv:2302.09964, https://doi.org/10.48550/arXiv.2302.09964 (2023).

[10] F. Minganti, A. Mercurio, F. Mauceri, M. Scigliuzzo, S. Savasta, and V. Savona, "Phonon Pumping by Modulating the Ultrastrong Vacuum", arXiv preprint arXiv:2309.15891, https://doi.org/10.48550/arXiv.2309.15891 (2023).

Contents

Contents

Contents

CHAPTER 1

The basics of light-matter interaction

It is well-known that light and matter interact with each other. We know that a charged particle immersed in an electric field is subject to a force $\mathbf{F} = q\mathbf{E}$, where q is the charge of the particle and $\mathbf{E}$ is the electric field. The same particle also interacts with a magnetic field with a force $\mathbf{F} = q(\mathbf{v} \times \mathbf{B})$, where $\mathbf{v}$ and $\mathbf{B}$ are the velocity of the particles and the magnetic field, respectively.

Although we have already identified more or less what is called "*matter*", someone lacking knowledge in physics could encounter difficulty in identifying the representation of light described above. This definition will be explained later.

The task of this chapter is to give some elementary information about light-matter interaction and to introduce also some problems that might emerge with a wrong theoretical description.

1.1 What is matter?

If we ask someone what matter is, he may answer that it is anything that has mass and occupies space[1]. In other words: a table, a book, a glass, a hydrogen atom, an electron. All these objects are classified as matter, and, following Newton's second law, all of them obey the formula $\mathbf{F} = m\mathbf{a}$, where $\mathbf{a}$ is the acceleration of the object.

This intuitive idea of matter, of elementary particles or compounds of them, is in part modified by quantum mechanics, where any material system behaves like a wave. They obey certain wave equations, e.g., the Schrödinger equation

$$i\hbar \frac{\partial}{\partial t}\psi(\mathbf{r}, t) = -\frac{\hbar^2}{2m}\nabla^2\psi(\mathbf{r}, t) + V(\mathbf{r})\psi(\mathbf{r}, t)\,, \qquad (1.1)$$

where $\hbar$ is the reduced Planck constant, $V(\mathbf{r})$ is the potential, and $\psi(\mathbf{r}, t)$ is the system wavefunction. The solutions of this differential equation are called eigenstates of the system and depend on the potential $V(\mathbf{r})$.

The right-hand side of Eq. (1.1) is the result of the application of the system Hamiltonian to the wavefunction, in other words, $i\hbar\,\partial/\partial t\,\psi(\mathbf{r}, t) = \hat{H}\psi(\mathbf{r}, t)$, where

$$\hat{H} = -\frac{\hbar^2}{2m}\nabla^2 + V(\mathbf{r})\,. \qquad (1.2)$$

If the system is assumed to oscillate as e^{-iEt}, where E is the system energy, we can solve the time-independent part of the Schrödinger equation $\hat{H}\psi = E\psi$.

1.1.1 The quantum harmonic oscillator

As an example, here we consider the quantum harmonic oscillator. Classically, the harmonic oscillator is defined as a system subject to

---

[1]We may continue to explain what are mass and space, but we limit ourselves to leave the reader with the standard and intuitive idea he already has.

the force $\mathbf{F} = -k\mathbf{r}$, where k is the elastic constant. In other words, the force is proportional to the displacement from a stable point (in this case the origin).

Following the relation $\mathbf{F} = -\nabla V(\mathbf{r})$, we can say that the corresponding potential is $V(\mathbf{r}) = k/2 \; \mathbf{r}^2$. Inserting it inside Eq. (1.1), and considering only the one-dimensional case, we obtain the following eigenstates

$$\psi_n(x) = \frac{1}{\sqrt{2^n n!}} \left(\frac{m\omega}{\pi\hbar}\right)^{1/4} e^{-\frac{m\omega x^2}{2\hbar}} H_n\left(\sqrt{\frac{m\omega}{\hbar}}x\right) , \qquad (1.3)$$

where $\omega = \sqrt{k/m}$ is the resonance frequency of the oscillator and H_n is the n-th Hermite polynomial.

A useful way to describe the quantum harmonic oscillator is by using the ladder operators

$$\hat{a} = \sqrt{\frac{m\omega}{2\hbar}} \left(\hat{x} + i\frac{1}{m\omega}\hat{p}\right) \qquad (1.4a)$$

$$\hat{a}^\dagger = \sqrt{\frac{m\omega}{2\hbar}} \left(\hat{x} - i\frac{1}{m\omega}\hat{p}\right) , \qquad (1.4b)$$

note that the position $\hat{x}$ and conjugate momentum $\hat{p}$ are operators too. If we now write the eigenstates in Eq. (1.3) in the bra-ket notation ($\psi_n \to |n\rangle$), the ladder operators allow us to move from one eigenstate to the next or previous one:

$$\hat{a}\,|n\rangle = \sqrt{n}\,|n-1\rangle \qquad (1.5a)$$

$$\hat{a}^\dagger\,|n\rangle = \sqrt{n+1}\,|n+1\rangle , \qquad (1.5b)$$

and it is straightforward to recognize the creation ($\hat{a}^\dagger$) and annihilation ($\hat{a}$) operators. In this framework the system Hamiltonian in Eq. (1.2) of the quantum harmonic oscillator becomes

$$\hat{H} = \hbar\omega\left(\hat{a}^\dagger\hat{a} + \frac{1}{2}\right) . \qquad (1.6)$$
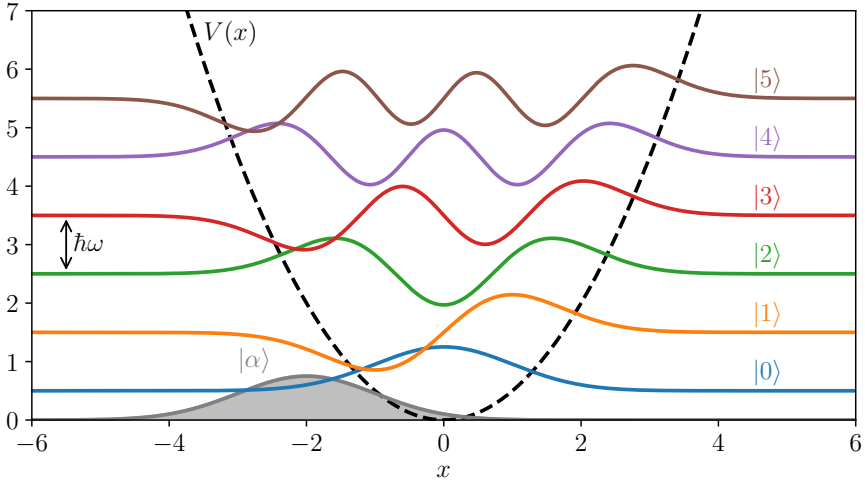
Figure 1.1: First eigenstates of one-dimensional the quantum harmonic oscillator, each of them vertically shifted by the corresponding eigenvalue. The grey-filled curve corresponds to a coherent state with $\alpha = -\sqrt{2}$. The used parameter are $m = 1$, $\omega = 1$, and $\hbar = 1$.

It is worth introducing the coherent state $|\alpha\rangle$ of the harmonic oscillator, defined as the eigenstate of the destroy operator, with eigenvalue α, in other words, $\hat{a}|\alpha\rangle = \alpha|\alpha\rangle$. It can be expressed analytically in terms of the eigenstates of the quantum harmonic oscillator

$$|\alpha\rangle = e^{-\frac{1}{2}|\alpha|^2} \sum_{n=0}^{\infty} \frac{\alpha^n}{\sqrt{n!}} |n\rangle \ , \tag{1.7}$$

and it can be seen as the most classic-like state since it has the minimum uncertainty $\Delta x \Delta p = \hbar/2$.

Figure 1.1 shows the first eigenstates of the quantum harmonic oscillator, each of them vertically shifted by the respective energy, while the grey-filled curve is a coherent state with $\alpha = -\sqrt{2}$. The black dashed curve is the potential, choosing $k = 1$, $m = 1$, and $\hbar = 1$.

It is worth noting that also the groundstate $|0\rangle$ has a nonzero energy ($E_0 = \hbar\omega/2$). This figure and most of other figures in this Thesis are obtained by using the Julia code, and a dedicated GitHub repository is available [11].

Although the quantum harmonic oscillator analogues can be seen in various scenarios (see, e.g., the quantum behavior of the electromagnetic field in Section 1.2), matter is often described by different Hamiltonians (e.g., that of the hydrogen atom) which may present nonlinear behaviors and energies not exactly equally spaced. Indeed, in this Thesis we will deal mostly with this kind of systems, which allow us to concentrate only to a few energy states (two o three) due to the high nonlinearity.

1.1.2 The double-well potential

One of the most intuitive systems that can be described by a nonlinear Hamiltonian is the double-well potential. Indeed, under certain parameters, the two lowest energy states of the system correspond to the symmetric and the antisymmetric superposition of the left and right side of the potential, making an ideal two-level system (TLS).

The potential of the one-dimensional double-well system is

$$V(x) = -\frac{\mu}{2}x^2 + \frac{\lambda}{4}x^4 \,, \tag{1.8}$$

where $\mu, \lambda > 0$ are the parameters of the potential. The potential and the first eigenstates for $m = 1$, $\mu = 150$ and $\lambda = 300$ are depicted in Figure 1.2. The black dashed line represents the potential $V(x)$, while the first three eigenstates of the system are represented by the colored lines, each one being vertically offset by its corresponding eigenvalue. It's evident that the energy difference between the first two states $|\psi_0\rangle$ and $|\psi_1\rangle$ is significantly less than that between the second and third states, indicating a high degree of anharmonicity.

It is often useful to reduce the Hamiltonian of the double-well system to a two-level system, which is a system with only two energy levels. Indeed, by performing the projection $\hat{P} = |\psi_0\rangle\langle\psi_0| + |\psi_1\rangle\langle\psi_1|$,
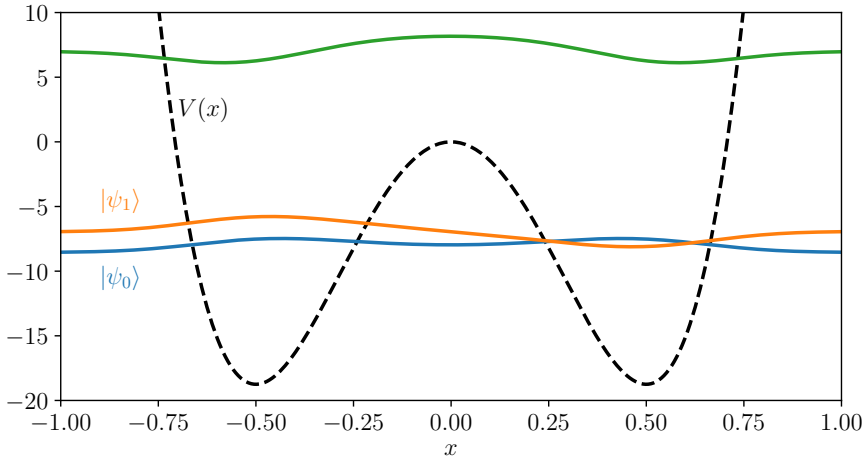
Figure 1.2: Double-well potential for $m = 1$, $\mu = 150$ and $\lambda = 300$. The black dashed curve is the potential $V(x)$, the colored lines are the first three eigenstates of the system, each vertically shifted by the corresponding eigenvalue. As can be seen, the difference in energy between the first two states is much smaller than the difference between the second and the third one, showing an high anharmonicity.

the Hamiltonian of the double-well system reduces to

$$\hat{H}_{\mathrm{TL}} = \hat{P}\left[\frac{\hat{p}^2}{2m} + V(\hat{x})\right]\hat{P} = \frac{\hbar\omega_{1,0}}{2}\hat{\sigma}_z\,, \tag{1.9}$$

where $\omega_{1,0} = \omega_1 - \omega_0$ is the frequency difference between the first two energy levels, and $\hat{\sigma}_z = |\psi_1\rangle\langle\psi_1| - |\psi_0\rangle\langle\psi_0|$ is the Pauli matrix. The eigenstates of the Hamiltonian in Eq. (1.9) are the symmetric and antisymmetric superposition of the left and right side of the potential, respectively

$$|\psi_0\rangle = \frac{1}{\sqrt{2}}\left(|\psi_{\mathrm{L}}\rangle + |\psi_{\mathrm{R}}\rangle\right) \tag{1.10a}$$

$$|\psi_1\rangle = \frac{1}{\sqrt{2}}\left(|\psi_{\mathrm{L}}\rangle - |\psi_{\mathrm{R}}\rangle\right)\,. \tag{1.10b}$$

1.2 What is light?

A person lacking knowledge in physics might be more confused than before in understanding the concept of matter, probably due to the wave behavior introduced by quantum mechanics. Here, instead, we clarify what physicists usually call "*light*", which should be much easier to understand. We start by introducing the classical view, defining the relationships between the electric and magnetic fields, which are expressed by the Maxwell equations. We then introduce the quantum point of view of light, showing that it can be seen as an infinite amount of quantum harmonic oscillators.

1.2.1 The classical concept of light

Classically, light is an electromagnetic wave, that can travel in the vacuum at the speed of $c = 299792458$ m/s. The wave nature of light comes from the Maxwell equations

$$\nabla \times \mathbf{E} + \frac{\partial \mathbf{B}}{\partial t} = 0 \tag{1.11a}$$

$$\nabla \times \mathbf{H} - \frac{\partial \mathbf{D}}{\partial t} = \mathbf{J} \tag{1.11b}$$

$$\nabla \cdot \mathbf{D} = \rho \tag{1.11c}$$

$$\nabla \cdot \mathbf{B} = 0 \,, \tag{1.11d}$$

where $\mathbf{J}$ and ρ are the density current and the density of charge, respectively. In the empty space both $\mathbf{J}$ and ρ are null, while $\mathbf{D} = \varepsilon_0 \mathbf{E}$ and $\mathbf{B} = \mu_0 \mathbf{H}$, with ε_0 the electric permittivity and μ_0 the magnetic permeability in the vacuum.

The Maxwell equations written above are still valid if we express the fields in terms of a vector potential $\mathbf{A}(\mathbf{r}, t)$ and a scalar potential $\phi(\mathbf{r}, t)$

$$\mathbf{E} = -\frac{\partial \mathbf{A}}{\partial t} - \nabla \phi \tag{1.12a}$$

$$\mathbf{B} = \nabla \times \mathbf{A} \,, \tag{1.12b}$$

and Eqs. (1.11a) to (1.11d) remain unchanged under a gauge transformation

$$\mathbf{A}' = \mathbf{A} + \nabla\chi\,, \quad \phi' = \phi - \frac{\partial\chi}{\partial t}\,, \tag{1.13}$$

with $\chi = \chi(\mathbf{r}, t)$ any scalar function. As a result, we can choose $\phi = 0$ and $\nabla \cdot \mathbf{A} = 0$, known as the Coulomb gauge. Substituting Eq. (1.12a) and (1.12b) into Eq. (1.11b), and taking advantage of the Coulomb gauge conditions and the vector identity $\nabla \times \nabla \times \mathbf{A} = \nabla(\nabla \cdot \mathbf{A} - \nabla^2\mathbf{A})$, we obtain

$$\left(\nabla^2 - \frac{1}{c^2}\frac{\partial^2}{\partial t^2}\right)\mathbf{A}(\mathbf{r}, t) = 0\,, \tag{1.14}$$

which is the well-known wave equation of light. Here $c = (\mu_0\varepsilon_0)^{-1/2} = 299792458$ m/s is the speed of light in the vacuum. The vector potential $\mathbf{A}(\mathbf{r}, t)$, which intrinsically contains both the electric and magnetic field, oscillates in space and time. Thus, as stated previously, light is an electromagnetic wave.

1.2.2 The quantum concept of light

We now promote light to a quantum object by simply placing a small cap over the symbols $\mathbf{E} \to \hat{\mathbf{E}}$, $\mathbf{B} \to \hat{\mathbf{B}}$ and $\mathbf{A} \to \hat{\mathbf{A}}$. Joking aside, quantization of the electromagnetic field is a relatively intuitive procedure, since waves, by their nature, have a connection to the properties of the harmonic oscillator. We start by writing the total energy stored in the electromagnetic field

$$E = \frac{1}{2}\int_V \mathrm{d}^3\mathbf{r}\left(\varepsilon_0\mathbf{E}^2 + \frac{1}{\mu_0}\mathbf{B}^2\right)\,, \tag{1.15}$$

where the spatial integration is performed in the volume V in which the field is considered. It can be the whole space or a finite volume of a specific geometry. Here we consider the field within a cubic volume of side L with periodic boundary conditions. If we write $\mathbf{A}(\mathbf{r}, t)$ as

a product of a spatial and a temporal part, the spatial part of the solution of Eq. (1.14) is a plane wave of the form $e^{\pm i\mathbf{k}\cdot\mathbf{r}}$, where $\mathbf{k}$ is the wavevector, and the temporal part is $e^{\mp i\omega t}$, where $\omega = c|\mathbf{k}|$ is the angular frequency. The spatial part is periodic in the volume V, and the temporal part is periodic in the time interval $T = 2\pi/\omega$. Because of the boundary conditions, the allowed values of $\mathbf{k}$ are restricted to $k_x = 2\pi n_x/L$, $k_y = 2\pi n_y/L$, and $k_z = 2\pi n_z/L$, where n_x, n_y, and n_z are integers. To account for the vector character of $\mathbf{A}$ we introduce the unitary polarization vector $\mathbf{e}_{\mathbf{k},\lambda}$, which has to be orthogonal to $\mathbf{k}$ to satisfy $\nabla \cdot \mathbf{A} = 0$. Here, the index λ refers to the polarization of the wave. Now the vector potential can be written as

$$\mathbf{A}(\mathbf{r},t) = \sum_{\mathbf{k},\lambda} \left[A_{\mathbf{k},\lambda}(t)\mathbf{u}_{\mathbf{k},\lambda}(\mathbf{r}) + A^*_{\mathbf{k},\lambda}(t)\mathbf{u}^*_{\mathbf{k},\lambda}(\mathbf{r}) \right], \qquad (1.16)$$

where the spatial functions are of the form $\mathbf{u}_{\mathbf{k},\lambda}(\mathbf{r}) = \mathbf{e}_{\mathbf{k},\lambda}e^{i\mathbf{k}\cdot\mathbf{r}}$, and they are mutually orthogonal

$$\frac{1}{V} \int_V \mathrm{d}^3\mathbf{r}\, \mathbf{u}_{\mathbf{k},\lambda}(\mathbf{r}) \cdot \mathbf{u}_{\mathbf{k}',\lambda'}(\mathbf{r}) = \delta_{\mathbf{k},\mathbf{k}'}\delta_{\lambda,\lambda'}. \qquad (1.17)$$

while the temporal functions must satisfy the differential equation

$$\ddot{A}_{\mathbf{k},\lambda}(t) + \omega_{\mathbf{k}}^2 A_{\mathbf{k},\lambda}(t) = 0, \qquad (1.18)$$

with $\omega_{\mathbf{k}} = c|\mathbf{k}|$ the angular frequency of the wave. The solution of this equation is of the form $A_{\mathbf{k},\lambda}(t) = A^0_{\mathbf{k},\lambda}e^{-i\omega_{\mathbf{k}}t}$, where $A^0_{\mathbf{k},\lambda}$ is a complex constant. Following the relations of the electric and magnetic field in Eqs. (1.12a) and (1.12b), we can write the electric and magnetic field operators as

$$\hat{\mathbf{E}}(\mathbf{r},t) = i\sum_{\mathbf{k},\lambda} \left[\omega_{\mathbf{k}}A_{\mathbf{k},\lambda}(t)\mathbf{u}_{\mathbf{k},\lambda}(\mathbf{r}) - \omega_{\mathbf{k}}A^*_{\mathbf{k},\lambda}(t)\mathbf{u}^*_{\mathbf{k},\lambda}(\mathbf{r}) \right] \qquad (1.19a)$$

$$\hat{\mathbf{B}}(\mathbf{r},t) = i\sum_{\mathbf{k},\lambda} \mathbf{k} \times \left[A_{\mathbf{k},\lambda}(t)\mathbf{u}_{\mathbf{k},\lambda}(\mathbf{r}) + A^*_{\mathbf{k},\lambda}(t)\mathbf{u}^*_{\mathbf{k},\lambda}(\mathbf{r}) \right]. \qquad (1.19b)$$

Using the expansion of $\mathbf{A}$ in Eq. (1.16) and the orthogonality of the spatial functions in Eq. (1.17), we can write the energy stored in the electromagnetic field in Eq. (1.15) as

$$E = \varepsilon_0 V \sum_{\mathbf{k},\lambda} \omega_{\mathbf{k}}^2 \left(A_{\mathbf{k},\lambda}^0 A_{\mathbf{k},\lambda}^{0*} + A_{\mathbf{k},\lambda}^{0*} A_{\mathbf{k},\lambda}^0 \right) = 2\varepsilon_0 V \sum_{\mathbf{k},\lambda} \omega_{\mathbf{k}}^2 \left| A_{\mathbf{k},\lambda}^0 \right|^2 . \quad (1.20)$$

By writing $A_{\mathbf{k},\lambda}^0 = \sqrt{\frac{\hbar}{2\varepsilon_0 V \omega_{\mathbf{k}}}} a_{\mathbf{k},\lambda}$, we can write the energy in Eq. (1.20) as

$$E = \sum_{\mathbf{k},\lambda} \hbar \omega_{\mathbf{k}} \left(a_{\mathbf{k},\lambda} a_{\mathbf{k},\lambda}^* + a_{\mathbf{k},\lambda}^* a_{\mathbf{k},\lambda} \right) , \quad (1.21)$$

and, by performing a change of variables from $a_{\mathbf{k},\lambda}$ and its complex conjugate to the real variables $q_{\mathbf{k},\lambda}$ and $p_{\mathbf{k},\lambda}$, where

$$q_{\mathbf{k},\lambda} = \sqrt{\frac{\hbar}{2\omega_{\mathbf{k}}}} \left(a_{\mathbf{k},\lambda} + a_{\mathbf{k},\lambda}^* \right) \quad (1.22a)$$

$$p_{\mathbf{k},\lambda} = -i\sqrt{\frac{\hbar \omega_{\mathbf{k}}}{2}} \left(a_{\mathbf{k},\lambda} - a_{\mathbf{k},\lambda}^* \right) , \quad (1.22b)$$

the electromagnetic energy becomes

$$E = \frac{1}{2} \sum_{\mathbf{k},\lambda} \left(p_{\mathbf{k},\lambda}^2 + \omega_{\mathbf{k}}^2 q_{\mathbf{k},\lambda}^2 \right) , \quad (1.23)$$

which resembles the Hamiltonian of a quantum harmonic oscillator with unitary mass and frequency $\omega_{\mathbf{k}}$, with $q_{\mathbf{k},\lambda}$ and $p_{\mathbf{k},\lambda}$ the position and momentum operators, respectively.

Up to now we have manipulated the classical equations of light to reach Eq. (1.23), which is a sum of uncoupled harmonic oscillators. The quantization of the electromagnetic field is performed by promoting the position and momentum to quantum operators $q_{\mathbf{k},\lambda} \to \hat{q}_{\mathbf{k},\lambda}$ and $p_{\mathbf{k},\lambda} \to \hat{p}_{\mathbf{k},\lambda}$, which satisfy the commutation relations

$$[\hat{q}_{\mathbf{k},\lambda}, \hat{p}_{\mathbf{k}',\lambda'}] = i\hbar \delta_{\mathbf{k},\mathbf{k}'} \delta_{\lambda,\lambda'} , \quad [\hat{q}_{\mathbf{k},\lambda}, \hat{q}_{\mathbf{k}',\lambda'}] = [\hat{p}_{\mathbf{k},\lambda}, \hat{p}_{\mathbf{k}',\lambda'}] = 0 . \quad (1.24)$$

Furthermore, also the classical coefficients $a_{\mathbf{k},\lambda}$ are automatically promoted to quantum operators $\hat{a}_{\mathbf{k},\lambda}$, because of the relations in Eqs. (1.22a) and (1.22b). The resulting operators $\hat{a}_{\mathbf{k},\lambda}$ and $\hat{a}_{\mathbf{k},\lambda}^{\dagger}$ are the annihilation and creation operators of the electromagnetic field, respectively. Using the commutation relations in Eq. (1.24), we obtain the usual commutation relations of the ladder operators

$$\left[\hat{a}_{\mathbf{k},\lambda}, \hat{a}_{\mathbf{k}',\lambda'}^{\dagger}\right] = \delta_{\mathbf{k},\mathbf{k}'}\delta_{\lambda,\lambda'}\,, \quad [\hat{a}_{\mathbf{k},\lambda}, \hat{a}_{\mathbf{k}',\lambda'}] = \left[\hat{a}_{\mathbf{k},\lambda}^{\dagger}, \hat{a}_{\mathbf{k}',\lambda'}^{\dagger}\right] = 0\,, \quad (1.25)$$

and the total Hamiltonian of the electromagnetic field finally becomes

$$\hat{H} = \sum_{\mathbf{k},\lambda} \hbar\omega_{\mathbf{k}} \left(\hat{a}_{\mathbf{k},\lambda}^{\dagger}\hat{a}_{\mathbf{k},\lambda} + \frac{1}{2}\right)\,. \qquad (1.26)$$

As ironically stated at the beginning of this section, we have quantized the electromagnetic field by simply placing a small cap over the symbols $\mathbf{E} \to \hat{\mathbf{E}}$, $\mathbf{B} \to \hat{\mathbf{B}}$ and $\mathbf{A} \to \hat{\mathbf{A}}$. Thus, we finally have

$$\hat{\mathbf{A}}(\mathbf{r}, t) = \sum_{\mathbf{k},\lambda} \sqrt{\frac{\hbar}{2\varepsilon_0 V \omega_{\mathbf{k}}}} \mathbf{e}_{\mathbf{k},\lambda} \left(\hat{a}_{\mathbf{k},\lambda}e^{i(\mathbf{k}\cdot\mathbf{r}-\omega_{\mathbf{k}}t)} + \text{h.c.}\right) \qquad (1.27a)$$

$$\hat{\mathbf{E}}(\mathbf{r}, t) = i\sum_{\mathbf{k},\lambda} \sqrt{\frac{\hbar\omega_{\mathbf{k}}}{2\varepsilon_0 V}} \mathbf{e}_{\mathbf{k},\lambda} \left(\hat{a}_{\mathbf{k},\lambda}e^{i(\mathbf{k}\cdot\mathbf{r}-\omega_{\mathbf{k}}t)} - \text{h.c.}\right) \qquad (1.27b)$$

$$\hat{\mathbf{B}}(\mathbf{r}, t) = i\sum_{\mathbf{k},\lambda} \sqrt{\frac{\hbar}{2\varepsilon_0 V \omega_{\mathbf{k}}}} \mathbf{k} \times \mathbf{e}_{\mathbf{k},\lambda} \left(\hat{a}_{\mathbf{k},\lambda}e^{i(\mathbf{k}\cdot\mathbf{r}-\omega_{\mathbf{k}}t)} + \text{h.c.}\right)\,. \qquad (1.27c)$$

1.2.3 Field quantization in a cavity

The prototypical example of confined electromagnetic field is the one-dimensional cavity, which is a region of space enclosed by perfectly reflecting walls. As in the previous section, the solution of the spatial part of the Maxwell equation in Eqs. (1.11a) to (1.11d) under this boundary conditions leads to an infinite and discrete set of solutions.

As sketched in Fig. 1.3, in the case of linear polarization of the electromagnetic field, their spatial part is of the form $\mathbf{E}(\mathbf{r}, t) =$
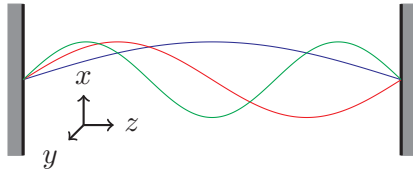
Figure 1.3: First three modes of the electromagnetic field $\mathbf{A}(\mathbf{r})$ in a cavity. The blue, red and green curves represent the first, second and third mode, respectively.

$\mathbf{e}_x E(z,t)$, $\mathbf{B}(\mathbf{r},t) = \mathbf{k} \times \mathbf{e}_x B(z,t) = \mathbf{e}_y B(z,t)$, and $\mathbf{A}(\mathbf{r},t) = \mathbf{e}_x A(z,t)$, where $\mathbf{e}_x$ and $\mathbf{e}_y$ are the unitary vectors along the x and y axis, respectively. Imposing the boundary conditions $E(0,t) = E(L,t) = 0$ that the electric field vanishes at the walls, we can write the spatial solution of the form $\sin(k_n z)$, with $k_n = n\pi/L$ and $n = 1, 2, \ldots$, and each spatial solution has the frequency $\omega_n = c k_n$. The quantized fields become

$$\hat{\mathbf{A}}_n(\mathbf{r}) = \sqrt{\frac{\hbar}{\varepsilon_0 V \omega_n}} \mathbf{e}_x \sin(k_n z) \left(\hat{a}_n + \hat{a}_n^\dagger \right) \tag{1.28a}$$

$$\hat{\mathbf{E}}_n(\mathbf{r}) = -i\sqrt{\frac{\hbar \omega_n}{\varepsilon_0 V}} \mathbf{e}_x \sin(k_n z) \left(\hat{a}_n - \hat{a}_n^\dagger \right) \tag{1.28b}$$

$$\hat{\mathbf{B}}_n(\mathbf{r}) = \frac{1}{c} \sqrt{\frac{\hbar \omega_n}{\varepsilon_0 V}} \mathbf{e}_y \cos(k_n z) \left(\hat{a}_n + \hat{a}_n^\dagger \right) . \tag{1.28c}$$

When the electromagnetic field inside a cavity interacts with a two-level system with resonance frequency ω_{eg}, we can assume that only one mode of the cavity is near resonance with the two-level system. In this conditions we can consider only one mode of the electromagnetic field, and the Hamiltonian becomes that of a single quantum harmonic oscillator

$$\hat{H}_n = \hbar \omega_n \left(\hat{a}_n^\dagger \hat{a}_n + \frac{1}{2} \right) . \tag{1.29}$$

It is worth noting the dependence of the amplitude of the electromagnetic field in Eqs. (1.28a) to (1.28c) on the volume V of the

cavity. Reducing the volume of the cavity will increase the amplitude of the field, and this will be useful for achieving large light-matter coupling and the ultrastrong coupling regime, as we will see in Section 1.4.2.

1.3 The interaction between light and matter

The physics behind the Maxwell equation expressed in Eqs. (1.11a) to (1.11d) can be described, in the case of a single particle interacting with the electromagnetic field, by the following Lagrangian [12, 13]

$$L(\mathbf{q}, \dot{\mathbf{q}}, \mathbf{A}, \dot{\mathbf{A}}) = \frac{1}{2} m \dot{\mathbf{q}}^2 + \int_V \mathcal{L}(\mathbf{q}, \dot{\mathbf{q}}, \mathbf{A}(\mathbf{r}), \dot{\mathbf{A}}(\mathbf{r}), \phi(\mathbf{r})) \, \mathrm{d}^3\mathbf{r} \,, \quad (1.30)$$

where the first term is the kinetic energy of the particle, and the second term inside the integral is the Lagrangian density of the electromagnetic field

$$\mathcal{L}(\mathbf{q}, \dot{\mathbf{q}}, \mathbf{A}(\mathbf{r}), \dot{\mathbf{A}}(\mathbf{r}), \phi(\mathbf{r})) = \frac{\varepsilon_0}{2} \left[\left(\dot{\mathbf{A}} + \nabla \phi \right)^2 - c^2 \left(\nabla \times \mathbf{A} \right)^2 \right] \\ + \mathbf{J}(\mathbf{r}) \cdot \mathbf{A}(\mathbf{r}) - \rho(\mathbf{r})\phi(\mathbf{r}) \,. \quad (1.31)$$

Here m is the particle mass, $\mathbf{q}$ and $\dot{\mathbf{q}}$ are the position and velocity of the particle, respectively, while $\mathbf{J}(\mathbf{r})$ and $\rho(\mathbf{r})$ are the density current and the density of charge, respectively.

It is worth noting that the Lagrangian written above is in an arbitrary gauge, considering the electric and magnetic fields as in Eqs. (1.12a) and (1.12b). This automatically ensures that Eqs. (1.11a) and (1.11d) are satisfied. In the case of a single electron, with a fixed proton at the origin (hydrogen atom), we have

$$\mathbf{J}(\mathbf{r}) = -e\dot{\mathbf{q}}\delta(\mathbf{r} - \mathbf{q}) \,, \quad \rho(\mathbf{r}) = q\delta(\mathbf{r} - \mathbf{q}) + e\delta(\mathbf{r}) \,, \quad (1.32)$$

where $-e$ is the charge of the electron. They clearly satisfy the continuity equation

$$\nabla \cdot \mathbf{J} + \dot{\rho} = 0 \,. \quad (1.33)$$

13

The Maxwell equation in Eq. (1.11b) can be obtained from the Euler-Lagrange equation with respect to $\mathbf{A}$, which is

$$\frac{\mathrm{d}}{\mathrm{d}t}\frac{\partial L}{\partial \dot{\mathbf{A}}} - \frac{\partial L}{\partial \mathbf{A}} = 0 . \tag{1.34}$$

Indeed, we obtain

$$c^2 \nabla \left(\nabla \cdot \mathbf{A} \right) - c^2 \nabla^2 \mathbf{A} + \nabla \dot{\phi} + \ddot{\mathbf{A}} - \frac{\mathbf{J}}{\varepsilon_0} = 0 , \tag{1.35}$$

which is identical to Eq. (1.11b). The fourth and final Maxwell equation in Eq. (1.11c) follows upon taking the divergence of Eq. (1.33) and using the definition of $\mathbf{J}$ and ρ in Eq. (1.32).

For the particle motion, the Lorentz force is derived from the Euler-Lagrange equation with respect to $\mathbf{q}$, which leads to

$$m\ddot{\mathbf{q}} = -e \left(\mathbf{E} + \dot{\mathbf{q}} \times \mathbf{B} \right) . \tag{1.36}$$

As can be seen in the definition of the Lagrangian in Eq. (1.30), $\mathbf{q}$ and $\mathbf{A}$ are the only independent dynamical variables, with ϕ determinable via them by the equations of motion. The momenta conjugate to $\mathbf{q}$ and $\mathbf{A}$ are

$$\mathbf{p} = \frac{\partial L}{\partial \dot{\mathbf{q}}} = m\dot{\mathbf{q}} - e\mathbf{A}(\mathbf{q}) \tag{1.37a}$$

$$\mathbf{\Pi}(\mathbf{r}) = \frac{\partial L}{\partial \dot{\mathbf{A}}} = -\varepsilon_0 \mathbf{E}(\mathbf{r}) , \tag{1.37b}$$

and the canonical procedure yields the Hamiltonian

$$H = \mathbf{p} \cdot \dot{\mathbf{q}} + \int_V \mathrm{d}^3 r \left[\mathbf{\Pi}(\mathbf{r}) \cdot \dot{\mathbf{A}}(\mathbf{r}) \right] - L , \tag{1.38}$$

which leads to

$$H = \frac{1}{2m} \left(\mathbf{p} + e\mathbf{A} \right)^2 + \frac{1}{2} \int_V \mathrm{d}^3 r \left(\frac{\mathbf{\Pi}^2}{\varepsilon_0} + \frac{B^2}{\mu_0} \right) . \tag{1.39}$$

In the equation written above, there is an extra term equal to

$$\int_V d^3\mathbf{r} \left[(\nabla \cdot \mathbf{\Pi} + \rho)\,\phi \right],$$

but, it is clear from Eqs. (1.11c) and (1.37b) that this term is identically zero.

1.3.1 General gauge transformation

As previously stated in Eq. (1.13), we can perform a gauge transformation of the form

$$\mathbf{A}'(\mathbf{r}) = \mathbf{A}(\mathbf{r}) - \nabla\chi(\mathbf{r}), \quad \phi'(\mathbf{r}) = \phi(\mathbf{r}) + \dot{\chi}(\mathbf{r}), \qquad (1.40)$$

leaving the fields and particle equations of motion unchanged. Here $\chi(\mathbf{r})$ is an arbitrary scalar function, called generating function. It is moreover useful to introduce a gauge density $\tilde{\chi}$ such that

$$\chi(\mathbf{r}) = \int_V d^3\mathbf{r}'\,\tilde{\chi}(\mathbf{r}, \mathbf{r}', \{\mathbf{A}(\mathbf{r}')\}), \qquad (1.41)$$

which will be written in the shorthand form $\tilde{\chi}(\mathbf{r}, \mathbf{r}')$ in the subsequent equations.

The Lagrangian density $\mathscr{L}'$ in the new gauge is given by Eq. (1.31) but with the old potentials replaced by the new ones

$$\begin{aligned}
\mathscr{L}' &= \mathscr{L}(\mathbf{q}, \dot{\mathbf{q}}, \mathbf{A}'(\mathbf{r}), \dot{\mathbf{A}}'(\mathbf{r}), \phi'(\mathbf{r})) \\
&= \mathscr{L}(\mathbf{q}, \dot{\mathbf{q}}, \mathbf{A}(\mathbf{r}) - \nabla\chi(\mathbf{r}), \dot{\mathbf{A}}(\mathbf{r}) - \nabla\dot{\chi}(\mathbf{r}), \phi(\mathbf{r}) + \dot{\chi}(\mathbf{r})).
\end{aligned}$$

Thus from Eqs. (1.30) and (1.31) we have

$$L' = L - \int_V d^3\mathbf{r} \left[\mathbf{J} \cdot \nabla\chi + \rho\dot{\chi} \right], \qquad (1.42)$$

and, since $\tilde{\chi}$ depends on the time through $\mathbf{A}$, we have

$$\begin{aligned}
L' &= L + e\dot{\mathbf{q}} \cdot \nabla\chi(\mathbf{q}) - \int_V d^3\mathbf{r}\,\rho(\mathbf{r}) \int_V d^3\mathbf{r}' \frac{\partial\tilde{\chi}(\mathbf{r}, \mathbf{r}')}{\partial\mathbf{A}(\mathbf{r}')} \cdot \dot{\mathbf{A}}(\mathbf{r}') \\
&= L + e\dot{\mathbf{q}} \cdot \nabla\chi(\mathbf{q}) - \int_V d^3\mathbf{r}\,\dot{\mathbf{A}}(\mathbf{r}) \cdot \int_V d^3\mathbf{r}' \frac{\partial\tilde{\chi}(\mathbf{r}, \mathbf{r}')}{\partial\mathbf{A}(\mathbf{r})}\rho(\mathbf{r}').
\end{aligned} \qquad (1.43)$$

We now continue to take $\mathbf{q}$ and $\mathbf{A}$ as the canonical variables, while the conjugate momenta become

$$\mathbf{p}' = \frac{\partial L'}{\partial \dot{\mathbf{q}}} = m\dot{\mathbf{q}} - e\mathbf{A}(\mathbf{q}) + e\nabla\chi(\mathbf{q}) \tag{1.44a}$$

$$\mathbf{\Pi}'(\mathbf{r}) = \frac{\partial L'}{\partial \dot{\mathbf{A}}} = \varepsilon_0 \left[\dot{\mathbf{A}}(\mathbf{r}) + \nabla\phi(\mathbf{r}) \right] - \mathbf{P}(\mathbf{r}), \tag{1.44b}$$

where we have introduced the polarization density

$$\mathbf{P}(\mathbf{r}) = \int_V d^3\mathbf{r}' \frac{\partial\tilde{\chi}(\mathbf{r},\mathbf{r}')}{\partial\mathbf{A}(\mathbf{r})}\rho(\mathbf{r}'). \tag{1.45}$$

By comparison with the original conjugate momenta $\mathbf{p}$ and $\mathbf{\Pi}(\mathbf{r})$ of the old Lagrangian L in Eqs. (1.37a) and (1.37b), the new momenta are related to the old ones by

$$\mathbf{p}' = \mathbf{p} + e\nabla\chi(\mathbf{q}) \tag{1.46a}$$

$$\mathbf{\Pi}'(\mathbf{r}) = \mathbf{\Pi}(\mathbf{r}) - \mathbf{P}(\mathbf{r}). \tag{1.46b}$$

The new Hamiltonian H' is obtained from the same procedure as in Eq. (1.38), and it is given by

$$H' = \frac{1}{2m} \left(\mathbf{p}' + e\mathbf{A} - e\nabla\chi \right)^2 + \frac{1}{2}\int_V d^3\mathbf{r} \left(\frac{(\mathbf{\Pi}' + \mathbf{P})^2}{\varepsilon_0} + \frac{B'^2}{\mu_0} \right), \tag{1.47}$$

and it is straightforward to verify that the equations of motion for $\mathbf{q}$ and $\mathbf{A}$ are unchanged.

The vector potential can be separated by a longitudinal and transverse part

$$\mathbf{A} = \mathbf{A}^{\|}(\mathbf{r}) + \mathbf{A}^{\perp}(\mathbf{r}), \tag{1.48}$$

where, by using the longitudinal and transverse delta functions, we have

$$\mathbf{A}_i^{\|}(\mathbf{r}) = \sum_j \int_V d^3\mathbf{r}' \, A_j(\mathbf{r}')\delta_{ij}^{\|}(\mathbf{r} - \mathbf{r}') \tag{1.49a}$$

$$\mathbf{A}_i^{\perp}(\mathbf{r}) = \sum_j \int_V d^3\mathbf{r}' \, A_j(\mathbf{r}')\delta_{ij}^{\perp}(\mathbf{r} - \mathbf{r}'). \tag{1.49b}$$

The two parts satisfy the relations

$$\nabla \times \mathbf{A}^{\parallel}(\mathbf{r}) = 0 \tag{1.50a}$$

$$\nabla \cdot \mathbf{A}^{\perp}(\mathbf{r}) = 0 \,. \tag{1.50b}$$

Thus, it is clear that the general gauge transformation in Eq. (1.40) changes only the longitudinal component $\mathbf{A}^{\parallel}$ of the vector potential, while the transverse component $\mathbf{A}^{\perp}$ remains unchanged. In the next discussion below, we will explicitly derive the form of χ for two of the most used gauges, namely the Coulomb gauge and the Power-Zienau-Woolley (P.Z.W.) gauge.

1.3.2 Coulomb gauge

The Coulomb gauge corresponds to a frame in which the particle momentum $\mathbf{p}$ is coupled to only the transverse part of the vector potential $\mathbf{A}^{\perp}$. The generating function χ is given by

$$\nabla \chi_C(\mathbf{r}) = \mathbf{A}^{\parallel}(\mathbf{r}) \,, \tag{1.51}$$

and the transformed vector potential has

$$\mathbf{A}_C^{\parallel}(\mathbf{r}) = 0 \,, \quad \nabla \cdot \mathbf{A}_C(\mathbf{r}) = 0 \,. \tag{1.52}$$

The required generator of the Coulomb gauge is therefore [13]

$$\chi_C(\mathbf{r}) = \frac{1}{4\pi} \sum_j \int_V \mathrm{d}^3\mathbf{r}' \, A_j(\mathbf{r}') \nabla'_j \frac{1}{|\mathbf{r} - \mathbf{r}'|} \,, \tag{1.53}$$

and the polarization in the Coulomb gauge becomes

$$P_{Cj}(\mathbf{r}) = \frac{1}{4\pi} \nabla_j \int_V \mathrm{d}^3\mathbf{r}' \, \rho(\mathbf{r}') \frac{1}{|\mathbf{r} - \mathbf{r}'|} \,, \tag{1.54}$$

and thus

$$\mathbf{P}_C(\mathbf{r}) = -\varepsilon_0 \mathbf{E}^{\parallel}(\mathbf{r}) \,, \tag{1.55}$$

which satisfies the relation

$$\nabla \cdot \mathbf{P}_C(\mathbf{r}) = -\rho(\mathbf{r}) \,. \tag{1.56}$$

The momentum conjugate to $\mathbf{A}_C$ is obtained from Eqs. (1.44b) and (1.55) and it is given by

$$\mathbf{\Pi}_C(\mathbf{r}) = -\varepsilon_0 \mathbf{E}(\mathbf{r}) + \varepsilon_0 \mathbf{E}^{\parallel}(\mathbf{r}) = -\varepsilon_0 \mathbf{E}^{\perp}(\mathbf{r}) \,, \tag{1.57}$$

which gives the transverse electric field.

The Hamiltonian can be written in the Coulomb gauge by using Eqs. (1.47), (1.55) and (1.57). Moreover, by expanding the integral involving $\mathbf{\Pi}_C$ and $\mathbf{P}_C$, and considering that the contribution of their dot product is zero since they are a transverse vector and a longitudinal vector, respectively, we obtain

$$\begin{aligned}
H_C = &\frac{1}{2m} \left(\mathbf{p} + e\mathbf{A}^{\perp} \right)^2 + \frac{1}{2} \int_V \mathrm{d}^3\mathbf{r} \left(\frac{\mathbf{\Pi}_C^2}{\varepsilon_0} + \frac{B_C^2}{\mu_0} \right) \\
&+ \frac{1}{2\varepsilon_0} \int_V \mathrm{d}^3\mathbf{r} \, \mathbf{P}_C^2 \,,
\end{aligned} \tag{1.58}$$

To derive the exact form of the last term in the equation written above, we can use the charge density considered in Eq. (1.32) and the relation in Eq. (1.54), which leads to

$$P_{Cj}(\mathbf{r}) = -\frac{e}{4\pi} \nabla_j \left(\frac{1}{|\mathbf{q} - \mathbf{r}|} - \frac{1}{\mathbf{r}} \right) \,, \tag{1.59}$$

and the last term of Eq. (1.58) represents the Coulomb energies of the charged particles

$$\frac{1}{2\varepsilon_0} \int_V \mathrm{d}^3\mathbf{r} \, \mathbf{P}_C^2 = -\frac{e^2}{4\pi\varepsilon_0 |\mathbf{q}|} + \text{infinite electron self energy} \,. \tag{1.60}$$

Note that the Coulomb potential between the two charged particles (where the proton was considered fixed at the origin) was not introduced

in the initial Lagrangian, but it emerged through the interaction with the electromagnetic field.

To promote these fields to quantum operators, we can use the same procedure as in Section 1.2.2 for the quantization of the electromagnetic field. By promoting $\mathbf{q}$, $\mathbf{p}$, $\mathbf{A}_C$ and $\mathbf{\Pi}_C$ to operators, we obtain the following commutation relations

$$[\hat{q}_i, \hat{p}_{C\,j}] = i\hbar\delta_{ij}\,, \quad \left[\hat{A}_i(\mathbf{r}), \hat{\Pi}_{C\,j}(\mathbf{r}')\right] = i\hbar\delta_{ij}^{\perp}(\mathbf{r} - \mathbf{r}')\,, \tag{1.61}$$

1.3.3 Power-Zienau-Woolley gauge

The Power-Zienau-Woolley (P.Z.W.) is sometimes called the multipolar gauge [14]. Let's consider the following polarization vector

$$\mathbf{P}_M(\mathbf{r}) = -e \int_0^1 \mathrm{d}\lambda\, \mathbf{q}\delta(\mathbf{r} - \lambda\mathbf{q})\,, \tag{1.62}$$

and we can see that [13]

$$\nabla \cdot \mathbf{P}_M(\mathbf{r}) = e\delta(\mathbf{r} - \mathbf{q}) - e\delta(\mathbf{r}) = -\rho(\mathbf{r})\,. \tag{1.63}$$

By explicitly introducing the dependence of the polarization vector on the position of the particle $\mathbf{q}$, $\mathbf{P}_M(\mathbf{r}, \mathbf{q})$, the gauge generator density $\tilde{\chi}_M$ of the P.Z.W. gauge can be derived from Eqs. (1.45) and (1.62) and the charge density in Eq. (1.32), and it is given by

$$\tilde{\chi}_M(\mathbf{r}, \mathbf{r}') = \frac{1}{e}\mathbf{A}(\mathbf{r}') \cdot \mathbf{P}_M(\mathbf{r}, \mathbf{r}')\,. \tag{1.64}$$

The gauge generator χ_M is then obtained from Eqs. (1.41) and (1.64) and it is given by

$$\chi_M(\mathbf{r}) = -\int_V \mathrm{d}^3\mathbf{r}' \int_0^1 \mathrm{d}\lambda\, \mathbf{A}(\mathbf{r}') \cdot \mathbf{r}\delta(\mathbf{r}' - \lambda\mathbf{r})\,, \tag{1.65}$$

and the respective gradient is

$$\nabla\chi_M(\mathbf{r}) = \mathbf{A}(\mathbf{r}) - \frac{1}{e}\int_V \mathrm{d}^3\mathbf{r}'\, \theta(\mathbf{r}', \mathbf{r}) \times \mathbf{B}(\mathbf{r}')\,, \tag{1.66}$$

19

where

$$\theta(\mathbf{r}', \mathbf{q}) = -e \int_0^1 d\lambda\, \lambda \mathbf{q} \delta(\mathbf{r}' - \lambda \mathbf{q})\,. \tag{1.67}$$

Using Eqs. (1.13) and (1.66), the vector potential in the P.Z.W. gauge is given by

$$\mathbf{A}_M(\mathbf{r}) = \frac{1}{e} \int_V d^3\mathbf{r}'\, \theta(\mathbf{r}', \mathbf{r}) \times \mathbf{B}(\mathbf{r}')\,, \tag{1.68}$$

which, in the special case where $\mathbf{B} = 0$, $\mathbf{A}_M(\mathbf{r}) = 0$. However, in general we have that the divergence is not zero $\nabla \cdot \mathbf{A}_M(\mathbf{r}) \neq 0$, in contrary to the Coulomb gauge case.

The conjugate momentum to $\mathbf{A}_M$ is obtained from Eq. (1.44b)

$$\mathbf{\Pi}_M(\mathbf{r}) = -\varepsilon_0 \mathbf{E}(\mathbf{r}) - \mathbf{P}_M(\mathbf{r}) = -\mathbf{D}(\mathbf{r})\,, \tag{1.69}$$

where $\mathbf{D}(\mathbf{r})$ is the electric displacement field. The Hamiltonian in the P.Z.W. gauge can be once again derived from the canonical transformation in Eq. (1.47), and it is given by

$$\begin{aligned} H_M = & \frac{1}{2m}\left(\mathbf{p} + e\mathbf{A}_M\right)^2 + \frac{1}{2}\int_V d^3\mathbf{r}\left(\frac{\mathbf{\Pi}_M^2}{\varepsilon_0} + \frac{B_M^2}{\mu_0}\right) \\ & + \frac{1}{2\varepsilon_0}\int_V d^3\mathbf{r}\,\mathbf{P}_M^2 + \frac{1}{\varepsilon_0}\int_V d^3\mathbf{r}\,\mathbf{P}_M \cdot \mathbf{\Pi}_M\,. \end{aligned} \tag{1.70}$$

For the quantization procedure, we have the same commutation relations as in Eq. (1.61)

$$[\hat{q}_i, \hat{p}_{Mj}] = i\hbar\delta_{ij}\,, \quad \left[\hat{A}_i(\mathbf{r}), \hat{\Pi}_{Mj}(\mathbf{r}')\right] = i\hbar\delta_{ij}^{\perp}(\mathbf{r} - \mathbf{r}')\,. \tag{1.71}$$

Indeed, the vector potential $\mathbf{A}$ remains arbitrary, but its longitudinal part dows not affect the commutation relations because of the transversality of $\mathbf{\Pi}_M$. Thus, despite $\mathbf{A}^{\parallel}$ is not zero, it does not affect the dynamics.

1.3.4 Gauge transformations in quantum mechanics

In quantum mechanics, the gauge transformations are performed by a unitary transformation directly acting on the Hamiltonian and the wave function. It is simple to understand why, since the gauge transformations leave the Maxwell equations (and so the dynamics behind them) unchanged, such transformations should not affect the physical observables (expectation values of the operators), the Schrödinger equation and the probability density. The Schrödinger equation says that, for the Hamiltonian in Eq. (1.39) and a quantum state $|\psi\rangle$, the time evolution of the state is given by

$$i\hbar \frac{\partial}{\partial t} |\psi\rangle = \hat{H} |\psi\rangle \,. \tag{1.72}$$

Consider now a unitary transformation which leads to a new Hamiltonian $\hat{H}_U$ and a new state $|\psi\rangle_U$ given by

$$\hat{H}_U = \hat{U}\hat{H}\hat{U}^\dagger \,, \quad |\psi\rangle_U = \hat{U}|\psi\rangle \,, \tag{1.73}$$

any expectation value of an operator $\hat{O}$ is unchanged

$$\langle\psi|\hat{O}|\psi\rangle = \langle\psi|\hat{U}^\dagger\hat{U}\hat{O}\hat{U}^\dagger\hat{U}|\psi\rangle = \langle\psi|_U \hat{O}_U |\psi\rangle_U \,. \tag{1.74}$$

We now show that, when $\hat{U} = \exp(-i\hat{\Lambda})$ where $\hat{\Lambda} = -e\chi_C(\hat{\mathbf{q}})/\hbar$ or $\hat{\Lambda} = -e\chi_M(\hat{\mathbf{q}})/\hbar$, we obtain the Hamiltonian in the Coulomb gauge in Eq. (1.58) and the Hamiltonian in the P.Z.W. gauge in Eq. (1.70), respectively. We first note that $\hat{\Lambda}$ depends only on $\hat{\mathbf{q}}$ and $\hat{\mathbf{A}}$, but not on their conjugate momenta $\hat{\mathbf{p}}$ and $\hat{\mathbf{\Pi}}$. Thus, this unitary transformation changes only the momenta and not the coordinates

$$\begin{aligned}\hat{H}_U =& \hat{U}\hat{H}(\hat{\mathbf{q}}, \hat{\mathbf{p}}, \hat{\mathbf{A}}, \hat{\mathbf{\Pi}})\hat{U}^\dagger \\ =& \hat{H}(\hat{\mathbf{q}}, \hat{U}\hat{\mathbf{p}}\hat{U}^\dagger, \hat{\mathbf{A}}, \hat{U}\hat{\mathbf{\Pi}}\hat{U}^\dagger) = \hat{H}(\hat{\mathbf{q}}, \hat{\mathbf{p}}_U, \hat{\mathbf{A}}, \hat{\mathbf{\Pi}}_U)\,.\end{aligned} \tag{1.75}$$

By taking for example $\hat{\Lambda} = -e\chi_M(\hat{\mathbf{q}})/\hbar$, we have for $\hat{p}$

$$\begin{aligned}\hat{\mathbf{p}}_U =& \hat{U}\hat{\mathbf{p}}\hat{U}^\dagger = \hat{\mathbf{p}} - i\left[\hat{\Lambda}, \hat{\mathbf{p}}\right] + \frac{i^2}{2!}\left[\hat{\Lambda}, \left[\hat{\Lambda}, \hat{\mathbf{p}}\right]\right] + \dots \\ =& \hat{\mathbf{p}} + e\nabla\chi_M(\hat{\mathbf{q}})\,,\end{aligned} \tag{1.76}$$

where we have used the Baker-Campbell-Hausdorff formula $\exp(\hat{A})\,\hat{B}\exp(-\hat{A}) = \hat{B} + [\hat{A}, \hat{B}] + \frac{1}{2!}[\hat{A}, [\hat{A}, \hat{B}]] + \dots$ and Eq. (1.71) for the commutator $[\hat{\Lambda}, \hat{\mathbf{p}}]$. In Eq. (1.76), the terms with higher order in $\hat{\Lambda}$ are zero because $\hat{\Lambda}$ depends only on $\hat{\mathbf{q}}$. Thus, we have that $\hat{\mathbf{p}}_U = \hat{\mathbf{p}} + e\nabla\chi_M(\hat{\mathbf{q}})$, which is the momentum in the P.Z.W. gauge in Eq. (1.46a). Similarly, we can show that $\hat{\mathbf{\Pi}}_U = \hat{\mathbf{\Pi}} - \hat{\mathbf{P}}_M(\hat{\mathbf{r}})$, which is the momentum in the P.Z.W. gauge in Eq. (1.46b).

1.4 The interaction of light with a two-level atom

In this section we consider an electron in a one-dimensional double-well potential, like in Section 1.1.2, and we couple it to a single mode of the electromagnetic field (e.g., a cavity mode as in Section 1.2.3). We start by writing the Hamiltonian in the Coulomb gauge, as in Eq. (1.58)

$$\hat{H}_C = \frac{1}{2m}\left[\hat{p} + e\hat{A}_x\right]^2 + V(\hat{x}) + \hbar\omega_c\hat{a}^\dagger\hat{a}, \qquad (1.77)$$

where $\hat{A}_x = A_0(\hat{a} + \hat{a}^\dagger)$ with $A_0 = \sqrt{\hbar/(\varepsilon_0 V\omega_c)}\sin(k_x z_0)$ is the x component of the vector potential expressed in Eq. (1.28a), which is evaluated at the position of the electron z_0 (since we are assuming that it can only move in the x direction). Moreover, ω_c is the resonance frequency of the electromagnetic field, and $V(x) = -\mu/2x^2 + \lambda/4x^4$ is the double-well potential as in Eq. (1.8).

Under these conditions, the vector potential is constant with respect to the electron, meaning we are under the dipole approximation[2]. In this case, we can write the Hamiltonian in the P.Z.W. gauge through the unitary transformation $\hat{H}_D = \hat{T}\hat{H}_C\hat{T}^\dagger$, where

$$\hat{T} = \exp\left(i\frac{e}{\hbar}\hat{x}\hat{A}_x\right), \qquad (1.78)$$

---

[2]In this case this is trivial, since we are limited to only one dimension and the field varies in another dimension (z in this case).

obtaining

$$
\begin{aligned}
\hat{H}_D =& \frac{1}{2m}\hat{p}^2 + V(\hat{x}) + \hbar\omega_c\hat{a}^\dagger\hat{a} \\
&+ ie\omega_c A_0\left(\hat{a} - \hat{a}^\dagger\right)\hat{x} + \frac{e^2 A_0^2\omega_c}{\hbar}\hat{x}^2\,.
\end{aligned}
\tag{1.79}
$$

In the case of constant vector potential, the P.Z.W. gauge is usually called the dipole gauge [12, 15]. Now, as in Section 1.1.2, we assume that the double-well potential is such that the bounded electron has the first two energy levels ($|g\rangle$ and $|e\rangle$) well separated from the others, allowing to perform the two levels approximation through the projection operator $\hat{P} = |g\rangle\langle g| + |e\rangle\langle e|$, and we obtain the Hamiltonian in the dipole gauge projected

$$
\begin{aligned}
\hat{\mathcal{H}}_D =& \hat{P}\hat{H}_D\hat{P} \\
=& \frac{\hbar\omega_{eg}}{2}\hat{\sigma}_z + \hbar\omega_c\hat{a}^\dagger\hat{a} - i\hbar g_D\left(\hat{a} - \hat{a}^\dagger\right)\hat{\sigma}_x + \frac{e^2 A_0^2\omega_c x_{eg}^2}{\hbar}\,,
\end{aligned}
\tag{1.80}
$$

where $g_D = -e\omega_c A_0 x_{eg}/\hbar$ (with $x_{eg} = \langle e|\hat{x}|g\rangle$) is the dipole coupling constant, and $\omega_{eg} = (E_e - E_g)/\hbar$ is the transition frequency between the two levels. The last term in Eq. (1.80) is a constant energy shift, since $\hat{P}\hat{x}^2\hat{P} = x_{eg}^2(|g\rangle\langle g| + |e\rangle\langle e|)$ for the parity symmetry of the system $V(x) = V(-x)$, and it can be neglected.

1.4.1 The Jaynes-Cummings model

The Hamiltonian in Eq. (1.80) describes the quantum Rabi model (QRM), which is the full quantum treatment of the semiclassical model of a two-level system interacting with an oscillating classical field [16]. However, when the coupling strength g is much smaller than the energy separation between the two levels ($g \ll \omega_{eg}$), we can perform the rotating wave approximation (RWA) by neglecting the counter-rotating terms $\hat{a}\hat{\sigma}_-$ and $\hat{a}^\dagger\hat{\sigma}_+$, obtaining the well-known Jaynes-Cummings (JC) model [17]

$$
\hat{\mathcal{H}}_{JC} = \frac{\hbar\omega_{eg}}{2}\hat{\sigma}_z + \hbar\omega_c\hat{a}^\dagger\hat{a} + \hbar g\left(\hat{a}\hat{\sigma}_+ + \hat{a}^\dagger\hat{\sigma}_-\right)\,,
\tag{1.81}
$$

where we performed a unitary transformation $\hat{a} \rightarrow i\hat{a}$. Withing this approximation, the eigenstates can be found analytically [18]. Indeed, the JC Hamiltonian can be block-diagonalized, obtaining the following set of eigenstates

$$
\begin{aligned}
|n, +\rangle &= \cos\left(\frac{\alpha_n}{2}\right) |n, e\rangle + \sin\left(\frac{\alpha_n}{2}\right) |n+1, g\rangle \\
|n, -\rangle &= \sin\left(\frac{\alpha_n}{2}\right) |n, e\rangle - \cos\left(\frac{\alpha_n}{2}\right) |n+1, g\rangle ,
\end{aligned}
\tag{1.82}
$$

where $\alpha_n = \arctan[2g\sqrt{n+1}/(\omega_{eg} - \omega_c)]$. The corresponding eigenvalues are

$$
E_{n,\pm} = \hbar\omega_c(n + \frac{1}{2}) \pm \frac{1}{2}\hbar\sqrt{(\omega_{eg} - \omega_c)^2 + 4g^2(n+1)} . \tag{1.83}
$$

The Jaynes-Cummings model in Eq. (1.81) conserves the total number of particles ($[\hat{\mathcal{H}}_{JC}, \hat{a}^\dagger\hat{a} + \hat{\sigma}_+\hat{\sigma}_-] = 0$) and the parity of the system ($[\hat{\mathcal{H}}_{JC}, \hat{\Pi}(\phi)] = 0$), where $\hat{\Pi}(\phi) = \exp\left[i\phi(\hat{a}^\dagger\hat{a} + \hat{\sigma}_+\hat{\sigma}_-)\right]$ is the parity operator and ϕ is an arbitrary phase [19].

The dynamics of the Jaynes-Cummings Hamiltonian is quite simple to understand. If we consider the resonance condition $\omega_c = \omega_{eg}$ and we start with the state $|n, e\rangle$, the system will oscillate between $|n, e\rangle$ and $|n+1, g\rangle$ with a frequency $g\sqrt{n+1}$. This means that the probability to find the atom in the excited state oscillates like $P_e(t) = \cos^2(g\sqrt{n+1}t)$, which is the so-called Rabi oscillation. The vacuum Rabi oscillation is a coherent oscillation between the two states, and it is a consequence of the coherent coupling between the two levels.

The main antagonist of this coherent oscillation is the dissipation, which is always present when considering the interaction with an environment. If we call γ the dissipation rate of the system, we can set a scale regime as a function of the ratio g/γ. When this ratio is smaller than one we are the the so called *weak coupling* regime, while when it is larger than one we are in the *strong coupling* regime. The Rabi oscillations can be seen only in the strong coupling regime, since
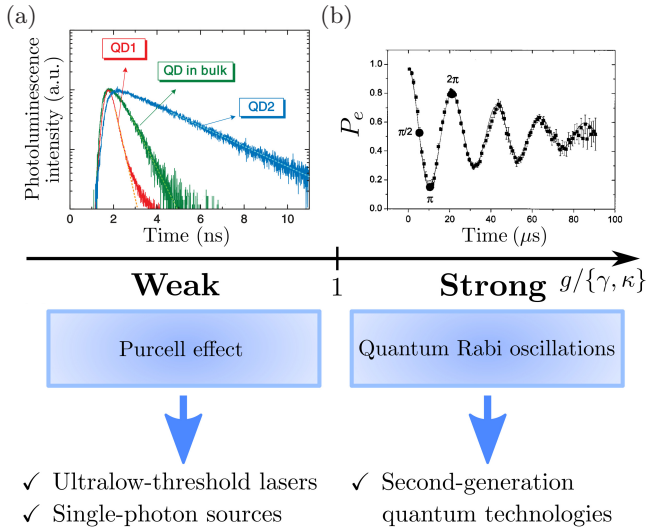
Figure 1.4: Scale of regimes of light-matter interaction, comparing the coupling strength g to the dissipation rates γ, κ of the cavity and the atom, respectively. (a) Weak coupling: experimental demonstration of full control of the spontaneous-emission dynamics of single quantum dots (QDs) interacting with a photonic-crystal nanocavity [20]. The plot shows the micro-photoluminescence of InGaAs QDs in different situations: when they match the cavity frequency, when they don't, and when there is no cavity at all. Compared with the case without any cavity, the QDs decay more quickly in a resonant cavity and more slowly in an off-resonant cavity. This is an example of the Purcell effect. (b) Strong coupling: vacuum ($n = 0$) Rabi oscillations of Rydberg atoms coupled to a superconducting microwave cavity [21]. The plot shows the probability of finding the atom in the excited state as a function of time. The oscillations are a consequence of the coherent coupling between the two systems, and the damping is due to the dissipation.

in the weak coupling regime the dissipation is too strong to allow the coherent oscillation between the two systems. In 1983 Haroche and co-workers were able to observe the Rabi oscillation for the first time, using a collection of Rydberg atoms in a microwave cavity [22]. The strong coupling was soon also achieved in several experimental

architectures, involving single atoms interacting with microwave and optical cavities [21, 23, 24], quasi-2D electronic excitations (Wannier excitons) [25], quantum dots [26] and superconducting circuits [27]. Although the weak coupling regime might be considered less interesting, it can give rise to a rich collection of interesting phenomena, such as the Purcell effect, which is the enhancement or the suppression of the spontaneous emission of an atom in a cavity [28, 29]. Indeed, as shown in Fig. 1.4 (a), the spontaneous emission of a quantum dot can be enhanced or suppressed by placing it in a resonant or off-resonant cavity, respectively [20]. Compared with the case without any cavity, the QDs decay more quickly in a resonant cavity (which enhances the density of states that the QDs can decay to) and more slowly in an off-resonant cavity (which shields the QD from the environment). This is an example of the Purcell effect. On the other hand, in the strong coupling regime, the coherent coupling between the two systems gives rise to the so-called vacuum Rabi oscillations, as shown in Fig. 1.4 (b). The oscillations are a consequence of the coherent coupling between the two systems, and the damping is due to the dissipation.

If in one hand the ratio g/γ between the coupling strength and the dissipation rate is important to let the coherences observable, it is not a good scale for describing the relative strength. Indeed, in all the experimental observations we cited up to now, the largest value of coupling strength was three orders of magnitude smaller than the bare energies of the system. For this reason, the ratio $\eta = g/\omega$ can give us more information about the system itself. Indeed, we have already seen that the RWA is a valid valid approximation when the coupling strength is much smaller than the energy separation between the two levels. But when this condition does not hold anymore, and we have $g \simeq \omega$, the properties of the interacting system can change dramatically. For instance, by using the quantum Rabi Hamiltonian in Eq. (1.80), which still contains the counter rotating terms, we can see that the number of total excitations is no longer conserved $[\hat{\mathcal{H}}_D, \hat{a}^\dagger \hat{a} + \hat{\sigma}_+ \hat{\sigma}_-] \neq 0$. Allowing the system to present several peculiar phenomena, involving virtual photons, creation of particles from the vacuum, and so on. This is

only an anticipation of what we will see in the next sections, where we will concentrate on two other regimes of light-matter interaction: the ultrastrong coupling regime (USC) and the deep strong coupling regime (DSC), which are characterized by $\eta \simeq 1/10$ and $\eta > 1$, respectively.

1.4.2 The ultrastrong coupling regime

In the previous discussion, we anticipated the concept of ultrastrong and deep strong coupling regimes. Although reaching this regimes is not easy, in the last decades there was an increasing interest in achieving larger η values [30, 31]. The choice was to consider the coupling of many atoms to the same cavity mode, as correctly predicted by the Dicke model [32], this leads to enhanced coupling that scales with the square root of the number of dipoles $g \propto \sqrt{N}$. The second choice was to use different degrees of freedom, whose coupling is not bounded by the small value of the fine structure constant $\alpha \simeq 1/137$, which is the natural dimensionless parameter emerging in a perturbative treatment in quantum electrodynamics (QED).

The first path was investigated, where the possibility of achieving the USC regime could be observed in intersubband polaritons, due to the large number of electrons [35]. In 2009, the USC regime was observed for the first time in a microcavity-embedded doped GaAs quantum wells with $\eta \simeq 0.11$. The second path was mainly investigated in the context of superconducting circuits, where in 2010 a normalized coupling up to $\eta \simeq 0.12$ was obtained [33, 36].

Fig. 1.5 shows two main experimental results for the observation of USC and DSC. In Fig. 1.5(a) a microwave spectroscopy was performed on a system featuring a superconducting flux qubit connected to a coplanar-waveguide resonator [33]. The plot illustrates the cavity's transmission as a function of the probe frequency, denoted as ω_{probe}, and the flux offset, which adjusts the qubit's frequency. This distinctive avoided level crossing indicates a process that doesn't conserve the total number of excitations. It describes the interaction between a state initially containing a single photon in the third resonator mode
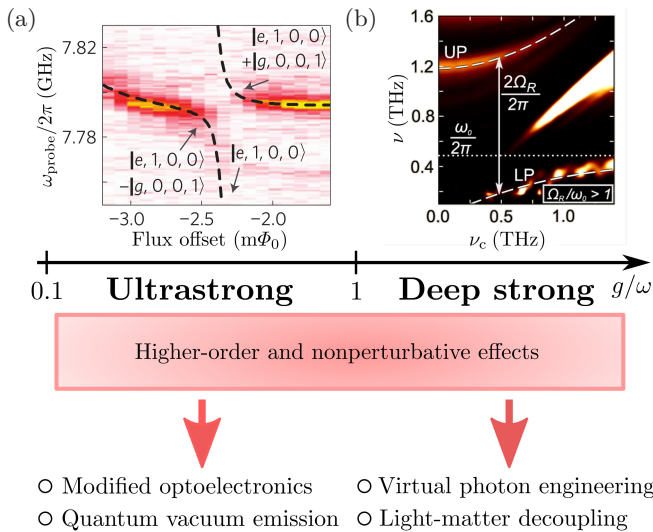
Figure 1.5: Scale of regimes of light-matter interaction, comparing the coupling strength g to the bare energies ω of the cavity and the atom. (a) Ultrastrong coupling: microwave spectroscopy of a system with a superconducting flux qubit coupled to a coplanar-waveguide resonator [33]. The plot shows the cavity transmission as a function of probe frequency ω_{probe} and flux offset, which tunes the qubit frequency. This avoided level crossing is a signature of a process that does not conserve the total number of excitations, since it describes the interaction between a first state that has a single photon in the third resonator mode and a second one that has one qubit excitation and one photon in the first resonator mode. (b) Deep strong coupling: magneto-THz transmission measurements on a THz metamaterial coupled to the cyclotron resonance of a 2D electron gas [34]. The splitting between the lower polariton (LP) and upper polariton (UP) levels in the point of the arrow is a measure of the coupling strength. In this work, a record $\eta = 1.43$ was reached.

and another state with one qubit excitation and one photon in the first resonator mode. This process is a signature of the USC regime, since it is a direct consequence of the counter-rotating terms. Fig. 1.5(b) shows the magneto-THz transmission measurements that were conducted on a THz metamaterial coupled to the cyclotron resonance of a 2D

electron gas [34]. The separation between the lower polariton (LP) and upper polariton (UP) levels at the arrow's location serves as a measure of the strength of the coupling. In this study, an impressive $\eta = 1.43$ coupling strength was achieved, which is currently the larges value ever reported.

Nowadays, this regime has been achieved in a great variety of systems and settings [30, 31]. The experimental progress in USC physics has motivated many studies showing interesting new effects enabled or boosted by this regime [36–71], predicting a changing in ground state chemical reactions [64], observing a modification of the ground state current resistivity [65]. Several studies explored higher-order processes [48, 49, 53, 57–59], such as multiphoton Rabi oscillations [48, 49] and a single photon exciting multiple atoms [53, 71].

1.4.3 Breakdown of gauge invariance in the USC regime

The careful reader would have already wondered why in the beginning of Section 1.4 we performed the gauge transformation to project the atom in the two-level approximation. Of course, nobody avoids us to perform the truncation on the Hamiltonian in the Coulomb gauge expressed in Eq. (1.77). Unexpectedly, this choice would lead to a completely different and wrong result when approaching to the USC regime.

Certainly gauge invariance is a crucial property that remains valid within the global Hilbert space, but it becomes compromised when operating within a specific subspace [72, 73]. As an example, some physical observables show a marked dependence on the chosen gauge. Consider the historical example of two-photon (1s-2s) absorption in the hydrogen atom [73]: the effect is zero within the Coulomb gauge and in a two-level approximation. However, when expanding the number of levels, convergence to the exact result is significantly slower in the Coulomb gauge than in the dipole gauge. These gauge-related complexities are further exacerbated in the context of USC interactions, as elaborated in Ref. [74].

We start by considering the Hamiltonian in the Coulomb gauge in Eq. (1.77), and we expand it

$$
\begin{aligned}
\hat{H}_C = {} & \frac{1}{2m}\hat{p}^2 + V(\hat{x}) + \hbar\omega_c\hat{a}^\dagger\hat{a} \\
& + \frac{eA_0}{m}\hat{p}\left(\hat{a} + \hat{a}^\dagger\right) + \frac{q^2 A_0^2}{2m}\left(\hat{a} + \hat{a}^\dagger\right)^2 .
\end{aligned}
\tag{1.84}
$$

We can easily see that the diagonal terms are zero ($\langle g|\hat{p}|g\rangle = \langle e|\hat{p}|e\rangle = 0$) since the eigenstates are stationary. On the other hand, the off-diagonal terms are not zero ($\langle g|\hat{p}|e\rangle = \langle e|\hat{p}|g\rangle^* \neq 0$) since, using Eqs. (1.10a) to (1.10b) they describes the tunneling process between the left and right states. By expressing the momentum as $\hat{p} = -i\hbar\partial_x$, we can write $\hat{P}\hat{p}\hat{P} = x_{eg}\omega_{eg}m\hat{\sigma}_y$, where $x_{eg} = \langle e|\hat{x}|g\rangle$, and $\hat{P} = |g\rangle\langle g| + |e\rangle\langle e|$ is the projection operator on the two-level subspace. In this way, the truncated Hamiltonian in the Coulomb gauge becomes

$$
\hat{\mathcal{H}}_C = \frac{\hbar\omega_{eg}}{2}\hat{\sigma}_z + \hbar\omega_c\hat{a}^\dagger\hat{a} + \hbar g_C\left(\hat{a} + \hat{a}^\dagger\right)\hat{\sigma}_y + D\left(\hat{a} + \hat{a}^\dagger\right)^2 , \tag{1.85}
$$

where $g_C = -e\omega_{eg}A_0 x_{eg}/\hbar$ is the coupling strength in the Coulomb gauge, and $D = e^2 A_0^2/(2m)$ is the well-known diamagnetic term.

The Hamiltonian in the Coulomb gauge, however, cannot be obtained by a unitary transformation from the Hamiltonian in the dipole gauge of Eq. (1.80), meaning that all the observables may be different. Indeed, as shown in Fig. 1.6, the first eigenvalues of the Hamiltonian in the Coulomb gauge are different from the eigenvalues of the Hamiltonian in the dipole gauge, where the latter is the correct one, since we compared the results with the full non truncated Hamiltonian in Eq. (1.84)[3]. This is a clear example of the breakdown of gauge invariance in the USC regime. The parameters used for the double-well potential are $\alpha = 400$, $\beta = 250$, while $\omega_c = \omega_{eg}$. We changed

---

[3]We can also compare the results with the Hamiltonian in the dipole gauge expressed in Eq. (1.80). Obviously, the results are the same, since the non truncated Hamiltonians are linked by a gauge transformation.
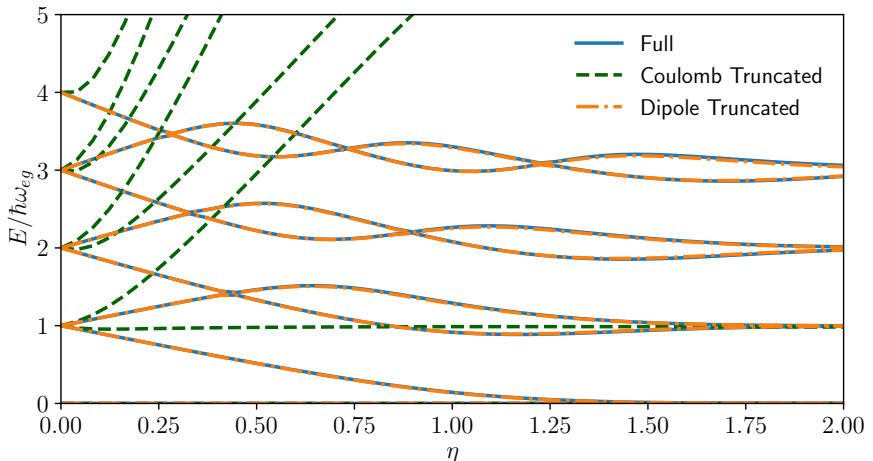
Figure 1.6: Comparison of the first eigenvalues of the single electron in a double-well potential interacting with a single mode cavity field. The blue lines correspond to the full Hamiltonian in Eq. (1.84), but the same results can be obtained from the Hamiltonian in the dipole gauge in Eq. (1.79). The orange lines correspond to the dipole gauge truncated to a two-level system, thus using Eq. (1.80). The green lines, instead, correspond to the truncated Coulomb gauge Hamiltonian in Eq. (1.85). As can be seen, Coulomb gauge reproduces wrong results. The parameters used for the potential are $\alpha = 400$, $\beta = 250$, while $\omega_c = \omega_{eg}$. We changed the normalized coupling η by changing the value of A_0.

the normalized coupling η by changing the value of A_0, following the relation $A_0 = \eta/(-ex_{eg})$ and choosing $e = -1$ for simplicity. Playing around a bit with the code in the dedicated GitHub repository [11], the reader can try to adjust the potential parameters and see that the truncate dipole gauge coincides with the full Hamiltonian only at high atom non-linearities.

At this moment we may ask ourselves what is the cause of this breakdown of gauge invariance. The answer was given in 2019 [75], stating that this problem is related to the non-locality that the atom potential acquires under a projection to a reduced Hilbert space

$V(\hat{x}) \to V(\hat{x}, \hat{x}')$, while it has been shown by several works [76–78] that a non-local potential can be expressed as a momentum-dependent operator $V(\hat{x}, \hat{p})$. Thus, to preserve gauge invariance, we have to perform the minimal coupling replacement $\hat{p} \to \hat{p} + e\hat{A}_x$ also in the non-local potential. Fig. 1.7 shows this problem in a visible way, where $|V(\hat{x}, \hat{x}')|$ is shown for various values of the truncation: $N = 100$, $N = 20$, $N = 5$ and $N = 2$, with the same parameters of Fig. 1.6 for the atom potential. As can be seen, the non-locality of the potential increases as we decrease the number of levels, and this is the reason why the Coulomb gauge fails to reproduce the correct results. In the dipole gauge, there is no minimal coupling replacement applied to the atom part, but, as we will see soon, there is a minimal coupling applied to the cavity field. This concept is crucial for most of the topics of this thesis, since we will see that the dipole gauge is not always well defined.

The problem was bypassed in the following way. First, we note that the full Hamiltonian in the Coulomb gauge in Eq. (1.84) can be written as

$$\hat{H}_C = \hat{U}\hat{H}_a\hat{U}^\dagger + \hat{H}_f, \tag{1.86}$$

where

$$\hat{H}_a = \frac{1}{2m}\hat{p}^2 + V(\hat{x}) \tag{1.87a}$$

$$\hat{H}_f = \hbar\omega_c\hat{a}^\dagger\hat{a}, \tag{1.87b}$$

and $\hat{U} = \hat{T}^\dagger$, where $\hat{T}$ is the unitary transformation in Eq. (1.78) that brings the Hamiltonian in the Coulomb gauge to the dipole gauge. To this end, we can write the Hamiltonian in the dipole gauge as

$$\begin{aligned} \hat{H}_D = \hat{T}\hat{H}_C\hat{T}^\dagger &= \hat{T}\hat{U}\hat{H}_a\hat{U}^\dagger\hat{T}^\dagger + \hat{T}\hat{H}_f\hat{T}^\dagger \\ &= \hat{H}_a + \hat{T}\hat{H}_f\hat{T}^\dagger = \hat{H}_a + \hat{U}^\dagger\hat{H}_f\hat{U}. \end{aligned} \tag{1.88}$$

where we can see that an opposite minimal coupling is applied only to the field part of the Hamiltonian, while the atom part is left unchanged.

$$|V(\hat{x}, \hat{x}')|$$
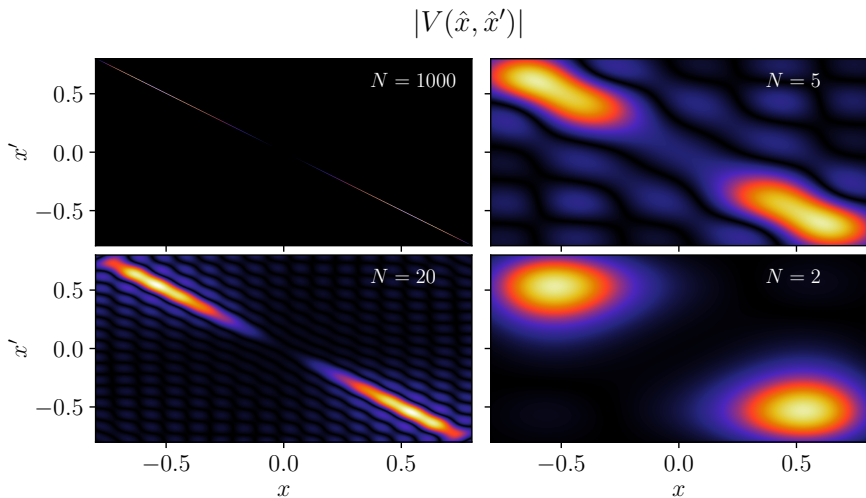
Figure 1.7: Non-locality of the double-well potential. The plot shows $|V(\hat{x}, \hat{x}')|$ for various values of the truncation: $N = 100$, $N = 20$, $N = 5$ and $N = 2$. As can be seen, the non-locality of the potential increases as we decrease the number of levels. The parameters used for the potential are $\alpha = 400$, $\beta = 250$.

By applying now the projection into a two-level system to the Hamiltonian in the Coulomb gauge in Eq. (1.86), we obtain the standard quantum Rabi Hamiltonian in the Coulomb gauge expressed in Eq. (1.85) $\hat{\mathcal{H}}_C = \hat{P}\hat{U}\hat{H}_a\hat{U}^\dagger\hat{P} + \hat{H}_f$, which we have already seen that it produces wrong results.

The key point to bypass this problem is to take into account the projected Hilbert space already before applying the minimal coupling replacement [75]. In other words, we have

$$\hat{\mathcal{H}}_C = \hat{\mathcal{U}}\hat{\mathcal{H}}_a\hat{\mathcal{U}}^\dagger + \hat{H}_f \,, \tag{1.89}$$

where $\hat{\mathcal{H}}_a = (\hbar\omega_{eg}/2)\hat{\sigma}_z$ is the already projected atom Hamiltonian,

and

$$
\begin{aligned}
\hat{\mathcal{U}} &= \exp\left[-i\frac{e}{\hbar}\hat{A}_x\hat{P}\hat{x}\hat{P}\right] \\
&= \exp\left[i\eta\left(\hat{a}+\hat{a}^\dagger\right)\hat{\sigma}_x\right].
\end{aligned}
\tag{1.90}
$$

By using again the Baker-Campbell-Hausdorff formula, we finally have the correct quantum Rabi Hamiltonian in the Coulomb gauge

$$
\hat{\mathcal{H}}_C = \frac{\hbar\omega_{eg}}{2}\left\{\hat{\sigma}_z\cos\left[2\eta\left(\hat{a}+\hat{a}^\dagger\right)\right] + \hat{\sigma}_y\sin\left[2\eta\left(\hat{a}+\hat{a}^\dagger\right)\right]\right\} + \hbar\omega_c\hat{a}^\dagger\hat{a},
\tag{1.91}
$$

which is linked to the quantum Rabi Hamiltonian in the dipole gauge through the unitary transformation

$$
\hat{\mathcal{H}}_D = \hat{\mathcal{T}}\hat{\mathcal{H}}_C\hat{\mathcal{T}}^\dagger = \hat{\mathcal{H}}_a + \hat{\mathcal{U}}^\dagger\hat{H}_f\hat{\mathcal{U}},
\tag{1.92}
$$

and thus reproduces the same results.

It should be stressed once again that this procedure is valid only in the dipole approximation, that is when the field can be considered constant with respect to the atom dipole. Moreover, the same Hamiltonian in the Coulomb gauge was recently obtained by using lattice gauge theory [79]. In the next sections we will address this issue in more detail, showing that, besides the gauge-invariance of the Hamiltonian, several issues may appear when treating ultrastrongly coupled open quantum systems, photodetection, and pure dephasing, showing that the dipole gauge is not always the most intuitive gauge to use.

CHAPTER 2

Open quantum systems and photodetection in the USC regime

In the previous chapter we have seen the foundamentals of cavity QED, focusing on the quantum Rabi model and its gauge ambiguities arising in the ultrastrong coupling regime. We treated the problem in the Hamiltonian level, which mean that we considered the composite system atom plus cavity as a closed quantum system. However, a closed system is a theoretical construct, which is useful to understand the intrinsic properties of it, but may be not so useful to describe the real world, where every system is in interaction with one or a multiple set of environments.

We already bypassed the gauge problem regarding the correct form of the quantum Rabi Hamiltonian in the Coulomb gauge. But, are we sure that everything is now solved? What happens to the gauge invariance when considering an open quantum system in the USC regime? Is the dipole gauge of the quantum Rabi Hamiltonian always correctly defined in the case of photodetection? In this chapter we will answer to all these questions. A little spoiler on the last question: no.

2.1 Photodetection in the USC regime

Photons are typically counted using photodetectors, where photon absorption causes a change in the detector's microscopic state. This change is then amplified to produce a classical signal, such as electric current, which is observed by the experimenter. Different photodetectors have varying response times and sensitivities to photon frequencies. The specific detection mechanism is essential for interpreting experiments involving photons. Optical photodetectors often use photo-ionization, where a photon absorption leads to the creation of free electrons and ions, generating a macroscopic current [80]. In semiconductor photodetectors, photon absorption above a certain energy threshold excites electrons and holes, which, under the influence of an electric field, create electron-hole pairs, resulting in a macroscopic current [80]. Understanding these processes is crucial for interpreting photon detection experiments.

Let's consider that before detection, the field exists in a pure state denoted as $|\Psi\rangle$. When a photon is absorbed, the resulting state of the field, denoted as $|\Psi_f\rangle$, is obtained by applying the operator $E^+(\mathbf{r}, t)$, which includes the annihilation operators of the field modes, to the initial state. In mathematical terms, this is represented as $|\Psi_f\rangle \propto E^+(r, t)|\Psi\rangle$. The probability of detecting the photon, along with the transition from the initial state $|\Psi\rangle$ to the final state $|\Psi\rangle_f$, is thus directly proportional to [81]

$$P_{\text{det}} \propto \left| \langle \Psi_f | E^+(\mathbf{r}, t) | \Psi \rangle \right|^2, \tag{2.1}$$

and the total probability of photodetection $w(\mathbf{r}, t)$ is obtained by summing over all possible final states $|\Psi_f\rangle$:

$$
\begin{aligned}
w(\mathbf{r}, t) &= \sum_f \left| \langle \Psi_f | E^+(\mathbf{r}, t) | \Psi \rangle \right|^2 \\
&= \sum_f \langle \Psi | E^-(\mathbf{r}, t) | \Psi_f \rangle \langle \Psi_f | E^+(\mathbf{r}, t) | \Psi \rangle \\
&= \langle \Psi | E^-(\mathbf{r}, t) E^+(\mathbf{r}, t) | \Psi \rangle .
\end{aligned}
\tag{2.2}
$$

Obviously, if the state is not pure, and it is expressed by a density matrix $\hat{\rho}$ we have that the photodetection probability is given by

$$w(\mathbf{r}, t) = \text{Tr}\left[\rho E^{-}(\mathbf{r}, t) E^{+}(\mathbf{r}, t)\right] . \tag{2.3}$$

In the case of a single mode field, where the the system is governed by quantum Harmonic oscillator $\hat{H}_f = \omega_c \hat{a}^\dagger \hat{a}$, as in Eq. (1.29), and the electric field is defined as $\hat{E} = i\omega_c A_0(\hat{a} - \hat{a}^\dagger)$. The part of the electric field with positive frequency is $\hat{E}^+ = i\omega_c A_0 \hat{a}$, since it can be easily seen that the time evolution of this operator is $\hat{E}^+(t) = \exp(i\hat{H}_f t)\hat{E}^+\exp(-i\hat{H}_f t) = \hat{E}^+\exp(-i\omega_c t)$, and the photodetection probability for a given pure state $|\Psi\rangle$ is thus proportional to the number of photons

$$w(\mathbf{r}, t) \propto \langle \Psi | \hat{a}^\dagger \hat{a} | \Psi \rangle . \tag{2.4}$$

Now, we may ask if this is always valid, or what happens if we consider the photodetection in the USC regime. First, let's consider the Jaynes-Cummings model as in Section 1.4.1, and we ask what is the photodetection probability if the system is in the ground state. We already know that this model is exactly solvable, and the ground state is $|\psi_{\text{GS}}\rangle = |0, g\rangle$ at any coupling strength. It is straightforward to see that the photodetection probability is always zero, but this is not the case when taking into account the counter-rotating terms and thus passing to the quantum Rabi model. The ground state of the quantum Rabi model is no longer equal to $|0, g\rangle$, but it is a superposition of all the bare states. When not taking into account the parity symmetry breaking of the atom, i.e. $V(\hat{x}) = V(-\hat{x})$, the quantum Rabi model conserves the parity of the system $[\hat{H}, \hat{\Pi}(\pi)] = 0$ (where $\hat{H}$ and $\hat{\Pi}(\theta) = \exp[i\theta(\hat{a}^\dagger \hat{a} + \hat{\sigma}_+ \hat{\sigma}_-)]$ are the system Hamiltonian and the phase-dependent parity operator, respectively), but it does not conserve the total number of excitations $[\hat{H}, \hat{a}^\dagger \hat{a} + \hat{\sigma}_+ \hat{\sigma}_-] \neq 0$. Thus, the ground state of the quantum Rabi Hamiltonian is of the form

$$|\psi_{\text{GS}}\rangle = \sum_n \left(c_n^{(1)} |2n, g\rangle + c_n^{(2)} |2n+1, g\rangle \right) , \tag{2.5}$$
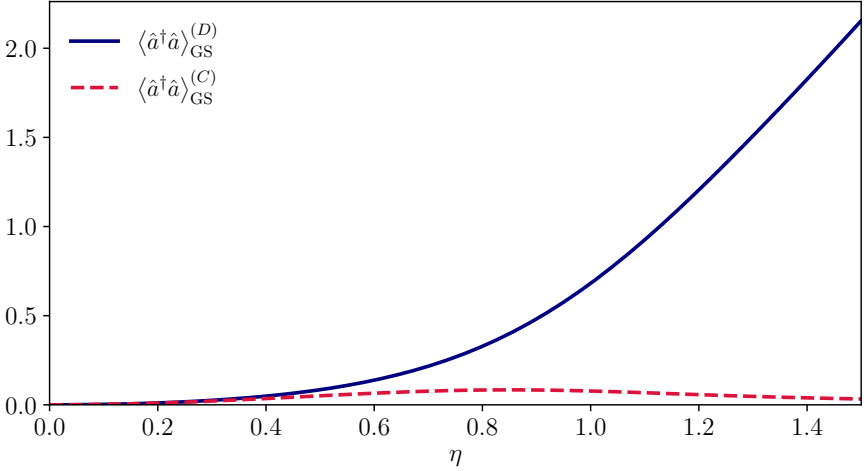
Figure 2.1: Expectation value of $\hat{a}^\dagger \hat{a}$ in the groundstate of the quantum Rabi Hamiltonian in both the dipole gauge in Eq. (1.80) (blue solid line) and the Coulomb gauge in Eq. (1.91) (red dashed line). As can be easily seen, this quantity is not zero, and it is even a gauge-dependent variable. The parameters are $\omega_c = 1$, $\omega_{eg} = 1$.

and it can be easily seen that

$$\langle \psi_{\text{GS}} | \hat{a}^\dagger \hat{a} | \psi_{\text{GS}} \rangle \neq 0 \,. \tag{2.6}$$

Fig. 2.1 shows the expectation value of $\hat{a}^\dagger \hat{a}$ in the groundstate of the quantum Rabi Hamiltonian in both the dipole gauge in Eq. (1.80) and the Coulomb gauge in Eq. (1.91). As can be easily seen, this quantity is not zero, and it is even a gauge-dependent variable. This is a clear example of the fact that the photodetection probability defined in Eq. (2.4) is not always valid, and it is even a gauge-dependent quantity when we approach the USC regime.

Following Glauber's approach [81], we need to revisit the positive frequency part of the field when we are in the USC regime. We start by writing the electric field operator in the basis of the eigenstates of

the system

$$\hat{E} = i\omega_c A_0 \sum_{j,k} \langle j|\hat{a} - \hat{a}^\dagger|k\rangle \, |j\rangle\langle k| \, , \tag{2.7}$$

and the definition of the positive frequency part is now given by

$$\hat{E}^+ = i\omega_c A_0 \sum_{j,k>j} \langle j|\hat{a} - \hat{a}^\dagger|k\rangle \, |j\rangle\langle k| \, . \tag{2.8}$$

The photodetection probability is now given by Eq. (2.2) with the positive frequency part of the electric field defined in Eq. (2.8). Indeed, it has been shown that this is the correct way to calculate the real photon rate at any light-matter coupling strength [82–84]. Obviously, the eigenstates $|j\rangle$ and the operators depend on the gauge we are considering, like any change of basis. In the following, we will discuss about the gauge invariance of photodetection at arbitrary light-matter coupling strengths.

2.1.1 Photodetection in the Coulomb gauge

In Section 1.4.3 we derived the correct form of the quantum Rabi Hamiltonian in the Coulomb gauge, which is given by Eq. (1.91), which we rewrite here for the sake of clarity

$$\hat{H}_C = \omega_c \hat{a}^\dagger \hat{a} + \frac{\omega_{eg}}{2} \left\{ \hat{\sigma}_z \cos\left[2\eta\left(\hat{a} + \hat{a}^\dagger\right)\right] + \hat{\sigma}_y \sin\left[2\eta\left(\hat{a} + \hat{a}^\dagger\right)\right] \right\} . \tag{2.9}$$

As we already have seen, the Hamiltonian written above can be obtained starting from the light-matter Hamiltonian in the absence of interaction $\hat{\mathcal{H}}_0 = \hat{\mathcal{H}}_a + \hat{\mathcal{H}}_f$, where $\hat{\mathcal{H}}_a = \omega_{eg}\hat{\sigma}_z/2$ and $\hat{\mathcal{H}}_f = \omega_c\hat{a}^\dagger\hat{a}$, by applying a suitable unitary transformation (generalized minimal coupling transformation) to $\hat{\mathcal{H}}_a$ only [75, 79]. Specifically,

$$\hat{\mathcal{H}}_C = \hat{\mathcal{U}}\hat{\mathcal{H}}_a\hat{\mathcal{U}}^\dagger + \hat{\mathcal{H}}_f \, , \tag{2.10}$$

where

$$\hat{\mathcal{U}} = \exp\left[i\eta\left(\hat{a} + \hat{a}^\dagger\right)\hat{\sigma}_x\right] . \tag{2.11}$$

We observe that in the Coulomb gauge, the canonical field momentum is not modified by the interaction with the matter component, i.e., $\hat{\Pi} = -\varepsilon_0 \hat{E}$ (ε_0 vacuum permittivity), such that, in this framework, the electric field operator can be written as we already said

$$\hat{E} = i\omega_c A_0 \left(\hat{a} - \hat{a}^\dagger \right) , \tag{2.12}$$

and, by using the system eigenstates, its positive frequency part is as in Eq. (2.8), that here we rewrite considering ω_c and A_0 as simple scaling factors, and so that does not influence the photon rate calculations

$$\hat{E}^+ = i \sum_{j,k>j} \langle j|\hat{a} - \hat{a}^\dagger|k \rangle \, |j\rangle\langle k| . \tag{2.13}$$

By using the following relation [85]

$$\omega_c \langle j|\hat{a} - \hat{a}^\dagger|k \rangle = \omega_{kj} \langle j|\hat{a} + \hat{a}^\dagger|k \rangle , \tag{2.14}$$

Eq. (2.13) can be written also as

$$\hat{E}^+ = i \sum_{j,k>j} \frac{\omega_{kj}}{\omega_c} \langle j|\hat{a} + \hat{a}^\dagger|k \rangle \, |j\rangle\langle k| . \tag{2.15}$$

By using the simple input-output theory [86], results analogous to w can be obtained for the rate w^{out} of emitted photons detected by a detector placed outside the cavity [82, 87]. However, the output field operators can display a different dependence on ω_{kj}, arising from the density of states of the output modes and from the frequency dependence of the coupling coefficient, which (for example) depends on the mirror reflectivity in a standard microcavity. More generally, the output field operator, in the Coulomb gauge, can be written as

$$\hat{E}_{\text{out}}^+ = i \sum_{j,k>j} \alpha(\omega_{kj}) \langle j|\hat{a} + \hat{a}^\dagger|k \rangle \, |j\rangle\langle k| , \tag{2.16}$$

where $\alpha(\omega)$ represents the specific dependence on frequency, which varies according to the model. A more comprehensive input-output

theory can be established using quantized quasinormal modes, as discussed in various studies [88–90].

It's important to note that photodetection is a process of energy absorption. Therefore, it's logical to assume that photon detection rates approach zero as frequencies ω approach zero. Any realistic analysis that covers a broad frequency range should also consider dispersion in the material model. However, incorporating this aspect would make the study system-dependent, which is beyond the scope of this general framework.

2.1.2 Photodetection in the dipole gauge

The quantum Rabi Hamiltonian can also be expressed in the dipole gauge, as in Eq. (1.80), which, again, we rewrite here for the sake of clarity

$$\hat{H}_D = \omega_c \hat{a}^\dagger \hat{a} + \frac{\omega_{eg}}{2} \hat{\sigma}_z - i\omega_c \eta \left(\hat{a} - \hat{a}^\dagger \right) \hat{\sigma}_x + \omega_c \eta^2 \hat{\sigma}_x^2 . \tag{2.17}$$

The Hamiltonian written above is linked to the one in the Coulomb gauge by a gauge transformation $\hat{H}_D = \hat{\mathcal{U}}^\dagger \hat{H}_C \hat{\mathcal{U}}$, where $\hat{\mathcal{U}}$ is expressed in Eq. (2.11). In the dipole gauge, the field conjugate momentum is modified by the interaction with the matter system, and it is proportional to the electric displacement (induction) field, as in Eq. (1.69). In the case of a constant single mode cavity field we have [2]

$$\hat{\Pi}' = -\hat{D} = -i\varepsilon_0 \omega_c A_0 \left(\hat{a} - \hat{a}^\dagger \right) , \tag{2.18}$$

Thus, the electric field operator cannot be expanded in terms of photon operators only. Indeed, due to the fact that $\hat{D} = \varepsilon_0 \hat{E}' + \hat{P}$ (for a dipole in free space), where $\hat{P}$ is the electric polarization, the electric field operator in the dipole gauge has to be expanded as

$$\hat{E}' = i\omega_c A_0 \left(\hat{a}' - \hat{a}'^\dagger \right) , \tag{2.19}$$

where

$$\hat{a}' = \hat{\mathcal{U}}^\dagger \hat{a} \hat{\mathcal{U}} = \hat{a} + i\eta \hat{\sigma}_x \tag{2.20}$$

41

is the photon operator in the new basis of the dipole gauge [84]. Furthermore, the operator $\hat{a}'$ and $\hat{a}'^{\dagger}$ obey to the usual commutation relations of the bosonic operators, i.e. $[\hat{a}', \hat{a}'^{\dagger}] = 1$.

The photodetection probability can be obtained following the same procedure as in Section 2.1.1. First, we need to write the electric field operator $\hat{E}'$ in the basis of the eigenstates of the system, and than we take only the positive frequency part of it[1]

$$\hat{E}'^{+} = i \sum_{j,k>j} \langle j'|\hat{a}' - \hat{a}'^{\dagger}|k'\rangle \, |j'\rangle\langle k'| \; . \tag{2.21}$$

The main error that is usually made consists to consider the electric field operator in the dipole gauge as

$$\hat{E}_{\text{wrong}} = i\omega_c A_0 \left(\hat{a} - \hat{a}^{\dagger}\right) \tag{2.22}$$

instead of Eq. (2.19), which is valid only at very low coupling strengths. By considering the wrong electric field operator would lead to gauge-dependent photon emission. Indeed, Eq. (2.21) is linked to Eq. (2.13) by the same unitary transformation $\hat{\mathcal{U}}$, which means that the photodetection rate w is equal in both gauges.

As done in Section 2.1.1, we have the relation

$$\omega_c \, \langle j'|\hat{a}' - \hat{a}'^{\dagger}|k'\rangle = \omega_{kj} \, \langle j'|\hat{a}' + \hat{a}'^{\dagger}|k'\rangle \; , \tag{2.23}$$

and the positive frequency part of the electric field becomes

$$\hat{E}'^{+} = i \sum_{j,k>j} \frac{\omega_{kj}}{\omega_c} \, \langle j'|\hat{a}' + \hat{a}'^{\dagger}|k'\rangle \, |j'\rangle\langle k'| \; . \tag{2.24}$$

Finally, in analogy to the whole discussion of this section, it is possible to define the field operators describing the qubit emission $w_a = \langle \hat{\Sigma}^{-}\hat{\Sigma}^{+} \rangle$, where

$$\hat{\Sigma}^{+} = i \sum_{j,k>j} \frac{\omega_{kj}}{\omega_{eg}} \, \langle j|\hat{\sigma}_x|k\rangle \, |j\rangle\langle k| \; . \tag{2.25}$$

---

[1]Here again we consider ω_c and A_0 as simple scaling factors, and so that does not influence the photon rate calculations.

Considering a standard cavity QED system, for example, the cavity emission rate corresponds to the photon flux escaping one of the mirrors, while the qubit emission rate corresponds to the spontaneous emission directly from the qubit, that can be collected by a detector placed orthogonally to the axis connecting the two mirrors [91, 92].

2.2 Open quantum systems in the USC regime

Let's consider a generic open quantum system, which is in interaction with an environment. The total Hamiltonian of the system is given by

$$\hat{H}_{\text{tot}} = \hat{H}_S + \hat{H}_R + \hat{\mathcal{V}}, \tag{2.26}$$

where $\hat{H}_S$ is the Hamiltonian of the system, $\hat{H}_R$ is the Hamiltonian of the environment (reservoir), and $\hat{\mathcal{V}}$ is the interaction Hamiltonian between the system and the environment. We are interested in the dynamics of the reduced density matrix of the system, which is obtained by tracing out the environment degrees of freedom $\hat{\rho}_S = \text{Tr}_R[\hat{\rho}_{\text{tot}}]$. Usually, the dynamics of the reduced density matrix is governed by the standard master equation

$$\frac{\mathrm{d}}{\mathrm{d}t}\hat{\rho}_S = \mathcal{L}_{\text{std}}\hat{\rho}_S, \tag{2.27}$$

where

$$\mathcal{L}_{\text{std}}\hat{\rho}_S = - i \left[\hat{H}_S, \hat{\rho}_S\right] + \sum_n \gamma_n n_{\text{th}}(\omega_n, T_n)\mathcal{D}\left[\hat{S}_n\right]\hat{\rho}_S \\ + \sum_n \gamma_n \left[n_{\text{th}}(\omega_n, T_n) + 1\right]\mathcal{D}\left[\hat{S}_n^\dagger\right]\hat{\rho}_S, \tag{2.28}$$

and

$$\mathcal{D}\left[\hat{S}\right]\hat{\rho} = \frac{1}{2}\left[2\hat{S}\hat{\rho}\hat{S}^\dagger - \hat{S}^\dagger\hat{S}\hat{\rho} - \hat{\rho}\hat{S}^\dagger\hat{S}\right] \tag{2.29}$$

are the standard Liouvillian and the Lindblad dissipator, respectively. $n_{\text{th}}(\omega_n, T_n) = [\exp(\hbar\omega_n/k_{\text{B}}T_n) - 1]^{-1}$ is the thermal population of

the n-th reservoir describing the number of excitations at a given temperature T_n, k_B is the Boltzmann constant, and γ_n is the dissipation rate. The operators $\hat{S}_n$ are the system operators that couple to the environment, and they are usually expressed in terms of the bare system operators, e.g., $\hat{a}$ or $\hat{\sigma}_-$. For low coupling strengths η, the standard master equation in Eq. (2.27) can be used to accurately describe many cavity QED and circuit QED experiments [93–96].

This approach is derived by doing several assumptions: i) the environment is a macroscopic system described by an infinite number of quantum harmonic oscillators, which are all in thermal equilibrium at a given temperature T. For instance, this is the case of the open radiation field that behaves as a reservoir for an atom [97, 98]; ii) the interaction between the system and the environment is weak, and that the system is initially uncorrelated with the environment; iii) the system is Markovian, i.e. that the memory time of the environment is much shorter than the characteristic time of the system dynamics [86, 97, 98]. Moreover, to derive the standard master equation in Eq. (2.27), the interaction Hamiltonian is expressed in terms of the bare system operators, e.g, $\hat{a}$ or $\hat{\sigma}_-$, and subsequently applying a RWA after having traced out the bath degrees of freedom. However, this is a valid procedure when $\hat{H}_S$ represents a single system (e.g., a cavity field or an atom) or a set of weakly interacting subsystems (e.g., a Jaynes-Cummings Hamiltonian), but it is no longer valid when the system is composed by ultrastrongly coupled subsystems. This is straightforward to understand if we remember the discussion in Section 2.1, where, for instance, we have seen that the bare fields operators $\hat{a}$ and $\hat{a}^\dagger$ does not describe anymore the process of annihilation and creation of photons, respectively.

A suggestion comes again from Section 2.1, where the expression of the field in terms of positive and negative frequencies in the eigenstate basis was given to obtain the correct photodetection rate. Indeed, a master equation specific for ultrastrongly coupled systems was derived [99]. This approach is based on the same assumptions as the standard master equation, but the interaction Hamiltonian is

expressed in terms of the eigenstates $|j\rangle$ of the system, sometimes knows as *dressed master equation*, which is

$$\frac{\mathrm{d}}{\mathrm{d}t}\hat{\rho}_S = \mathcal{L}_{\mathrm{dr}}\hat{\rho}_S , \qquad (2.30)$$

where

$$\begin{aligned}
\mathcal{L}_{\mathrm{dr}}\hat{\rho}_S = & -i\left[\hat{H}_S, \hat{\rho}_S\right] + \sum_n \sum_{j,k>j} \Gamma_{jk}^{(n)} n_{\mathrm{th}}(\omega_{kj}, T_n) \mathcal{D}\left[|k\rangle\langle j|\right] \hat{\rho}_S \\
& + \sum_n \sum_{j,k>j} \Gamma_{jk}^{(n)} \left[n_{\mathrm{th}}(\omega_{kj}, T_n) + 1\right] \mathcal{D}\left[|j\rangle\langle k|\right] \hat{\rho}_S ,
\end{aligned} \qquad (2.31)$$

and $\Gamma_{jk}^{(n)} = \gamma_n \omega_{kj} |\langle j|\hat{S}_n + \hat{S}_n^\dagger|k\rangle|^2$. First we note that the dissipation occurs through the projection operators $|j\rangle\langle k|$ in the energy eigenstates of the system, allowing a direct transition between them. Second, the thermal population $n_{\mathrm{th}}(\omega_{kj}, T_n)$ is now a function of the energy difference between the states $|j\rangle$ and $|k\rangle$, and not anymore of the bare frequencies ω_n. Third, the dissipation rates $\Gamma_{jk}^{(n)}$ are now a function of the bare system operators $\hat{S}_n$ and not anymore a constant factor.

This master equation is able to correctly describe the dissipation involving ultrastrongly coupled systems, however, it is only valid in the absence of degenerate transitions, i.e., $\omega_{jk} \neq \omega_{lm} \, \forall \, j, k, l, m$. Indeed, as in the case of the standard master equation in Eq. (2.27), a RWA was applied after having traced out the bath degrees of freedom. This is a strong limitation, when considering harmonic systems as in the weak coupling regime and in the deep strong coupling (DSC) regime (see, e.g., the correct energy levels in Fig. 1.6).

Recently, a more general approach was proposed [100], which was derived again in the basis of the eigenstates of the system, but without applying the post-trace RWA. The full derivation of this *generalized master equation* (GME) is given in Appendix A, while here we just report the final result

$$\frac{\mathrm{d}}{\mathrm{d}t}\hat{\rho}_S = \mathcal{L}_{\mathrm{gme}}\hat{\rho}_S , \qquad (2.32)$$

with

$$\frac{\mathrm{d}}{\mathrm{d}t}\hat{\rho}_S(t) = -i\left[\hat{H}_S, \hat{\rho}_S(t)\right] + \frac{1}{2}\sum_n \sum_{\substack{j,k>j \\ l,m>l}} \Gamma^{(n)}(\omega_{ml}) \Big\{$$

$$\left[\hat{S}_{lm}^{(n)\dagger}\hat{\rho}_S(t)\hat{S}_{jk}^{(n)} - \hat{S}_{jk}^{(n)}\hat{S}_{lm}^{(n)\dagger}\hat{\rho}_S(t)\right] n_{\mathrm{th}}(\omega_{ml}, T_n)$$

$$+ \left[\hat{S}_{lm}^{(n)}\hat{\rho}_S(t)\hat{S}_{jk}^{(n)\dagger} - \hat{S}_{jk}^{(n)\dagger}\hat{S}_{lm}^{(n)}\hat{\rho}_S(t)\right] \left[n_{\mathrm{th}}(\omega_{ml}, T_n) + 1\right]$$

$$+ \left[\hat{S}_{jk}^{(n)\dagger}\hat{\rho}_S(t)\hat{S}_{lm}^{(n)} - \hat{\rho}_S(t)\hat{S}_{lm}^{(n)}\hat{S}_{jk}^{(n)\dagger}\right] n_{\mathrm{th}}(\omega_{ml}, T_n)$$

$$+ \left[\hat{S}_{jk}^{(n)}\hat{\rho}_S(t)\hat{S}_{lm}^{(n)\dagger} - \hat{\rho}_S(t)\hat{S}_{lm}^{(n)\dagger}\hat{S}_{jk}^{(n)}\right] \left[n_{\mathrm{th}}(\omega_{ml}, T_n) + 1\right]\Big\} ,$$

$$(2.33)$$

where $\Gamma^{(n)}(\omega) = \tilde{\gamma}_n\omega$ is the frequency-dependent dissipation rate, specific for an ohmic bath, and $\hat{S}_{jk}^{(n)} = \langle j|\hat{S}_n|k\rangle\,|j\rangle\langle k|$ with $\hat{S}_n$ the n-th system operator the couples to the n-th bath. It is worth noting that here $\tilde{\gamma}_n$ are dimensionless parameters, because the real decay rate is $\Gamma^{(n)}(\omega)$, which is a function of the frequency ω. Thus, it is sometimes useful to define the decay rate at the specific bare frequency $\gamma_n \equiv \Gamma^{(n)}(\omega_n) = \tilde{\gamma}\omega_n$. The equation above can be rewritten as

$$\mathcal{L}_{\mathrm{gme}}\hat{\rho}_S = -i\left[\hat{H}_S, \hat{\rho}_S\right]$$

$$+ \frac{1}{2}\sum_n \left[\hat{\mathcal{S}}_{n,1}^-\hat{\rho}_S\hat{\mathcal{S}}_n^+ + \hat{\mathcal{S}}_n^-\hat{\rho}_S\hat{\mathcal{S}}_{n,1}^+ - \hat{\mathcal{S}}_n^+\hat{\mathcal{S}}_{n,1}^-\hat{\rho}_S - \hat{\rho}_S\hat{\mathcal{S}}_{n,1}^+\hat{\mathcal{S}}_n^- \right.$$

$$\left. + \hat{\mathcal{S}}_{n,2}^+\hat{\rho}_S\hat{\mathcal{S}}_n^- + \hat{\mathcal{S}}_n^+\hat{\rho}_S\hat{\mathcal{S}}_{n,2}^- - \hat{\mathcal{S}}_n^-\hat{\mathcal{S}}_{n,2}^+\hat{\rho}_S - \hat{\rho}_S\hat{\mathcal{S}}_{n,2}^-\hat{\mathcal{S}}_n^+\right] ,$$

$$(2.34)$$

and

$$\hat{\mathcal{S}}_n^+ = \sum_{j,k>j} \langle j|\hat{S}_n|k\rangle\,|j\rangle\langle k| , \tag{2.35a}$$

$$\hat{\mathcal{S}}_{n,1}^+ = \sum_{j,k>j} \Gamma^{(n)}(\omega_{kj})n_{\mathrm{th}}(\omega_{kj}, T_n)\,\langle j|\hat{S}_n|k\rangle\,|j\rangle\langle k| , \tag{2.35b}$$

$$\hat{\mathcal{S}}_{n,2}^+ = \sum_{j,k>j} \Gamma^{(n)}(\omega_{kj})\left[n_{\mathrm{th}}(\omega_{kj}, T_n) + 1\right]\langle j|\hat{S}_n|k\rangle\,|j\rangle\langle k| . \tag{2.35c}$$

This generalized master equation contains the minimal amount of approximations which can be summarized in only the Born and Markov approximations. Moreover, it is valid for any light-matter coupling strength, and it is able to describe the dissipation of ultrastrongly coupled systems even in the presence of degenerate transitions. It is easy to see that, in the limit of weak coupling, the generalized master equation reduces to the standard master equation in Eq. (2.27).

In the interaction picture, each term of Eq. (2.33), barring the last one, oscillates at frequencies $\pm(\omega_{ml} - \omega_{kj})$. When $|\omega_{ml} - \omega_{kj}|$ greatly exceeds the system's damping rates $\Gamma^{(n)}$, these terms offer minimal contributions to the master equation's integration. Therefore, $|\omega_{ml} - \omega_{kj}|$ can be considered comparable to the system linewidths.

Despite the rapid oscillations in Eq. (2.33) due to transitions with large frequency differences (absent post-trace RWA in the dressed master equation), they should not significantly contribute if $|\omega_{ml} - \omega_{kj}| > \Gamma^{(n)}$. However, they can substantially prolong computation time and induce computational instabilities, particularly evident when computing log-scaled spectra. To mitigate these issues, we employ a low-pass filter function in Eq. (2.33) to diminish the contribution of dissipator terms with high frequency differences [100]. This filter function can take any low-pass filter form, such as a step-like or sigmoid-like shape. Here, we use a gaussian shape of the form

$$\mathcal{F}_n(\omega_{ml} - \omega_{kj}) = \exp\left[-\frac{(\omega_{ml} - \omega_{kj})^2}{2\sigma_n^2}\right], \qquad (2.36)$$

where σ_n is the standard deviation of the gaussian function. Here we choose $\sigma_n = 100\Gamma^{(n)}(\omega_n)$. With this choice, the filtered generalized master equation cannot be expressed in a form like Eq. (2.34), but we need to use Eq. (2.33) with the low-pass filter. In the limit $\sigma_n \to 0$ we obtain the dressed master equation in Eq. (2.31), and in the limit $\sigma_n \to \infty$ we obtain the unfiltered generalized master equation in Eqs. (2.33) and (2.34).

2.3 Emission spectrum of an open quantum system

For stochastic stationary fields, the emission spectrum is defined as the Fourier transform of the two-time correlation function of the electric field operator [80, 86]

$$S(\omega) = \lim_{t \to \infty} \int_{-\infty}^{+\infty} d\tau \, e^{-i\omega\tau} \left\langle \hat{E}^-(t+\tau)\hat{E}^+(t) \right\rangle, \qquad (2.37)$$

which allows one to obtain information on the frequency of the emitted photons and, indirectly, on the system dynamics.

Equation (2.37) can be derived semi-analytically if we know the eigenvalues and the eigenvectors of the Liouvillian superoperator $\mathcal{L}$. Indeed, starting from the two-times correlation function in Eq. (2.37) and considering for simplicity the closed dynamics involving the total Hamiltonian between the system ed the environment expressed in Eq. (2.26), we have

$$
\begin{aligned}
\left\langle \hat{A}(t+\tau)\hat{B}(t) \right\rangle &= \mathrm{Tr}\left[e^{i\hat{H}_{\mathrm{tot}}(t+\tau)} \hat{A} e^{-i\hat{H}_{\mathrm{tot}}(t+\tau)} e^{i\hat{H}_{\mathrm{tot}}t} \hat{B} e^{-i\hat{H}_{\mathrm{tot}}t} \hat{\rho}_0 \right] \\
&= \mathrm{Tr}\left[e^{i\hat{H}_{\mathrm{tot}}\tau} \hat{A} e^{-i\hat{H}_{\mathrm{tot}}\tau} \hat{B} e^{-i\hat{H}_{\mathrm{tot}}t} \hat{\rho}_0 e^{i\hat{H}_{\mathrm{tot}}t} \right] \\
&= \mathrm{Tr}\left[e^{i\hat{H}_{\mathrm{tot}}\tau} \hat{A} e^{-i\hat{H}_{\mathrm{tot}}\tau} \hat{B} \hat{\rho}(t) \right].
\end{aligned}
$$
$$(2.38)$$

The equation written above still represents the entire dynamics of the system and the environment. We now perform the quantum regression theorem by tracing out the bath degrees of freedom [86, 97], and we can express everything in terms of the reduced density matrix of the system $\hat{\rho}_S(t) = \exp(\mathcal{L}t)\hat{\rho}_S(0)$, which is governed in terms of the Liouvillian superoperator $\mathcal{L}$. It is worth noting that the process of tracing out the bath can be safely done because the correlation function written above involves only system operators and because we are assuming that the Born-Markov approximations can be done.

When we perform the limit $t \to \infty$, the density matrix $\hat{\rho}_S(t)$ approaches the steadystate $\hat{\rho}_{S,ss}$, and the correlation function becomes

$$\left\langle \hat{A}(t + \tau)\hat{B}(t) \right\rangle_{t \to \infty} = \mathrm{Tr}\left[\hat{A}e^{-i\hat{H}_{\mathrm{tot}}\tau} \hat{B}\hat{\rho}_{ss}e^{i\hat{H}_{\mathrm{tot}}\tau} \right], \tag{2.39}$$

which, by applying the quantum regression theorem, becomes

$$\left\langle \hat{A}(t + \tau)\hat{B}(t) \right\rangle_{t \to \infty} = \left\langle \hat{A}(\tau)\hat{B}(0) \right\rangle_{ss} = \mathrm{Tr}\left[\hat{A}\; e^{\mathcal{L}\tau}\left(\hat{B}\hat{\rho}_{S,ss} \right) \right]. \tag{2.40}$$

Finally, for stationary systems, the correlation function has the property

$$\left\langle \hat{A}(\tau)\hat{B}(0) \right\rangle_{ss} = \left\langle \hat{A}(-\tau)\hat{B}(0) \right\rangle_{ss}^{*}, \tag{2.41}$$

which allows us to write the emission spectrum in Eq. (2.37) as

$$S(\omega) = 2\,\mathrm{Re}\left[\int_0^\infty \mathrm{d}\tau\, e^{-i\omega\tau} \left\langle \hat{E}^{-}(\tau)\hat{E}^{+}(0) \right\rangle_{ss} \right]. \tag{2.42}$$

The whole procedure is simple. First, we calculate the steadystate of the system, which can be derived using various iterative algorithms [101], which usually use the vectorization of the density matrix as discussed in Appendix B. Then, we initialize the system with the pseudo-state $\hat{R}(0) = \hat{E}^{+}\hat{\rho}_{ss}$, and we evolve it in time using the Liouvillian superoperator $\mathcal{L}$. Finally, we calculate the expectation value

$$\left\langle \hat{E}^{-}(\tau)\hat{E}^{+}(0) \right\rangle_{ss} = \mathrm{Tr}\left[\hat{E}^{-}\hat{R}(\tau) \right], \tag{2.43}$$

and we then use Eq. (2.42) to obtain the emission spectrum.

As we already said, the emission spectrum can be obtained analytically, if we know the eigenvalues and the eigenvectors of the Liouvillian superoperator $\mathcal{L}$. Indeed, To fully determine the dynamics of the system, one has to know all the spectrum of the Liouvillian superoperator, whose eigenmatrices and eigenvalues are defined via the relation

$$\mathcal{L}\hat{\rho}_n = \lambda_n \hat{\rho}_n. \tag{2.44}$$

Thus, we can use the eigenstates of the Liouvillian as a basis to expand any system operator $\hat{A} = \sum_n c_n \hat{\rho}_n$ [102]. Moreover, it can be proved that, for a generic Liouvillian in a Lindblad form, $\lambda_{n,R} \equiv \mathrm{Re}[\lambda_n] < 0$ [86, 97]. The physical reason is that the real part $\lambda_{n,R}$ of the eigenvalues of the Liouvillian superoperator is related to the relaxation of the system, and so it has to be negative. The imaginary part $\lambda_{n,I}$ of the eigenvalues is related to the coherences and oscillations of the system. The steadystate $\hat{\rho}_{\mathrm{ss}} = \hat{\rho}_0$ of the system is the only eigenmatrix with eigenvalue equal to zero. Indeed, the steadystate is the only state which satisfies the equation $\mathcal{L}\hat{\rho}_{\mathrm{ss}} = 0$.

Considering $\hat{R}(0)$ as the initial state, if we expand it in the eigenbasis of the Liouvillian superoperator, i.e., $\hat{R}(0) = \sum_n c_n \hat{\rho}_n$, the time evolution becomes[2]

$$\hat{R}(t) = c_0 \hat{\rho}_0 + \sum_{n>0} c_n e^{\lambda_n t} \hat{\rho}_n \,. \tag{2.45}$$

By using Eq. (2.45) in Eq. (2.43), the spectrum of the emitted field in Eq. (2.42) becomes

$$S(\omega) = 2\,\mathrm{Re}\left\{ \sum_{n>0} c_n \,\mathrm{Tr}\left[\hat{E}^-\hat{\rho}_n\right] \int_0^\infty \mathrm{d}\tau \, e^{(\lambda_n - i\omega)\tau} \right\}\,, \tag{2.46}$$

where we have not considered the contribution of the steadystate $\hat{\rho}_0$ because it produces only a delta function centered at $\omega = 0$. The integral in Eq. (2.46) can be easily calculated, since

$$\int_0^\infty \mathrm{d}\tau \, e^{p\tau} = -\frac{1}{p}\,, \quad \mathrm{Re}[p] < 0\,, \tag{2.47}$$

and the analytical expression of the emission spectrum finally becomes

$$S(\omega) = 2\sum_{n>0} \mathrm{Re}\left\{ c_n \,\mathrm{Tr}\left[\hat{E}^-\hat{\rho}_n\right] \frac{-\lambda_{n,R} - i\left(\omega - \lambda_{n,I}\right)}{\left(\omega - \lambda_{n,I}\right)^2 + \lambda_{n,R}^2} \right\}\,, \tag{2.48}$$

---

[2]In general, in the case of the decomposition of a physical density matrix, the coefficient c_0 is one. This ensures that when $t \to \infty$ the state approaches to the steadystate $\hat{\rho}_0$. But in this case $\hat{R}(0) = \hat{E}^+\hat{\rho}_0$ is not a physical density matrix, and so c_0 is not necessarily equal to one.

which, in general, is a sum of Lorentzian functions centered at the eigenfrequencies $\lambda_{n,I}$ of the Liouvillian superoperator, with a width given by the real part $\lambda_{n,R}$ of the eigenvalues.

In the density matrix vectorization framework discussed in Appendix B, any operator living in the Hilbert space becomes a vector $\hat{S} \to \vec{S}$, and the Liouvillian becomes a matrix $\overline{\overline{\mathcal{L}}}$ which is not Hermitian. Thus, the decomposition coefficients of the vectorized operator $\vec{R}(0) = (\hat{I} \otimes \hat{E}^+)\vec{\rho}_0$ in the eigenbasis of the Liouvillian are

$$c_n = \vec{\sigma}_n \cdot \vec{R}(0) = \vec{\sigma}_n \cdot \left(\hat{I} \otimes \hat{E}^+\right) \cdot \vec{\rho}_0 \,, \tag{2.49}$$

where $\vec{\sigma}_n$ is the n-th left-eigenvector of the Liouvillian $\overline{\overline{\mathcal{L}}}$, with $\vec{\sigma}_n \cdot \overline{\overline{\mathcal{L}}} = \lambda_n \vec{\sigma}_n$.

The main effort is to calculate the eigenvalues and the eigenvectors of the Liouvillian superoperator. Usually, the vectorization of the density matrix is used to express the Liouvillian in a matrix form (see Appendix B), which allows us to use standard numerical linear algebra algorithms to calculate the eigenvalues and the eigenvectors.

In the spectrum of the emitted field, the positive frequency part of the field $\hat{E}^+$ is expressed in Eq. (2.15) for the Coulomb gauge and in Eq. (2.24) for the dipole gauge (which is obviously linked to that in the Coulomb gauge by a unitary transformation $\hat{\mathcal{U}}$). Obviously, $\hat{E}^-$ is defined as the conjugate transposed of $\hat{E}^+$ in Eqs. (2.15) and (2.24), respectively.

2.4 Photon emission spectrum from incoherent pumping of the atom: from weak to deep strong coupling

In this section, we will leverage the latest advancements to present a comprehensive view of light emission from the quantum Rabi model under incoherent pumping, spanning from weak to deep strong light-matter interaction. As the light-matter coupling strength transitions

from extremely weak to deep strong coupling regimes, the QRM's spectrum, initially quasi-harmonic, evolves into a strongly anharmonic one at higher couplings. Upon reaching the deep strong limit, it reverts back to a harmonic behavior. In the weak coupling regime, ignoring the counter-rotating terms and employing the conventional quantum optics master equation usually yields precise results. However, in the USC regime, this master equation falls short in accurately depicting the emission spectra. This issue can be partially addressed by employing the master equation in the dressed basis [99] [refer to Eq. (2.30)], a methodology that incorporates the interaction between system components in deriving the dissipators. Nevertheless, this robust approach may also fail to accurately describe the QRM's emission in both weak and deep strong coupling regimes. To overcome these challenges, we examine the system's incoherent emission at any coupling strength using the generalized master equation (GME) given in Eq. (2.32). This equation is applicable for systems exhibiting harmonic, quasi-harmonic, and anharmonic spectra [2, 100, 103]. A parallel analysis has been conducted in the strong coupling regime using the JC model and the conventional quantum optics master equation, which are suitable in this regime [92].

The incoherent stimulation of the qubit is characterized by its coupling with a thermal reservoir at a specific effective temperature $\mathcal{T}_a \equiv k_{\mathrm{B}} T / \omega_{eg} \neq 0$. We have assumed a zero temperature ($\mathcal{T}_c = 0$) cavity-reservoir for all results, implying that the cavity emission is a result of its interaction with the qubit.

The eigenstates of the quantum Rabi Hamiltonian are derived through standard numerical diagonalization in a truncated, yet adequately large finite-dimensional, Hilbert space. We take into account the Hilbert space resulting from the tensor product of the qubit basis $\{|g\rangle, |e\rangle\}$, and the basis composed of the first $N+1$ photonic Fock states up to the N-photon state $|N\rangle$. The truncation number N is selected to ensure that the lowest M energy eigenvalues and corresponding eigenvectors of interest do not change significantly when N is increased. All results are obtained by solving the GME in Eq. (2.32) using the

Liouvillian $\mathcal{L}_{\mathrm{gme}}$ in Eq. (2.33) for the density matrix of the cavity-qubit in the dressed basis, including the lowest M energy levels. The truncation number M is chosen to achieve convergence. Specifically, we verify that the results (emission rates and spectra) do not change significantly when M is increased.

In the subsequent discussion, for convenience, we adopt an alternative notation for the eigenstates of the QRM, drawing parallels with the notation employed for labeling the eigenstates of the JCM in Eq. (1.82). As previously mentioned in Section 1.4.1, at zero detuning $[\Delta \equiv (\omega_c - \omega_{eg})/\omega_{eg} = 0]$, the excited eigenstates of the JC Hamiltonian can be expressed as $|n_\pm\rangle = (|n, g\rangle \pm |n-1, e\rangle)/\sqrt{2}$. The eigenstates of the QRM, beyond the strong coupling regime, do not exhibit a similar simple structure. In this context, when beneficial, we denote them by extending the aforementioned JC notation with a tilde. In this notation, $|\tilde{0}\rangle$ represents the ground state, and $|\tilde{n}_\pm\rangle$ characterizes an eigenstate of the quantum Rabi Hamiltonian. It should be noted that $|\tilde{n}_\pm\rangle$ approaches the corresponding JC state $|n_\pm\rangle$ for $\eta \ll 1$. With this notation, the energy eigenstates preserve their parity (corresponding to the parity of the integer number $\tilde{n}$) regardless of the value of η.

2.4.1 Zero atom-cavity detuning

Here we consider the case of zero atom-cavity detuning, i.e., $\Delta = 0$. To demonstrate the validity of the approach discussed up to now, which takes into account gauge-invariance and a proper modeling of the system-environment interaction, we calculate the photon emission rate w in the dipole gauge using the Hamiltonian in Eq. (2.17) and the generalized master equation in Eq. (2.32), with the system-bath interaction operators $\hat{S}_c = \hat{E}' = i(\hat{a} - \hat{a}^\dagger) - 2\eta\hat{\sigma}_x$ and $\hat{S}_a = \hat{\sigma}_x$ for the cavity and the atom, respectively. Furthermore, it is compared with different photon rates: i) w_{dr} in the dipole gauge using the dressed master equation in Eq. (2.30) and the same system-bath interaction operators $\hat{S}_c$ and $\hat{S}_a$; ii) the photon rate w_{wrong} in the dipole gauge using the wrong electric field in Eq. (2.22) as the cavity system-bath
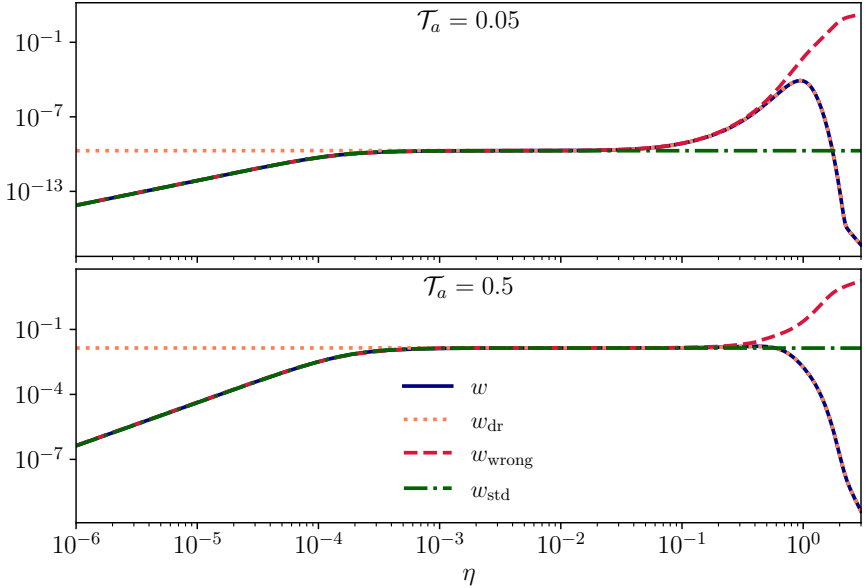
Figure 2.2: Photon emission rate as a function of the normalized coupling strength η for $\mathcal{T}_a = 0.05$ and $\mathcal{T}_a = 0.5$ in the upper and lower panel, respectively. The blue solid line represents the photon rate using the gauge-invariant approach and the GME. It is compared with the gauge invariant approach but using the dressed master equation (orange dotted line), with the wrong electric field (red dashed line), and with the Jaynes-Cummings Hamiltonian with the standard master equation (green dot-dashed line). The used parameters are $\omega_{eg} = 1$, $\omega_c = 1$, $\gamma_c = 10^{-3}\omega_{eg}$, and $\gamma_a = 10^{-4}\omega_{eg}$.

interaction operator (which is a usual mistake); iii) the photon rate w_{std} using the Jaynes-Cummings Hamiltonian in Eq. (1.81) and the standard master equation in Eq. (2.27) with the jump operators $\hat{S}_{c,\text{std}} = \hat{a}$ and $\hat{S}_{a,\text{std}} = \hat{\sigma}_-$ for the cavity and the qubit, respectively.

The blue solid line of Fig. 2.2 corresponds to the emission rate w using the gauge-invariant approach and the GME. We can distinguish four regions. The first one is from $10^{-5} < \eta \lesssim (\gamma_c + \gamma_a)/(2\omega_{eg})$ (where

$\gamma_c = 10^{-3}\omega_{eg}$ and $\gamma_a = 10^{-4}\omega_{eg}$), and it coincides with weak coupling regime, where an increasing photon emission rate is a signature of the Purcell effect [28, 29]. Indeed, by increasing the coupling strength, the thermal excitations of the atom can be more easily transferred to the cavity field, and so the photon emission rate increases. The second region is from $10^{-3} \lesssim \eta \lesssim 10^{-1}$, corresponding to the strong coupling regime, where the photon emission rate is almost constant. In this region, the coupling is strong enough to allow the total sharing of the excitations. By increasing further the coupling beyond the onset of USC ($\eta > 0.1$), a strong enhancement of the cavity emission can be observed at low temperature $\mathcal{T}_a = 5 \times 10^{-2}$. It originates from the decrease of the transition frequency $\omega_{\tilde{1}_-,\tilde{0}}$ between the lowest excited state and the ground state for increasing values of η [see Fig. 2.3]. The strong decrease of $\omega_{\tilde{1}_-,\tilde{0}}$ enables the increase of the occupancy of the state $|\tilde{1}_-\rangle$ at very low effective temperatures. Such a population growth determines an increase in the emission rate (of photons at frequency $\omega_{\tilde{1}_-,\tilde{0}}$), which can be observed in Fig. 2.2. The same behavior is not observed at a significantly higher temperature. In this case, the state $|\tilde{1}_-\rangle$ can already be populated at small values of η.

As η surpasses the DSC regime ($\eta > 1$), w experiences a swift decline. This pattern is indicative of the widely recognized light-matter decoupling phenomenon [104, 105], where light and matter essentially separate from each other. An intriguing outcome of this seemingly paradoxical phenomenon is the reversal of the Purcell effect, causing the spontaneous emission rate, typically expected to rise with the strength of light-matter coupling, to approach zero for sufficiently strong couplings. This prediction was made in the context of bosonic matter excitations interacting with a multi-mode optical resonator (generalized Hopfield model), utilizing the Coulomb gauge. The decoupling effect has recently been forecasted for any light-matter system derived from the minimal coupling substitution of electronic momentum [105]. By employing the so-called asymptotic decoupling frame, it was demonstrated that the electronic system tends towards
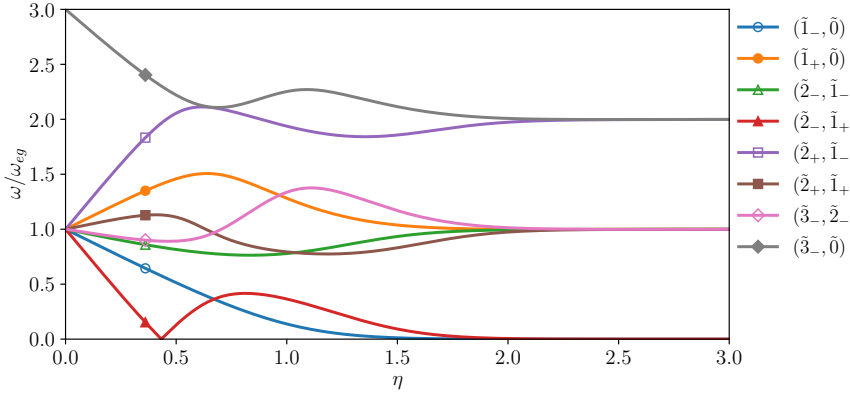
Figure 2.3: Normalized energy levels and transition energies versus η, for $\Delta = 0$. Only the parity-allowed transition energies $|\omega_k - \omega_j|/\omega_{eg}$ are shown for the lowest eigenstates of the QRM.

localization as the coupling intensifies due to an increase in effective mass. This localization effect triggers the decoupling of the light-matter system.

As can be easily seen in Fig. 2.2, the dressed master equation (orange dotted line) reproduces the same results as the generalized master equation (blue solid line), except for low coupling strengths $\eta \lesssim 10^{-3}$, where the dressed master equation shows an unphysical photon emission rate. Indeed, we have to remember that the emitted photons come from the thermal reservoir of the atom, which shares its excitation to the cavity due to the interaction. But if this interaction vanishes, the atom excitations are not able to be transferred to the cavity, with a resulting decreasing of the photon emission rate. The reason why the dressed master equation fails in this regime is due to de harmonicity of the system at these couplings, as discussed in Section 2.2.

The red dashed line shows the photon rate when using the wrong electric field in Eq. (2.22) as the cavity system-bath interaction operator
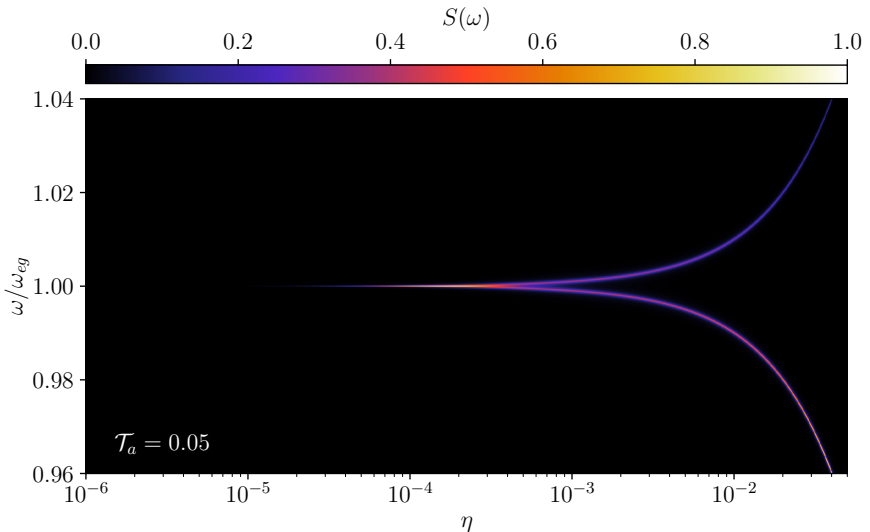
Figure 2.4: Cavity emission spectrum as a function of the normalized coupling strength η for $\mathcal{T}_a = 0.05$. This figure directly shows the Purcell effect process of the weak coupling regime and the vacuum Rabi splitting of the strong coupling regime. The used parameters are the same as in Fig. 2.2.

and also as photodetection operator. As expected, it fails at the onset of the USC ($\eta \gtrsim 10^{-1}$), showing a photon emission rate orders of magnitudes larger than the correct one. Moreover, no decoupling effect is present.

Finally, the photon rate using the Jaynes-Cummings Hamiltonian in Eq. (1.81) and the standard master equation in Eq. (2.27) with the jump operators $\hat{S}_{c,\text{std}} = \hat{a}$ and $\hat{S}_{a,\text{std}} = \hat{\sigma}_-$ for the cavity and the qubit, respectively, is shown as the green dot-dashed line. It is able to correctly reproduce the photon emission rate only in the weak and strong coupling regimes, but it fails beyond the strong coupling regime, showing a plateau instead of the decoupling effect.

The cavity emission spectrum under the incoherent weak excitation

of the qubit ($\mathcal{T}_a = 5 \times 10^{-2}$) in both weak and strong coupling regimes ($10^{-6} < \eta < 5 \times 10^{-2}$) is depicted in Figure 2.4. The spectrum is normalized with respect to its maximum value, such that it is bounded to one. The shift from the weak coupling regime (represented by a single spectral line) to the strong coupling regime (represented by split lines) is clearly noticeable. The two lines correspond to the transitions $|\tilde{1}_\pm\rangle \to |\tilde{0}\rangle$, denoted as $(\tilde{1}_-, \tilde{0})$ and $(\tilde{1}_+, \tilde{0})$ in Fig. 2.3. As η increases, the emission line brightens in the weak coupling regime. In the strong coupling regime, an asymmetry in the relative intensity of the two lines becomes apparent when they are sufficiently split. This is a direct result of the higher population of the lower-energy excited state $|\tilde{1}_-\rangle$ compared to the higher-energy state $|\tilde{1}_+\rangle$ at $\mathcal{T}_a = 5 \times 10^{-2}$. This behavior cannot be replicated using the standard quantum-optics master equation where reservoir occupations are calculated at bare transition frequencies (in the absence of light-matter interaction), see, e.g., Section 2.4.3.

The logarithmic cavity emission spectra as a function of the normalized coupling strength η is depicted in Figure 2.5. These spectra, calculated at four distinct temperatures, illustrate the transition of the emission spectra from strong to DSC regimes. Each of the four spectra is normalized to the maximum value of the spectrum at $\mathcal{T}_a = 0.5$. Unlike light-matter systems governed by a harmonic Hamiltonian (refer to Ref. [106] for instance), the spectra in this highly anharmonic scenario become significantly complex when the system is sufficiently excited. At an extremely low temperature ($\mathcal{T}_a = 5 \times 10^{-2}$), only a few spectral lines are visible, with the two most prominent ones corresponding to the transitions $(\tilde{1}_\pm, \tilde{0})$ [refer to Fig. 2.3].

It should be noted that due to parity symmetry [19, 30], the transition $(\tilde{1}_+, \tilde{1}_-)$ is prohibited. As anticipated, at such a low temperature, the emission from the lowest excited level at frequency $\omega_{\tilde{1}_-,\tilde{0}}$ is dominant. As η increases (up to approximately $\eta \simeq 1$), the intensity of the line $\omega_{\tilde{1}_-,\tilde{0}}$ rises due to a decrease in the ratio $\omega_{\tilde{1}_-,\tilde{0}}/(\omega_{eg}\mathcal{T}_a)$, leading to an increase in the excited state population $\rho_{\tilde{1}_-,\tilde{1}_-}$. However, for $\eta \gtrsim 1$, this population begins to decrease as a
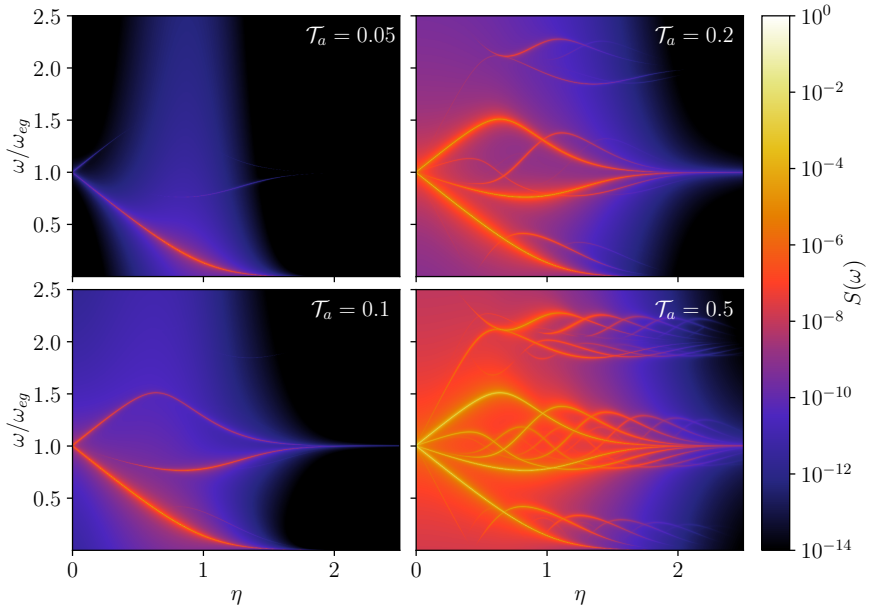
Figure 2.5: Cavity emission spectrum in log scale as a function of the normalized coupling strength η between the strong and the deep strong coupling regimes, for $\mathcal{T}_a = 0.05, 0.1, 0.2, 0.5$. The spectra are normalized with respect to the maximum value of the spectrum at $\mathcal{T}_a = 0.5$, at higher temperatures it is possible to see several lines which are avoided in the JC model. The used parameters are the same as in Fig. 2.2.

result of decoupling between light-matter and qubit-reservoir. This trend aligns with the corresponding emission rate depicted in Fig. 2.2.

When further increasing the temperature ($\mathcal{T}_a = 0.1$ and $\mathcal{T}_a = 0.2$), additional energy levels get populated and additional spectral lines appear. Most of these correspond to transitions indicated in Fig. 2.3. In the low-frequency range at $\mathcal{T}_a = 0.2$, in addition to the transition $(\tilde{1}_-, \tilde{0})$, a new spectral line at $|\omega_{\tilde{2}_-, \tilde{1}_-}|$ appears. The crossing between the energy levels $\omega_{\tilde{2}_-}$ and $\omega_{\tilde{1}_-}$, occurring at $\eta \sim \bar{\eta} = 0.43$, manifests as a low spectral line approaching $\omega = 0$ as $\eta \to \bar{\eta}$, and then (after the
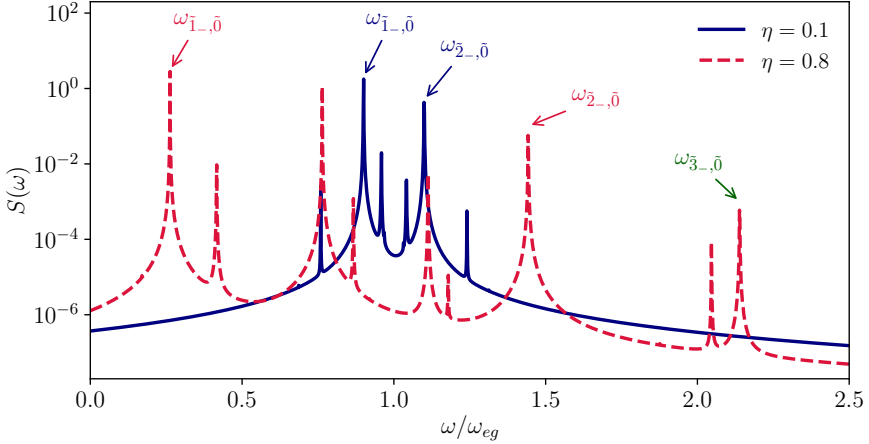
Figure 2.6: Cavity emission spectrum in log scale as a function of the normalized frequency ω/ω_{eg} for $\mathcal{T}_a = 0.2$ with $\eta = 0.1$ (blue solid) and $\eta = 0.8$ (red dashed). Each spectrum can be obtained by cutting the corresponding spectrum in Fig. 2.5 at the corresponding value of η. The spectrum at $\eta = 0.8$ presents also the transition $(\tilde{3}_-, \tilde{0})$ which is not allowed in the Jaynes-Cummings model. The used parameters are the same as in Fig. 2.5.

crossing), moving away from $\omega = 0$. At higher frequencies ($\omega/\omega_{eg} \sim 1$), other two crossing spectral lines become clearly visible.

As shown in Fig. 2.3, they correspond to the transitions $(\tilde{2}_+, \tilde{1}_+)$ and $(\tilde{3}_-, \tilde{2}_-)$. Still at higher frequencies, other two lines are observable for $\eta \gtrsim 0.4$: they correspond to the transitions $(\tilde{2}_+, \tilde{1}_-)$ and $(\tilde{3}_-, \tilde{0})$. In the latter, the involved states differ by a number of excitations $\Delta\tilde{n} = 3$ and it is a forbidden transition in the JC model (See, e.g., Section 2.4.3). This transition is enabled by the presence of the counter-rotating terms in the QRM of Eq. (2.17) and represents a clear example of USC physics [30, 31], beyond the JCM. The spectra obtained at $\mathcal{T}_a = 0.5$ display still richer structures with the appearance of additional lines originated by higher energy levels that get populated at this effective temperature.
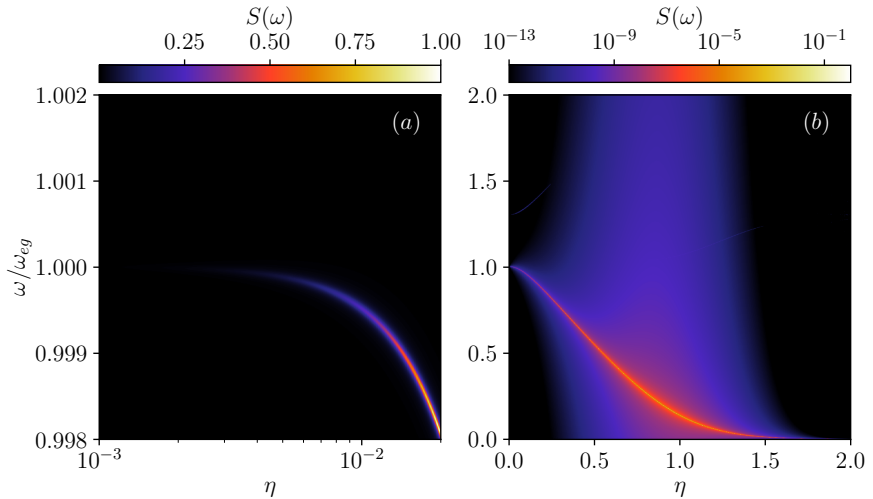
Figure 2.7: Cavity emission spectrum as a function of the normalized coupling strength η for $\mathcal{T}_a = 0.05$ and $\Delta = 0.3$. (a) in the weak and strong coupling regime; (b) in the USC and DSC regime. The main difference with respect to Fig. 2.4 is the presence of only one peak related to the qubit-like transition $\left|\tilde{1}_-\right\rangle \to \left|\tilde{0}\right\rangle$. The used parameters are the same as in Fig. 2.2.

Figure 2.6 shows the cavity emission spectrum for two different values of the coupling strength $\eta = 0.1$ and $\eta = 0.8$ at $\mathcal{T}_a = 0.2$. Each spectrum can be obtained by cutting the corresponding spectrum in Fig. 2.5 at the corresponding value of η. Moreover, the spectrum at $\eta = 0.8$ presents also the transition $(\tilde{3}_-, \tilde{0})$ which is not allowed in the Jaynes-Cummings model. The presence of this transition is a clear signature of the USC physics, which is not present in the JCM.

2.4.2 Positive atom-cavity detuning

Here we consider the case of positive detuning $\Delta = 0.3$, which implies $\omega_c/\omega_{eg} = 1.3$. This is an interesting case because we can distinguish the properties of the resonance peaks due to the detuning. As expected,
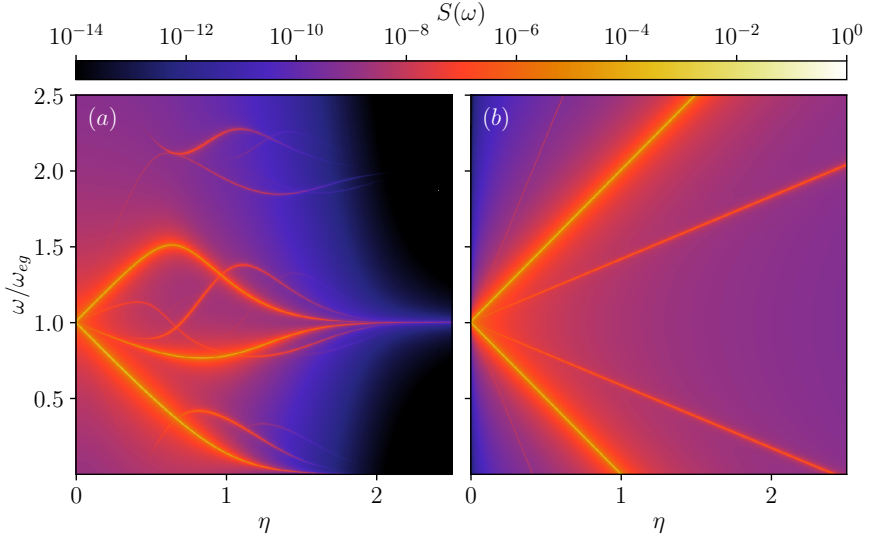
Figure 2.8: Comparison of the cavity emission spectrum as a function of the normalized coupling strength η for $\mathcal{T}_a = 0.2$ between: (a) the gauge-invariant approach with the use of the generalized master equation; (b) the Jaynes-Cummings model with the standard master equation. Apart from the fact that the resonances become very different beyond $\eta \gtrsim 0.2$ because of the different Hamiltonians in use, the JC model is not able to reproduce the peak at $\omega \simeq 2$, corresponding to the transition $(\tilde{3}_-, \tilde{0})$, which is a clear signature of the USC physics. The used parameters are the same as in Fig. 2.2.

the large detuning significantly reduces the energy transfer from the qubit to the cavity for $\eta \ll \Delta$.

As can be seen from Fig. 2.7, the cavity starts to emit photons at both the cavity and qubit transition frequency for $\eta \gtrsim 10^{-2}$. Surprisingly, the cavity emits with more intensity at the qubit frequency ω_{eg}, because in this coupling regime $\omega_{\tilde{1}_-, \tilde{0}} \simeq \omega_{eg}$ and because the thermal population $n_{\text{th}}(\omega_{kj}, T)$ is larger at ω_{eg} rather then ω_c. Compared to Fig. 2.4 (where $\Delta = 0$), this resonance, which is relative to the transition $(\tilde{1}_-, \tilde{0})$, appears at a higher coupling strength, due to
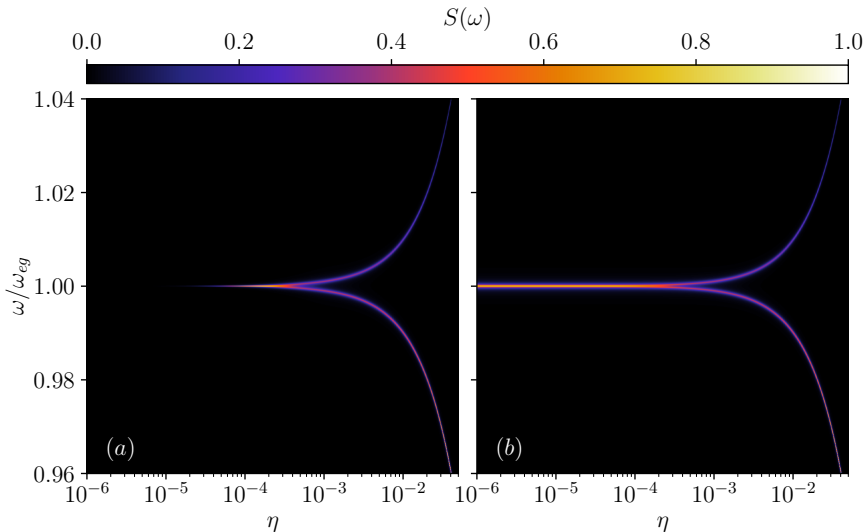
Figure 2.9: Comparison of the cavity emission spectrum as a function of the normalized coupling strength η for $\mathcal{T}_a = 0.05$ between: (a) the gauge-invariant approach with the use of the generalized master equation; (b) the gauge-invariant approach with the use of the dressed master equation. It is clear that for low coupling strengths the dressed master equation fails, because the system becomes harmonic. The used parameters are the same as in Fig. 2.2.

the detuning.

2.4.3 Comparison with other models

Now we compare the results obtained with the gauge-invariant approach and the GME with the ones obtained with the Jaynes-Cummings model and the standard master equation.

In Fig. 2.8 we compare the emission spectrum of the cavity as a function of the dimensionless coupling strength η using the gauge-invariant method with the generalized master equation (panel a) and the Jaynes-Cummings model with the standard master equation (panel

b). The resonances diverge significantly for $\eta \gtrsim 0.2$ due to the distinct Hamiltonians employed, but, more interestingly, the JC model fails to reproduce the peak at $\omega \approx 2$, which corresponds to the transition $(\tilde{3}_-, \tilde{0})$ and is a clear indicator of the USC regime. We used the same parameters as in Fig. 2.2 with $\mathcal{T}_a = 0.2$.

In Fig. 2.9, we compare the emission spectrum of the cavity as a function of the dimensionless coupling strength η using the gauge-invariant method with the generalized master equation (panel a) and the gauge-invariant method with the dressed master equation (panel b). It is evident that the dressed master equation breaks down for low coupling strengths, because the system becomes harmonic. We used the same parameters as in Fig. 2.2 with $\mathcal{T}_a = 0.05$.

CHAPTER 3

Spontaneous scattering of Raman photons without vibrational degrees of freedom

In the previous section we investigated the photon emission under a thermal pumping of the atom. The purpose of that study was to analyze the properties of the emitted light, which comes only from the interaction with the atom. The incoherent (thermal) pumping is relatively simple to model, because we are often dealing with time-independent models.

In this section, however, we study the properties of USC systems under coherent pumping (e.g., a laser), and we demonstrate that in cavity-QED systems, spontaneous Raman scattering of incoming radiation can be detected without the need for external amplification or linkage to any vibrational freedom. As the cavity-QED system nears the ultrastrong coupling domain, Raman scattering events manifest as resonances in the emission spectrum, becoming distinctly noticeable. We offer a quantum mechanical portrayal of this phenomenon, establishing that the ultrastrong coupling between light and matter

is an essential prerequisite for detecting Raman scattering. This phenomenon, coupled with its pronounced sensitivity to the parameters of the system, paves the way for novel methods of characterizing cavity QED configurations and generating quantum light states.

The Raman effect describes the inelastic scattering of radiation by matter, in which scattered photons are produced with a frequency which is either lower (Stokes photons) or larger (anti-Stokes photons) than the frequency of the incident field [107–109]. Within the realm of quantum optics and cavity quantum electrodynamics (cQED), this scattering is typically regulated and stimulated through a secondary resonant drive [110–119] or a cavity [120–124]. This forms the foundation for numerous pivotal coherent control techniques such as coherent population trapping [110, 111], electromagnetic induced transparency [113, 114], or stimulated Raman adiabatic passage [116–119].

However, the conventional method to observe *spontaneous* Raman scattering of photons without any external stimulation is when the incident light interacts with phonons in a material [107–109]. This interaction reveals the molecular vibrational modes of the sample, making this effect a useful spectroscopic tool for material characterization [125–130].

The Raman processes are enhanced by plasmons in surface-enhanced Raman spectroscopy [131–133], allowing single-molecule sensitivity [131, 132], and reaching regimes where the quantum nature of the vibrational and electromagnetic modes is important [134–136]. As a result, several recent theoretical works have developed fully quantum mechanical descriptions of Raman scattering [137–141], leading to the field of molecular optomechanics, where the interaction between phonons and plasmonic cavity phonons is described by an optomechanical Hamiltonian [142, 143].

In this section, we show the possibility of observing spontaneous Raman scattering in cQED systems that, unlike molecular optomechanics, have no vibrational degrees of freedom. A key feature of the quantum description of Raman scattering is that the underlying

process does not conserve the total number of particles: for example, in a Stokes process, a single laser photon of a given energy becomes a single photon with lower energy plus a vibrational excitation—a phonon. The underlying Hamiltonian must therefore not conserve the total number of excitations, which happens in optomechanical interaction Hamiltonians of the form $\hat{V}_{OM} = g_{OM}\hat{a}^\dagger\hat{a}(\hat{b} + \hat{b}^\dagger)$ that appear in molecular optomechanics (with $\hat{a}$ and $\hat{b}$ annihilation operators of photon and phonon modes, respectively).

Now, instead of an optomechanical system, let us consider the case of a single mode cavity field interacting with a dipole, as depicted in Fig. 3.1(a), which we already know that it is modeled by the quantum Rabi Hamiltonian. We will demonstrate that the presence of the counter rotating terms is crucial for the observation of Raman scattering. Indeed, in the absence of these terms (Jaynes-Cummings model), the Hamiltonian conserves the total number of excitations (see, e.g., Section 1.4.1), and therefore the Raman scattering is forbidden. Similarly to the optomechanical case, the full QRM that describes the dynamics in the USC does not conserve the total number of excitations. We present that the observation of spontaneous Raman scattering of photons from an incident field is an additional distinctive process of the USC regime [4]. Specifically, we provide clear evidence of these processes in the emission spectra of a coherently-driven cQED system in the USC regime [2, 103]. This finding positions USC-cQED as a unique context where Raman Stokes and anti-Stokes photons are spontaneously generated without the involvement of any vibrational degree of freedom. In addition to precise numerical calculations that demonstrate the effect, we reinforce these results with forecasts from a comprehensive quantum depiction of the Raman scattering process.

3.1 Theoretical model

The quantum Rabi Hamiltonian describes the interaction of a single mode cavity field with a two-level atom. In the presence of a coherent

drive, the Hamiltonian becomes time-dependent, and the gauge-invariant approach to describe emission spectrum might be slightly different [103]. Here we will resort to the sensor method developed in Ref. [144], adding an ancillary sensor two-level atom of resonance frequency ω_s, which is weakly coupled to the cavity to not perturb the system. This approach has been shown to produce equivalent results to the quantum regression theorem in the USC limit [103]. In this way, the total Hamiltonian in the dipole gauge, without the external coherent drive, is given by

$$
\begin{aligned}
\hat{\mathcal{H}} = {} & \omega_c \hat{a}^\dagger \hat{a} + \frac{\omega_{eg}}{2}\hat{\sigma}_z + \frac{\omega_s}{2}\hat{\sigma}_z^{(s)} - i\eta\omega_c \left(\hat{a} - \hat{a}^\dagger\right)\hat{\sigma}_p \\
& - \eta_s\omega_c \left[i\left(\hat{a} - \hat{a}^\dagger\right) - 2\eta\hat{\sigma}_p\right]\hat{\sigma}_x^{(s)},
\end{aligned}
\tag{3.1}
$$

where $\hat{\sigma}_i^{(s)}$ are the Pauli operators of the sensor atom, η_s is the coupling strength between the sensor atom and the cavity, and $\hat{\sigma}_p = \cos(\theta)\hat{\sigma}_x + \sin(\theta)\hat{\sigma}_z$ is the polarization operator of the atom, which includes the possibility of a permanent dipole moment, parametrized by θ. Finite values of θ break the parity symmetry of the quantum Rabi Hamiltonian [19, 30], which means that the Hamiltonian non longer commutes with the parity operator $\hat{\Pi} = \exp[i\pi(\hat{a}^\dagger\hat{a} + \hat{\sigma}_+\hat{\sigma}_-)]$. Taking as an example the double-well potential examined in Section 1.1.2, this behavior of the atom can be obtained by considering an asymmetric double-well potential $(V(\hat{x}) \neq V(-\hat{x}))$, while in superconducting architectures it can be obtained with an external magnetic field in a flux qubit [33, 55]. The Hamiltonian in Eq. (3.1) is obtained from a gauge-invariant approach, taking into account two atoms instead of one [145].

The coherent drive is modeled through the term

$$
\hat{\mathcal{H}}_{\mathrm{drive}}(t) = \Omega \left[i\left(\hat{a} - \hat{a}^\dagger\right) - 2\eta\hat{\sigma}_p\right]\cos(\omega_{\mathrm{L}}t),
\tag{3.2}
$$

where Ω is the laser amplitude and ω_{L} is the laser frequency. It is worth reminding that it describes a coherent electric field in the dipole gauge, since $\hat{E} = i(\hat{a} - \hat{a}^\dagger) - 2\eta\hat{\sigma}_p$. Moreover, such as any Raman
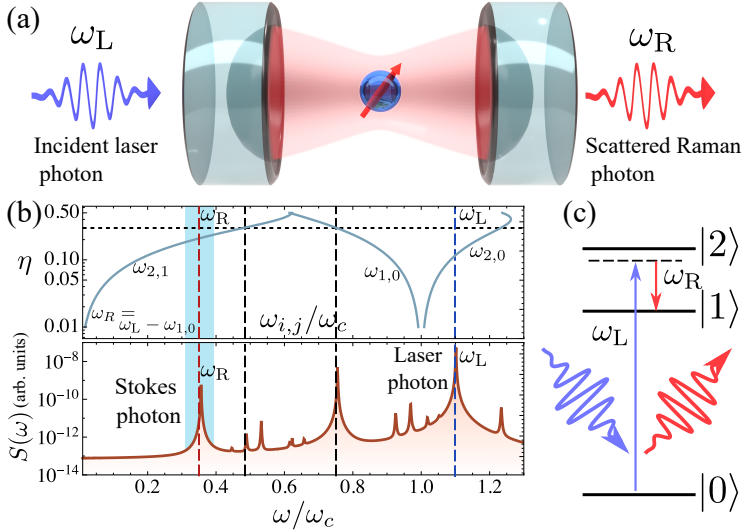
Figure 3.1: Illustration of the Raman scattering process. (a) Scheme of the cavity QED system examined in this study: a quantum emitter interacts with a single cavity mode in the ultrastrong-coupling regime and spontaneously emits a Raman photon from an incident excitation field. (b) Top: Transition energies between the first two excited eigenstates of the light-matter system and the ground state, as a function of the normalized coupling parameter η. Bottom: Emission spectrum for $\omega_c = \omega_{eg} = 1$, $\eta = 0.3$, $\omega_L = 1.1\omega_c$, $\gamma_c = \gamma_a = 10^{-3}\omega_c$ and $\gamma_s = 10^{-3}\omega_s$. The red line denotes the frequency at which Stokes photons are emitted. (c) The incident photon with frequency ω_L is scattered by the atom, resulting in a photon with frequency ω_R.

process, we are dealing with an open quantum system. Therefore, we use the generalized master equation in Eq. (2.33) with the following jump operators: $\hat{S}_c = i(\hat{a} - \hat{a}^\dagger) - 2\eta\hat{\sigma}_p$, $\hat{S}_a = \hat{\sigma}_p$, and $\hat{S}_s = \hat{\sigma}_x^{(s)}$ for the cavity, the atom, and the sensor, respectively.

Since counter-rotating terms in Eq. (3.2) cannot be straightforwardly eliminated in the USC regime, the dynamics will yield a time-dependent density matrix, even at long times. Thus, the density

matrix at long times will oscillate around an average steady state $\hat{\rho}(t) = \hat{\rho}_{ss} + \delta\hat{\rho}(t)$. However, here we consider $\Omega \ll \eta\omega_c$, which means that we can neglect the last term $\delta\hat{\rho}(t)$ and consider only the time-averaged steady state $\hat{\rho}_{ss}$. The question now is how to get $\hat{\rho}_{ss}$ since we are dealing with a time-dependent problem. The direct solution is to integrate the generalized master equation at long times and then average the density matrix over the one time period $T_L = 2\pi/\omega_L$. However, this approach is computationally expensive, since we have to integrate the time-dependent master equation for a long time. A more efficient approach is to use the Floquet theory to expand the density matrix in Fourier components, imposing that $\hat{\rho}(t) = \hat{\rho}(t + T_L)$ when $t \to \infty$. Here we use an iterative algorithm to obtain $\hat{\rho}_{ss}$ without the need to integrate the master equation for a long time. The full derivation is explained in Appendix C, where a matrix continued fraction recursion is used [146–148]. Here we limit ourselves to show the final result.

First, in the Liouvillian space, we can divide the driving term arising from Eq. (3.2) into two parts $\mathcal{L}_{\mp 1}$, with positive and negative frequency, respectively. If the periodicity of the density matrix holds, we can expand it in Fourier components as

$$\hat{\rho}(t) = \sum_{n=-\infty}^{+\infty} \hat{\rho}_n e^{in\omega_L t}, \tag{3.3}$$

and the time-averaged steady state density matrix $\hat{\rho}_{ss}$ can be found as the nullspace of the superoperator

$$\mathcal{L}_{\text{eff}} = \mathcal{L}_0 + \mathcal{L}_1 \mathcal{T}_{-1} + \mathcal{L}_{-1} \mathcal{S}_1, \tag{3.4}$$

where

$$\mathcal{S}_n = -\left[(\mathcal{L}_0 - in\omega_L) + \mathcal{L}_{-1}\mathcal{S}_{n+1} \right]^{-1} \mathcal{L}_1 \tag{3.5a}$$

$$\mathcal{T}_n = -\left[(\mathcal{L}_0 - in\omega_L) + \mathcal{L}_1\mathcal{T}_{n-1} \right]^{-1} \mathcal{L}_{-1}, \tag{3.5b}$$

and choosing an $n_{\max}$ such that $\mathcal{S}_{n_{\max}} = 0$ and $\mathcal{T}_{-n_{\max}} = 0$, meaning that the $n_{\max}$-th Fourier component of the density matrix is negligible.

We can now assume that the the cavity emission spectrum is proportional to the stationary emission rate of the qubit sensor

$$S(\omega_s) \propto \mathrm{Tr}\left[\hat{\Sigma}_s^- \hat{\Sigma}_s^+ \hat{\rho}_{ss}\right] ,$$ (3.6)

with

$$\hat{\Sigma}_s^+ = \sum_{j,k>j} \frac{\omega_{kj}}{\omega_s} \langle j|\hat{\sigma}_x^{(s)}|k\rangle |j\rangle\langle k| ,$$ (3.7)

as discussed in Section 2.1.

3.2 The Raman scattering process in cavity QED

Figure 3.1(b) depicts an example of the emission spectrum. Here and in the following we fix, unless stated otherwise, $\omega_{eg} = \omega_c$, $\theta = \pi/6$, $\eta = 0.3$, $\eta_s = 10^{-5}$, $\Omega = 5 \times 10^{-3}\omega_c$, $\gamma_c = \gamma_a = 10^{-3}\omega_c$, and $\omega_L = 1.1\omega_c$. Upon initial observation, a resonance peak at the laser frequency is noticeable, along with additional peaks corresponding to transition energies between the light-matter eigenstates, as shown in the top panel of Fig. 3.1(b). Another peak can be seen, which is associated with the spontaneous scattering of a Stokes photon. The Raman process leading to this peak is illustrated in Fig. 3.1(c). Through a second-order process, an input laser photon with frequency ω_L transforms into a Raman photon with lower energy ω_R and a light-matter excitation of energy ω_1. Given that energy must be conserved, the Stokes photon's energy is expected to be $\omega_R = \omega_L - \omega_1$, indicating a linear dependence on the laser excitation.

In order to understand the origin of Raman peaks and their reliance on system parameters like η or θ, we formulate a comprehensive quantum representation of the Raman scattering process. We assume that the cavity is linked to a wide quasi-continuum of modes with $\hat{H}_b = \sum_q \omega_q \hat{b}_q^\dagger \hat{b}_q$, which encompasses the incident radiation field and the dispersed Raman photons. The entire system Hamiltonian is

3. Spontaneous scattering of Raman photons without vibrational degrees of freedom

$\hat{H}_{\text{total}} = \hat{H}_R + \hat{H}_b + \hat{V}_b$, where $\hat{H}_R$ is the quantum Rabi Hamiltonian ($\hat{\mathcal{H}}$ above, excluding the sensor and drive terms) and

$$\hat{V}_b = \sum_q g_q (\hat{b}_q + \hat{b}_q^\dagger)[i(\hat{a} - \hat{a}^\dagger) - 2\eta\hat{\sigma}_p] \,. \tag{3.8}$$

Subsequently, we treat $\hat{H}_R + \hat{H}_b$ as the undisturbed, raw Hamiltonian, and we represent $\hat{H}_R$ in diagonal form as $\hat{H}_R = \sum_j \omega_j |j\rangle\langle j|$. The Raman scattering process can be portrayed by second-order perturbation theory under the constant perturbation $\hat{V}_b$. We consider an initial state $|I_i\rangle = |i, n_L, n_R\rangle$, where the first entry labels the eigenstates of $\hat{H}_R$, n_L labels the photon number in the input mode—the laser drive—with frequency ω_L, and n_R denotes the photon number in the output mode of frequency ω_R, where Raman photons are being emitted. We are considering here only the two modes involved in the scattering process; all other modes of the quasi-continuum are assumed to be in zero-photon states throughout the process. The energy of the initial state is $\omega_{I,i} = \omega_i + \omega_L n_L + \omega_R n_R$. Then, we consider a final state $|F_f\rangle = |f, n_L - 1, n_R + 1\rangle$, with energy $\omega_{F,f} = \omega_f + \omega_L(n_L - 1) + \omega_R(n_R + 1)$. Energy conservation implies $\omega_{F,f} = \omega_{I,i}$, and therefore, for a specific choice of initial and final states i and f, the energy of the corresponding Raman photons is

$$\omega_R = \omega_R^{(f,i)} \equiv \omega_L - (\omega_f - \omega_i). \tag{3.9}$$

$|F_f\rangle$ is connected to the initial state $|I_i\rangle$ by a second-order process involving an intermediate virtual state. It is possible to identify two kinds of intermediate states, $|T_1\rangle$ and $|T_2\rangle$, describing respectively the process (i) where a photon is first absorbed from the input state: $|T_1\rangle = |j, n_L - 1, n_R\rangle$, with energy $\omega_{T_1} = \omega_j + \omega_L(n_L - 1) + \omega_R n_R$; and the process (ii) where a photon is first emitted into the output mode: $|T_2\rangle = |j, n_L, n_R + 1\rangle$, with energy $\omega_{T_2} = \omega_j + \omega_L n_L + \omega_R(n_R + 1)$.

The rate of the process $|I_i\rangle \to |F_f\rangle$ given by the Fermi golden rule, for a given ω_L, i and f, is

$$W_{f,i}(\omega_L, \omega_R) = 2\pi g_R^2 g_L^2 n_L(n_R + 1)|M_{f,i}|^2 \delta(\omega_R - \omega_R^{(f,i)}) \,, \tag{3.10}$$

where $\omega_{f,i} = \omega_f - \omega_i$ and

$$M_{f,i}(\omega_L, \omega_R) = \sum_j \left(\frac{X_{f,j} X_{j,i}}{\omega_{T_1} - \omega_{I_i}} + \frac{X_{f,j} X_{j,i}}{\omega_{T_2} - \omega_{I_i}} \right), \qquad (3.11)$$

with $X_{f,j} \equiv \langle f | i(\hat{a} - \hat{a}^\dagger) - 2\eta\hat{\sigma}_p | j \rangle$. Notice that $\omega_{T_1} - \omega_{I,i} = \omega_{j,i} - \omega_L$, and $\omega_{T_2} - \omega_{I,i} = \omega_{j,i} + \omega_R^{(f,i)}$. The total scattering rate for the process is obtained by summing over all possible initial and final states, which will be constrained by the energy-conservation condition in (3.10), giving

$$W(\omega_L, \omega_R) = \sum_{f,i} W_{f,i}(\omega_L, \omega_R) \rho_i^{ss}(1 - \rho_f^{ss}), \qquad (3.12)$$

where ρ_k^{ss} is the steady-state occupation probability of the eigenstate $|k\rangle$ of $\hat{H}_R$. For a system at very low temperatures and low driving which is mostly in the ground state, so that $\rho_0^{ss} \approx 1$, we obtain $W(\omega_L, \omega_R) = \sum_f W_{f,0}(\omega_L, \omega_R)$. Therefore, if Raman spectroscopy is performed by probing cQED systems that are close to the ground state, only the family of Raman processes that start from $|0\rangle$ are expected to be observed.

The above-mentioned quantum scattering process is characterized by resonances in the emission spectrum, which are centered at the frequencies $\omega_R^{(f,i)}$. These resonances have a characteristic feature that distinguishes them from peaks arising from standard radiative transitions: their central frequency $\omega_R^{(f,i)}$ depends linearly on the laser frequency ω_L. This linear relationship results in resonance peaks that form straight lines in the excitation-emission spectrum, which is the emission spectra for varying driving frequencies. This characteristic serves as definitive evidence that these peaks are a result of the inelastic, spontaneous scattering of laser photons via the quantum process described above. Numerical simulations of the excitation-emission spectra for a cavity-QED system are depicted in Fig. 3.2 for two distinct temperatures $\mathcal{T} \equiv k_B T / \omega_c$ of both the cavity and the atom, with $\mathcal{T} = 0$ for the panel (a) and $\mathcal{T} = 0.15$ for the panel (b). The most prominent Raman peaks are labeled in Fig. 3.3(a). At
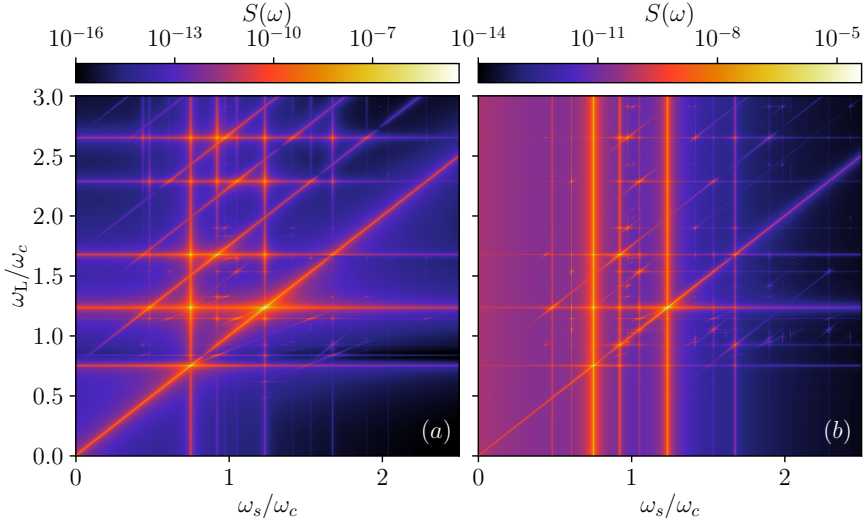
Figure 3.2: Emission spectra of a cQED system in the USC regime, where several Raman processes are clearly visible. (a) at $\mathcal{T} = 0$, where the Stokes are predominantly visible, with the hyper-Raman processes also visible; (b) at $\mathcal{T} = 0.15$, where the anti-Stokes processes becomes more visible. The used parameters are the same as in Fig. 3.1(b).

lower temperatures, the most noticeable peaks are Stokes processes that originate from the ground state of the light-matter system and terminate at an excited state $|f\rangle$ (these Stokes processes are denoted as $\omega_S^{(f0)}$). As predicted by Eq. (3.12), Stokes processes that initiate from an excited state are barely visible or not visible at all at lower temperatures; in Fig. 3.3(a), we emphasize the process $\omega_S^{(21)}$—which starts in $|1\rangle$ and ends in $|2\rangle$—as it can be discerned in certain regions of the displayed spectra. Similarly, the emission of anti-Stokes photons with frequencies exceeding the drive frequency is only clearly observable at non-zero temperatures: these processes necessitate that the energy of the final state of the cQED system is less than that of the initial one, implying that the initial state must be an excited state with
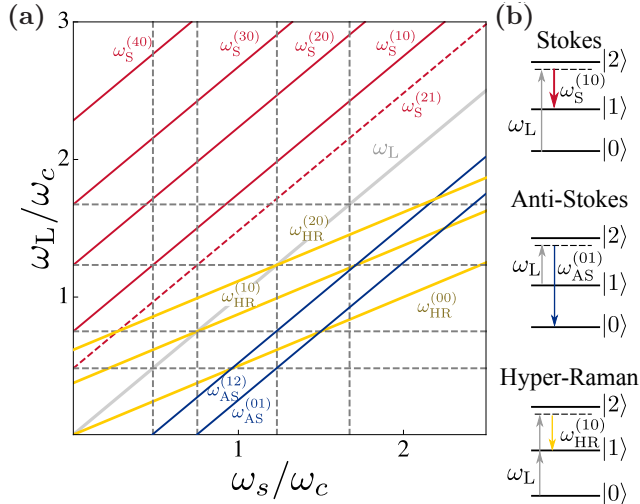
Figure 3.3: (a) Identification of some processes visible in Fig. 3.2(a,b), which include Stokes processes starting from $|0\rangle$ (solid red), Stokes process starting from $|1\rangle$ (dashed red), anti-Stokes (solid blue), and hyper-Raman (solid yellow). (b) Schematic representation of the Raman processes involved in this setup: Stokes, anti-Stokes, and hyper-Raman.

a significant stationary occupation probability. These simulations also reveal that higher-order, hyper-Raman processes can be faintly detected in the excitation emission spectra. These processes scatter two incident laser photons into a Raman photon, and thus energy conservation dictates that the frequency of the hyper-Raman photons must be $\omega_R^{(fi)} = 2\omega_L - (\omega_f - \omega_i)$. Consequently, these processes can be identified in the excitation-emission spectra as straight lines with double the slope of standard Raman processes.

3.3 Comparison with perturbation theory

The characteristics discussed above become more pronounced when one enters the ultrastrong coupling regime, where $\eta \gtrsim 0.1$, leading to significant values for the matrix elements $X_{k,j}$ in Eq. (3.10). In fact, Fig. 3.4(a) presents the computation of the scattering rate W as a function of η using Eq. (3.12) for the Stokes process $|0\rangle \to |1\rangle$, which is most noticeable in a system near the ground state, in comparison to the intensity of the corresponding Raman peak computed in the excitation emission spectra. By selecting the scaling factors in Eq. (3.10) as: $g_L^2 n_L = (\Omega/2)^2$, $n_R \approx 0$, $g_R = \eta_s \omega_c$, and converting the delta function into a Lorentzian shape, which accounts for detector losses $\delta(0) \approx 1/(\pi \gamma_s^2)$, we achieve a satisfactory match with the emission spectrum derived from Eq. (3.6).

Apart from the strong correlation between both results, which validates our explanation of the fundamental quantum process, we emphasize the exponential growth of peak intensity with η. Furthermore, the discrepancy at low η values in Fig. 3.4(a) is not indicative of a breakdown in perturbation theory, but rather arises from numerical simulation tolerances and a background signal originating from other system resonance tails. Far below the USC regime, small scattering rates make it extremely difficult to observe Raman processes in cavity QED systems, as demonstrated in Fig. 3.4(c), where it is nearly impossible to detect the first Stokes peak for $\eta = 0.01$.

It is instructive to explore potential Raman processes in a cQED system with $\eta \ll 1$, which can be accurately described by a Jaynes-Cummings Hamiltonian. The eigenstates of this system form doublets $|j_\pm\rangle$ that also serve as eigenstates of total excitation number $\hat{N} = \hat{a}^\dagger \hat{a} + \hat{\sigma}_+ \hat{\sigma}_-$, i.e., $\hat{N} |j_\pm\rangle = j |j_\pm\rangle$. This implies that only those Raman processes conserving total excitation number are permitted, i.e., those whose initial and final states belong to the same doublet. Since processes initiating and terminating in the ground state result in $\omega_R = \omega_L$ and hence do not yield energy-shifted photons, it is not possible to observe key Raman processes involving the ground state
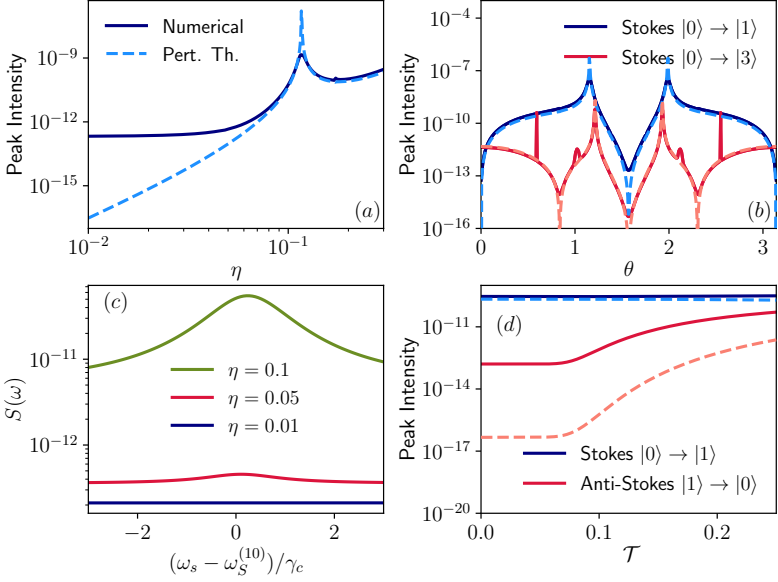
Figure 3.4: Comparison of the perturbation theory prediction with the numerical simulations. (a) The maximum peak intensity of the Stokes process $|0\rangle \to |1\rangle$ as a function of the normalized coupling strength η. (b) Peak intensity of the Stokes processes $|0\rangle \to |1\rangle$ and $|0\rangle \to |3\rangle$ as a function of the parity parameter θ. (c) Emission spectrum of the Stokes process $|0\rangle \to |1\rangle$ around $\omega_S^{(10)}$ for different values of η. (d) Peak intensity of both Stokes and anti-Stokes processes between the states $|0\rangle$ and $|1\rangle$ as a function of the normalized temperature $\mathcal{T}$. These figures show an high agreement between the perturbation theory and the numerical simulations. The used parameters are the same as in Fig. 3.1(b).

in a Jaynes Cummings system. Peaks that might be observed under these conditions, such as ω_S^{21} and ω_{AS}^{21}, are barely discernible even within the ultrastrong-coupling regime, as shown in Fig. 3.4(a,b), and necessitate a stationary population of excited states, which could introduce additional dephasing sources. We therefore conclude that Raman photon emission from coherently driven cavity QED systems is fundamentally a characteristic effect of the USC coupling limit.

The presence or absence of specific Raman peaks can offer insights into microscopic parameters, such as the static dipole moment represented by θ. Each peak displays a unique θ dependence, as demonstrated in Fig. 3.4(b) with two specific instances, the Stokes peaks $\omega_S^{(10)}$ and $\omega_S^{(30)}$, indicating that this dependence is accurately captured by our quantum process description based on perturbation theory. This instance underscores that in certain scenarios—like for $\omega_R^{(10)}$—the violation of parity symmetry ($\theta \neq 0$) is essential for the observation of the corresponding Raman peak. When $\theta = 0$, QRM eigenstates also serve as parity eigenstates, hence only Raman processes preserving parity, such as $|0\rangle \rightarrow |3\rangle$, will exhibit a non-zero scattering rate. Lastly, Fig. 3.4(d) reveals that our quantum model offers a reliable qualitative forecast for the varying temperature dependence of Stokes and anti-Stokes peaks, indicating that the intensity of Stokes peaks is marginally reduced, while the intensity of anti-Stokes peaks can be amplified by several orders of magnitude, which can be attributed to the corresponding rise in the stationary population of excited states.

3.4 Implications of Raman peaks for spectroscopy: Fisher Information

The development of strategies to enhance the characterization of cavity QED systems is a crucial endeavor, considering their fundamental role in numerous quantum technology architectures. The introduction and comprehension of Raman scattering processes in this study bear significant relevance for the spectroscopic characterization of cavity QED systems through the examination of excitation-emission spectra, thereby considerably augmenting the information these measurements yield about the system's internal parameters. In essence, we can markedly boost the accuracy of internal parameter estimation by ensuring that not only are the spectral features associated with direct transitions between eigenstates accurately fitted by our cavity-QED model, but also the Raman scattering peaks. To provide quantitative

substantiation for these assertions, we scrutinize this issue from the standpoint of quantum parameter estimation [149–156]. As a pertinent example, we contemplate a scenario where our system is characterized by the quantum Rabi model Hamiltonian described above, and we are tasked with estimating the light-matter coupling parameter η from an emission spectrum measurement.

A measurement strategy is represented by a positive operator-valued measurement (POVM) Λ, a set of operators $\{\hat{\Lambda}_\mu\}$, where $\mu \in \{1, 2, \ldots, M\}$ labels different possible measurement outcomes, and $\sum_\mu \Lambda_\mu = \mathbb{1}$. For a given unknown parameter η, the probability for each measurement outcome follows a distribution $P(\mu|\eta) = \text{Tr}[\rho_\eta \Lambda_\mu]$, where ρ_η is the η-dependent density matrix of the system. The uncertainty in the estimation of η, $\Delta^2\eta$, is bounded by the Fisher information of the probability distribution, $\Delta^2\eta \geq 1/F$, defined as

$$F = \text{E}\left[\left(\frac{d\log P(\mu|\eta)}{d\eta}\right)^2\right]. \tag{3.13}$$

In Ref. [157], an expression for the Fisher information associated to measurements of emission spectra was derived. The measurement of the emission spectrum $S(\omega)$ is described as a collection of independent measurements over a discretized set of N frequency points $\vec{\omega} = [\omega_1, \omega_2, \ldots, \omega_N]$. For each frequency point ω_i the probability distribution of the measurement of the spectrum is a Poissonian distribution with mean value $S(\omega_i)$, leading to Fisher information

$$F = \sum_{i=1}^{N} \frac{1}{S(\omega_i, \eta)} \left[\frac{\partial S(\omega_i, \eta)}{\partial \eta}\right]^2. \tag{3.14}$$

Applying the Cramér-Rao bound, this quantity allows us to evaluate the metrological potential of spectrum measurements for estimating an unknown η. We can isolate the contribution to the Fisher information from different regions of the spectrum. Here, we separate contributions from two different frequency ranges; one centered around a direct
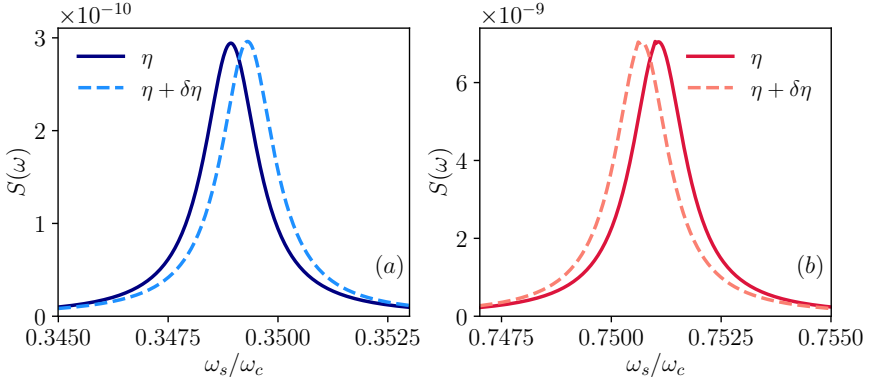
Figure 3.5: Variation of the emission spectrum with the coupling strength $\eta = 0.3$ and $\delta\eta = 0.0005$ as an estimation of the Fisher information. (a) Variation of the Stokes peak $|0\rangle \rightarrow |1\rangle$. (b) Variation of the direct peak $|1\rangle \rightarrow |0\rangle$. Although the Stokes peak is 4% the intensity of the direct peak, its Fisher information is still 4% the Fisher information of the direct peak, stating that the relative information is equal. The used parameters are the same as in Fig. 3.1(b).

transition from eigenstate $|1\rangle$ to ground state $|0\rangle$, and one around the Raman peak corresponding to Stokes process $|0\rangle \rightarrow |1\rangle$, labeled as $\omega_{\mathrm{S}}^{(10)}$. The spectral peaks measured in both frequency ranges are displayed in Fig. 3.5(a-b), with the same parameters of Fig. 3.1(b). A small change in η imprints a change in these spectral forms. Our calculation shows that the total intensity of the Raman peak is 4% the intensity of the direct peak, but its Fisher information is still 4% that of the direct peak, meaning that the relative information is equal, and that the Raman peak contains significant information about η, despite its small intensity. We stress that the intensity peaks and the derived Fisher information may change by changing the properties of the environment, such as the density of states, leading to a different spectral shape varying ω_s [4]. Here we limited ourselves to consider the only environment introduced in this Thesis, which is the ohmic bath.

This example illustrates how Raman peaks emerging in ultra

strong coupling regime contain significant information about internal parameters of system. Their correct description and understanding is crucial for accurate characterization of cavity QED setups via spectroscopic measurements.

This example underscores a significant distinction between Raman photons spontaneously scattered by cavity QED systems and those scattered through coupling to phononic degrees of freedom. In the absence of phonons, the process is entirely encapsulated by a quantum Rabi Hamiltonian, and all spectral features can be fitted by such a model (for instance, the central frequency is wholly determined by the transition energies between different eigenstates of the quantum Rabi Hamiltonian). Conversely, in the case of Raman scattering due to phonon coupling, the frequency of a scattered Stokes photon, ω_{S}, would be offset from the laser frequency ω_{L} by an amount equivalent to the frequency ω_m of the phonon mode:

$$\omega_{\mathrm{S}} = \omega_{\mathrm{L}} - \omega_m \, , \qquad (3.15)$$

which is a parameter that is independent of the cavity QED system. This implies that it would not be feasible to fit such a peak with only a quantum Rabi model. This crucial difference between both scenarios enables us to ascertain the origin of the observed Raman peaks and unambiguously identify instances where these originate from the purely cavity QED effect that we present in this work.

CHAPTER 4

Pure dephasing of light and matter in the USC and DSC regimes

In the previous chapters, we focused on the gauge-invariant description of open quantum systems in the ultrastrong coupling regime, on the photodetection under coherent and incoherent pumping. We have seen that the standard master equation fails when approaching to the USC regime, and that the mathematical description of the fields may vary depending on the gauge chosen. Taking as an example the electric field, we have seen in Section 2.1 that in the Coulomb gauge it is defined as

$$\hat{E}_C = i\omega_c A_0 \left(\hat{a} - \hat{a}^\dagger \right) , \tag{4.1}$$

because the photonic canonical momentum $\hat{\Pi}_C = -\varepsilon_0 \hat{E}$ is not modified by the interaction with the matter (see also Section 1.3 for the full derivation). On the other hand, in the multipolar (or dipole) gauge, the canonical momentum is proportional to the electric displacement field

$$\hat{\Pi}_D = -\hat{D}_D = -i\varepsilon_0 \omega_c A_0 \left(\hat{a} - \hat{a}^\dagger \right) , \tag{4.2}$$

where

$$\hat{D} = \varepsilon_0 \hat{E}_D + \hat{P}, \tag{4.3}$$

and $\hat{P}$ is the polarization operator of the matter. This implies that the electric field in the dipole gauge is

$$\hat{E}_D = -\frac{1}{\varepsilon_0} \left(\hat{\Pi}_D + \hat{P} \right) = i\omega_c A_0 \left(\hat{a} - \hat{a}^\dagger \right) - 2\omega_c A_0 \eta \hat{\sigma}_x, \tag{4.4}$$

for the case of a truncated two-level matter system.

We have also seen that the truncation operation of the matter system is not always a safe operation. Specifically, since in the Coulomb gauge the canonical momentum of the matter system is modified by the interaction with the electromagnetic field, the truncation has to be performed in the dipole gauge, where the matter canonical momentum is not modified. Although a proper way to derive the correct version of the truncated light-matter Hamiltonian in the Coulomb gauge was presented [75, 79] (See also Section 1.4.3), the key point is that the application of certain operations on a subsystem is safer in that gauge where the canonical momentum is not modified. The truncation of the matter eigenstates is much safe in the dipole gauge, while the definition of photodetection and photonic losses in the dipole gauge is not so intuitive as in the Coulomb gauge.

To further extend this concept, we now ask ourselves what is the energy of the electromagnetic field when it interacts with matter. We already know from Section 1.2 that the Hamiltonian of a single mode cavity field is $\hat{H}^{(c)} = \omega_c(\hat{a}^\dagger \hat{a} + 1/2)$[1]. This arises from Eq. (1.15) which express the energy as an integral in space of $\mathbf{E}^2(\mathbf{r})$ and $\mathbf{B}^2(\mathbf{r})$. Now, while in the Coulomb gauge the energy associated to the n-th mode is

---

[1]We remind that we choose $\hbar = 1$

related to the Hamiltonian

$$\hat{\mathcal{H}}_C^{(c)} = \frac{1}{2}\left(\varepsilon_0\hat{E}_C^2 + \frac{1}{\mu_0}\hat{B}_C^2\right)$$

$$= \frac{1}{2}\left[-\varepsilon_0 A_0^2\omega_c^2\left(\hat{a}-\hat{a}^\dagger\right)^2 + \frac{A_0^2\omega_c^2}{\mu_0 c^2}\left(\hat{a}+\hat{a}^\dagger\right)^2\right] \qquad (4.5)$$

$$= \omega_c\left(\hat{a}^\dagger\hat{a}+\frac{1}{2}\right),$$

where $A_0 = \sqrt{1/(2\varepsilon_0\omega_c)}$, in the dipole gauge it is related to the Hamiltonian

$$\hat{\mathcal{H}}_D^{(c)} = \frac{1}{2}\left(\varepsilon_0\hat{E}_D^2 + \frac{1}{\mu_0}\hat{B}_D^2\right)$$

$$= \frac{1}{2}\left\{\varepsilon_0 A_0^2\omega_c^2\left[i\left(\hat{a}-\hat{a}^\dagger\right)-2\eta\hat{\sigma}_x\right]^2 + \frac{A_0^2\omega_c^2}{\mu_0 c^2}\left(\hat{a}+\hat{a}^\dagger\right)^2\right\} \qquad (4.6)$$

$$= \omega_c\left(\hat{a}^\dagger\hat{a}+\frac{1}{2}\right) - i\eta\omega_c\left(\hat{a}-\hat{a}^\dagger\right)\hat{\sigma}_x + \eta^2\omega_c,$$

which is very different from Eq. (4.5), especially when $\eta \gtrsim 0.1$.

The same holds for the matter system. In the Coulomb gauge, the energy associated to the matter system is related to the Hamiltonian

$$\hat{\mathcal{H}}_C^{(a)} = \frac{\omega_{eg}}{2}\left\{\hat{\sigma}_z\cos\left[2\eta\left(\hat{a}+\hat{a}^\dagger\right)\right] + \hat{\sigma}_y\sin\left[2\eta\left(\hat{a}+\hat{a}^\dagger\right)\right]\right\}, \qquad (4.7)$$

while in the dipole gauge

$$\hat{\mathcal{H}}_D^{(a)} = \frac{\omega_{eg}}{2}\hat{\sigma}_z. \qquad (4.8)$$

Moreover, by looking at Eqs. (1.89) and (1.92), we see that $\hat{\mathcal{H}}_D^{(c)} = \omega_c\hat{\mathcal{U}}^\dagger\hat{a}^\dagger\hat{a}\hat{\mathcal{U}} = \omega_c\hat{a}_D^\dagger\hat{a}_D$ and $\hat{\mathcal{H}}_C^{(a)} = (\omega_{eg}/2)\hat{\mathcal{U}}\hat{\sigma}_z\hat{\mathcal{U}}^\dagger = (\omega_{eg}/2)\hat{\sigma}_{z,C}$, where $\hat{\mathcal{U}} = \exp[i\eta(\hat{a}+\hat{a}^\dagger)\hat{\sigma}_x]$ is the operator that links the two gauges, as defined in Eq. (1.90).

Here we see that the intuitive definition of the energy related to one of the two subsystems holds only in the gauge where the momentum

of that specific subsystem is unchanged. In the other gauge, there is still a valid definition of energy, but it may be more or less different depending on the coupling strength. This may change the way to treat problems such as pure dephasing, where a stochastic perturbation of the single subsystem is taken into account [5].

4.1 The concept of pure dephasing

In Section 2.2, an open quantum system, which is a quantum system that interacts with an environment, was examined. This interaction results in an energy relaxation time T_1 that is linked to a specific optical transition. When an atom is in a continuum of modes of a free electromagnetic field, the decay of the population of an excited state also leads to the decay of polarization, causing decoherence. In situations where only energy relaxation mechanisms are present, such transverse relaxation time is $T_2 = 2T_1$ [98, 158]. However, quantum systems with optical transitions can be influenced by additional dephasing mechanisms that cause the decay of dipole coherence without altering the system's populations. These pure dephasing effects can be caused by environmental field fluctuations that affect the phases of the emitter wave functions [159–164]. Typically, the phase (transverse) relaxation time is less than or equal to twice the energy relaxation time: $T_2 \leq 2T_1$. In optical spectroscopy, the full width at half maximum (FWHM) of homogeneous broadening corresponds to $2/T_2$. Decoherence is known to eliminate quantum coherence and quantum correlations [165, 166], and this process accelerates as the *size* of a quantum system increases [167]. This explains why quantum superpositions are not observed in the macroscopic world [168]. Decoherence can significantly impact and limit quantum information processing (QIP) [169, 170], and depending on the specific environment, methods to protect qubits from dephasing have been suggested [171–174].

Devices for QIP, secure communication, and high-precision sensing have been developed by combining various systems from photons,

atoms, and spins to mesoscopic superconducting and nanomechanical structures. The complementary functionalities of these hybrid quantum systems could be crucial for advancing new quantum technologies [44, 175, 176]. It is interesting to understand how the decoherence of one or more subsystems can affect the performance of the entire system, which is relevant for enhancing the performance of quantum devices [99, 100].

Cavity [166] and circuit [27, 44] quantum electrodynamics (QED) systems are some of the most researched hybrid quantum systems. They play a crucial role in quantum optics and in developing new quantum technologies [177–180]. Pure dephasing can significantly influence these systems' performance. For instance, it has been demonstrated that pure dephasing can enhance the performance of nanophotonic devices like single-photon sources and nanolasers by serving as a valuable resource for solid-state emitters [181].

Decoherence effects in hybrid quantum systems are often introduced by using the standard quantum optics master equation in Eq. (2.27), which we already know that it may fail a large coupling strengths. The dressed master equation in Eq. (2.30), which was derived in Ref. [99], is valid beyond the strong coupling regime, but it fails wen the system becomes harmonic, such as in the weak coupling and the deep strong coupling regimes. Moreover, the authors in Ref. [99] derived also a master equation involving only pure dephasing effects, originating from the energy fluctuations of the subsystems. However, this model considered the energy perturbation coming from the bare Hamiltonian of the subsystem, rather than taking into account the effects of the interaction between the subsystems. The main task of this chapter is to fix this issue, deriving a gauge-invariant master equation for the pure dephasing of light and matter in the USC and DSC regimes. We present results for two prototypical models of cavity QED: the quantum Rabi model (QRM) and the Hopfield model. However, the approach here considered can also be applied to describe more complex light-matter systems.
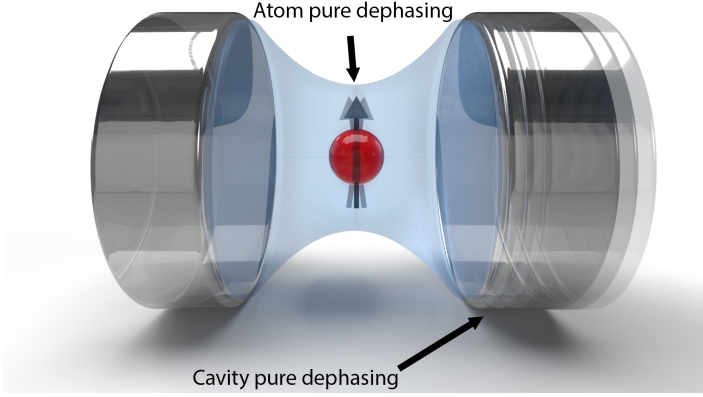
Figure 4.1: Pictorial representation of a two-level system interacting with a single-mode cavity field, when both subsystems are affected by pure dephasing.

4.2 Pure dephasing in the quantum Rabi model

Pure dephasing effects on both the atom and electromagnetic field are in general described by introducing two zero-mean stochastic functions $f_c(t), f_a(t)$ modulating their resonance frequency. In this way, the perturbation Hamiltonian can be written as

$$\hat{\mathcal{V}}_{\text{dep}}(t) = f_c(t)\hat{a}^\dagger\hat{a} + f_a(t)\hat{\sigma}_z \,. \tag{4.9}$$

The standard way to convert this perturbation into a master equation is to consider the following terms in addition to the standard master equation in Eq. (2.27)

$$\frac{\mathrm{d}}{\mathrm{d}t}\hat{\rho} = \mathcal{L}_{\text{std}}\hat{\rho} + \frac{\gamma_\phi^{(c)}}{2}\mathcal{D}\left[\hat{a}^\dagger\hat{a}\right]\hat{\rho} + \frac{\gamma_\phi^{(a)}}{2}\mathcal{D}\left[\hat{\sigma}_z\right]\hat{\rho}\,, \tag{4.10}$$

which, for low coupling strengths η, can be used to accurately describe many cavity QED and circuit QED experiments [93–96]. This master equation, however, fails to describe losses and pure dephasing at larger coupling strengths ($\eta \gtrsim 0.1$), and a theoretical derivation of pure

dephasing valid also in the USC and DSC regimes was derived [99]. As for the dressed master equation in Eq. (2.30), it was derived by expanding $\hat{\mathcal{V}}_{\text{dep}}(t)$ in the basis of the eigenstates of the total system Hamiltonian. For the sake of simplicity, we consider stochastic functions with a low-frequency spectral density (with respect to the relevant transition frequencies of the system). The resulting master equation can be written as

$$\frac{\mathrm{d}}{\mathrm{d}t}\hat{\rho} = - i\left[\hat{H}_s, \hat{\rho}\right] + \frac{\gamma_\phi^{(c)}}{2}\mathcal{D}\left[\hat{\Phi}\right]\hat{\rho} + \frac{\gamma_\phi^{(a)}}{2}\mathcal{D}\left[\hat{\Xi}\right]\hat{\rho}, \qquad (4.11)$$

where $\hat{\Phi} = \sum_j \langle j|\hat{\sigma}_z|j\rangle\,|j\rangle\langle j|$ and $\hat{\Xi} = \sum_j \langle j|\hat{a}^\dagger\hat{a}|j\rangle\,|j\rangle\langle j|$, with $|j\rangle$ being the eigenstates of $\hat{H}_s$. The bare dephasing rates $\gamma_\phi^x = 2S_f(0)$ are determined by the low-frequency spectral densities $S_f^{(x)}(\omega)$ of $f_x(t)$, with $x = q, c$. Additional dephasing terms can appear, when the spectral density functions $S_f(\omega)$ are not negligible at the transition frequencies of the system (see Appendix D).

However, as already stated in the beginning of this chapter, the operators $\hat{a}^\dagger\hat{a}$ and $\hat{\sigma}_z$ do not describe always the contribution related to the cavity and atom energies, respectively. For example, the energy of the cavity field in the dipole gauge is related to the operator $\hat{\mathcal{H}}_D^{(c)} = \omega_c\hat{a}_D^\dagger\hat{a}_D$, where $\hat{a}_D = \hat{a} + i\eta\hat{\sigma}_x$. On the other hand, the energy of the atom in the Coulomb gauge is related to the operator $\hat{\mathcal{H}}_C^{(a)} = (\omega_{eg}/2)\hat{\sigma}_{z,C}$, where $\hat{\sigma}_{z,C} = \hat{\sigma}_z\cos[2\eta(\hat{a}+\hat{a}^\dagger)] + \hat{\sigma}_y\sin[2\eta(\hat{a}+\hat{a}^\dagger)]$. Thus, the perturbation term in Eq. (4.9) does not describes correctly the process of pure dephasing. The correct procedure is to consider the following perturbation terms, depending on the gauge considered

$$\hat{\mathcal{V}}_{C,\phi}(t) = f_a(t)\hat{\sigma}_{z,C} + f_c(t)\hat{a}^\dagger\hat{a} \qquad \text{(in Coulomb gauge)}, \qquad (4.12a)$$

$$\hat{\mathcal{V}}_{D,\phi}(t) = f_a(t)\hat{\sigma}_z + f_c(t)\hat{a}_D^\dagger\hat{a}_D \qquad \text{(in dipole gauge)}. \qquad (4.12b)$$

To better understand why this is the correct procedure, let us consider the quantum Rabi Hamiltonian in the dipole gauge

$$\hat{\mathcal{H}}_D = \omega_c\hat{a}_D^\dagger\hat{a}_D + \frac{\omega_{eg}}{2}\hat{\sigma}_z - i\eta\omega_c\left(\hat{a} - \hat{a}^\dagger\right)\hat{\sigma}_x + \omega_c\eta^2, \qquad (4.13)$$

and we now add a perturbation of both the resonance frequencies of the cavity and the atom $\omega_c \to \omega_c + f_c(t)$ and $\omega_{eg} \to \omega_{eg} + 2f_a(t)$, through stochastic zero-mean functions $f_c(t)$ and $f_a(t)$, respectively. The Hamiltonian can be written as

$$
\begin{aligned}
\hat{\mathcal{H}}_{D,\phi}(t) = &\ [\omega_c + f_c(t)]\,\hat{a}^\dagger\hat{a} + \frac{\omega_{eg} + 2f_a(t)}{2}\hat{\sigma}_z \\
&- i\eta\,[\omega_c + f_c(t)]\left(\hat{a} - \hat{a}^\dagger\right)\hat{\sigma}_x + (\omega_c + f_c(t))\,\eta^2 \\
= &\ \omega_c\hat{a}^\dagger\hat{a} + \frac{\omega_{eg}}{2}\hat{\sigma}_z - i\eta\omega_c\left(\hat{a} - \hat{a}^\dagger\right)\hat{\sigma}_x + \omega_c\eta^2 \qquad (4.14)\\
&+ f_c(t)\hat{a}^\dagger\hat{a} + f_a(t)\hat{\sigma}_z - i\eta f_c(t)\left(\hat{a} - \hat{a}^\dagger\right)\hat{\sigma}_x + f_c(t)\eta^2 \\
= &\ \hat{\mathcal{H}}_D + f_c(t)\hat{a}_D^\dagger\hat{a}_D + f_a(t)\hat{\sigma}_z = \hat{\mathcal{H}}_D + \hat{\mathcal{V}}_{D,\phi}(t)\,,
\end{aligned}
$$

which results in the same additional term presented in Eq. (4.12b). The same procedure can be applied to the Coulomb gauge, where the Hamiltonian is

$$
\hat{\mathcal{H}}_C = \omega_c\hat{a}^\dagger\hat{a} + \frac{\omega_{eg}}{2}\left\{\hat{\sigma}_z\cos\left[2\eta\left(\hat{a} + \hat{a}^\dagger\right)\right] + \hat{\sigma}_y\sin\left[2\eta\left(\hat{a} + \hat{a}^\dagger\right)\right]\right\}\,.
$$
$$(4.15)$$

Again, we now add a perturbation of both the resonance frequencies of the cavity and the atom $\omega_c \to \omega_c + f_c(t)$ and $\omega_{eg} \to \omega_{eg} + 2f_a(t)$, and the Hamiltonian can be written as

$$
\begin{aligned}
\hat{\mathcal{H}}_{C,\phi}(t) = &\ [\omega_c + f_c(t)]\,\hat{a}^\dagger\hat{a} + \frac{\omega_{eg} + 2f_a(t)}{2}\left\{\hat{\sigma}_z\cos\left[2\eta\left(\hat{a} + \hat{a}^\dagger\right)\right]\right. \\
&+ \left.\hat{\sigma}_y\sin\left[2\eta\left(\hat{a} + \hat{a}^\dagger\right)\right]\right\} \\
= &\ \hat{\mathcal{H}}_C + f_c(t)\hat{a}^\dagger\hat{a} + f_a(t)\left\{\hat{\sigma}_z\cos\left[2\eta\left(\hat{a} + \hat{a}^\dagger\right)\right]\right. \\
&+ \left.\hat{\sigma}_y\sin\left[2\eta\left(\hat{a} + \hat{a}^\dagger\right)\right]\right\} \\
= &\ \hat{\mathcal{H}}_C + f_c(t)\hat{a}^\dagger\hat{a} + f_a(t)\hat{\sigma}_{z,C} = \hat{\mathcal{H}}_C + \hat{\mathcal{V}}_{C,\phi}(t)\,,
\end{aligned}
$$
$$(4.16)$$

which, as expected, results in the same additional term presented in Eq. (4.12a). As derived in Appendix D, the resulting master equation

has the same form of Eq. (4.11), but with the correct operators $\hat{\Phi}$ and $\hat{\Xi}$, depending on the gauge considered. It is worth noting that Eqs. (4.14) and (4.16) are linked through the same gauge transformation that links the two Hamiltonians without dephasing terms: $\hat{\mathcal{H}}_{C,\phi}(t) = \hat{\mathcal{U}}\hat{\mathcal{H}}_{D,\phi}(t)\hat{\mathcal{U}}^\dagger$, while $\hat{\mathcal{H}}_C + \hat{\mathcal{V}}_{\text{dep}}(t) \neq \hat{\mathcal{U}}[\hat{\mathcal{H}}_D + \hat{\mathcal{V}}_{\text{dep}}(t)]\hat{\mathcal{U}}^\dagger$, which means that, in the latter case, the results are not gauge-invariant.

In the following, we label the QRM states as in Section 2.4, by generalizing the notation of the Jaynes-Cummings (JC) model. In particular, $|\tilde{0}\rangle$ denotes the ground state, and $|\tilde{n}_\pm\rangle$ the states that tend to the JC states $|n_\pm\rangle$, when the coupling vanishes. Moreover, we use not-primed (primed) states to indicate the Coulomb (dipole) gauge states. As an example we analyze pure dephasing effects on the two lowest transitions in the QRM: $\alpha_\pm \equiv (\tilde{1}_\pm, \tilde{0})$, and considering only atom pure dephasing ($f_c(t) = 0$). In the interaction picture, from Eq. (4.11), we obtain (see Appendix D)

$$\dot{\tilde{\rho}}_{\alpha'_\pm}(t) = -\left(\gamma_\phi^{\alpha'_\pm}/2\right)\tilde{\rho}_{\alpha'_\pm}(t),\tag{4.17}$$

with

$$\gamma_\phi^{\alpha'_\pm} = \frac{\gamma_\phi^{(q)}}{2}\left|\sigma_z^{\tilde{1}'_\pm,\tilde{1}'_\pm} - \sigma_z^{\tilde{0}',\tilde{0}'}\right|^2.\tag{4.18}$$

Moreover, we observe that the obtained dephasing rates are gauge invariant ($\gamma_\phi^{\alpha'_\pm} = \gamma_\phi^{\alpha_\pm}$), because the expectation values are unitary invariant, when transforming both operator and states: $\gamma_\phi^{\alpha_\pm} = \gamma_\phi^{(q)}|\sigma_{z,C}^{\tilde{1}_\pm,\tilde{1}_\pm} - \sigma_{z,C}^{\tilde{0},\tilde{0}}|^2/2$.

The normalized atom pure dephasing $\gamma_\phi^{\alpha_\pm}/\gamma_\phi^{(q)}$ as a function of the coupling strength η, and with a small detuning $\Delta \equiv \omega_c - \omega_{eg} = -10^{-3}\omega_c$, is depicted in Fig. 4.2. The upper panel illustrates the accurate rates, which are derived by considering the appropriate operator $\hat{\sigma}_{z,C}$ in the Coulomb gauge (or $\hat{\sigma}_z$ if the dipole gauge was selected). The lower panel presents the rates calculated by employing the operator $\hat{\sigma}_z$ in the Coulomb gauge, revealing a noticeable deviation
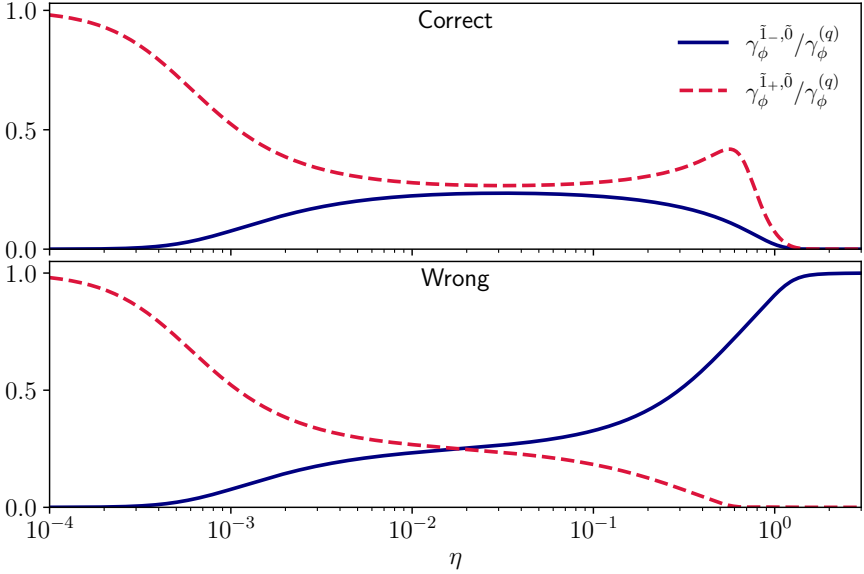
Figure 4.2: Normalized atom pure dephasing rates $\gamma_\phi^{\alpha'_\pm}/\gamma_\phi^{(q)}$ for the two lowest transitions in the QRM, as a function of the coupling strength η, and with a small detuning $\Delta/\omega_c = -10^{-3}$. The upper panel shows the correct rates, obtained by taking into account the correct operator $\hat{\sigma}_{z,C}$ in the Coulomb gauge (or $\hat{\sigma}_z$ if we had chosen the dipole gauge). The lower panel shows the rates obtained by using the operator $\hat{\sigma}_z$ in the Coulomb gauge, which shows a clear discrepancy with the correct rates.

from the accurate rates. This discrepancy arises because the operator $\hat{\sigma}_z$ in the Coulomb gauge does not represent the energy of the atom, as discussed at the start of this chapter.

In the scenario of small coupling strength, where $|\tilde{1}_+\rangle$ approaches $|e, 0\rangle$ and $|\tilde{1}_-\rangle$ approaches $|g, 1\rangle$, the conventional outcomes are reinstated, and only the $(\tilde{1}_+, \tilde{0})$ transition is influenced by the atom pure dephasing. As anticipated, when the coupling is or the same order of magnitude of the detuning, pure dephasing is distributed between the two transitions, since the energy eigenstates $|\tilde{1}_\pm\rangle$ tend to evolve into

an evenly balanced superposition of $|e, 0\rangle$ and $|g, 1\rangle$. For normalized coupling strengths $\eta > 0.1$ (the USC regime), pure dephasing becomes less potent for the transition $(\tilde{1}_-, \tilde{0})$, until at higher couplings (the DSC regime), both transitions tend to become immune to dephasing. This pattern mirrors two observations: i) as the energy of $|\tilde{1}_-, \tilde{0}\rangle$ nears zero, the energy fluctuations of the atom have a negligible effect on this transition's broadening; ii) the phenomenon of light-matter decoupling [2, 105], extensively discussed in Section 2.4, is clearly visible. Conversely, the bottom panel of Fig. 4.2 displays an incorrect large pure dephasing rate for the lowest energy transition.

4.3 Pure dephasing in the Hopfield model

A comparable examination can be conducted for polaritons. We take into account the most basic version of the Hopfield model [182], which characterizes the interaction of a single-mode electromagnetic resonator with a bosonic matter field (with the bosonic annihilation $\hat{b}$ and creation $\hat{b}^\dagger$ operators) that models certain collective matter excitations. The system Hamiltonian in the dipole gauge is given by

$$\hat{H}_{\mathrm{D}} = \hat{H}_0 + i\lambda\omega_c \left(\hat{a}^\dagger - \hat{a} \right) \left(\hat{b} + \hat{b}^\dagger \right) + \omega_c \lambda^2 \left(\hat{b} + \hat{b}^\dagger \right)^2 , \qquad (4.19)$$

where $\hat{H}_0 = \omega_c \hat{a}^\dagger \hat{a} + \omega_x \hat{b}^\dagger \hat{b}$, and λ represents the normalized coupling strength. A similar model can be derived in the Coulomb gauge [145]

$$\hat{H}_C = \hat{H}_0 - i\omega_x \lambda \left(\hat{b}^\dagger - \hat{b} \right) \left(\hat{a}^\dagger + \hat{a} \right) + \omega_x \lambda^2 \left(\hat{a}^\dagger + \hat{a} \right)^2 . \qquad (4.20)$$

These two Hamiltonians can be directly derived by generalized minimal coupling replacements: $H_C = \omega_c \hat{a}^\dagger \hat{a} + \omega_x \hat{T} \hat{b}^\dagger \hat{b} \hat{T}^\dagger$ and $H_D = \omega_c \hat{T}^\dagger \hat{a}^\dagger \hat{a} \hat{T} + \omega_x \hat{b}^\dagger \hat{b}$, where $\hat{T} = \exp[i\lambda(\hat{a} + \hat{a}^\dagger)(\hat{b} + \hat{b}^\dagger)]$ [145]. As is well known, the interaction leads to polaritonic resonances, which are a result of the mixing of the two bosonic modes. It is feasible to diagonalize the system by expressing the photon and exciton operators

in terms of polaritonic (bosonic) operators [182]. For $\mu = 1, 2$ (lower and upper polariton, respectively), we have

$$\hat{y} = \sum_{\mu=1}^{2} (U_y^\mu P_\mu - V_y^\mu P_\mu), (y = \hat{a}, \hat{b}). \tag{4.21}$$

The diagonalization process determines both polariton eigenfrequencies Ω_μ, which are gauge invariant, and the Hopfield coefficients, which are gauge dependent. Consequently, the polariton operators are also gauge dependent. We use primed operators and coefficients for the dipole gauge.

Dephasing effects can be modeled by introducing the perturbation Hamiltonian, assuming the light-matter interaction is negligible,

$$\hat{\mathcal{V}}_{\text{dep}}(t) = f_c(t)\hat{a}^\dagger \hat{a} + f_x(t)\hat{b}^\dagger \hat{b}, \tag{4.22}$$

which represents the random fluctuation of the resonance frequencies of the components. When the light-matter interaction is included, it becomes clear that Eq. (4.22) is not accurate, and its corrected form depends on the gauge:

$$\hat{\mathcal{V}}_{D,\phi}(t) = f_c(t)\hat{a}_D^\dagger \hat{a}_D + f_x(t)\hat{b}^\dagger \hat{b} \qquad \text{(in dipole gauge)}, \tag{4.23a}$$

$$\hat{\mathcal{V}}_{C,\phi}(t) = f_c(t)\hat{a}^\dagger \hat{a} + f_x(t)\hat{b}_C^\dagger \hat{b}_C \qquad \text{(in Coulomb gauge)}. \tag{4.23b}$$

where $\hat{a}_D = \hat{T}^\dagger \hat{a}\hat{T} = \hat{a} + i\lambda(\hat{b} + \hat{b}^\dagger)$ and $\hat{b}_C = \hat{T}\hat{b}\hat{T}^\dagger = \hat{b} - i\lambda(\hat{a} + \hat{a}^\dagger)$. Here, $\hat{a}_D$ ($\hat{b}_C$) is the *physical* photonic (excitonic) annihilation operator in the dipole (Coulomb) gauge. By *physical*, we refer to the operators that describe the annihilation of the physical quanta of the fields [145]. The polariton pure dephasing rates can be calculated by expanding Eqs. (4.23a) and (4.23b) in terms of the polariton operators, and then applying the standard master equation method to obtain the Lindbladian terms, similar to the results of the previous section. From the derived master equation, we get $\partial_t \langle \hat{P}_\mu \rangle = (-i\Omega_\mu - \gamma_\phi^\mu/2)\langle \hat{P}_\mu \rangle$, where

$$\gamma_\phi^\mu = \gamma_\phi^{(c)} \left(|U_a^\mu|^2 + |V_a^\mu|^2 \right) + \gamma_\phi^{(x)} \left(\left| U_b^{\mu\prime} \right|^2 + \left| V_b^{\mu\prime} \right|^2 \right). \tag{4.24}$$
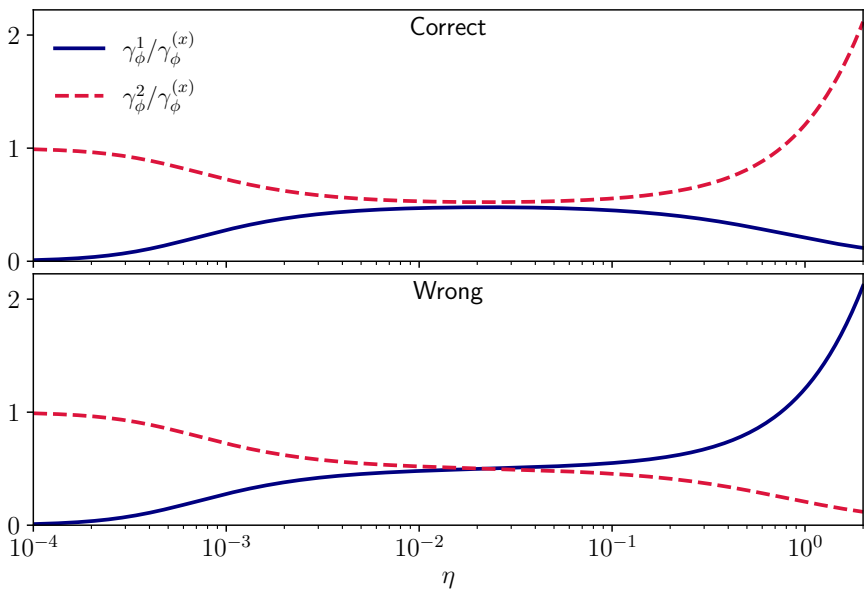
Figure 4.3: Normalized pure dephasing rates $\gamma_\phi^\mu / \gamma_\phi^{(x)}$ of the collective matter degrees of freedom for the two polariton modes, as a function of the coupling strength λ, and with a small detuning $\Delta/\omega_c = -10^{-3}$. The upper panel shows the correct rates. The lower panel shows the rates obtained by using the operator $\hat{b}^\dagger \hat{b}$ in the Coulomb gauges, respectively, which again shows a clear discrepancy with the correct rates.

This outcome can significantly differ from what would be obtained starting from Eq. (4.22) and disregarding changes in subsystems-observables induced by interaction. Fig. 4.3 displays normalized pure dephasing rates for two polariton modes $(\gamma_\phi^\mu / \gamma_\phi^{(x)})$, considering zero photonic noise $(\gamma_\phi^{(c)} = 0)$, and $\Delta/\omega_c = -10^{-3}$. We observe that at high coupling rates, lower polariton dephasing rate tends to zero. This effect is due to lower polariton resonance frequency rapidly approaching zero for $\lambda \to \infty$, regardless of detuning. This implies that any minor fluctuation of resonance frequencies of components does not induce

fluctuations and hence no dephasing in polariton mode. For comparison, lower panel of Fig. 4.3 shows incorrect result $\gamma_\phi^\mu/\gamma_\phi^{(x)} = |U_b^\mu|^2 + |V_b^\mu|^2$, obtained by neglecting changes in form of subsystems-observables, which can be induced by interaction. Evident differences emerge when entering the USC regime with $\lambda \sim 0.1$. Moreover, at larger coupling rates, in the DSC regime, the behavior of the lower and upper polaritons is clearly inverted.

To conclude this chapter, it is worth mentioning that the procedure adopted here can be extended to other situations. For example, when taking into account non-linearities in the cavity field, they must be treated adequately, taking care of the gauge invariance [1]. In this case, the trivial introduction of the non-linearities is only valid in the Coulomb gauge.

CHAPTER 5

Photon condensation in approximate models

Phase transitions at equilibrium between a standard state and a photon condensate state (also referred to as superradiant phase transitions) are a subject of intense debate in research, with theories proposing their existence and no-go theorems contradicting each other over the past forty years. Recent no-go theorems have established that gauge invariance prohibits second-order phase transitions to a photon condensate state when the cavity-photon mode is assumed to be spatially uniform. Nevertheless, it has been theoretically postulated that a group of three-level systems interacting with light can exhibit a first-order phase transition to a photon condensate state. In this chapter, we present a general no-go theorem that is also applicable to truncated, gauge-invariant models, which prohibits both first-order and second-order superradiant phase transitions in the absence of a magnetic field coupling [3]. Specifically, we consider the cases of interacting electrons in a lattice and M-level systems.

5.1 Introduction to photon condensation

In the previous chapter, we have seen the effects of pure dephasing in the Hopfield model. This model was initially introduced to describe the interaction of the electromagnetic field with a harmonic resonant polarization density of a three-dimensional (3D) dielectric crystal. Nowadays, it is used to describe the interaction between free or confined light and different kinds of collective excitations, such as optical phonons, excitons in nanostructures, magnons, and plasmonic crystals, which can be described as bosonic fields. However, the simplest model describing the interaction of collective excitations with light is the Dicke model [32]. The Dicke model is a fundamental model in the theory of light-matter interactions [30, 183–185]. It characterizes a group of N identical two-level systems coherently coupled to the same bosonic mode $\hat{a}$, which arises from the quantization of the electromagnetic field inside a cavity of volume V. As its name suggests, it was first introduced by Robert H. Dicke [32], with the aim of describing the "emission of coherent radiation" obtained by considering a "radiating gas as a single quantum-mechanical system". He dubbed such process "super-radiant emission".

In the thermodynamic limit ($N \to \infty$, $V \to \infty$, with $N/V =$ constant) and when the light-matter coupling strength exceeds a critical value, the Dicke model undergoes an equilibrium second-order thermal phase transition [186, 187] between a normal and a "super-radiant" phase. In the zero-temperature limit, the phase transition persists and corresponds to a quantum phase transition [188–191]. The super-radiant phase is characterized by a macroscopic number of coherent photons, $\langle \hat{a} \rangle \sim \sqrt{N}$, and by a macroscopic number of excitations in the matter sector. To avoid confusion with the Dicke non-equilibrium super-radiant emission [32], we here follow Refs. [192, 193] and dub the equilibrium super-radiant phase transition as "photon condensation".

In the Coulomb gauge, a careful derivation of the Dicke model starting from a microscopic condensed-matter model with electronic degrees of freedom leads to an additional diamagnetic term [194],

proportional to $(\hat{a} + \hat{a}^\dagger)^2$, which is usually neglected by utilizing a (wrong) "weak-coupling argument". It was soon understood [194–196] that such additional term is crucial to preserve the gauge invariance property of the model. Only when both terms generated by the minimal coupling substitution $\hat{\mathbf{p}} \rightarrow \hat{\mathbf{p}} + e\mathbf{A}$, (i.e. the paramagnetic light-matter coupling and the diamagnetic term) are retained, does one have a gauge-invariant theory satisfying the Thomas-Reiche-Kuhn (TRK) sum rule [85, 197]. The occurrence of photon condensation in such a generalized Dicke model is forbidden [194, 198, 199].

Despite its significance, the Dicke model is not all-encompassing. In recent years, research have expanded beyond it by investigating interactions between matter degrees of freedom and quantized electromagnetic fields in a variety of other models and physical systems. Many of these "beyond-Dicke" systems, including three-level systems [200, 201], graphene [202], ferroelectric materials [203], superconducting circuits [199, 204–206], and strongly correlated (a.k.a. quantum) materials [207], have been predicted to exhibit photon condensation.

A series of no-go theorems for photon condensation in a single-mode spatially-uniform cavity field have been published [192, 208–212], demonstrating that gauge invariance prohibits photon condensation even in such "beyond-Dicke" systems. Often, these theorems have been countered by "go theorems" [199, 213, 214]. The topic of photon condensation remains a contentious theoretical issue.

Currently, the most recent no-go theorem is reported in Ref. [192], where the authors demonstrated that photon condensation is forbidden by gauge invariance for generic non-relativistic interacting electron systems coupled to a spatially-uniform cavity mode. The proof is based on linear response theory and uses the smallness of the order parameter $\alpha = \langle \hat{a} \rangle$. It is therefore valid only for second-order phase transitions, where $\alpha \ll 1$ at the phase transition, and changes continuously. It is now clear that a natural path to overcome such theorem is to consider spatially-varying cavity fields [193, 215, 216]. In these recent works, photon condensation has been shown to occur and is essentially a magneto-static instability [193, 215–217]. Apparently,

another possibility to bypass the hypothesis of such theorem could be to consider a first-order phase transition [200, 216], where the order parameter α abruptly changes from zero (in the normal phase) to a finite value (in the photon condensate phase). As a matter of fact, that first-order phase transitions were a valuable possibility to overcome the no-go theorem was first discussed some time ago [204, 218]. In these works, an ensemble of three level systems coupled to single uniform mode undergoes to first-order phase transition. Indeed, according to Refs. [204, 218] systems displaying first-order phase-transitions were thought as valuable candidates to realize photon condensation.

These results are, however, in contrast with a rather general no-go theorem presented already in 1978 [195]. In this work, an ensemble of electrons in the presence of single-particle potentials and interacting with a uniform electromagnetic mode is considered and it is shown that superradiant phase transitions (of any order) to a photon condensate are forbidden. In this proof, no truncation is taken and the full infinite-dimensional Hilbert space is retained. However, it is often impractical to deal with an exponentially large Hilbert space. Hence, when performing explicit calculations in atomic systems, or more generally, in many-body systems, approximate (truncated) models are customarily employed.

However, we already know that such approximations can spoil gauge invariance (see Section 1.4.3). Since no-go theorems are closely related to gauge-invariance, it is natural to conclude that the super-radiant phase transition that can be found in these approximate models (e.g. in the three-level systems discussed in Refs. [200, 216]) is a fictitious effect due to the Hilbert space truncation. In this chapter, we extend the no-go theorem for photon condensation of Ref. [195] for gauge-invariant truncated models of light-matter interacting systems [3].

5.2 Gauge invariance, photon condensation, and no-go theorem in interacting electron systems

5.2.1 Interacting electrons in the continuum

We consider a quantum many-body system of interacting electrons, following the notation of Ref. [219]. In second quantization, the electronic Hamiltonian can be written as

$$\hat{H}_{\mathrm{el}} = \hat{H}_0 + \hat{H}_{\mathrm{ee}} \,, \tag{5.1}$$

where the one-body part, $\hat{H}_0$, reads as following

$$\hat{H}_0 = \int \mathrm{d}\mathbf{r} \ \hat{\psi}^\dagger(\mathbf{r}) h_0(\mathbf{r}) \hat{\psi}(\mathbf{r}) \,, \tag{5.2}$$

with

$$h_0(\mathbf{r}) = -\frac{\nabla^2}{2m} + V(\mathbf{r}) \,, \tag{5.3}$$

while the electron-electron interaction contribution is given by

$$\hat{H}_{\mathrm{ee}} = \int \mathrm{d}\mathbf{r} \ \mathrm{d}\mathbf{r}' \ \hat{\psi}^\dagger(\mathbf{r}) \, \hat{\psi}^\dagger(\mathbf{r}') \, U(|\mathbf{r} - \mathbf{r}'|) \, \hat{\psi}(\mathbf{r}') \, \hat{\psi}(\mathbf{r}) \,. \tag{5.4}$$

Here, $V(\mathbf{r})$ and $U(|\mathbf{r} - \mathbf{r}'|)$ represent a generic one-body and two-body interaction potential, respectively.

The electron system is invariant under a global phase transformation $\hat{\psi}(\mathbf{r}) \to e^{i\theta}\hat{\psi}(\mathbf{r})$, and the associate Noether current reads

$$\hat{\mathbf{J}}(\mathbf{r}) = \hat{\psi}^\dagger(\mathbf{r}) \, (-i\nabla) \, \hat{\psi}(\mathbf{r}) + \mathrm{H}.c. \,. \tag{5.5}$$

However, the system is not invariant under a local phase transformation, $\hat{\psi}(\mathbf{r}) \to e^{i\theta(\mathbf{r})}\hat{\psi}(\mathbf{r})$. Such invariance can be restored by introducing the interaction with the electromagnetic field, by employing a minimal coupling scheme. Considering the Coulomb gauge—the effects of the

scalar potential being already described by $V(\mathbf{r})$ and $U(|\mathbf{r} - \mathbf{r}'|)$—the total light-matter Hamiltonian is given by:

$$\hat{H}_C = \int d\mathbf{r}\, \hat{\psi}^\dagger(\mathbf{r}) h_C(\mathbf{r}) \hat{\psi}(\mathbf{r}) + \hat{H}_{ee} + \hat{H}_{ph}\,, \qquad (5.6)$$

where

$$h_C(\mathbf{r}) = \hat{T}_{\mathbf{A}} + V(\mathbf{r})\,, \qquad (5.7)$$

and

$$\hat{T}_{\mathbf{A}} = \frac{1}{2m}\left[-i\nabla + e\hat{\mathbf{A}}(\mathbf{r})\right]^2\,. \qquad (5.8)$$

Here, $e > 0$ is the elementary electron charge, c is the speed of light, and $\hat{\mathbf{A}}(\mathbf{r})$ is the space-dependent field operator vector describing the electromagnetic field in the Coulomb gauge. The Hamiltonian of the free field is given by

$$\hat{H}_{ph} = \frac{1}{2}\int d\mathbf{r}\left\{\frac{\hat{\boldsymbol{\Pi}}^2(\mathbf{r})}{\varepsilon_0} + \frac{[\nabla \times \hat{\mathbf{A}}(\mathbf{r})]^2}{\mu_0}\right\}\,, \qquad (5.9)$$

where $\hat{\boldsymbol{\Pi}}(\mathbf{r})$ is the conjugate momentum.

In this work, for simplicity, we will consider a single mode decomposition of the fields [219],

$$\hat{\mathbf{A}}(\mathbf{r}) = \mathbf{A}_0(\mathbf{r})(\hat{a} + \hat{a}^\dagger)\,, \qquad (5.10a)$$

$$\hat{\boldsymbol{\Pi}}(\mathbf{r}) = i\boldsymbol{\Pi}_0(\mathbf{r})(\hat{a} - \hat{a}^\dagger)\,. \qquad (5.10b)$$

Notice that such single-mode approximation has been widely adopted in the Literature [186–188, 192, 199–201, 203, 204, 207, 209, 215–217, 219] in the context of photon condensation.

In terms of the single-mode photon creation ($\hat{a}^\dagger$) and annihilation ($\hat{a}$) operators, the field Hamiltonian reduces to

$$\hat{H}_{ph} = \omega_{ph}\hat{a}^\dagger\hat{a}\,. \qquad (5.11)$$

A transformation of both the electronic and electromagnetic fields of the form

$$\hat{\psi}(\mathbf{r}) \rightarrow e^{i\theta(\mathbf{r})}\hat{\psi}(\mathbf{r}) \tag{5.12a}$$

$$\hat{\mathbf{A}}(\mathbf{r}) \rightarrow \hat{\mathbf{A}}(\mathbf{r}) - \frac{1}{e}\nabla\theta(\mathbf{r}) , \tag{5.12b}$$

leaves the Hamiltonian in Eq. (5.6) invariant, which aligns with the gauge principle. We note that Eq. (5.6) omits the Zeeman coupling between the electron's spin and the magnetic component of the electromagnetic field. The exclusion of this term is justified either when the magnetic field is zero or when it can be disregarded in the spatial region where the field interacts with the electron system, as, for instance, in the dipole approximation.

In situations where the interaction of the matter system with the magnetic field can be overlooked, the vector potential involved in the interaction terms can be locally expressed as the gradient of a scalar field.

$$\mathbf{A}_0(\mathbf{r}) = \nabla\chi(\mathbf{r}) . \tag{5.13}$$

In the dipole approximation, $\chi(\mathbf{r})$ can be expressed as $\chi(\mathbf{r}) = \mathbf{r} \cdot \mathbf{A}_0$, with $\mathbf{A}_0$ being spatially uniform. Strict application of the dipole approximation (uniform vector potential) to semiconductors implies a total disregard of propagation effects within the medium. To neglect the interaction of the electron system with the magnetic field in an extended system such as a semiconductor, one can partition the entire medium into numerous cells of identical volume V_{cell} and apply the dipole approximation to each cell [220, 221]. The cell should be significantly smaller than the field wavelength (the typical choice is to take the unit cell of the crystal as such a unit). This partial relaxation of the dipole approximation (extended dipole approximation) can be realized using Eq. (5.13). We emphasize that Eq. (5.13) implies that the magnetic field $\mathbf{B}$ in the spatial region where the electronic field is non-negligible is zero, i.e., $\mathbf{B}(\mathbf{r}) \equiv \nabla \times \mathbf{A}_0(\mathbf{r}) = \nabla \times \nabla\chi(\mathbf{r}) = 0$.

When the interaction of the matter system with the magnetic field can be neglected, the minimal coupling replacement can also

be implemented by applying a unitary transformation to the bare electronic Hamiltonian. The unitary operator transforms the electronic field operators as follows [219]:

$$\hat{\mathcal{U}}\hat{\psi}(\mathbf{r})\hat{\mathcal{U}}^{\dagger} = e^{ie\chi(\mathbf{r})(\hat{a}+\hat{a}^{\dagger})}\hat{\psi}(\mathbf{r}) \,, \tag{5.14}$$

where

$$\hat{\mathcal{U}} = \exp\left[-ie(\hat{a}+\hat{a}^{\dagger})\int d\mathbf{r}\ \hat{\psi}^{\dagger}(\mathbf{r})\chi(\mathbf{r})\hat{\psi}(\mathbf{r})\right] \,. \tag{5.15}$$

Equation Eq. (5.14) is demonstrated in Ref. [3].

We stress that only the electronic Hamiltonian has to be transformed applying the unitary operator in Eq. (5.15), while the photonic field $\hat{a}$ is unchanged. The Hamiltonian in Eq. (5.6) can be rewritten as

$$\hat{H}_{\mathrm{C}} = \hat{H}_{\mathrm{ph}} + \hat{\mathcal{U}}(\hat{H}_0 + \hat{H}_{\mathrm{ee}})\hat{\mathcal{U}}^{\dagger} \,. \tag{5.16}$$

In theory, the equation presented can be further simplified by recognizing that the unitary transformation $\hat{\mathcal{U}}$ has no impact on the electron-electron interaction contribution to the Hamiltonian [219]. This can be expressed as $\hat{\mathcal{U}}\hat{H}_{\mathrm{ee}}\hat{\mathcal{U}}^{\dagger} = \hat{H}_{\mathrm{ee}}$. However, for the purpose of this proof, we won't rely on this property. In the Coulomb gauge, $\hat{H}_{\mathrm{C}}$ represents the complete Hamiltonian that describes light, matter, and their interactions.

We will now establish a no-go theorem for photon condensation by demonstrating that the expectation value of the photonic operator in the ground state is zero, denoted as the super-radiant order parameter: $\langle\hat{a}\rangle = 0$. In the following, we will provide a proof by contradiction. If there exists a ground state $|\psi_0\rangle$ characterized by a non-zero super-radiant order parameter $\alpha \equiv \langle\psi_0|\hat{a}|\psi_0\rangle \neq 0$, then it is feasible to find another state $|\psi\rangle$ with lower energy, contrary to the assumption that $|\psi_0\rangle$ is the ground state. Specifically, we extend a procedure from first-quantization to the second quantization framework, as developed in prior work [195]. It is worth noting that many theoretical analyses of photon condensation [193, 199, 215, 217], including those predicting its occurrence, neglect light-matter entanglement and assume that the

system's ground state factorizes into matter and light wave-functions, using a mean-field approximation for the light-matter interaction. In our approach, we do not make use of this assumption.

Let us consider the following unitary operator,

$$\hat{\mathcal{T}} = \hat{\mathcal{D}}(\alpha) \exp\left[-i2e\,\mathrm{Re}(\alpha)\int d\mathbf{r}\,\hat{\psi}^\dagger(\mathbf{r})\chi(\mathbf{r})\hat{\psi}(\mathbf{r})\right]\,, \tag{5.17}$$

where $\hat{\mathcal{D}}(\alpha) = \exp(-\alpha^*\hat{a} + \alpha\hat{a}^\dagger)$ is the displacement operator characterized by a displacement α. Photonic operators transform under the displacement as,

$$\hat{\mathcal{D}}(\alpha)\hat{a}\hat{\mathcal{D}}(\alpha)^\dagger = \hat{a} - \alpha\,, \tag{5.18}$$

The electronic and photonic fields transform under $\hat{\mathcal{T}}$ as,

$$\hat{\mathcal{T}}\hat{\psi}(\mathbf{r})\hat{\mathcal{T}}^\dagger = e^{i2e\,\mathrm{Re}(\alpha)\chi(\mathbf{r})}\hat{\psi}(\mathbf{r}) \tag{5.19a}$$

$$\hat{\mathcal{T}}\hat{a}\hat{\mathcal{T}}^\dagger = \hat{a} - \alpha\,, \tag{5.19b}$$

where in the second line we considered that the operator $\exp\left[-i2e\,\mathrm{Re}(\alpha)\int d\mathbf{r}\,\hat{\psi}^\dagger(\mathbf{r})\chi(\mathbf{r})\hat{\psi}(\mathbf{r})\right]$ does not act on the photonic sector and then Eq. (5.18) to transform the photon operator.

We remind that we assumed as an hypothesis that the Hamiltonian of Eq. (5.16) has a ground state $|\psi_0\rangle$ with a non-vanishing expectation value of the photonic annihilation operator ($\alpha \equiv \langle\psi_0|\hat{a}|\psi_0\rangle \neq 0$). We now consider the state $|\psi\rangle = \hat{\mathcal{T}}^\dagger|\psi_0\rangle$. By means of Eq. (5.19b) we can prove that such state has zero order parameter,

$$\langle\psi|\hat{a}|\psi\rangle = \langle\psi_0|\hat{\mathcal{T}}\hat{a}\hat{\mathcal{T}}^\dagger|\psi_0\rangle = 0, \tag{5.20}$$

where we employed the assumption $\langle\psi_0|\hat{a}|\psi_0\rangle = \alpha$. In the following we show that the trial state $|\psi\rangle = \hat{\mathcal{T}}^\dagger|\psi_0\rangle$ has lower energy than $|\psi_0\rangle$, contradicting the initial assumption that $|\psi_0\rangle$ is the ground state.

First, we can prove that,

$$\hat{\mathcal{D}}(\alpha)\hat{\mathcal{U}}^\dagger\hat{\mathcal{D}}(\alpha)^\dagger = \exp\left[-i2e\,\mathrm{Re}(\alpha)\int d\mathbf{r}\,\hat{\psi}^\dagger(\mathbf{r})\chi(\mathbf{r})\hat{\psi}(\mathbf{r})\right]\hat{\mathcal{U}}^\dagger, \tag{5.21}$$

where we used that, by means of Eq. (5.19b), $\hat{\mathcal{D}}(\alpha)(\hat{a} + \hat{a}^\dagger)\hat{\mathcal{D}}(\alpha)^\dagger = (\hat{a} + \hat{a}^\dagger) - 2\,\mathrm{Re}(\alpha)$. Before proceeding, it is useful to consider the operators product $\hat{\mathcal{U}}^\dagger\hat{\mathcal{T}}^\dagger$,

$$\hat{\mathcal{U}}^\dagger\hat{\mathcal{T}}^\dagger = \hat{\mathcal{D}}^\dagger(\alpha)\hat{\mathcal{D}}(\alpha)\hat{\mathcal{U}}^\dagger\hat{\mathcal{D}}^\dagger(\alpha)\exp\left[i2e\,\mathrm{Re}(\alpha)\int d\mathbf{r}\,\hat{\psi}^\dagger(\mathbf{r})\chi(\mathbf{r})\hat{\psi}(\mathbf{r})\right],\tag{5.22}$$

where we expressed $\hat{\mathcal{T}}$ by using the definition in Eq. (5.17) and we inserted a product of displacement operators by means of the identity $\hat{\mathcal{D}}^\dagger(\alpha)\hat{\mathcal{D}}(\alpha) = 1$. By using Eq. (5.21) the previous expression can be simplified as,

$$\hat{\mathcal{U}}^\dagger\hat{\mathcal{T}}^\dagger = \hat{\mathcal{D}}^\dagger(\alpha)\hat{\mathcal{U}}^\dagger.\tag{5.23}$$

Now we evaluate the total Coulomb Hamiltonian on the trial state $|\psi\rangle = \hat{\mathcal{T}}^\dagger|\psi_0\rangle$,

$$\langle\psi|\hat{H}_\mathrm{C}|\psi\rangle = \langle\psi_0|\left[\hat{\mathcal{T}}\hat{\mathcal{U}}(\hat{H}_0 + \hat{H}_\mathrm{ee})\hat{\mathcal{U}}^\dagger\hat{\mathcal{T}}^\dagger + \hat{\mathcal{T}}\hat{H}_\mathrm{ph}\hat{\mathcal{T}}^\dagger\right]|\psi_0\rangle.\tag{5.24}$$

On one hand, the matter Hamiltonian can be simplified as,

$$\langle\psi_0|\hat{\mathcal{T}}\hat{\mathcal{U}}(\hat{H}_0 + \hat{H}_\mathrm{ee})\hat{\mathcal{U}}^\dagger\hat{\mathcal{T}}^\dagger|\psi_0\rangle = \langle\psi_0|\hat{\mathcal{U}}^\dagger(\hat{H}_0 + \hat{H}_\mathrm{ee})\hat{\mathcal{U}}|\psi_0\rangle,\tag{5.25}$$

where we used the property $\hat{\mathcal{U}}^\dagger\hat{\mathcal{T}}^\dagger = \hat{\mathcal{D}}^\dagger(\alpha)\hat{\mathcal{U}}^\dagger$ given in Eq. (5.23) and the fact that the displacement operator leaves invariant the matter Hamiltonian $\hat{H}_0 + \hat{H}_\mathrm{ee}$, $\hat{\mathcal{D}}(\alpha)(\hat{H}_0 + \hat{H}_\mathrm{ee})\hat{\mathcal{D}}^\dagger(\alpha) = \hat{H}_0 + \hat{H}_\mathrm{ee}$. On the other hand, by means of Eq. (5.19b), we can calculate the average value of the photonic Hamiltonian $\hat{H}_\mathrm{ph}$,

$$\langle\psi_0|\hat{\mathcal{T}}\hat{H}_\mathrm{ph}\hat{\mathcal{T}}^\dagger|\psi_0\rangle = \langle\psi_0|\left[\omega_\mathrm{ph}(\hat{a}^\dagger\hat{a} + |\alpha|^2) - \omega_\mathrm{ph}(\alpha\hat{a}^\dagger + \alpha^*\hat{a})\right]|\psi_0\rangle.\tag{5.26}$$

, By using that, by construction, we have $\langle\psi_0|\hat{a}|\psi_0\rangle = \alpha$, Eq. (5.26) simplifies to,

$$\langle\psi_0|\hat{\mathcal{T}}\hat{H}_\mathrm{ph}\hat{\mathcal{T}}^\dagger|\psi_0\rangle = \omega_\mathrm{ph}\left(\hat{a}^\dagger\hat{a} - |\alpha|^2\right).\tag{5.27}$$

By combining Eq. (5.27) and Eq. (5.25) and the definition of the total Coulomb Hamiltonian in Eq. (5.16) we have,

$$\langle\psi|\hat{H}_{\mathrm{C}}|\psi\rangle = \langle\psi_0|\hat{H}_{\mathrm{C}}|\psi_0\rangle - \omega_{\mathrm{ph}}|\alpha|^2\,. \tag{5.28}$$

Noticing that $\omega_{\mathrm{ph}}|\alpha|^2$ is by hypothesis a positive and strictly non-zero quantity we have,

$$\langle\psi|\hat{H}_{\mathrm{C}}|\psi\rangle < \langle\psi_0|\hat{H}_{\mathrm{C}}|\psi_0\rangle\,. \tag{5.29}$$

This equation implies that the state $|\psi_0\rangle$, which has a non-vanishing expectation value of the photon annihilation operator $\hat{a}$, is not the real ground state of the system, since the state $|\psi\rangle$, which was built specifically to have a vanishing expectation value, has a lower energy. This concludes the proof by contradiction that super-radiant phase transitions to a photon condensate is forbidden for any interacting light-matter system which can be described by an effective Hamiltonian as Eq. (5.16)

We close by noticing that this result applies also to the case of a multi-mode cavity field, provided that it still corresponds to the physical situation of $\mathbf{B} = \mathbf{0}$. In the absence of a magnetic field, the most general coupling to a transverse electric field is given by the following unitary transformation,

$$\hat{\mathcal{U}} = \exp\left[-ie\sum_i(\hat{a}_i + \hat{a}_i^\dagger)\int\mathrm{d}\mathbf{r}\ \hat{\psi}^\dagger(\mathbf{r})\chi_i(\mathbf{r})\hat{\psi}(\mathbf{r})\right]\,, \tag{5.30}$$

While Eq. (5.6) neglects the Zeeman coupling, our main conclusion can be easily generalized also to the case in which such coupling is present. The Zeeman coupling is proportional to the scalar product of the electron spin operator and the magnetic field, i.e. $\hat{\sigma} \cdot \hat{\mathbf{B}}(\mathbf{r})$. Since in this work $\mathbf{B}(\mathbf{r}) = \nabla \times \mathbf{A}_0(\mathbf{r}) = \mathbf{0}$, the Zeeman coupling does not alter the above analysis.

Finally, we stress that the photon condensate order parameter has been defined as $\langle\hat{a}\rangle$ in the Coulomb gauge. The quantity $\langle\hat{a}\rangle$ is not a

physical, gauge-invariant quantity [84, 213, 214]. For example, in the dipolar gauge, $\langle \hat{a} \rangle$ measures spontaneous polarization of matter, which is a signature of ferroelectricity [203]. In contrast, In contrast, we here choose as order parameter the displacement field due to transverse photons, which coincides with $\langle \hat{a} \rangle$ only in the Coulomb gauge. This is a well defined gauge-invariant quantity and our no-go theorem manifests in other gauges as the absence of a transverse electromagnetic field. Of course, when applying a gauge (unitary) transformation, invariant expectation values are obtained only transforming accordingly both the quantum states and the operators, see, e.g., Ref [84].

5.2.2 Interacting electrons on a lattice

The methodology delineated earlier is extendable to scenarios involving electron interactions on a lattice, which involves a discretized spatial domain. The primary distinctions from the continuous scenario encompass: (i) the transformation of the integral into a discrete summation ($\int d\mathbf{r} \to \sum_{\mathbf{r}_i}$), (ii) the substitution of the electronic field with a fermionic annihilation operator ($\hat{\psi}(\mathbf{r}) \to \hat{c}_{\mathbf{r}_i}$, adhering to the anti-commutation property $\{\hat{c}_{\mathbf{r}_i}, \hat{c}_{\mathbf{r}_j}^\dagger\} = \delta_{\mathbf{r}_i, \mathbf{r}_j}$). Consequently, the Hamiltonians for one-body electron and electron-electron interaction, articulated in Eqs. (5.2) and (5.4) respectively, become

$$\hat{H}_0 = \sum_{\mathbf{r}_i, \mathbf{r}_j} \tau_{\mathbf{r}_i, \mathbf{r}_j} \hat{c}_{\mathbf{r}_i}^\dagger \hat{c}_{\mathbf{r}_j} \tag{5.31a}$$

$$\hat{H}_{\text{ee}} = \sum_{\mathbf{r}_i, \mathbf{r}_j} U_{\mathbf{r}_i, \mathbf{r}_j} \hat{c}_{\mathbf{r}_i}^\dagger \hat{c}_{\mathbf{r}_j}^\dagger \hat{c}_{\mathbf{r}_j} \hat{c}_{\mathbf{r}_i} , \tag{5.31b}$$

where $\tau_{\mathbf{r}_i, \mathbf{r}_j} = \Omega_{\mathbf{r}_i} \delta_{\mathbf{r}_i, \mathbf{r}_j} + t_{\mathbf{r}_i} \delta_{\langle \mathbf{r}_i, \mathbf{r}_j \rangle}$ describes the on-site energies and the near-neighbor hopping factors (where $\langle \mathbf{r}_i, \mathbf{r}_j \rangle$ denotes near-neighbor sites), while $U_{\mathbf{r}_i, \mathbf{r}_j}$ is a symmetric operator, since the electron-electron interaction potential $U(|\mathbf{r} - \mathbf{r}'|)$ expressed in Eq. (5.4) depends only on the distance between the two points $\mathbf{r}$ and $\mathbf{r}'$.

However, in general, the truncation of the Hilbert space, could introduce some kind of spatial non-locality in the electron-electron

interaction [78]. Hence, it can be useful to also consider the generalized version of $\hat{H}_{\text{ee}}$ which includes also non-local effects

$$\hat{H}_{\text{ee}}^{\text{nl}} = \sum_{\substack{\mathbf{r}_i, \mathbf{r}_j \\ \mathbf{r}_l, \mathbf{r}_m}} U_{\mathbf{r}_i, \mathbf{r}_j}^{\mathbf{r}_l, \mathbf{r}_m} \hat{c}_{\mathbf{r}_i}^{\dagger} \hat{c}_{\mathbf{r}_j}^{\dagger} \hat{c}_{\mathbf{r}_m} \hat{c}_{\mathbf{r}_l} . \tag{5.32}$$

The previous Hamiltonian appears for example in the context of non-Fermi liquid states of matter. With a suitable choice of the parameters $U_{\mathbf{r}_i, \mathbf{r}_j}^{\mathbf{r}_l, \mathbf{r}_m}$ it indeed coincides with the so-called SYK model [222, 223]. The generalized electron-electron interaction term $\hat{H}_{\text{ee}}^{\text{nl}}$ reduces to the usual interaction Hamiltonian $\hat{H}_{\text{ee}}$ for

$$U_{\mathbf{r}_i, \mathbf{r}_j}^{\mathbf{r}_l, \mathbf{r}_m} = U_{\mathbf{r}_i, \mathbf{r}_j} \delta_{\mathbf{r}_i, \mathbf{r}_l} \delta_{\mathbf{r}_j, \mathbf{r}_m} . \tag{5.33}$$

The interaction with a single-mode cavity field is again introduced by applying a unitary transformation to the electronic fields (which now become the fermionic operators $\hat{c}_{\mathbf{r}_i}$) in a manner similar to Eq. (5.14), that is

$$\hat{\mathcal{U}} \hat{c}_{\mathbf{r}_i} \hat{\mathcal{U}}^{\dagger} = e^{ie\chi_{\mathbf{r}_i}(\hat{a} + \hat{a}^{\dagger})} \hat{c}_{\mathbf{r}_i} , \tag{5.34}$$

with

$$\hat{\mathcal{U}} = \exp\left[-ie(\hat{a} + \hat{a}^{\dagger}) \sum_{\mathbf{r}_i} \chi_{\mathbf{r}_i} \hat{c}_{\mathbf{r}_i}^{\dagger} \hat{c}_{\mathbf{r}_i}\right] . \tag{5.35}$$

Eq. (5.34), can be seen as the equivalent of the Peierls substitution [224]. Such procedure can be regarded as a particular instance of lattice gauge theory, the general method developed by Wilson for studying non-perturbative relativistic gauge theories on a lattice [225]. The obtained coupled light-matter Hamiltonian is similar to the continuum case expressed in Eq. (5.16),

$$\hat{H}_{\text{C}} = \hat{H}_{\text{ph}} + \hat{\mathcal{U}} \left(\hat{H}_0 + \hat{H}_{\text{ee}}^{\text{nl}}\right) \hat{\mathcal{U}}^{\dagger} , \tag{5.36}$$

where $\hat{H}_{\text{ph}}$ is defined in Eq. (5.11) and signifies the bare photonic Hamiltonian. It's important to note that, as we have taken into account the generalized form of the electron-electron interaction

term that includes non-locality, $\hat{H}_{\text{ee}}^{\text{nl}}$ might not commute with $\hat{\mathcal{U}}$ any longer. However, this characteristic is not a prerequisite for the proof, which remains valid in this instance as well. We do note that the existence of such a non-local potential suggests that the resultant comprehensive light-matter Hamiltonian will incorporate supplementary terms originating from $\hat{\mathcal{U}}\hat{H}_{\text{ee}}^{\text{nl}}\hat{\mathcal{U}}^{\dagger}$. These terms are vital to maintain gauge invariance, even when an effective non-local potential is present [75].

The proof of the no-go theorem for interacting electrons systems on a lattice is now straightforward, and it follows the same steps applied to the continuum case in Section 5.2.1. We start by introducing the lattice version of the unitary operator expressed in Eq. (5.17)

$$\hat{\mathcal{T}} = \exp\left[-ie2\operatorname{Re}(\alpha)\sum_{\mathbf{r}_i}\chi_{\mathbf{r}_i}\hat{c}_{\mathbf{r}_i}^{\dagger}\hat{c}_{\mathbf{r}_i}\right]\hat{\mathcal{D}}(\alpha)\,, \tag{5.37}$$

which transforms the electronic and photonic operators as

$$\hat{\mathcal{T}}\hat{c}_{\mathbf{r}_i}\hat{\mathcal{T}}^{\dagger} = e^{ie2\operatorname{Re}(\alpha)\chi_{\mathbf{r}_i}}\hat{c}_{\mathbf{r}_i}\,, \tag{5.38a}$$

$$\hat{\mathcal{T}}\hat{a}\hat{\mathcal{T}}^{\dagger} = \hat{a} - \alpha\,. \tag{5.38b}$$

Once again, we now suppose that the system described by the Hamiltonian (5.36) has a ground state $|\psi_0\rangle$ with a non-vanishing expectation value of the photonic annihilation operator. We now construct a trial state $|\psi\rangle = \hat{\mathcal{T}}^{\dagger}|\psi_0\rangle$ with the property $\langle\psi|\hat{a}|\psi\rangle = 0$. Following similar steps Section 5.2.1 we can prove the property, $\hat{\mathcal{U}}^{\dagger}\hat{\mathcal{T}}^{\dagger} = \hat{\mathcal{D}}^{\dagger}(\alpha)\hat{\mathcal{U}}^{\dagger}$, corresponding to Eq. (5.23). It is useful to note that,

$$\hat{\mathcal{T}}\hat{\mathcal{U}}(\hat{H}_0 + \hat{H}_{\text{ee}})\hat{\mathcal{U}}^{\dagger}\hat{\mathcal{T}}^{\dagger} = \hat{\mathcal{U}}\hat{\mathcal{D}}(\alpha)(\hat{H}_0 + \hat{H}_{\text{ee}})\hat{\mathcal{D}}^{\dagger}(\alpha)\hat{\mathcal{U}}^{\dagger} = \hat{\mathcal{U}}(\hat{H}_0 + \hat{H}_{\text{ee}})\hat{\mathcal{U}}^{\dagger}\,, \tag{5.39}$$

where we used Eq. (5.23) and the fact that $\hat{\mathcal{D}}(\alpha)$ commutes with $\hat{H}_0 + \hat{H}_{\text{ee}}$. Hence, the total energy of the the trial state $|\psi\rangle$ reads:

$$\langle\psi|\hat{H}_{\text{C}}|\psi\rangle = \langle\psi_0|\left[\hat{\mathcal{U}}(\hat{H}_0 + \hat{H}_{\text{ee}})\hat{\mathcal{U}}^{\dagger} + \hat{\mathcal{T}}\hat{H}_{\text{ph}}\hat{\mathcal{T}}^{\dagger}\right]|\psi_0\rangle\,. \tag{5.40}$$

From Eq. (5.40) and employing Eq. (5.38b), the energy finally reads,

$$\langle\psi|\hat{H}_C|\psi\rangle = \langle\psi_0|\hat{H}_C|\psi_0\rangle - \hbar\omega_{\mathrm{ph}}|\alpha|^2 \,. \tag{5.41}$$

Again, we find that $|\psi_0\rangle$ cannot be the ground state of the system, since there is a lower energy state $|\psi\rangle$ with the property that $\langle\psi|\hat{a}|\psi\rangle = 0$, forbidding the superradiant phase transition for such system.

As observed, the incorporation of approximations, such as the conversion of continuous space into a lattice, could lead to a form of spatial non-locality. Moreover, in the realm of solid-state physics, the shift from the continuum to the lattice is typically executed in a marginally different manner. For instance, in line with the tight-binding method, it is feasible to accommodate multiple orbitals at each lattice site. As suggested in Ref. [219], we can assign the orbital index μ to each site within the tight-binding framework. Under these circumstances, the Hamiltonians for one-body electron and non-local electron-electron interaction transform respectively into

$$\hat{H}_0 = \sum_{\mathbf{r}_i,\mathbf{r}_j} \sum_{\mu_1,\mu_2} \tau_{\mathbf{r}_i,\mathbf{r}_j,\mu_1,\mu_2} \hat{c}^\dagger_{\mathbf{r}_i,\mu_1} \hat{c}_{\mathbf{r}_j,\mu_2} \tag{5.42a}$$

$$\hat{H}_{\mathrm{ee}}^{\mathrm{nl}} = \sum_{\substack{\mathbf{r}_i,\mathbf{r}_j \\ \mathbf{r}_l,\mathbf{r}_m}} \sum_{\substack{\mu_1,\mu_2 \\ \mu_3,\mu_3}} U^{\mathbf{r}_l,\mathbf{r}_m,\mu_3,\mu_4}_{\mathbf{r}_i,\mathbf{r}_j,\mu_1,\mu_2} \hat{c}^\dagger_{\mathbf{r}_i,\mu_1} \hat{c}^\dagger_{\mathbf{r}_j,\mu_2} \hat{c}_{\mathbf{r}_m,\mu_3} \hat{c}_{\mathbf{r}_l,\mu_4} \,,$$

and the unitary operator $\hat{\mathcal{U}}$ becomes

$$\hat{\mathcal{U}} = \exp\left[-ie(\hat{a} + \hat{a}^\dagger) \sum_{\mathbf{r}_i} \sum_{\mu} \chi_{\mathbf{r}_i,\mu} \; \hat{c}^\dagger_{\mathbf{r}_i,\mu} \hat{c}_{\mathbf{r}_i,\mu}\right] \,. \tag{5.43}$$

The proof of the no-go theorem follows the same procedure applied to the previous two cases.

5.3 Gauge invariance, photon condensation, and no-go theorem in M-level systems

Prior to advancing with the demonstration of the no-go theorem for a truncated model, we revisit the methodology to formulate M-level models that uphold gauge-invariance, notwithstanding the truncation of the Hilbert space. It is already established that the truncated minimal coupling substitution, presented in Section 1.4.3, is associated with the broad framework of lattice gauge theory and the so-called Peierls substitution [79]. In this context, we establish that this association persists even for M-level systems. The Hamiltonian for any M-level system can be expressed in the eigenstates $|m\rangle$ basis as follows:

$$\hat{h}_0 = \sum_{m=1}^{M} \epsilon_m |m\rangle\langle m| \, . \tag{5.44}$$

In the Coulomb gauge, and in the case of a single-mode spatially uniform vector potential $A = A_0(\hat{a} + \hat{a}^\dagger)$, such system can be coupled to A as following [75]

$$\hat{h}_{\mathrm{C}} = \hat{\mathcal{U}}_1 \hat{h}_0 \hat{\mathcal{U}}_1^\dagger + \hat{\mathcal{H}}_{\mathrm{ph}} \, , \tag{5.45}$$

where $\hat{\mathcal{H}}_{\mathrm{ph}} = \hbar\omega_{\mathrm{ph}}\hat{a}^\dagger\hat{a}$ is the cavity Hamiltonian, and $\hat{\mathcal{U}}_1 = \exp[-ieA_0\hat{X}(\hat{a} + \hat{a}^\dagger)]$ has the purpose of carrying out the minimal coupling replacement within the dipole approximation. Here $\hat{X} = \hat{P}\hat{x}\hat{P}$ (with $\hat{P} = \sum_{m=1}^{M} |m\rangle\langle m|$) represents the truncated position operator.

We now consider a collection of N identical, non-interacting M-level atoms. The total bare Hamiltonian is

$$\hat{\mathcal{H}}_0 = \sum_{n=1}^{N} \sum_{m=1}^{M} \epsilon_m |m_n\rangle\langle m_n| \, , \tag{5.46}$$

and, by applying the method discussed above, we get the total interacting light-matter Hamiltonian:

$$\hat{\mathcal{H}}_{\mathrm{C}} = \hat{\mathcal{U}} \hat{\mathcal{H}}_0 \hat{\mathcal{U}}^\dagger + \hat{\mathcal{H}}_{\mathrm{ph}} \, , \tag{5.47}$$

where $\hat{\mathcal{U}} = \exp[-ieA_0 \sum_n \hat{X}_n(\hat{a}+\hat{a}^\dagger)]$, and $\hat{X}_n$ is the truncated position operator corresponding to the n-th atom.

We proceed to demonstrate that, given the Hamiltonian of a typical M-level matter system in interaction with an electromagnetic field possesses the structure outlined in Eq. (5.47), the photon annihilation operator $\hat{a}$ is incapable of having a non-zero expectation value in this system's ground state. We validate this using a methodology akin to the one employed in Section 5.2, which is grounded on the technique formulated in Ref. [195] for the conventional minimal coupling replacement scenario. We suppose that the ground state $|\psi_0\rangle$ of a system described by the Hamiltonian (5.47) has the property that $\langle\psi_0|\hat{a}|\psi_0\rangle \neq 0$. We introduce the following unitary operator:

$$\hat{\mathcal{T}} = \exp\left[-ieA_0 2\,\mathrm{Re}(\alpha) \sum_n \hat{X}_n\right] \hat{\mathcal{D}}(\alpha)\,, \qquad (5.48)$$

which has the property of shifting the electron momentum and, in particular, to shift the photon operators

$$\hat{\mathcal{T}}\hat{a}\hat{\mathcal{T}}^\dagger = \hat{a} - \alpha\,. \qquad (5.49)$$

Again, we construct the trial state as $|\psi\rangle = \hat{\mathcal{T}}^\dagger |\psi_0\rangle$, which is characterized by a zero order parameter,

$$\langle\psi|\hat{a}|\psi\rangle = 0\,. \qquad (5.50)$$

Similarly to Section 5.2, by means of Eq. (5.49), we can prove that,

$$\hat{\mathcal{D}}(\alpha)\hat{\mathcal{U}}^\dagger\hat{\mathcal{D}}^\dagger(\alpha) = \exp\left[-ieA_0 2\,\mathrm{Re}(\alpha) \sum_n \hat{X}_n\right] \hat{\mathcal{U}}^\dagger\,, \qquad (5.51)$$

and following the steps of Section 5.2 we can prove Eq. (5.23), $\hat{\mathcal{U}}^\dagger\hat{\mathcal{T}}^\dagger = \hat{\mathcal{D}}^\dagger(\alpha)\hat{\mathcal{U}}^\dagger$, also for the present case. The energy of the trial state $|\psi\rangle$ reads,

$$\langle\psi|\hat{\mathcal{H}}_\mathrm{C}|\psi\rangle = \langle\psi_0|\left[\hat{\mathcal{T}}\hat{\mathcal{U}}\hat{\mathcal{H}}_0\hat{\mathcal{U}}^\dagger\hat{\mathcal{T}}^\dagger + \hat{\mathcal{T}}\hat{\mathcal{H}}_\mathrm{ph}\hat{\mathcal{T}}^\dagger\right]|\psi_0\rangle\,. \qquad (5.52)$$

By means of Eq. (5.23) and Eq. (5.49), the energy reads,

$$\langle \psi | \hat{\mathcal{H}}_{\mathrm{C}} | \psi \rangle = \langle \psi_0 | \hat{\mathcal{H}}_{\mathrm{C}} | \psi_0 \rangle - \omega_{\mathrm{ph}} |\alpha|^2 \,. \tag{5.53}$$

Eq. (5.53) implies that the state $|\psi_0\rangle$, which has a non-vanishing expectation value of the photon annihilation operator $\hat{a}$, is not the real ground state of the system, since a lower energy state $|\psi\rangle$, which was built specifically to have a vanishing expectation value, has a lower energy. This ends the proof by contradiction. We have shown that the true ground-state of $\hat{\mathcal{H}}_{\mathrm{C}}$ is characterized by a vanishing super-radiant order parameter $\langle \hat{a} \rangle$.

5.3.1 Mapping onto a tight-binding lattice

As discussed in Section 1.4, under the dipole approximation, a two-level atom's interaction with the electromagnetic field can be equivalently portrayed as a double-well system. This system considers only the two lowest energy eigenstates, which subsequently corresponds to a two-site system interacting with a cavity field [79]. In this context, we broaden this concept to a generic M-level system, illustrating that it can be represented as a linear chain of sites interconnected by hopping processes (i.e., a tight-binding lattice).

We now define the following operator,

$$\hat{R} = -eA_0 \hat{x} \,. \tag{5.54}$$

In the basis of the eigenstates $|m\rangle$, $\hat{R}$ can be expressed as

$$\hat{R} = \sum_{m_1=0}^{M-1} \sum_{m_2=0}^{M-1} R_{m_1,m_2} |m_1\rangle \langle m_2| \,. \tag{5.55}$$

Since $\hat{R}$ is an Hermitian operator, it defines a basis of eigenvectors $|r\rangle$ such that:

$$\hat{R} |r\rangle = \lambda_r |r\rangle \,. \tag{5.56}$$

Recalling Eq. (5.54), the states $|r\rangle$ are also eigenvectors of the position operator, i.e. $\hat{x}|r\rangle = x_r |r\rangle$, with $\lambda_r = -eA_0 x_r$. As we will show momentarily, this local basis of eigenstates of the position operator $\hat{x}$ defines a natural lattice representation of the Hamiltonian $\hat{h}_0$.

We now introduce the unitary transformation $\hat{O}$, which connects the energy basis $|m\rangle$ with the position basis $|r\rangle$. Its matrix elements will be denoted by the symbol $O_{r,m} \equiv \langle r|\hat{O}|m\rangle$. By definition, the following property holds true:

$$\delta_{r_1,r_2}\lambda_{r_1} = \sum_{m_1=0}^{M-1} \sum_{m_2=0}^{M-1} O_{r_1,m_1} R_{m_1,m_2} O^\dagger_{m_2,r_2} . \tag{5.57}$$

As this identity shows, the transformation $\hat{O}$ diagonalizes the position operator $\hat{R}$.

The lattice representation of the matter Hamiltonian $\hat{h}_0$ is given by

$$\hat{h}_0 = \sum_{r_1=0}^{M-1} \sum_{r_2=0}^{M-1} t_{r_1,r_2} |r_1\rangle \langle r_2| , \tag{5.58}$$

where the hopping matrix t_{r_1,r_2} is defined by

$$t_{r_1,r_2} = \sum_{m=0}^{M-1} O_{r_1,m} \epsilon_m O^\dagger_{m,r_2} . \tag{5.59}$$

It is worth noting that the Hamiltonian written above is on the same form of the one-body Hamiltonian on a lattice described by Eq. (5.2).

We are now in the position to write the Hamiltonian $\hat{h}_c$ (defined by Eq. (5.45)) in terms of the eigenvectors $|m\rangle$ of the position operator:

$$\begin{aligned}
\hat{h} &= \sum_{r_1=0}^{M-1} \sum_{r_2=0}^{M-1} e^{i\lambda_{r_1}(\hat{a}+\hat{a}^\dagger)} t_{r_1,r_2} e^{-i\lambda_{r_2}(\hat{a}+\hat{a}^\dagger)} |r_1\rangle \langle r_2| \\
&= \sum_{r_1=0}^{M-1} \sum_{r_2=0}^{M-1} e^{-ie(x_{r_1}-x_{r_2})(\hat{a}+\hat{a}^\dagger)} t_{r_1,r_2} |r_1\rangle \langle r_2| .
\end{aligned} \tag{5.60}$$

This is the main result of this Section. It shows that the coupled Hamiltonian $\hat{h}_c$ has the exact same form of a tight-binding lattice model coupled to light via the Peierls substitution. In fact, the Peierls approach was originally formulated to examine electron systems interacting with static magnetic fields, within the context of the tight-binding approximation. The Peierls substitution can be perceived as a precursor to lattice gauge theory, which is the comprehensive method devised by Wilson for investigating non-perturbative relativistic gauge theories on a lattice [225], or in the field of condensed matter physics, for scrutinizing quantum simulations of lattice gauge theories [226]. In this discussion, we have demonstrated that these two methodologies align when one operates in the position basis $|m\rangle$. Consequently, within the lattice basis, the Peierls substitution emerges as the most universal instrument for coupling matter with a singular cavity mode.

5.3.2 Example: a ladder three-level system

We now consider the particular case of a three-level ladder atom, which can be described as a three-site system with inversion symmetry, as depicted in Fig. 5.1. In this Section we show that, in stark contrast to the conclusions of Refs. [200, 201], such system does not display photon condensation.

The bare Hamiltonian of a single three-level ladder atom, expressed in the lattice representation (see Eq. (5.58)), reads as following:

$$\hat{h}_0 = \sum_{i=-1}^{1} \epsilon_i \, |i\rangle\langle i| + t(|-1\rangle\langle 0| + |0\rangle\langle 1| + \text{H.c.}) . \tag{5.61}$$

We consider here a system with parity symmetry, so that the selection rules for a three-level ladder atom apply: $\epsilon_{-1} = \epsilon_1$. From now on, we also fix $\epsilon_{-1} = \epsilon_1 = 0$. According to gauge lattice theory, the interaction with the electromagnetic field can be obtained by introducing the Wilson parallel transporter [225]. The resulting Hamiltonian, after applying the dipole approximation (uniform field),
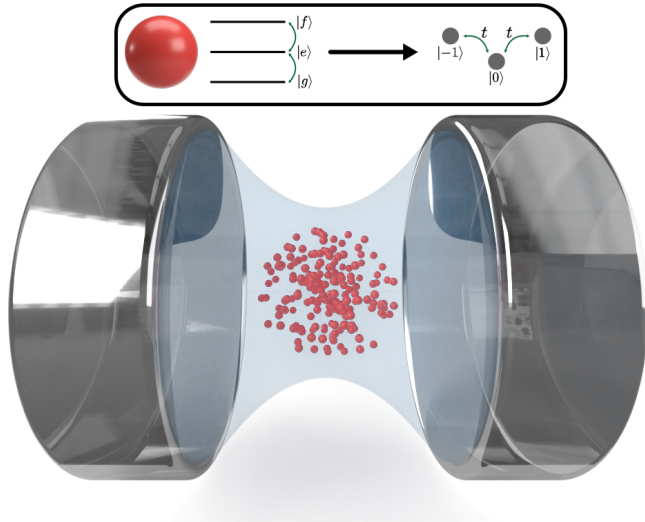
Figure 5.1: Graphical depiction of a group of three-level atoms interacting with a cavity field. Each atom, viewed in a ladder configuration, can be interpreted as a three-site system with nearest neighbor hopping and parity symmetry. The interaction with the electromagnetic field, according to the lattice gauge theory, can be derived using the Wilson parallel transporter.

is

$$\hat{h}_{\text{tot}} = \hat{\mathcal{H}}_{\text{ph}} + \hat{h}\,, \tag{5.62}$$

where $\hat{H}_{\text{ph}}$ is the free-photon Hamiltonian and $\hat{h}$ is the atomic Hamiltonian, now invariant under arbitrary (site-dependent) phase transformations:

$$\hat{h} = \epsilon_0 \left|0\right\rangle\!\left\langle0\right| + [te^{-i\gamma(\hat{a}^\dagger + \hat{a})}(\left|-1\right\rangle\!\left\langle0\right| + \left|0\right\rangle\!\left\langle1\right|) + \text{H.c.}]\,, \tag{5.63}$$

accordingly to Eq. (5.60). Her, $\gamma = -edA_0$ with d the distance between two adjacent sites. For simplicity, we assume a single mode optical resonator: $\hat{H}_{\text{ph}} = \hbar\omega_{\text{ph}}\hat{a}^\dagger\hat{a}$, with the field coordinate $\hat{A} = A_0(\hat{a}^\dagger + \hat{a})$, where A_0 is the vacuum fluctuation amplitude.

117

The Hamiltonian in Eq. (5.63) can also be written as

$$\hat{h} = \hat{\mathcal{U}}_1 \hat{h}_0 \hat{\mathcal{U}}_1^\dagger \, , \tag{5.64}$$

where

$$\hat{\mathcal{U}}_1 = \exp\left[-ie\hat{x}_L\hat{A}\right] \, , \tag{5.65}$$

and $\hat{x}_L$ is the lattice coordinate, i.e. $\hat{x}_L = d\sum_j j\,|j\rangle\langle j|$.

Let us now consider a collection of N identical, non-interacting three-level ladder atoms. The total Hamiltonian is

$$\hat{\mathcal{H}} = \hat{\mathcal{H}}_{\text{ph}} + \epsilon_0\hat{\Sigma}_{0,0} + t[e^{-i\gamma(\hat{a}^\dagger+\hat{a})}(\hat{\Sigma}_{-1,0} + \hat{\Sigma}_{0,1}) + \text{H.c.}] \, , \tag{5.66}$$

where

$$\hat{\Sigma}_{i,j} = \sum_{k=1}^{N} |i_k\rangle\langle j_k| \, . \tag{5.67}$$

Equation (5.66) can be written compactly as

$$\hat{\mathcal{H}} = \hat{\mathcal{H}}_{\text{ph}} + \hat{\mathcal{U}}\hat{H}_0\hat{\mathcal{U}}^\dagger \tag{5.68}$$

where

$$\hat{H}_0 = \epsilon_0\hat{\Sigma}_{0,0} + t\left(\hat{\Sigma}_{-1,0} + \hat{\Sigma}_{0,1} + \text{H.c.}\right) \tag{5.69}$$

and

$$\hat{\mathcal{U}} = \exp\left[i\frac{\gamma}{2}\left(\hat{a} + \hat{a}^\dagger\right)\sum_{j=1}^{N} j\,\hat{\Sigma}_{j,j}\right] \, . \tag{5.70}$$

When the system's Hamiltonian is cast in the form of Eq. (5.68), the theorem demonstrated in the beginning of the section, showing that no photon condensation can occur, can be readily applied to this case.

5.4 Towards superradiant phase transitions in magnonic systems

In this section we briefly discuss the magnon-photon interaction in the context of cavity QED. One of the most interesting features of this systems is the Zeeman-like coupling between the collective spin waves (magnons) and the electromagnetic field. Is has been shown that this coupling does not have any $\hat{A}^2$ term in the Hamiltonian, and thus there is the possibility to achieve photon condensation under certain parameters [217]. Recently, the ultrastrong coupling between magnons and photons has been achieved [7], showing a negligible contribution of the diamagnetic term in the parameters fitting, and thus confirming the theory of Zeeman-like coupling.

The interaction between magnetic excitations and electromagnetic radiation has recently become a central focus in numerous research fields such as magnonics, spintronics, magneto-opto-mechanics, and information processing due to its potential for the development of hybrid systems and devices [227–230]. The manipulation of magnon-photon coupling and cooperativity is a crucial aspect for harnessing the unique functionalities associated with the coherent dynamics in these systems. New applications, including memory devices [231], coherent spin pumping [232], haloscopes for axion detection [233], microwave-optical transducers [234] and coherent microwave sources [235] have already been explored. A current challenge is the creation of all-on-chip devices for their efficient integration into microwave circuits [230].

In the typical scenario of a ferromagnetic sample embedded in a microwave resonator, spin waves couple with resonant electromagnetic modes [236] and the system can be modeled by combining Maxwell and Landau-Lifshitz-Gilbert (LLG) equations [237, 238]. This classical description is remarkably effective in the case of the ferrimagnetic Yttrium Iron Garnet (YIG) [229], which has been extensively studied due to its combination of several optimal features, including the exceptionally low damping of magnetization precession [239].

In the quantum regime, spin waves are collective (bosonic) excitations (magnons) that may coherently interact with cavity photons [240, 241], and its interaction is well described by the Dicke model because of the Zeeman interaction. The USC regime was first reported in the case of mm-size YIG crystals in 3D cavities [46, 242–245] and few other magnetic materials [67, 246–248]. In view of the realization of scalable architectures, small magnets coupled to superconducting planar resonant geometries have been recently designed and observed to achieve the (ultra-)strong coupling regime [249–256].

In this section, we illustrate the attainment of high coupling rates by placing the magnetic film in direct contact with the superconducting resonator. In our setup, the excitation of spin waves occurs at the superconductor/ferrimagnet interface, where the amplitude of the microwave field reaches its peak. The optimized magnon-photon coupling leads to collective coupling strengths as large as 0.2 times the cavity frequency. Data analysis, conducted with a modified Hopfield model for which we provide an exact solution, also reveals negligible diamagnetic coupling for magnon excitations in YIG [7].

5.4.1 Theoretical model

We model our system by considering a quantized single-mode electro-magnetic field (with ω_c cavity frequency) interacting with an ensemble of magnetic moments. We consider collective operators for the spin ensemble, the quantization of both spin excitations and the electro-magnetic field which allows us to introduce the respective bosonic operators $\hat{a}$ and $\hat{b}$. Due to the vanishing orbital angular momentum of Fe^{3+} in YIG [238], we expect a prominent Zeeman interaction of the type $\hat{\mathcal{H}}_Z = -g_e \hat{\sigma} \cdot \mu_B \hat{\mathbf{h}}$ for a single spin. Here $[\hat{\sigma}_j, \hat{\sigma}_k] = i\epsilon_{jkl}\hat{\sigma}_l$ are the Pauli operators, $\hat{\mathbf{h}}$ is the magnetic field component of the cavity resonator while μ_B is the Bohr magneton and $g_e \approx 2$ in the case of a simple electron. However, to not exclude the possibility of having orbital angular momentum contributions in our hybrid system, we also

consider this degree of freedom including a diamagnetic term, which comes from the usual minimal coupling replacement.

The total Hamiltonian then reads ($\hbar = 1$)

$$
\begin{aligned}
\hat{\mathcal{H}} = {} & \omega_c \hat{a}^\dagger \hat{a} + \frac{\omega_b}{2} \sum_{j=1}^{N} \sigma_z^{(j)} + \frac{\lambda}{2\sqrt{N}} \sum_{j=1}^{N} \sigma_x^{(j)} \left(\hat{a} + \hat{a}^\dagger \right) \\
& + \beta \left(\hat{a} + \hat{a}^\dagger \right)^2 ,
\end{aligned}
\tag{5.71}
$$

where $\hat{a}$ ($\hat{a}^\dagger$) is the photon annihilation (creation) operator, ω_c is the cavity resonance frequency, ω_b is the resonance frequency of a single spin, λ is the collective light-matter coupling, and β is the coefficient of the diamagnetic term.

By using the collective spin operators $\hat{J}_z \equiv (1/2) \sum_{j=1}^{N} \hat{\sigma}_z^{(j)}$ and $\hat{J}_x = \hat{J}_+ + \hat{J}_- \equiv (1/2) \sum_{j=1}^{N} \hat{\sigma}_x^{(j)}$, we can apply the Holstein-Primakoff transformations [257]

$$
\hat{J}_z \to \hat{b}^\dagger \hat{b} - \frac{N}{2} , \quad \hat{J}_+ \to \hat{b}^\dagger \sqrt{N - \hat{b}^\dagger \hat{b}} , \quad \hat{J}_- = \hat{J}_+^\dagger ,
\tag{5.72}
$$

where $\hat{b}$ and $\hat{b}^\dagger$ are the magnon annihilation and creation operators respectively, which obey to the standard bosonic commutation relations. In the thermodynamic limit (i.e. $N \to \infty$) we can approximate $\hat{J}_+ \approx \sqrt{N} \hat{b}^\dagger$. Then, by applying the Holstein-Primakoff transformation, we obtain:

$$
\hat{\mathcal{H}} = \omega_c \hat{a}^\dagger \hat{a} + \omega_b \hat{b}^\dagger \hat{b} + \lambda \left(\hat{b} + \hat{b}^\dagger \right) \left(\hat{a} + \hat{a}^\dagger \right) + \beta \left(\hat{a} + \hat{a}^\dagger \right)^2 ,
\tag{5.73}
$$

that is the well-known Hopfield Hamiltonian [182].

We consider the dependence of the magnon resonance frequency ω_b to the external magnetic field H_0 as described by $\omega_b = \sqrt{\omega_H(\omega_H + \omega_M)} + \Delta$, leaving as the sole free parameter the energy shift Δ characterizing high frequency magnons for the next step of our investigation. In our analysis we also leave as free parameters the

cavity frequency ω_c, the collective coupling λ and the factor of the diamagnetic term β.

The Hamiltonian in Eq. (5.73) can be expressed in terms of two non-interacting harmonic oscillators $\hat{\mathcal{H}} = \Omega_- \hat{P}_-^\dagger \hat{P}_- + \Omega_+ \hat{P}_+^\dagger \hat{P}_+$, where $\hat{P}_\pm$ are the polariton operators, which are linear combinations of light and matter operators $\hat{P}_\mu = c_1^{(\mu)} \hat{a} + c_2^{(\mu)} \hat{b} + c_3^{(\mu)} \hat{a}^\dagger + c_4^{(\mu)} \hat{b}^\dagger$, with $\mu = \pm$. To fit our parameters, we need first to find the polariton frequencies, and, being a proper bosonic excitation of the system, the operator $\hat{P}_\mu$ fulfills the equation of motion of the harmonic oscillator $[\hat{P}_\mu, \hat{\mathcal{H}}] = \Omega_\mu \hat{P}_\mu$. Since the polariton operator $\hat{P}_\mu$ is a linear combination of the light and matter operators, we need to calculate first the commutator of the latter with the Hamiltonian

$$
\begin{aligned}
\left[\hat{a}, \hat{\mathcal{H}}\right] &= \omega_c \hat{a} + \lambda \left(\hat{b} + \hat{b}^\dagger\right) \\
\left[\hat{b}, \hat{\mathcal{H}}\right] &= \omega_b \hat{b} + \lambda \left(\hat{a} + \hat{a}^\dagger\right) \\
\left[\hat{a}^\dagger, \hat{\mathcal{H}}\right] &= -\omega_c \hat{a}^\dagger - \lambda \left(\hat{b} + \hat{b}^\dagger\right) \\
\left[\hat{b}^\dagger, \hat{\mathcal{H}}\right] &= -\omega_b \hat{b}^\dagger - \lambda \left(\hat{a} + \hat{a}^\dagger\right),
\end{aligned}
$$

and the polariton frequencies Ω_μ are obtained by finding the positive eigenvalues of the following Hopfield matrix

$$
\mathcal{M} = \begin{pmatrix}
\omega_c + 2\beta & \lambda & -2\beta & -\lambda \\
\lambda & \omega_b & -\lambda & 0 \\
2\beta & \lambda & -\omega_c - 2\beta & -\lambda \\
\lambda & 0 & -\lambda & -\omega_b
\end{pmatrix}.
\tag{5.74}
$$

leading to:

$$
\Omega_\pm = \frac{1}{\sqrt{2}} \sqrt{\tilde{\omega}_c^2 + \omega_b^2 \pm \sqrt{(\tilde{\omega}_c^2 - \omega_b^2)^2 + 16\omega_c \omega_b \lambda^2}},
\tag{5.75}
$$

where $\tilde{\omega}_c = \sqrt{\omega_c(\omega_c + 4\beta)}$.

The aforementioned equation provides an excellent fit for the S_{21} spectrum peaks. The optimal fit result, depicted in Fig. 5.2, was
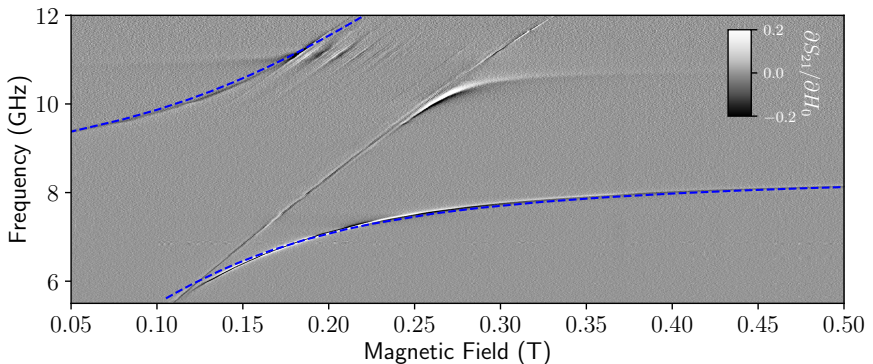
Figure 5.2: Best fit of the transmission spectrum obtained with the YIG film pressed on top of the superconducting YBCO CPW. The obtained parameters are: $\omega_c/2\pi = 8.65$ GHz, $\Delta/2\pi = 2.05$ GHz, $\lambda/2\pi = 2.002$ GHz, $\alpha/\sqrt{2\pi} = 3 \times 10^{-3}$ GHz$^{\frac{3}{2}}$. Image taken from Ref. [7].

achieved with these parameters: $\omega_c/2\pi = 8.65$ GHz, $\Delta/2\pi = 2.05$ GHz, and $\lambda/2\pi = 2.002$ GHz. Regarding the diamagnetic parameter β, the only nontrivial result (i.e., nonzero result from fit) was obtained by assuming a dependence on the magnon frequency: $\beta = \alpha/\sqrt{\omega_b}$, which can be justified by the fact that the presence of this term is dominant at low frequencies. With this assumption, we obtained $\alpha/\sqrt{2\pi} = 3 \times 10^{-3}$ GHz$^{\frac{3}{2}}$, corresponding to a value of the diamagnetic coefficient $\beta/2\pi \sim 10^{-3}$ GHz on resonance condition. The ratio between the collective coupling and the cavity frequency is approximately 0.23, fulfilling the criterion $\lambda/\omega_c > 0.1$ for USC. The fit confirms that the influence of the diamagnetic term is almost negligible leading us to conclude that the system couples to the resonator mainly through the spins. Notice that its value is more than two orders of magnitude smaller than the standard diamagnetic term for electric dipolar interactions $\beta_{\text{std}} = \lambda^2/\omega_b$. The smallness of the diamagnetic factor opens the possibility to achieve photon condensation in this systems [217].

Appendices

APPENDIX A

Master equation for ultrastrongly coupled systems

We start by considering a generic system interacting with reservoir (or environment), which is a large system with infinitely many states. Let the Hamiltonians be, respectively, $\hat{H}_S$ and $\hat{H}_R$, and the interaction Hamiltonian be $\hat{\mathcal{V}}$. The total Hamiltonian is then

$$\hat{H}_{\text{tot}} = \hat{H}_S + \hat{H}_R + \hat{\mathcal{V}}. \tag{A.1}$$

Here we model the environment as an infinite set of harmonic oscillators, with the corresponding creation and annihilation operators $\hat{b}_k^\dagger$ and $\hat{b}_k$, respectively. For instance, this is the case of the open radiation field that behaves as a reservoir for an atom [97, 98]. Now, let $\tilde{\rho}(t) = \exp(i\hat{H}_R t)\hat{\rho}(t)\exp(-i\hat{H}_R t)$ be the density matrix of the reservoir in the interaction picture[1], we then obtain the von Neumann equation in the interaction picture

$$\frac{\mathrm{d}}{\mathrm{d}t}\tilde{\rho} = -i\left[\tilde{\hat{\mathcal{V}}}(t), \tilde{\rho}(t)\right], \tag{A.2}$$

---

[1]From now on, we will consider $\hbar = 1$ to simplify the notation.

where the time dependence of $\tilde{\hat{\mathcal{V}}}(t)$ originates from the transformation to the interaction picture, $\tilde{\hat{\mathcal{V}}}(t) = \exp(i\hat{H}_R t)\hat{\mathcal{V}}\exp(-i\hat{H}_R t)$.

A.1 The Born-Markov approximation

We are now interested in the reduced dynamics of the system, which is obtained by tracing out the reservoir degrees of freedom from the total density matrix. Indeed, we can assume that the reservoir is basically unaffected by the system, and so we define the reduced density matrix as

$$\hat{\rho}_S(t) = \text{Tr}_R\left[\hat{\rho}_{\text{tot}}(t)\right] , \tag{A.3}$$

and we assume also that the two systems are uncoupled at $t = 0$, i.e. $\hat{\rho}_{\text{tot}}(0) = \hat{\rho}_S(0) \otimes \hat{\rho}_R(0)$. By integrating Eq. (A.2) we obtain

$$\tilde{\rho}(t) = \tilde{\rho}(0) - i \int_0^t \text{d}t' \left[\tilde{\hat{\mathcal{V}}}(t'), \tilde{\rho}(t')\right] . \tag{A.4}$$

Substituting this equation back again into Eq. (A.2) and tracing out the reservoir degrees of freedom, we get

$$\begin{aligned}
\frac{\text{d}}{\text{d}t}\tilde{\rho}_S(t) = &- i \,\text{Tr}_R\left[\tilde{\hat{\mathcal{V}}}(t), \tilde{\rho}(0)\right] \\
&- \int_0^t \text{d}t' \,\text{Tr}_R\left[\tilde{\hat{\mathcal{V}}}(t), \left[\tilde{\hat{\mathcal{V}}}(t'), \tilde{\rho}(t')\right]\right] ,
\end{aligned} \tag{A.5}$$

which can be iterated repeatedly to obtain a series expansion at various orders in the interaction Hamiltonian $\hat{\mathcal{V}}$. However, we limit ourselves to the second order, because we assume that the interaction is weak.

Then, we assume that the interaction Hamiltonian is linear in terms of the system and reservoir operators, and that it contains only off-diagonal matrix elements. Indeed, if some diagonal element is present in the interaction term $\hat{\mathcal{V}}$, it can be incorporated inside the diagonal part. We assume also that the density matrix of the environment is diagonal in the energy basis, because it represents a quantum system

in equilibrium at some temperature. If it were not in equilibrium, it would mean that it is still interacting with another system with similar dimensions of the environment itself. Under these conditions, we have

$$\mathrm{Tr}_R\left[\tilde{\hat{\mathcal{V}}}(t), \tilde{\hat{\rho}}(0)\right] = \mathrm{Tr}_R\left[\hat{\mathcal{V}}(t), \hat{\rho}_S(0) \otimes \hat{\rho}_R(0)\right] = 0\,, \qquad (A.6)$$

because, when performing the trace over the reservoir degrees of freedom, the interaction term contains only off-diagonal term and the environment density matrix is diagonal. Then, the first term in Eq. (A.5) vanishes.

As can be seen from Eq. (A.5), the time derivative of the density matrix at time t depends on the density matrix at all previous times t'. However, we can perform a few other simplifications. On the basis of our assumptions about the relative sizes of both S and R, as well as the weakness of the coupling between them, we can replace $\tilde{\hat{\rho}}(t')$ by $\tilde{\hat{\rho}}_S(t')\hat{\rho}_R(0)$, which means that the reservoir attains much faster compared to the time it takes to the system to change. Thus, we conclude that the reservoir correlations contained in the products $\tilde{\hat{\mathcal{V}}}(t)\tilde{\hat{\mathcal{V}}}(t')$ are sharply peaked around $t = t'$. We can therefore replace $\tilde{\hat{\rho}}(t')$ by $\tilde{\hat{\rho}}(t)$ in the second term of Eq. (A.5), obtaining

$$\frac{\mathrm{d}}{\mathrm{d}t}\tilde{\hat{\rho}}_S(t) = -\int_0^t \mathrm{d}t'\,\mathrm{Tr}_R\left[\tilde{\hat{\mathcal{V}}}(t), \left[\tilde{\hat{\mathcal{V}}}(t'), \tilde{\hat{\rho}}_S(t) \otimes \hat{\rho}_R(0)\right]\right]\,. \qquad (A.7)$$

By applying the change of variable $t' \to t - t'$, and extending the domain of the integration to infinity, we finally obtain the well-known Born-Markov master equation

$$\frac{\mathrm{d}}{\mathrm{d}t}\tilde{\hat{\rho}}_S(t) = -\int_0^\infty \mathrm{d}t'\,\mathrm{Tr}_R\left[\tilde{\hat{\mathcal{V}}}(t), \left[\tilde{\hat{\mathcal{V}}}(t - t'), \tilde{\hat{\rho}}_S(t) \otimes \hat{\rho}_R(0)\right]\right]\,, \qquad (A.8)$$

where the name comes from the Born approximation, which is the truncation of the series expansion of the von Neumann equation at the second order in $\tilde{\hat{\mathcal{V}}}$ and the Markov approximation, which is the assumption that the reservoir attains much faster compared to the time it takes to the system to change.

A.2 Generalized master equation without post-trace RWA

Up to now, we never specified the form of the interaction Hamiltonian $\hat{\mathcal{V}}$, but we already said that it is linear in terms of the system and reservoir operators and it is off-diagonal because it describes only interactions and not energy shifts. The form ho the interaction Hamiltonian is

$$\hat{\mathcal{V}} = \hat{\mathcal{S}} \left(\hat{\mathcal{B}} + \hat{\mathcal{B}}^\dagger \right) , \tag{A.9}$$

where $\hat{\mathcal{B}} = \sum_n g_n \hat{b}_n$, with g_n and $\hat{b}_n$ the coupling constant and the destroy operator of the n-th mode, respectively. $\hat{\mathcal{S}}$ is the system operator, which in the basis of the eigenstates of the system Hamiltonian $\hat{H}_S$ is

$$\hat{\mathcal{S}} = \sum_{j,k} S_{jk} |j\rangle\langle k| = \sum_{j,k} \hat{S}_{jk} , \tag{A.10}$$

which can contain both positive and negative frequencies. Due to the small coupling between the system and the reservoir, we can perform the rotating wave approximation

$$\hat{\mathcal{V}} = \hat{\mathcal{S}}^+ \hat{\mathcal{B}}^\dagger + \hat{\mathcal{S}}^- \hat{\mathcal{B}} , \tag{A.11}$$

where

$$\hat{\mathcal{S}}^+ = \sum_{j,k>j} S_{jk} |j\rangle\langle k| , \quad \hat{\mathcal{S}}^- = \left(\hat{\mathcal{S}}^+ \right)^\dagger . \tag{A.12}$$

In the interaction picture, we have that the bath operators oscillates as $\tilde{\mathcal{B}}(t) = \sum_n g_n e^{-i\omega_n t} \hat{b}_n$, where ω_n is the frequency of the n-th mode of the environment. On the other hand, the system operator oscillates as

$$\tilde{\hat{\mathcal{S}}}^+(t) = \sum_{j,k>j} \hat{S}_{jk} e^{-i\omega_{kj} t} = \sum_{j,k>j} \tilde{\hat{S}}_{jk}(t) , \tag{A.13}$$

and the interaction term in the interaction picture becomes

$$\tilde{\hat{\mathcal{V}}}(t) = \tilde{\hat{\mathcal{S}}}^+(t) \tilde{\hat{\mathcal{B}}}^\dagger(t) + \tilde{\hat{\mathcal{S}}}^-(t) \tilde{\hat{\mathcal{B}}}(t) . \tag{A.14}$$

By substituting this expression into Eq. (A.8) and expanding the commutators, we obtain

$$
\begin{aligned}
\frac{\mathrm{d}}{\mathrm{d}t}\tilde{\rho}_S(t) = \int_0^\infty \mathrm{d}t' \Big\{ &\Big[\tilde{\hat{\mathcal{S}}}^-(t-t')\tilde{\rho}_S(t)\tilde{\hat{\mathcal{S}}}^+(t) \\
&-\tilde{\hat{\mathcal{S}}}^+(t)\tilde{\hat{\mathcal{S}}}^-(t-t')\tilde{\rho}_S(t)\Big]\left\langle\tilde{\hat{\mathcal{B}}}^\dagger(t)\tilde{\hat{\mathcal{B}}}(t-t')\right\rangle_R \\
&+\Big[\tilde{\hat{\mathcal{S}}}^+(t-t')\tilde{\rho}_S(t)\tilde{\hat{\mathcal{S}}}^-(t) \\
&-\tilde{\hat{\mathcal{S}}}^-(t)\tilde{\hat{\mathcal{S}}}^+(t-t')\tilde{\rho}_S(t)\Big]\left\langle\tilde{\hat{\mathcal{B}}}(t)\tilde{\hat{\mathcal{B}}}^\dagger(t-t')\right\rangle_R \\
&+\Big[\tilde{\hat{\mathcal{S}}}^-(t)\tilde{\rho}_S(t)\tilde{\hat{\mathcal{S}}}^+(t-t') \\
&-\tilde{\rho}_S(t)\tilde{\hat{\mathcal{S}}}^+(t-t')\tilde{\hat{\mathcal{S}}}^-(t)\Big]\left\langle\tilde{\hat{\mathcal{B}}}^\dagger(t-t')\tilde{\hat{\mathcal{B}}}(t)\right\rangle_R \\
&+\Big[\tilde{\hat{\mathcal{S}}}^+(t)\tilde{\rho}_S(t)\tilde{\hat{\mathcal{S}}}^-(t-t') \\
&-\tilde{\rho}_S(t)\tilde{\hat{\mathcal{S}}}^-(t-t')\tilde{\hat{\mathcal{S}}}^+(t)\Big]\left\langle\tilde{\hat{\mathcal{B}}}(t-t')\tilde{\hat{\mathcal{B}}}^\dagger(t)\right\rangle_R \Big\},
\end{aligned}
\tag{A.15}
$$

where $\langle\cdot\rangle_R = \mathrm{Tr}_R\left[\cdot\hat{\rho}_R(0)\right]$ is the expectation value over the reservoir degrees of freedom. By using Eq. (A.13), and the relation $\tilde{\hat{S}}_{jk}(t-t') = \tilde{\hat{S}}_{jk}(t)e^{i\omega_{kj}t'}$, we obtain

$$
\begin{aligned}
\frac{\mathrm{d}}{\mathrm{d}t}\tilde{\rho}_s(t) = \sum_{\substack{j,k>j \\ l,m>l}} \Big\{ &\Big[\tilde{\hat{S}}_{lm}^\dagger(t)\tilde{\rho}_S\tilde{\hat{S}}_{jk}(t) - \tilde{\hat{S}}_{jk}(t)\tilde{\hat{S}}_{lm}^\dagger(t)\tilde{\rho}_S(t)\Big]\mathcal{G}_1(\omega_{ml}) \\
&+\Big[\tilde{\hat{S}}_{lm}(t)\tilde{\rho}_S(t)\tilde{\hat{S}}_{jk}^\dagger(t) - \tilde{\hat{S}}_{jk}^\dagger(t)\tilde{\hat{S}}_{lm}(t)\tilde{\rho}_S(t)\Big]\mathcal{G}_2(\omega_{ml}) \\
&+\Big[\tilde{\hat{S}}_{jk}^\dagger(t)\tilde{\rho}_S(t)\tilde{\hat{S}}_{lm}(t) - \tilde{\rho}_S(t)\tilde{\hat{S}}_{lm}(t)\tilde{\hat{S}}_{jk}^\dagger(t)\Big]\mathcal{G}_3(\omega_{ml}) \\
&+\Big[\tilde{\hat{S}}_{jk}(t)\tilde{\rho}_S(t)\tilde{\hat{S}}_{lm}^\dagger(t) - \tilde{\rho}_S(t)\tilde{\hat{S}}_{lm}^\dagger(t)\tilde{\hat{S}}_{jk}(t)\Big]\mathcal{G}_4(\omega_{ml}) \Big\},
\end{aligned}
\tag{A.16}
$$

where

$$\mathcal{G}_1(\omega) = \int_0^\infty \mathrm{d}t'\, e^{-i\omega t'} \left\langle \tilde{\hat{\mathcal{B}}}^\dagger(t)\tilde{\hat{\mathcal{B}}}(t-t') \right\rangle_R , \qquad (\text{A.17a})$$

$$\mathcal{G}_2(\omega) = \int_0^\infty \mathrm{d}t'\, e^{i\omega t'} \left\langle \tilde{\hat{\mathcal{B}}}(t)\tilde{\hat{\mathcal{B}}}^\dagger(t-t') \right\rangle_R , \qquad (\text{A.17b})$$

$$\mathcal{G}_3(\omega) = \int_0^\infty \mathrm{d}t'\, e^{i\omega t'} \left\langle \tilde{\hat{\mathcal{B}}}^\dagger(t-t')\tilde{\hat{\mathcal{B}}}(t) \right\rangle_R , \qquad (\text{A.17c})$$

$$\mathcal{G}_4(\omega) = \int_0^\infty \mathrm{d}t'\, e^{-i\omega t'} \left\langle \tilde{\hat{\mathcal{B}}}(t-t')\tilde{\hat{\mathcal{B}}}^\dagger(t) \right\rangle_R . \qquad (\text{A.17d})$$

One of the assumptions regarding the environment state was that it is in equilibrium at some temperature T, which means that $[\hat{H}_R, \hat{\rho}_R] = 0$. This implies that the reservoir correlation functions are time-translationally invariant, i.e. $\langle \tilde{\hat{\mathcal{B}}}^\dagger(t)\tilde{\hat{\mathcal{B}}}(t-t') \rangle_R = \langle \tilde{\hat{\mathcal{B}}}^\dagger(t')\tilde{\hat{\mathcal{B}}}(0) \rangle_R$. This can be proved by explicitly writing the bath operators in the interaction picture $\tilde{\hat{\mathcal{B}}}(t) = \sum_n g_n \exp(-i\omega_n t)\hat{b}_n$, and using the fact that the reservoir is in a stationary state. Then we have

$$\begin{aligned}
\left\langle \tilde{\hat{\mathcal{B}}}^\dagger(t)\tilde{\hat{\mathcal{B}}}(t-t') \right\rangle_R &= \sum_{n,m} g_n^* g_m e^{i\omega_{nm}t} e^{i\omega_m t'} \left\langle \hat{b}_n^\dagger \hat{b}_m \right\rangle_R \\
&= \sum_{n,m} g_n^* g_m e^{i\omega_{nm}t} e^{i\omega_m t'} n_{\mathrm{th}}(\omega_m, T)\delta_{nm} \qquad (\text{A.18}) \\
&= \sum_n |g_n|^2 e^{i\omega_n t'} n_{\mathrm{th}}(\omega_n, T) ,
\end{aligned}$$

which depends only on the time difference, which is t'. Where $n_{\mathrm{th}}(\omega, T) = [\exp(\hbar\omega/(k_B T)) - 1]^{-1}$ is the thermal population and k_B is the Boltzmann constant. Obviously, the same holds for the other correlation functions.

In general, we can also consider a continuum of modes, replacing the summation over n with an integral over the density of states, but for the purposes of this Thesis we are only interested in the so called

Ohmic baths, which means that we can consider

$$\mathcal{G}_1(\omega) = \mathcal{G}_3(\omega) = \frac{1}{2} n_{\text{th}}(\omega, T)\Gamma(\omega) \tag{A.19a}$$

$$\mathcal{G}_2(\omega) = \mathcal{G}_4(\omega) = \frac{1}{2}\left[n_{\text{th}}(\omega, T) + 1\right]\Gamma(\omega), \tag{A.19b}$$

where $\Gamma(\omega) = \tilde{\gamma}\omega$ is the frequency dependent decay rate.

By substituting these expressions into Eq. (A.16), and by passing to the Schrödinger picture, we obtain

$$
\begin{aligned}
\frac{\mathrm{d}}{\mathrm{d}t}\hat{\rho}_S(t) = &- i\left[\hat{H}_S, \hat{\rho}_S(t)\right] \\
&+ \frac{1}{2}\sum_{\substack{j,k>j \\ l,m>l}} \Gamma(\omega_{ml})\left\{\left[\hat{S}_{lm}^\dagger\hat{\rho}_S(t)\hat{S}_{jk} - \hat{S}_{jk}\hat{S}_{lm}^\dagger\hat{\rho}_S(t)\right]n_{\text{th}}(\omega_{ml})\right. \\
&+ \left[\hat{S}_{lm}\hat{\rho}_S(t)\hat{S}_{jk}^\dagger - \hat{S}_{jk}^\dagger\hat{S}_{lm}\hat{\rho}_S(t)\right]\left[n_{\text{th}}(\omega_{ml}) + 1\right] \\
&+ \left[\hat{S}_{jk}^\dagger\hat{\rho}_S(t)\hat{S}_{lm} - \hat{\rho}_S(t)\hat{S}_{lm}\hat{S}_{jk}^\dagger\right]n_{\text{th}}(\omega_{ml}) \\
&+ \left.\left[\hat{S}_{jk}\hat{\rho}_S(t)\hat{S}_{lm}^\dagger - \hat{\rho}_S(t)\hat{S}_{lm}^\dagger\hat{S}_{jk}\right]\left[n_{\text{th}}(\omega_{ml}) + 1\right]\right\},
\end{aligned}
\tag{A.20}
$$

which can be further simplified by using the following operators

$$\hat{\mathcal{S}}_1^+ = \sum_{j,k>j}\Gamma(\omega_{kj})n_{\text{th}}(\omega_{kj})\hat{S}_{jk} \tag{A.21a}$$

$$\hat{\mathcal{S}}_2^+ = \sum_{j,k>j}\Gamma(\omega_{kj})\left[n_{\text{th}}(\omega_{kj}) + 1\right]\hat{S}_{jk} \tag{A.21b}$$

and their Hermitian conjugates $\hat{\mathcal{S}}_1^-$ and $\hat{\mathcal{S}}_2^-$, respectively. And finally we have the generalized master equation in its simples form

$$
\begin{aligned}
\frac{\mathrm{d}}{\mathrm{d}t}\hat{\rho}_S(t) = &- i\left[\hat{H}_S, \hat{\rho}_S(t)\right] \\
&+ \frac{1}{2}\left[\hat{\mathcal{S}}_1^-\hat{\rho}_S(t)\hat{\mathcal{S}}^+ + \hat{\mathcal{S}}^-\hat{\rho}_S(t)\hat{\mathcal{S}}_1^+ - \hat{\mathcal{S}}^+\hat{\mathcal{S}}_1^-\hat{\rho}_S(t) - \hat{\rho}_S(t)\hat{\mathcal{S}}_1^+\hat{\mathcal{S}}^-\right. \\
&+ \left.\hat{\mathcal{S}}_2^+\hat{\rho}_S(t)\hat{\mathcal{S}}^- + \hat{\mathcal{S}}^+\hat{\rho}_S(t)\hat{\mathcal{S}}_2^- - \hat{\mathcal{S}}^-\hat{\mathcal{S}}_2^+\hat{\rho}_S(t) - \hat{\rho}_S(t)\hat{\mathcal{S}}_2^-\hat{\mathcal{S}}^+\right].
\end{aligned}
\tag{A.22}
$$

133

When examining the interaction scenario, each term in Eq. (A.20), with the exception of the final one, fluctuates at $\pm(\omega_{ml} - \omega_{kj})$. If the absolute value of $|\omega_{ml} - \omega_{kj}|$ surpasses the system's decay rates $\Gamma^{(n)}$ by a considerable margin, these elements yield insignificant additions to the integration of the master equation. As such, $|\omega_{ml} - \omega_{kj}|$ can be approximated to be on par with the linewidths of the system.

Even though Eq. (A.20) contains terms that oscillate rapidly due to transitions with substantial frequency disparities (which are not present following the post-trace RWA in the adorned master equation), they are unlikely to contribute significantly if $|\omega_{ml} - \omega_{kj}| > \Gamma^{(n)}$. Nevertheless, they can drastically inflate the computation duration and trigger computational instabilities, which can be prominent when generating log-scaled spectra. To counteract these challenges, we incorporate a low-pass filter function in Eq. (A.20), aiming to curtail the influence of dissipator terms associated with large frequency disparities [100]. This filter function can adopt any form of a low-pass filter, such as a step-like or sigmoid-like configuration.

APPENDIX B

Vectorization of the density matrix

In finite sizes Hilbert spaces, which are always the case in numerical simulations, the density matrix is represented by a square matrix ρ of dimension $N \times N$, where N is the dimension of the Hilbert space. The density matrix is Hermitian, which means that $\rho_{ij} = \rho_{ji}^*$, and positive semi-definite, which means that all its eigenvalues are non-negative. The density matrix is also normalized, which means that $\text{Tr}(\rho) = 1$. Its time evolution is given by the master equation

$$\frac{\mathrm{d}}{\mathrm{d}t}\hat{\rho} = \mathcal{L}\hat{\rho}\,, \tag{B.1}$$

where $\mathcal{L}$ is the Liouvillian superoperator. The Liouvillian superoperator is a linear operator acting on the space of operators. In numerical simulations, however, it is more convenient to represent the density matrix as a vector $\vec{\rho}$ of dimension N^2 and the Liouvillian superoperator as a matrix $\overline{\overline{\mathcal{L}}}$. The process of vectorization of the density matrix is relatively simple, but it is worth noting that it can be performed in row-major or column-major order. In general, the default reshape function in Python uses row-major order, while the reshape function in Julia uses column-major order. Assuming a column-major ordering,

B. Vectorization of the density matrix

the vectorization of a 2x2 density matrix is given by

$$\hat{\rho} = \begin{pmatrix} \rho_{11} & \rho_{12} \\ \rho_{21} & \rho_{22} \end{pmatrix} \quad \rightarrow \quad \vec{\rho} = \begin{pmatrix} \rho_{11} \\ \rho_{21} \\ \rho_{12} \\ \rho_{22} \end{pmatrix}. \tag{B.2}$$

The procedure to convert the Liouvillian is slightly more complicated. First, we need to distinguish between the left and right action of the Liouvillian subparts. The left action becomes

$$\mathcal{D}_L \left[\hat{S} \right] \hat{\rho} = \hat{S}\hat{\rho} \quad \rightarrow \quad \overline{\overline{\mathcal{D}}}_L \vec{\rho} = \left(\hat{I} \otimes \hat{S} \right) \vec{\rho}. \tag{B.3}$$

Indeed, taking as an example

$$\hat{S} = \begin{pmatrix} S_{11} & S_{12} \\ S_{21} & S_{22} \end{pmatrix}, \tag{B.4}$$

the action in the vectorized form is given by

$$
\begin{aligned}
\vec{\sigma} = \left(\hat{I} \otimes \hat{S} \right) \vec{\rho} &= \begin{pmatrix} S_{11} & S_{12} & 0 & 0 \\ S_{21} & S_{22} & 0 & 0 \\ 0 & 0 & S_{11} & S_{12} \\ 0 & 0 & S_{21} & S_{22} \end{pmatrix} \begin{pmatrix} \rho_{11} \\ \rho_{21} \\ \rho_{12} \\ \rho_{22} \end{pmatrix} \\
&= \begin{pmatrix} S_{11}\rho_{11} + S_{12}\rho_{21} \\ S_{21}\rho_{11} + S_{22}\rho_{21} \\ S_{11}\rho_{12} + S_{12}\rho_{22} \\ S_{21}\rho_{12} + S_{22}\rho_{22} \end{pmatrix}.
\end{aligned} \tag{B.5}
$$

It is straightforward to see that $\vec{\sigma}$ reshaped again in a 2x2 matrix gives $\hat{S}\hat{\rho}$.

In the same way, the right action becomes

$$\mathcal{D}_R \left[\hat{S} \right] \hat{\rho} = \hat{\rho}\hat{S} \quad \rightarrow \quad \overline{\overline{\mathcal{D}}}_R \vec{\rho} = \left(\hat{S}^T \otimes \hat{I} \right) \vec{\rho}, \tag{B.6}$$

where the transpose of $\hat{S}$ is taken because the action is on the right. The action in the vectorized form is given by

$$
\vec{\sigma} = \left(\hat{S}^T \otimes \hat{I} \right) \vec{\rho} = \begin{pmatrix} S_{11} & 0 & S_{21} & 0 \\ 0 & S_{11} & 0 & S_{21} \\ S_{12} & 0 & S_{22} & 0 \\ 0 & S_{12} & 0 & S_{22} \end{pmatrix} \begin{pmatrix} \rho_{11} \\ \rho_{21} \\ \rho_{12} \\ \rho_{22} \end{pmatrix}
$$
$$
= \begin{pmatrix} S_{11}\rho_{11} + S_{21}\rho_{12} \\ S_{11}\rho_{21} + S_{21}\rho_{22} \\ S_{12}\rho_{11} + S_{22}\rho_{12} \\ S_{12}\rho_{21} + S_{22}\rho_{22} \end{pmatrix} .
$$

(B.7)

Once again, it is straightforward to see that $\vec{\sigma}$ reshaped again in a 2x2 matrix gives $\hat{\rho}\hat{S}$. Now, the simultaneous action of the left and right subparts of the Liouvillian superoperator is simply given by the Kronecker product of the two matrices

$$
\mathcal{D}_{LR}\left[\hat{S}_1, \hat{S}_2 \right] \hat{\rho} = \hat{S}_1 \hat{\rho} \hat{S}_2 \quad \rightarrow \quad \overline{\overline{\mathcal{D}}}_{LR}\vec{\rho} = \left(\hat{S}_2^T \otimes \hat{S}_1 \right) \vec{\rho} .
$$

(B.8)

The vectorization procedure is very useful in numerical simulations. As an example, the steadystate of the system can be found by diagonalizing the Liouvillian $\overline{\overline{\mathcal{L}}}$ in its matrix form and taking the only eigenvector with eigenvalue equal to zero. Indeed, the steadystate is the only state which satisfies the equation

$$
\frac{\mathrm{d}}{\mathrm{d}t}\hat{\rho} = \mathcal{L}\hat{\rho} = 0 ,
$$

(B.9)

which is equivalent to the equation

$$
\overline{\overline{\mathcal{L}}}\vec{\rho} = 0\vec{\rho} .
$$

(B.10)

APPENDIX C

Matrix continued fractions algorithm for time-dependent Hamiltonians

As already mentioned in Chapter 3, dealing with time-dependent Hamiltonians is not always trivial. The time-dependence in quantum optics usually comes from a coherent drive, such as a laser. When dealing with harmonic systems, or in general, when the operator which couples the system with the coherent drive oscillates at one single frequency, the time dependence can be eliminated by a unitary transformation. However, this is not the case in the USC regime, where the system operator generally oscillates at different frequencies. For instance, if we consider the field operator $\hat{A} \equiv \hat{a} + \hat{a}^\dagger$, in the interaction picture we have

$$\hat{X}(t) = \sum_{j,k} e^{-i\omega_{kj}t} \langle j|\hat{a} + \hat{a}^\dagger|k\rangle |j\rangle\langle k| . \tag{C.1}$$

It is now clear that we must deal with time dependence. When performing numerical simulations this can lead to a huge computational

cost, because the standard iterative algorithms for finding the steady state [101] will fail because there is no time-independent steady state this time. Up to now, it seems that we have to solve the time-dependent generalized master equation in Eq. (2.33), integrating for a long time and then averaging over the steady state.

To overcome this problem, we can use the Floquet formalism and the expansion of the density matrix in Fourier components, solving a matrix continued fraction problem, and finding the averaged steady state [146–148]. Let us start first by defining the time-dependent equation of motion for the density matrix

$$\frac{\mathrm{d}}{\mathrm{d}t}\hat{\rho} = \left[\mathcal{L}_0 + \mathcal{L}_1 e^{i\omega_\mathrm{L} t} + \mathcal{L}_{-1} e^{-i\omega_\mathrm{L} t}\right]\hat{\rho}, \tag{C.2}$$

where $\mathcal{L}_{\pm 1}$ are the superoperators involving the drive. In the case of Chapter 3 we have[1]

$$\mathcal{L}_{\pm 1}\hat{\rho} = \frac{\Omega}{2}\left[i\left(\hat{a} - \hat{a}^\dagger\right) - 2\eta\hat{\sigma}_p, \hat{\rho}\right]. \tag{C.3}$$

The Floquet formalism implies that the density matrix at long times can be expanded in Fourier components of the form

$$\hat{\rho}(t) = \sum_{n=-\infty}^{+\infty} \hat{\rho}_n e^{in\omega_\mathrm{L} t}, \tag{C.4}$$

because all other transient terms will vanish at long times. Substituting the expansion in the equation of motion, we obtain

$$\sum_{n=-\infty}^{+\infty} in\omega_\mathrm{L}\hat{\rho}_n e^{in\omega_\mathrm{L} t} = \sum_{n=-\infty}^{+\infty} \left[\mathcal{L}_0 + \mathcal{L}_1 e^{i\omega_\mathrm{L} t} + \mathcal{L}_{-1} e^{-i\omega_\mathrm{L} t}\right]\hat{\rho}_n e^{in\omega_\mathrm{L} t}. \tag{C.5}$$

Equating the coefficients of the series yields the tridiagonal recursion relation

$$0 = \left(\mathcal{L}_0 - in\omega_\mathrm{L}\right)\hat{\rho}_n + \mathcal{L}_1\hat{\rho}_{n-1} + \mathcal{L}_{-1}\hat{\rho}_{n+1}. \tag{C.6}$$

---

[1]Note here that in this specific case $\mathcal{L}_1 = \mathcal{L}_{-1}$, because we are considering a cosine drive.

Such a recursion can be solved in different ways. The most common one is the matrix continued fraction method. Suppose that for $n \geqslant 0$ it is possible to find a sequence of superoperators $\mathcal{S}_n$ such that $\hat{\rho}_n = \mathcal{S}_n \hat{\rho}_{n-1}$. Then, the recursion relation becomes

$$[(\mathcal{L}_0 - in\omega_{\mathrm{L}})\,\mathcal{S}_n + \mathcal{L}_1 + \mathcal{L}_{-1}\mathcal{S}_{n+1}\mathcal{S}_n]\,\hat{\rho}_{n-1} = 0\,, \qquad (\text{C.7})$$

which yields

$$(\mathcal{L}_0 - in\omega_{\mathrm{L}})\,\mathcal{S}_n + \mathcal{L}_1 + \mathcal{L}_{-1}\mathcal{S}_{n+1}\mathcal{S}_n = 0\,, \qquad (\text{C.8})$$

or, equivalently,

$$\mathcal{S}_n = -\left[(\mathcal{L}_0 - in\omega_{\mathrm{L}}) + \mathcal{L}_{-1}\mathcal{S}_{n+1}\right]^{-1}\mathcal{L}_1\,. \qquad (\text{C.9})$$

This expressed $\mathcal{S}_n$ in terms of $\mathcal{S}_{n+1}$. We now assume that the contribution of the $n_{\max}$-th term is negligible, setting $\mathcal{S}_{n_{\max}} = 0$. Using now this recursion we can obtain all the superoperators, until we reach the last one $\mathcal{S}_1$. This is called a matrix continued fraction problem because the recursion relation can be written as

$$\mathcal{S}_1 = \frac{a_1}{b_1 + \frac{c_1 a_2}{b_2 + \frac{c_2 a_3}{b_3 + \dots}}}\,. \qquad (\text{C.10})$$

Similarly, if for $n \leqslant 0$ we can find a sequence of superoperators $\mathcal{T}_n$ such that $\hat{\rho}_n = \mathcal{T}_n \hat{\rho}_{n+1}$, then we have

$$[(\mathcal{L}_0 - in\omega_{\mathrm{L}})\,\mathcal{T}_n + \mathcal{L}_{-1} + \mathcal{L}_1\mathcal{T}_{n-1}\mathcal{T}_n]\,\hat{\rho}_{n+1} = 0\,, \qquad (\text{C.11})$$

which yields

$$(\mathcal{L}_0 - in\omega_{\mathrm{L}})\,\mathcal{T}_n + \mathcal{L}_{-1} + \mathcal{L}_1\mathcal{T}_{n-1}\mathcal{T}_n = 0\,, \qquad (\text{C.12})$$

or, equivalently,

$$\mathcal{T}_n = -\left[(\mathcal{L}_0 - in\omega_{\mathrm{L}}) + \mathcal{L}_1\mathcal{T}_{n-1}\right]^{-1}\mathcal{L}_{-1}\,. \qquad (\text{C.13})$$

C. Matrix continued fractions algorithm for time-dependent Hamiltonians

This expressed $\mathcal{T}_n$ in terms of $\mathcal{T}_{n-1}$. As before, we assume that the contribution of the $n_{\min}$-th term is negligible, setting $\mathcal{T}_{-n_{\min}} = 0$. Using now this recursion we can obtain all the superoperators, until we reach the last one $\mathcal{T}_{-1}$.

Having obtained $\mathcal{S}_1$ and $\mathcal{T}_{-1}$, we return the tridiagonal relation for $n = 0$, which is

$$\mathcal{L}_0 \hat{\rho}_0 + \mathcal{L}_1 \hat{\rho}_{-1} + \mathcal{L}_{-1} \hat{\rho}_1 = 0 \,, \tag{C.14}$$

and, noting that $\hat{\rho}_1 = \mathcal{S}_1 \hat{\rho}_0$ and $\hat{\rho}_{-1} = \mathcal{T}_{-1} \hat{\rho}_0$, we obtain

$$[\mathcal{L}_0 + \mathcal{L}_1 \mathcal{T}_{-1} + \mathcal{L}_{-1} \mathcal{S}_1] \hat{\rho}_0 = 0 \,. \tag{C.15}$$

Finally, the time-averaged steady state solution $\hat{\rho}_0$ can be found as the nullspace of the superoperator

$$\mathcal{L}_{\text{eff}} = \mathcal{L}_0 + \mathcal{L}_1 \mathcal{T}_{-1} + \mathcal{L}_{-1} \mathcal{S}_1 \,. \tag{C.16}$$

APPENDIX D

Derivation of the master equation for the pure dephasing

D.1   Pure dephasing in the quantum Rabi model

In this section, we explore how to accurately and describe pure dephasing effects in the quantum Rabi model (QRM), following the methodology outlined in Ref. [99] and taking into account both cavity and qubit decoherence. We begin by considering the quantum Rabi Hamiltonian with an added zero-mean stochastic modulation of the qubit resonance frequency $\hat{\mathcal{V}}^q_{\text{dep}} = f_q(t)\hat{\sigma}_z$. When we express the Hamiltonian in the dressed basis and transition to the interaction picture with respect to $\hat{\mathcal{V}}^q_{\text{dep}}$, we get

$$\hat{\mathcal{V}}^q_{\text{dep}}(t) = f(t)\sum_{j,k}\langle j|\hat{\sigma}_z|k\rangle\,|j\rangle\langle k|\,e^{i\omega_{jk}t}\,, \tag{D.1}$$

where $|j\rangle$ are the eigenstates of the total Hamiltonian and ω_{jk} are the transition frequencies. By expressing $f(t)$ in terms of its Fourier decomposition, and assuming that the main contribution to dephasing

results from a small frequency interval around ω_{jk} [99], we derive

$$\hat{\mathcal{V}}^q_{\text{dep}}(t) = \sum_{j,k} \sigma_z^{jk} |j\rangle\langle k| \, f_{-\omega_{jk}}(t) \,, \tag{D.2}$$

where

$$f_{\omega_{jk}}(t) = \sqrt{S_f(\omega_{jk})} \xi_{\omega_{jk}}(t) \,, \tag{D.3}$$

$S_f(\omega)$ is the spectral density of $f(t)$, and $\xi(\omega)$ such that $\langle \xi(\omega) \rangle = 0$ and $\langle \xi(\omega)\xi(\omega') \rangle = \delta(\omega - \omega')$ (i.e., corresponding to white noise). If the transition frequencies ω_{jk} are well-separated, we can treat each term of the above summation as an independent noise [99].

We can now formulate the dressed Lindbladian in case of qubit pure dephasing:

$$\mathcal{L}_{\text{dr}}\cdot = \mathcal{D}\left[\sum_j \Phi^j |j\rangle\langle j|\right]\cdot + \sum_{j,k\neq j} \Gamma_\phi^{jk} \, \mathcal{D}\left[|j\rangle\langle k|\right]\cdot \,, \tag{D.4}$$

where

$$\Phi^j = \sqrt{\frac{\gamma_\phi(0)}{2}} \sigma_z^{jj}, \tag{D.5}$$

and

$$\Gamma_\phi^{jk} = \frac{\gamma_\phi(\omega_{kj})}{2} \left|\sigma_z^{jk}\right|^2 \,. \tag{D.6}$$

The entire procedure described above can also be applied to the case of cavity pure dephasing, by considering the QRM Hamiltonian with an additional zero-mean stochastic modulation of the cavity resonance frequency $\hat{\mathcal{V}}^c_{\text{dep}} = f_c(t)\hat{a}^\dagger\hat{a}$. In this case, this stochastic perturbation, expressed in the dressed basis and in the interaction picture, becomes

$$\hat{\mathcal{V}}^c_{\text{dep}}(t) = \sum_{j,k} \langle j|\hat{a}^\dagger\hat{a}|k\rangle \, |j\rangle\langle k| \, f_{-\omega_{jk}}(t) \,, \tag{D.7}$$

while the Lindbladian remains in the same form of Eq. (D.4), with the only difference of Φ^j and Γ_ϕ^{jk}, which become respectively,

$$\Phi^j = \sqrt{\frac{\gamma_\phi(0)}{2}} \, \langle j|\hat{a}^\dagger \hat{a}|j\rangle \, , \tag{D.8a}$$

$$\Gamma_\phi^{jk} = \frac{\gamma_\phi(\omega_{kj})}{2} \left| \langle j|\hat{a}^\dagger \hat{a}|k\rangle \right|^2 \, . \tag{D.8b}$$

Nonetheless, as we have discussed in Chapter 4, the methodology outlined above does not yield the correct outcomes. Specifically, we have demonstrated that employing either the Coulomb or dipole gauge can lead to significantly different results. For instance, in the Coulomb gauge, the bare $\hat{\sigma}_z$ operator transforms into $\hat{\sigma}_{z,C} = \hat{\mathcal{U}}\hat{\sigma}_z\hat{\mathcal{U}}^\dagger$, as the minimal coupling is applied to the matter system. Meanwhile, the photonic operator $\hat{a}^\dagger\hat{a}$ transforms into $\hat{a}_D^\dagger\hat{a}_D = \hat{\mathcal{U}}^\dagger\hat{a}^\dagger\hat{a}\hat{\mathcal{U}}$ in the dipole gauge. Therefore, to accurately describe pure dephasing effects, we need to replace $\hat{\sigma}_z$ with $\hat{\sigma}_{z,C}$ in the Coulomb gauge and $\hat{a}^\dagger\hat{a}$ with $\hat{a}_D^\dagger\hat{a}_D$ in the dipole gauge in the Lindbladian given in Eq. (D.4).

D.2 Analytical derivation of the pure dephasing rates

By adopting the procedure described above, we are able to derive analytically the pure dephasing rates of both cavity and qubit. Starting from the Coulomb gauge and using Eq. (D.4), we discard the off-diagonal terms Γ_ϕ^{jk} since this contribution is significant only if the dephasing bath has a spectral weight at the potentially high frequency ω_{jk}, leading to the following equation:

$$\dot{\hat{\rho}} = -i\left[\hat{\mathcal{H}}_C, \hat{\rho}\right] + \frac{\gamma_\phi(0)}{2}\mathcal{D}\left[\sum_j \sigma_{z,C}^{jj}|j\rangle\langle j|\right]\hat{\rho}\,, \tag{D.9}$$

where $\sigma_{z,C}^{jj} = \langle j|\hat{\sigma}_{z,C}|j\rangle$. We now expand the Lindblad dissipator

$$
\mathcal{D}\left[\sum_j \sigma_{z,C}^{jj} |j\rangle\langle j|\right]\hat{\rho} = \frac{1}{2}\left[2\sum_j\sum_k \sigma_{z,C}^{jj}\sigma_{z,C}^{kk} |j\rangle\langle j|\,\hat{\rho}\,|k\rangle\langle k|\right.
$$
$$
- \sum_j\sum_k \sigma_{z,C}^{jj}\sigma_{z,C}^{kk} |k\rangle\langle k|\,|j\rangle\langle j|\,\hat{\rho} \tag{D.10}
$$
$$
\left.- \sum_j\sum_k \sigma_{z,C}^{jj}\sigma_{z,C}^{kk}\hat{\rho}\,|k\rangle\langle k|\,|j\rangle\langle j|\right],
$$

and we focus on the matrix element of the density matrix relative to the transition $(\tilde{1}_-, \tilde{0})$, but the same procedure can be applied to all the other transitions. The corresponding equation (in the interaction picture) for that matrix element becomes

$$
\frac{d}{dt}\hat{\rho}_{\tilde{1}_-,\tilde{0}}^{(I)} = \frac{\gamma_\phi(0)}{4}\langle\tilde{1}_-|\left[2\sum_j\sum_k \sigma_{z,C}^{jj}\sigma_{z,C}^{kk} |j\rangle\langle j|\,\hat{\rho}^{(I)}\,|k\rangle\langle k|\right.
$$
$$
\left.- \sum_j \left|\sigma_{z,C}^{jj}\right|^2 |j\rangle\langle j|\,\hat{\rho}^{(I)} - \sum_j \left|\sigma_{z,C}^{jj}\right|^2 \hat{\rho}^{(I)}\,|j\rangle\langle j|\,|\tilde{0}\rangle\right]
$$
$$
= \frac{\gamma_\phi(0)}{4}\left[2\sum_j\sum_k \sigma_{z,C}^{jj}\sigma_{z,C}^{kk}\langle\tilde{1}_-|\,|j\rangle\langle j|\,\hat{\rho}^{(I)}\,|k\rangle\langle k|\,|\tilde{0}\rangle\right.
$$
$$
- \sum_j \left|\sigma_{z,C}^{jj}\right|^2 \langle\tilde{1}_-|\,|j\rangle\langle j|\,\hat{\rho}^{(I)}\,|\tilde{0}\rangle \tag{D.11}
$$
$$
\left.- \sum_j \left|\sigma_{z,C}^{jj}\right|^2 \langle\tilde{1}_-|\,\hat{\rho}^{(I)}\,|j\rangle\langle j|\,|\tilde{0}\rangle\right]
$$
$$
= \frac{\gamma_\phi(0)}{4}\left[2\sigma_{z,C}^{\tilde{1}_-\tilde{1}_-}\sigma_{z,C}^{\tilde{0}\tilde{0}}\langle\tilde{1}_-|\,\hat{\rho}^{(I)}\,|\tilde{0}\rangle\right.
$$
$$
\left.- \left|\sigma_{z,C}^{\tilde{1}_-\tilde{1}_-}\right|^2 \langle\tilde{1}_-|\,\hat{\rho}^{(I)}\,|\tilde{0}\rangle - \left|\sigma_{z,C}^{\tilde{0}\tilde{0}}\right|^2 \langle\tilde{1}_-|\,\hat{\rho}^{(I)}\,|\tilde{0}\rangle\right]
$$
$$
= -\frac{\gamma_\phi(0)}{4}\left|\sigma_{z,C}^{\tilde{1}_-\tilde{1}_-} - \sigma_{z,C}^{\tilde{0}\tilde{0}}\right|^2 \hat{\rho}_{\tilde{1}_-,\tilde{0}}^{(I)}.
$$

By choosing the dipole gauge, one should replace $\sigma_{z,C}^{jj} \to \sigma_z^{jj}$. The same procedure is valid also for cavity pre dephasing, where we need to use $\hat{a}^\dagger \hat{a}$ in the Coulomb gauge and $\hat{a}_D^\dagger \hat{a}_D$ in the dipole gauge.

D.3 Pure dephasing in the Hopfield model

Here we analyze pure dephasing effects in the Hopfield model, following the procedure described in the previous sections and extending the results of Ref. [99]. Moreover, we consider both light and matter decoherence. First, it is useful to diagonalize the Hopfield Hamiltonian using the polaritonic operators [182], where the lower and upper polariton operators ($\mu = 1, 2$) can be defined as

$$\hat{P}_\mu = U_b^\mu \hat{b} + U_a^\mu \hat{a} + V_b^\mu \hat{b}^\dagger + V_a^\mu \hat{a}^\dagger \,. \tag{D.12}$$

Using the property

$$|U_b^\mu|^2 + |U_a^\mu|^2 - |V_b^\mu|^2 - |V_a^\mu|^2 = 1 \,, \tag{D.13}$$

which guarantee the correct polariton commutation rules [182], we can invert (D.12) in order to obtain

$$\hat{a} = \sum_{\mu=1}^{2} \left(U_a^\mu \hat{P}_\mu - V_a^\mu \hat{P}_\mu^\dagger \right) \,, \tag{D.14a}$$

$$\hat{b} = \sum_{\mu=1}^{2} \left(U_b^\mu \hat{P}_\mu - V_b^\mu \hat{P}_\mu^\dagger \right) \,. \tag{D.14b}$$

To describe the matter pure dephasing, we consider an additional zero-mean stochastic modulation of the matter resonance frequency $\hat{V}_{\text{dep}}^x = f_x(t) \hat{b}^\dagger \hat{b}$. In terms of the polaritonic operators we have

$$\hat{b}^\dagger \hat{b} = A_1 \hat{P}_1^\dagger \hat{P}_1 + A_2 \hat{P}_2^\dagger \hat{P}_2 + B_{12} \hat{P}_1^\dagger \hat{P}_2 + B_{21} \hat{P}_2^\dagger \hat{P}_1 \,, \tag{D.15}$$

with

$$A_\mu = |U_b^\mu|^2 + |V_b^\mu|^2 \,, \tag{D.16a}$$

$$B_{12} = B_{21}^* = U_b^{1*}U_b^2 + V_b^1 V_b^{2*} \,, \tag{D.16b}$$

where we have included only the terms which do not oscillate in time, or oscillate at low frequency, corresponding to applying the rotating wave approximation (RWA), and we have eliminated the constants derived from commutation rules, which have no dynamical consequences. Moving to the interaction picture, this contribution becomes

$$\hat{V}_{\text{dep}}^x(t) = f_x(t) \left[A_1 \hat{P}_1^\dagger \hat{P}_1 + A_2 \hat{P}_2^\dagger \hat{P}_2 \right.$$
$$\left. + e^{-i\omega_{21}t} B_{12} \hat{P}_1^\dagger \hat{P}_2 + e^{i\omega_{21}t} B_{21} \hat{P}_2^\dagger \hat{P}_1 \right] \,, \tag{D.17}$$

where $\omega_{21} = \omega_2 - \omega_1$ with the polaritonic eigenfrequencies ω_i. Eq. (D.17) can be written in a more compact form as

$$\hat{V}_{\text{dep}}^x = f_x(t) \left[\hat{D}_{12} + e^{-i\omega_{21}t} \hat{M}_{12} + e^{i\omega_{21}t} \hat{M}_{12}^\dagger \right] \,, \tag{D.18}$$

with

$$\hat{D}_{12} = A_1 \hat{P}_1^\dagger \hat{P}_1 + A_2 \hat{P}_2^\dagger \hat{P}_2 \,, \tag{D.19a}$$

$$\hat{M}_{12} = B_{12} \hat{P}_1^\dagger \hat{P}_2 \,, \tag{D.19b}$$

and using the results presented in the previous sections, we obtain

$$\hat{V}_{\text{dep}}^x(t) = f_0(t)\hat{D}_{12} + f_{\omega_{21}}(t)\hat{M}_{12} + f_{-\omega_{21}}(t)\hat{M}_{12}^\dagger \,, \tag{D.20}$$

with $f_\omega(t)$ expressed in Eq. (D.3). Thus, the resulting Lindbladian in the case of matter pure dephasing is

$$\mathcal{L}\cdot = \frac{1}{2}\gamma_\phi(\omega_{21})\mathcal{D}[\hat{M}_{12}]\cdot + \frac{1}{2}\gamma_\phi(-\omega_{21})\mathcal{D}[\hat{M}_{12}^\dagger]\cdot + \frac{1}{2}\gamma_\phi(0)\mathcal{D}[\hat{D}_{12}]\cdot \,, \tag{D.21}$$

with $\gamma_\phi(\omega) = 2S_f(\omega)$.

Conclusions

In conclusion, this Thesis provided a comprehensive exploration of light-matter interaction in the ultrastrong coupling (USC) regime. It began with a discussion on fundamental understanding of light-matter interaction, moving from a Lagrangian approach to a full quantum treatment. The Thesis addressed the breakdown of gauge invariance due to the truncation of the Hilbert space and proposed solutions to overcome these issues.

The Thesis then focused on the Coulomb and dipole gauges. Specifically, for the dipole gauge, it redefined aspects related to the electric field. It further elaborated on photodetection, deriving a generalized master equation with minimal assumptions. The application of this approach to incoherent and coherent pumping processes revealed unique phenomena observable in the USC regime.

The thesis also presented a gauge-invariant treatment of pure dephasing in the USC regime, demonstrating that standard approaches are insufficient when light-matter coupling strength is comparable to the frequency of the electromagnetic field. Lastly, it investigated the phenomenon of photon condensation, debunking previous claims of its existence in the absence of a magnetic field.

This Thesis has not explored some topics to which I have contributed in the last three years. First, the phenomenon of optomechanical two-

photon hopping [6]. In a membrane in the middle setup, where two cavities are separated by a mechanical membrane, the two cavities can exchange two photons through the virtual excitations of the membrane. And finally, all the works that are currently under review or in preparation. The effect of back-action and mechanically generated photons from a flying atom passing through a cavity [8]. The possibility of achieving the superradiant phase transition with an ensemble of model loop molecules [9]. The creation of coherent excitations of a mechanical membrane by modulating the properties of the ultrastrong vacuum of a cavity [10].

Overall, the main aim of this Thesis is to contribute to our understanding of light-matter interactions, particularly in the USC regime, showing some peculiar effects, and it challenged conventional approaches by introducing more accurate and comprehensive methods.

Bibliography

[1]   F. Mauceri, A. Mercurio, S. Savasta, and O. Di Stefano, "Ultrastrong coupling of a qubit with a nonlinear optical resonator", Phys. Rev. A **105**, 023719 (2022).

[2]   A. Mercurio, V. Macrì, C. Gustin, S. Hughes, S. Savasta, and F. Nori, "Regimes of cavity QED under incoherent excitation: From weak to deep strong coupling", Phys. Rev. Res. **4**, 023048 (2022).

[3]   G. Andolina, F. Pellegrino, A. Mercurio, O. Di Stefano, M. Polini, and S. Savasta, "A non-perturbative no-go theorem for photon condensation in approximate models", The European Physical Journal Plus **137**, 1 (2022).

[4]   V. Macrì, A. Mercurio, F. Nori, S. Savasta, and C. Sánchez Muñoz, "Spontaneous Scattering of Raman Photons from Cavity-QED Systems in the Ultrastrong Coupling Regime", Phys. Rev. Lett. **129**, 273602 (2022).

[5]   A. Mercurio, S. Abo, F. Mauceri, E. Russo, V. Macrì, A. Miranowicz, S. Savasta, and O. Di Stefano, "Pure Dephasing of Light-Matter Systems in the Ultrastrong and Deep-Strong Coupling Regimes", Phys. Rev. Lett. **130**, 123601 (2023).

[6]   E. Russo, A. Mercurio, F. Mauceri, R. Lo Franco, F. Nori, S. Savasta, and V. Macrì, "Optomechanical two-photon hopping", Phys. Rev. Res. **5**, 013221 (2023).

Bibliography

[7] A. Ghirri, C. Bonizzoni, M. Maksutoglu, A. Mercurio, O. Di Stefano, S. Savasta, and M. Affronte, "Ultrastrong Magnon-Photon Coupling Achieved by Magnetic Films in Contact with Superconducting Resonators", Phys. Rev. Appl. **20**, 024039 (2023).

[8] A. Mercurio, S. De Liberato, F. Nori, S. Savasta, and R. Stassi, "Flying atom back-reaction and mechanically generated photons from vacuum", arXiv preprint arXiv:2209.10419, https://doi.org/10.48550/arXiv.2209.10419 (2022).

[9] A. Mercurio, G. M. Andolina, F. Pellegrino, O. Di Stefano, P. Jarillo-Herrero, C. Felser, F. H. Koppens, S. Savasta, and M. Polini, "Photon condensation, Van Vleck paramagnetism, and chiral cavities", arXiv preprint arXiv:2302.09964, https://doi.org/10.48550/arXiv.2302.09964 (2023).

[10] F. Minganti, A. Mercurio, F. Mauceri, M. Scigliuzzo, S. Savasta, and V. Savona, "Phonon Pumping by Modulating the Ultrastrong Vacuum", arXiv preprint arXiv:2309.15891, https://doi.org/10.48550/arXiv.2309.15891 (2023).

[11] A. Mercurio, *GitHub repository for the code used in the Thesis*, 2023.

[12] C. Cohen-Tannoudji, J. Dupont-Roc, and G. Grynberg, "Lagrangian and Hamiltonian Approach to Electrodynamics, The Standard Lagrangian and the Coulomb Gauge", in *Photons and atoms* (John Wiley and Sons, Ltd, 1997) Chap. 2, pp. 79–168.

[13] M. Babiker and R. Loudon, "Derivation of the Power-Zienau-Woolley Hamiltonian in quantum electrodynamics by gauge transformation", Proceedings of the Royal Society of London. A. Mathematical and Physical Sciences **385**, 439 (1983).

[14] D. H. Kobe, "Gauge-invariant classical Hamiltonian formulation of the electrodynamics of nonrelativistic particles", American Journal of Physics **49**, 581 (1981).

[15] M. Wubs, L. G. Suttorp, and A. Lagendijk, "Multiple-scattering approach to interatomic interactions and superradiance in inhomogeneous dielectrics", Phys. Rev. A **70**, 053823 (2004).

[16] I. I. Rabi, "On the Process of Space Quantization", Phys. Rev. **49**, 324 (1936).

[17] E. Jaynes and F. Cummings, "Comparison of quantum and semiclassical radiation theories with application to the beam maser", Proceedings of the IEEE **51**, 89 (1963).

[18] P. Lambropoulos and D. Petrosyan, "Atom in an external radiation field", in *Fundamentals of quantum optics and quantum information* (Springer Berlin, Heidelberg, 2007) Chap. 3, pp. 73–117.

[19] D. Braak, "Symmetries in the quantum Rabi model", Symmetry **11**, 1259 (2019).

[20] W.-H. Chang, W.-Y. Chen, H.-S. Chang, T.-P. Hsieh, J.-I. Chyi, and T.-M. Hsu, "Efficient Single-Photon Sources Based on Low-Density Quantum Dots in Photonic-Crystal Nanocavities", Phys. Rev. Lett. **96**, 117401 (2006).

[21] M. Brune, F. Schmidt-Kaler, A. Maali, J. Dreyer, E. Hagley, J. M. Raimond, and S. Haroche, "Quantum Rabi Oscillation: A Direct Test of Field Quantization in a Cavity", Phys. Rev. Lett. **76**, 1800 (1996).

[22] Y. Kaluzny, P. Goy, M. Gross, J. M. Raimond, and S. Haroche, "Observation of Self-Induced Rabi Oscillations in Two-Level Atoms Excited Inside a Resonant Cavity: The Ringing Regime of Superradiance", Phys. Rev. Lett. **51**, 1175 (1983).

[23] D. Meschede, H. Walther, and G. Müller, "One-Atom Maser", Phys. Rev. Lett. **54**, 551 (1985).

[24] R. J. Thompson, G. Rempe, and H. J. Kimble, "Observation of normal-mode splitting for an atom in an optical cavity", Phys. Rev. Lett. **68**, 1132 (1992).

[25] C. Weisbuch, M. Nishioka, A. Ishikawa, and Y. Arakawa, "Observation of the coupled exciton-photon mode splitting in a semiconductor quantum microcavity", Phys. Rev. Lett. **69**, 3314 (1992).

[26] P. Lodahl, S. Mahmoodian, and S. Stobbe, "Interfacing single photons and single quantum dots with photonic nanostructures", Rev. Mod. Phys. **87**, 347 (2015).

[27] X. Gu, A. F. Kockum, A. Miranowicz, Y.-x. Liu, and F. Nori, "Microwave photonics with superconducting quantum circuits", Physics Reports **718**, 1 (2017).

[28] E. M. Purcell, H. C. Torrey, and R. V. Pound, "Resonance Absorption by Nuclear Magnetic Moments in a Solid", Phys. Rev. **69**, 37 (1946).

[29] E. M. Purcell, "Spontaneous Emission Probabilities at Radio Frequencies", Phys. Rev. **69**, 681 (1946).

[30] A. Frisk Kockum, A. Miranowicz, S. De Liberato, S. Savasta, and F. Nori, "Ultrastrong coupling between light and matter", Nature Reviews Physics **1**, 19 (2019).

[31] P. Forn-Díaz, L. Lamata, E. Rico, J. Kono, and E. Solano, "Ultrastrong coupling regimes of light-matter interaction", Rev. Mod. Phys. **91**, 025005 (2019).

[32] R. H. Dicke, "Coherence in Spontaneous Radiation Processes", Phys. Rev. **93**, 99 (1954).

[33] T. Niemczyk, F. Deppe, H. Huebl, E. Menzel, F. Hocke, M. Schwarz, J. Garcia-Ripoll, D. Zueco, T. Hümmer, E. Solano, et al., "Circuit quantum electrodynamics in the ultrastrong-coupling regime", Nature Physics **6**, 772 (2010).

[34] A. Bayer, M. Pozimski, S. Schambeck, D. Schuh, R. Huber, D. Bougeard, and C. Lange, "Terahertz light-matter interaction beyond unity coupling strength", Nano letters **17**, 6340 (2017).

[35] C. Ciuti, G. Bastard, and I. Carusotto, "Quantum vacuum properties of the intersubband cavity polariton field", Phys. Rev. B **72**, 115303 (2005).

[36] P. Forn-Díaz, J. Lisenfeld, D. Marcos, J. J. García-Ripoll, E. Solano, C. J. P. M. Harmans, and J. E. Mooij, "Observation of the Bloch-Siegert Shift in a Qubit-Oscillator System in the Ultrastrong Coupling Regime", Phys. Rev. Lett. **105**, 237001 (2010).

[37] G. Günter, A. A. Anappara, J. Hees, A. Sell, G. Biasiol, L. Sorba, S. De Liberato, C. Ciuti, A. Tredicucci, A. Leitenstorfer, et al., "Sub-cycle switch-on of ultrastrong light–matter interaction", Nature **458**, 178 (2009).

[38] Y. Todorov, A. M. Andrews, R. Colombelli, S. De Liberato, C. Ciuti, P. Klang, G. Strasser, and C. Sirtori, "Ultrastrong Light-Matter Coupling Regime with Polariton Dots", Phys. Rev. Lett. **105**, 196402 (2010).

[39] T. Schwartz, J. A. Hutchison, C. Genet, and T. W. Ebbesen, "Reversible Switching of Ultrastrong Light-Molecule Coupling", Phys. Rev. Lett. **106**, 196405 (2011).

[40] J.-Q. You and F. Nori, "Atomic physics and quantum optics using superconducting circuits", Nature **474**, 589 (2011).

[41] G. Scalari, C. Maissen, D. Turčinková, D. Hagenmüller, S. De Liberato, C. Ciuti, C. Reichl, D. Schuh, W. Wegscheider, M. Beck, et al., "Ultrastrong coupling of the cyclotron transition of a 2D electron gas to a THz metamaterial", Science **335**, 1323 (2012).

[42] M. Geiser, F. Castellano, G. Scalari, M. Beck, L. Nevou, and J. Faist, "Ultrastrong Coupling Regime and Plasmon Polaritons in Parabolic Semiconductor Quantum Wells", Phys. Rev. Lett. **108**, 106402 (2012).

[43] S. Kéna-Cohen, S. A. Maier, and D. D. Bradley, "Ultrastrongly Coupled Exciton–Polaritons in Metal-Clad Organic Semiconductor Microcavities", Advanced Optical Materials **1**, 827 (2013).

[44] Z.-L. Xiang, S. Ashhab, J. Q. You, and F. Nori, "Hybrid quantum circuits: Superconducting circuits interacting with other quantum systems", Rev. Mod. Phys. **85**, 623 (2013).

[45] C. Maissen, G. Scalari, F. Valmorra, M. Beck, J. Faist, S. Cibella, R. Leoni, C. Reichl, C. Charpentier, and W. Wegscheider, "Ultrastrong coupling in the near field of complementary split-ring resonators", Phys. Rev. B **90**, 205309 (2014).

[46] M. Goryachev, W. G. Farr, D. L. Creedon, Y. Fan, M. Kostylev, and M. E. Tobar, "High-Cooperativity Cavity QED with Magnons at Microwave Frequencies", Phys. Rev. Appl. **2**, 054002 (2014).

[47] J.-M. Pirkkalainen, S. Cho, F. Massel, J. Tuorila, T. Heikkilä, P. Hakonen, and M. Sillanpää, "Cavity optomechanics mediated by a quantum two-level system", Nature communications **6**, 6981 (2015).

[48] K. K. W. Ma and C. K. Law, "Three-photon resonance and adiabatic passage in the large-detuning Rabi model", Phys. Rev. A **92**, 023842 (2015).

[49] L. Garziano, R. Stassi, V. Macrì, A. F. Kockum, S. Savasta, and F. Nori, "Multiphoton quantum Rabi oscillations in ultrastrong cavity QED", Phys. Rev. A **92**, 063830 (2015).

Bibliography

[50] A. Baust, E. Hoffmann, M. Haeberlein, M. J. Schwarz, P. Eder, J. Goetz, F. Wulschner, E. Xie, L. Zhong, F. Quijandría, D. Zueco, J.-J. G. Ripoll, L. García-Álvarez, G. Romero, E. Solano, K. G. Fedorov, E. P. Menzel, F. Deppe, A. Marx, and R. Gross, "Ultrastrong coupling in two-resonator circuit QED", Phys. Rev. B **93**, 214501 (2016).

[51] F. Benz, M. K. Schmidt, A. Dreismann, R. Chikkaraddy, Y. Zhang, A. Demetriadou, C. Carnegie, H. Ohadi, B. De Nijs, R. Esteban, et al., "Single-molecule optomechanics in "picocavities"", Science **354**, 726 (2016).

[52] J. George, T. Chervy, A. Shalabney, E. Devaux, H. Hiura, C. Genet, and T. W. Ebbesen, "Multiple Rabi Splittings under Ultrastrong Vibrational Coupling", Phys. Rev. Lett. **117**, 153601 (2016).

[53] L. Garziano, V. Macrì, R. Stassi, O. Di Stefano, F. Nori, and S. Savasta, "One Photon Can Simultaneously Excite Two or More Atoms", Phys. Rev. Lett. **117**, 043601 (2016).

[54] P. Forn-Díaz, J. J. García-Ripoll, B. Peropadre, J.-L. Orgiazzi, M. Yurtalan, R. Belyansky, C. M. Wilson, and A. Lupascu, "Ultrastrong coupling of a single artificial atom to an electromagnetic continuum in the nonperturbative regime", Nature Physics **13**, 39 (2017).

[55] F. Yoshihara, T. Fuse, S. Ashhab, K. Kakuyanagi, S. Saito, and K. Semba, "Superconducting qubit–oscillator circuit beyond the ultrastrong-coupling regime", Nature Physics **13**, 44 (2017).

[56] F. Yoshihara, T. Fuse, S. Ashhab, K. Kakuyanagi, S. Saito, and K. Semba, "Characteristic spectra of circuit quantum electrodynamics systems from the ultrastrong- to the deep-strong-coupling regime", Phys. Rev. A **95**, 053824 (2017).

[57] A. F. Kockum, A. Miranowicz, V. Macrì, S. Savasta, and F. Nori, "Deterministic quantum nonlinear optics with single atoms and virtual photons", Phys. Rev. A **95**, 063849 (2017).

[58] A. F. Kockum, V. Macrì, L. Garziano, S. Savasta, and F. Nori, "Frequency conversion in ultrastrong cavity QED", Scientific reports **7**, 5313 (2017).

[59] R. Stassi, V. Macrì, A. F. Kockum, O. Di Stefano, A. Miranowicz, S. Savasta, and F. Nori, "Quantum nonlinear optics without photons", Phys. Rev. A **96**, 023818 (2017).

[60] B. Askenazi, A. Vasanelli, Y. Todorov, E. Sakat, J.-J. Greffet, G. Beaudoin, I. Sagnes, and C. Sirtori, "Midinfrared ultrastrong light–matter coupling for THz thermal emission", ACS photonics **4**, 2550 (2017).

[61] F. Barachati, J. Simon, Y. A. Getmanenko, S. Barlow, S. R. Marder, and S. Kéna-Cohen, "Tunable third-harmonic generation from polaritons in the ultrastrong coupling regime", Acs Photonics **5**, 119 (2018).

[62] F. Yoshihara, T. Fuse, Z. Ao, S. Ashhab, K. Kakuyanagi, S. Saito, T. Aoki, K. Koshino, and K. Semba, "Inversion of Qubit Energy Levels in Qubit-Oscillator Circuits in the Deep-Strong-Coupling Regime", Phys. Rev. Lett. **120**, 183601 (2018).

[63] E. Eizner, J. Brodeur, F. Barachati, A. Sridharan, and S. Kéna-Cohen, "Organic photodiodes with an extended responsivity using ultrastrong light–matter coupling", ACS Photonics **5**, 2921 (2018).

[64] L. A. Martínez-Martínez, R. F. Ribeiro, J. Campos-González-Angulo, and J. Yuen-Zhou, "Can ultrastrong coupling change ground-state chemical reactions?", ACS Photonics **5**, 167 (2018).

[65] G. L. Paravicini-Bagliani, F. Appugliese, E. Richter, F. Valmorra, J. Keller, M. Beck, N. Bartolo, C. Rössler, T. Ihn, K. Ensslin, et al., "Magneto-transport controlled by Landau polariton states", Nature Physics **15**, 186 (2019).

[66] J. Puertas Martínez, S. Léger, N. Gheeraert, R. Dassonneville, L. Planat, F. Foroughi, Y. Krupko, O. Buisson, C. Naud, W. Hasch-Guichard, et al., "A tunable josephson platform to explore many-body quantum optics in circuit-qed", npj Quantum Information **5**, 19 (2019).

[67] G. Flower, M. Goryachev, J. Bourhill, and M. E. Tobar, "Experimental implementations of cavity-magnon systems: from ultra strong coupling to applications in precision measurement", New Journal of Physics **21**, 095004 (2019).

[68] M. Jeannin, G. Mariotti Nesurini, S. Suffit, D. Gacemi, A. Vasanelli, L. Li, A. G. Davies, E. Linfield, C. Sirtori, and Y. Todorov, "Ultrastrong light–matter coupling in deeply subwavelength THz LC resonators", ACS photonics **6**, 1207 (2019).

[69] S.-P. Wang, G.-Q. Zhang, Y. Wang, Z. Chen, T. Li, J. S. Tsai, S.-Y. Zhu, and J. Q. You, "Photon-Dressed Bloch-Siegert Shift in an Ultrastrongly Coupled Circuit Quantum Electrodynamical System", Phys. Rev. Appl. **13**, 054063 (2020).

[70] J. Keller, G. Scalari, F. Appugliese, S. Rajabali, M. Beck, J. Haase, C. A. Lehner, W. Wegscheider, M. Failla, M. Myronov, D. R. Leadley, J. Lloyd-Hughes, P. Nataf, and J. Faist, "Landau polaritons in highly nonparabolic two-dimensional gases in the ultrastrong coupling regime", Phys. Rev. B **101**, 075301 (2020).

[71] V. Macrì, F. Nori, S. Savasta, and D. Zueco, "Spin squeezing by one-photon–two-atom excitation processes in atomic ensembles", Phys. Rev. A **101**, 053818 (2020).

[72] W. E. Lamb, "Fine Structure of the Hydrogen Atom. III", Phys. Rev. **85**, 259 (1952).

[73] F. Bassani, J. J. Forney, and A. Quattropani, "Choice of Gauge in Two-Photon Transitions: $1s - 2s$ Transition in Atomic Hydrogen", Phys. Rev. Lett. **39**, 1070 (1977).

[74] D. De Bernardis, P. Pilar, T. Jaako, S. De Liberato, and P. Rabl, "Breakdown of gauge invariance in ultrastrong-coupling cavity QED", Phys. Rev. A **98**, 053819 (2018).

[75] O. Di Stefano, A. Settineri, V. Macrì, L. Garziano, R. Stassi, S. Savasta, and F. Nori, "Resolution of gauge ambiguities in ultrastrong-coupling cavity quantum electrodynamics", Nature Physics **15**, 803 (2019).

[76] A. F. Starace, "Length and Velocity Formulas in Approximate Oscillator-Strength Calculations", Phys. Rev. A **3**, 1242 (1971).

[77] R. Girlanda, A. Quattropani, and P. Schwendimann, "Two-photon transitions to exciton states in semiconductors. Application to CuCl", Phys. Rev. B **24**, 2009 (1981).

[78] S. Ismail-Beigi, E. K. Chang, and S. G. Louie, "Coupling of Nonlocal Potentials to Electromagnetic Fields", Phys. Rev. Lett. **87**, 087402 (2001).

[79] S. Savasta, O. Di Stefano, A. Settineri, D. Zueco, S. Hughes, and F. Nori, "Gauge principle and gauge invariance in two-level systems", Phys. Rev. A **103**, 053703 (2021).

[80] P. Lambropoulos and D. Petrosyan, "Quantum Theory of Radiation", in *Fundamentals of quantum optics and quantum information* (Springer Berlin, Heidelberg, 2007) Chap. 2, pp. 45–72.

[81] R. J. Glauber, "The Quantum Theory of Optical Coherence", Phys. Rev. **130**, 2529 (1963).

[82] A. Ridolfo, M. Leib, S. Savasta, and M. J. Hartmann, "Photon Blockade in the Ultrastrong Coupling Regime", Phys. Rev. Lett. **109**, 193602 (2012).

[83] O. Di Stefano, A. F. Kockum, A. Ridolfo, S. Savasta, and F. Nori, "Photodetection probability in quantum systems with arbitrarily strong light-matter interaction", Scientific Reports **8**, 17825 (2018).

[84] A. Settineri, O. Di Stefano, D. Zueco, S. Hughes, S. Savasta, and F. Nori, "Gauge freedom, quantum measurements, and time-dependent interactions in cavity QED", Phys. Rev. Res. **3**, 023079 (2021).

[85] S. Savasta, O. Di Stefano, and F. Nori, "Thomas–Reiche–Kuhn (TRK) sum rule for interacting photons", Nanophotonics **10**, 465 (2020).

[86] C. Gardiner and P. Zoller, *Quantum noise: a handbook of Markovian and non-Markovian quantum stochastic methods with applications to quantum optics* (Springer Science & Business Media, 2004).

[87] L. Garziano, A. Ridolfo, R. Stassi, O. Di Stefano, and S. Savasta, "Switching on and off of ultrastrong light-matter interaction: Photon statistics of quantum vacuum radiation", Phys. Rev. A **88**, 063829 (2013).

[88] S. Franke, S. Hughes, M. K. Dezfouli, P. T. Kristensen, K. Busch, A. Knorr, and M. Richter, "Quantization of Quasinormal Modes for Open Cavities and Plasmonic Cavity Quantum Electrodynamics", Phys. Rev. Lett. **122**, 213901 (2019).

[89] S. Hughes, S. Franke, C. Gustin, M. Kamandar Dezfouli, A. Knorr, and M. Richter, "Theory and limits of on-demand single-photon sources using plasmonic resonators: a quantized quasinormal mode approach", ACS Photonics **6**, 2168 (2019).

[90] S. Franke, M. Richter, J. Ren, A. Knorr, and S. Hughes, "Quantized quasinormal-mode description of nonlinear cavity-QED effects from coupled resonators with a Fano-like resonance", Phys. Rev. Res. **2**, 033456 (2020).

[91] J. J. Sanchez-Mondragon, N. B. Narozhny, and J. H. Eberly, "Theory of Spontaneous-Emission Line Shape in an Ideal Cavity", Phys. Rev. Lett. **51**, 550 (1983).

[92] E. del Valle, F. P. Laussy, and C. Tejedor, "Luminescence spectra of quantum dots in microcavities. II. Fermions", Phys. Rev. B **79**, 235326 (2009).

[93] M. Brune, E. Hagley, J. Dreyer, X. Maître, A. Maali, C. Wunderlich, J. M. Raimond, and S. Haroche, "Observing the Progressive Decoherence of the "Meter" in a Quantum Measurement", Phys. Rev. Lett. **77**, 4887 (1996).

[94] S. Gleyzes, S. Kuhr, C. Guerlin, J. Bernu, S. Deleglise, U. Busk Hoff, M. Brune, J.-M. Raimond, and S. Haroche, "Quantum jumps of light recording the birth and death of a photon in a cavity", Nature **446**, 297 (2007).

[95] C. Guerlin, J. Bernu, S. Deleglise, C. Sayrin, S. Gleyzes, S. Kuhr, M. Brune, J.-M. Raimond, and S. Haroche, "Progressive field-state collapse and quantum non-demolition photon counting", Nature **448**, 889 (2007).

[96] A. Wallraff, D. I. Schuster, A. Blais, L. Frunzio, R.-S. Huang, J. Majer, S. Kumar, S. M. Girvin, and R. J. Schoelkopf, "Strong coupling of a single photon to a superconducting qubit using circuit quantum electrodynamics", Nature **431**, 162 (2004).

[97] H.-P. Breuer and F. Petruccione, *The Theory of Open Quantum Systems*, Oxford Graduate Texts (Oxford University Press, 2002).

[98] P. Lambropoulos and D. Petrosyan, "System-Reservoir Interaction", in *Fundamentals of quantum optics and quantum information* (Springer Berlin, Heidelberg, 2007) Chap. 4, pp. 119–149.

[99] F. Beaudoin, J. M. Gambetta, and A. Blais, "Dissipation and ultrastrong coupling in circuit QED", Phys. Rev. A **84**, 043832 (2011).

[100] A. Settineri, V. Macrí, A. Ridolfo, O. Di Stefano, A. F. Kockum, F. Nori, and S. Savasta, "Dissipation and thermal noise in hybrid quantum systems in the ultrastrong-coupling regime", Phys. Rev. A **98**, 053834 (2018).

[101] P. D. Nation, J. R. Johansson, M. P. Blencowe, and A. J. Rimberg, "Iterative solutions to the steady-state density matrix for optomechanical systems", Phys. Rev. E **91**, 013307 (2015).

[102] F. Minganti, A. Biella, N. Bartolo, and C. Ciuti, "Spectral theory of Liouvillians for dissipative phase transitions", Phys. Rev. A **98**, 042118 (2018).

[103] W. Salmon, C. Gustin, A. Settineri, O. Di Stefano, D. Zueco, S. Savasta, F. Nori, and S. Hughes, "Gauge-independent emission spectra and quantum correlations in the ultrastrong coupling regime of open system cavity-QED", Nanophotonics **11**, 1573 (2022).

[104] S. De Liberato, "Light-Matter Decoupling in the Deep Strong Coupling Regime: The Breakdown of the Purcell Effect", Phys. Rev. Lett. **112**, 016401 (2014).

[105] Y. Ashida, A. ç. İmamo ğlu, and E. Demler, "Cavity Quantum Electrodynamics at Arbitrary Light-Matter Coupling Strengths", Phys. Rev. Lett. **126**, 153603 (2021).

[106] S. Gambino, M. Mazzeo, A. Genco, O. Di Stefano, S. Savasta, S. Patane, D. Ballarini, F. Mangione, G. Lerario, D. Sanvitto, et al., "Exploring light–matter interaction phenomena under ultrastrong coupling regime", ACS Photonics **1**, 1042 (2014).

[107] Raman, Chandrasekhara Venkata and Krishnan, Kariamanikkam Srinivasa, "A new type of secondary radiation", Nature **121**, 501 (1928).

[108] A. Fainstein, B. Jusserand, and V. Thierry-Mieg, "Cavity-Polariton Mediated Resonant Raman Scattering", Phys. Rev. Lett. **78**, 1576 (1997).

[109] D. A. Long, *The Raman Effect: : A Unified Treatment of the Theory of Raman Scattering by Molecules* (John Wiley & Sons, Ltd, Chichester, UK, 2002).

[110] P. Jamonneau, G. Hétet, A. Dréau, J.-F. Roch, and V. Jacques, "Coherent Population Trapping of a Single Nuclear Spin Under Ambient Conditions", Phys. Rev. Lett. **116**, 043603 (2016).

[111] A. Donarini, M. Niklas, M. Schafberger, N. Paradiso, C. Strunk, and M. Grifoni, "Coherent population trapping by dark state formation in a carbon nanotube quantum dot", Nature communications **10**, 381 (2019).

[112] N. V. Vitanov, A. A. Rangelov, B. W. Shore, and K. Bergmann, "Stimulated Raman adiabatic passage in physics, chemistry, and beyond", Rev. Mod. Phys. **89**, 015006 (2017).

[113] M. Fleischhauer, A. Imamoglu, and J. P. Marangos, "Electromagnetically induced transparency: Optics in coherent media", Rev. Mod. Phys. **77**, 633 (2005).

[114] J. Long, H. S. Ku, X. Wu, X. Gu, R. E. Lake, M. Bal, Y.-x. Liu, and D. P. Pappas, "Electromagnetically Induced Transparency in Circuit Quantum Electrodynamics with Nested Polariton States", Phys. Rev. Lett. **120**, 083602 (2018).

[115] Y. Guo, C.-C. Shu, D. Dong, and F. Nori, "Vanishing and Revival of Resonance Raman Scattering", Phys. Rev. Lett. **123**, 223202 (2019).

[116] L. F. Wei, J. R. Johansson, L. X. Cen, S. Ashhab, and F. Nori, "Controllable Coherent Population Transfers in Superconducting Qubits for Quantum Computing", Phys. Rev. Lett. **100**, 113601 (2008).

[117] C.-C. Shu, J. Yu, K.-J. Yuan, W.-H. Hu, J. Yang, and S.-L. Cong, "Stimulated Raman adiabatic passage in molecular electronic states", Phys. Rev. A **79**, 023418 (2009).

[118] K. Kumar, A. Vepsäläinen, S. Danilin, and G. Paraoanu, "Stimulated Raman adiabatic passage in a three-level superconducting circuit", Nature communications **7**, 10628 (2016).

[119] G. Falci, P. Di Stefano, A. Ridolfo, A. D'Arrigo, G. Paraoanu, and E. Paladino, "Advances in quantum control of three-level superconducting circuit architectures", Fortschritte der Physik **65**, 1600077 (2017).

[120] F. Dimer, B. Estienne, A. S. Parkins, and H. J. Carmichael, "Proposed realization of the Dicke-model quantum phase transition in an optical cavity QED system", Phys. Rev. A **75**, 013804 (2007).

[121] S. Sun, J. L. Zhang, K. A. Fischer, M. J. Burek, C. Dory, K. G. Lagoudakis, Y.-K. Tzeng, M. Radulaski, Y. Kelaita, A. Safavi-Naeini, Z.-X. Shen, N. A. Melosh, S. Chu, M. Lon čar, and J. Vu čkovi ć, "Cavity-Enhanced Raman Emission from a Single Color Center in a Solid", Phys. Rev. Lett. **121**, 083601 (2018).

[122] M. Hennrich, T. Legero, A. Kuhn, and G. Rempe, "Vacuum-Stimulated Raman Scattering Based on Adiabatic Passage in a High-Finesse Optical Cavity", Phys. Rev. Lett. **85**, 4872 (2000).

[123] A. Kuhn, M. Hennrich, and G. Rempe, "Deterministic Single-Photon Source for Distributed Quantum Networking", Phys. Rev. Lett. **89**, 067901 (2002).

[124] T. M. Sweeney, S. G. Carter, A. S. Bracker, M. Kim, C. S. Kim, L. Yang, P. M. Vora, P. G. Brereton, E. R. Cleveland, and D. Gammon, "Cavity-stimulated Raman emission from a single quantum dot spin", Nature Photonics **8**, 442 (2014).

[125] A. Orlando, F. Franceschini, C. Muscas, S. Pidkova, M. Bartoli, M. Rovere, and A. Tagliaferro, "A comprehensive review on Raman spectroscopy applications", Chemosensors **9**, 262 (2021).

[126] A. Kudelski, "Analytical applications of Raman spectroscopy", Talanta **76**, 1 (2008).

[127] B. Pettinger, P. Schambach, C. J. Villagómez, and N. Scott, "Tip-enhanced Raman spectroscopy: near-fields acting on a few molecules", Annual review of physical chemistry **63**, 379 (2012).

[128] X.-M. Qian and S. M. Nie, "Single-molecule and single-nanoparticle SERS: from fundamental mechanisms to biomedical applications", Chemical Society Reviews **37**, 912 (2008).

[129] D. Yang and Y. Ying, "Applications of Raman spectroscopy in agricultural products and food analysis: A review", Applied Spectroscopy Reviews **46**, 539 (2011).

[130] R. Parimaladevi, V. Sathe, U. Mahalingam, et al., "Graphene boosted silver nanoparticles as surface enhanced Raman spectroscopic sensors and photocatalysts for removal of standard and industrial dye contaminants", Sensors and Actuators B: Chemical **281**, 679 (2019).

[131] K. Kneipp, Y. Wang, H. Kneipp, L. T. Perelman, I. Itzkan, R. R. Dasari, and M. S. Feld, "Single Molecule Detection Using Surface-Enhanced Raman Scattering (SERS)", Phys. Rev. Lett. **78**, 1667 (1997).

[132] S. Nie and S. R. Emory, "Probing single molecules and single nanoparticles by surface-enhanced Raman scattering", science **275**, 1102 (1997).

[133] J. Langer, D. Jimenez de Aberasturi, J. Aizpurua, R. A. Alvarez-Puebla, B. Auguié, J. J. Baumberg, G. C. Bazan, S. E. Bell, A. Boisen, A. G. Brolo, et al., "Present and future of surface-enhanced Raman scattering", ACS nano **14**, 28 (2019).

[134] R. Zhang, Y. Zhang, Z. Dong, S. Jiang, C. Zhang, L. Chen, L. Zhang, Y. Liao, J. Aizpurua, Y. e. Luo, et al., "Chemical mapping of a single molecule by plasmon-enhanced Raman scattering", Nature **498**, 82 (2013).

[135] W. Zhu and K. B. Crozier, "Quantum mechanical limit to plasmonic enhancement as observed by surface-enhanced Raman scattering", Nature communications **5**, 5228 (2014).

[136] A. Shalabney, J. George, J. a. Hutchison, G. Pupillo, C. Genet, and T. W. Ebbesen, "Coherent coupling of molecular resonators with a microcavity mode", Nature communications **6**, 5981 (2015).

[137] M. K. Schmidt, R. Esteban, A. González-Tudela, G. Giedke, and J. Aizpurua, "Quantum mechanical description of Raman scattering from molecules in plasmonic cavities", ACS nano **10**, 6291 (2016).

[138] P. Roelli, C. Galland, N. Piro, and T. J. Kippenberg, "Molecular cavity optomechanics as a theory of plasmon-enhanced Raman scattering", Nature nanotechnology **11**, 164 (2016).

[139] M. Kamandar Dezfouli and S. Hughes, "Quantum optics model of surface-enhanced Raman spectroscopy for arbitrarily shaped plasmonic resonators", ACS Photonics **4**, 1245 (2017).

[140] M. K. Dezfouli, R. Gordon, and S. Hughes, "Molecular optomechanics in the anharmonic cavity-QED regime using hybrid metal–dielectric cavity modes", ACS Photonics **6**, 1400 (2019).

[141] S. Hughes, A. Settineri, S. Savasta, and F. Nori, "Resonant Raman scattering of single molecules under simultaneous strong cavity coupling and ultrastrong optomechanical coupling in plasmonic resonators: Phonon-dressed polaritons", Phys. Rev. B **104**, 045431 (2021).

[142] P. Roelli, D. Martin-Cano, T. J. Kippenberg, and C. Galland, "Molecular Platform for Frequency Upconversion at the Single-Photon Level", Phys. Rev. X **10**, 031057 (2020).

[143] B. Gurlek, V. Sandoghdar, and D. Martin-Cano, "Engineering Long-Lived Vibrational States for an Organic Molecule", Phys. Rev. Lett. **127**, 123603 (2021).

[144] E. del Valle, A. Gonzalez-Tudela, F. P. Laussy, C. Tejedor, and M. J. Hartmann, "Theory of Frequency-Filtered and Time-Resolved N-Photon Correlations", Phys. Rev. Lett. **109**, 183601 (2012).

[145] L. Garziano, A. Settineri, O. Di Stefano, S. Savasta, and F. Nori, "Gauge invariance of the Dicke and Hopfield models", Phys. Rev. A **102**, 023718 (2020).

[146] A. Majumdar, A. Papageorge, E. D. Kim, M. Bajcsy, H. Kim, P. Petroff, and J. Vu čkovi ć, "Probing of single quantum dot dressed states via an off-resonant cavity", Phys. Rev. B **84**, 085310 (2011).

[147] A. Papageorge, A. Majumdar, E. D. Kim, and J. Vučković, "Bichromatic driving of a solid-state cavity quantum electrodynamics system", New Journal of Physics **14**, 013028 (2012).

[148] M. Maragkou, C. Sánchez-Muñoz, S. Lazi ć, E. Chernysheva, H. P. van der Meulen, A. González-Tudela, C. Tejedor, L. J. Martínez, I. Prieto, P. A. Postigo, and J. M. Calleja, "Bichromatic dressing of a quantum dot detected by a remote second quantum dot", Phys. Rev. B **88**, 075309 (2013).

[149] M. G. Paris, "Quantum estimation for quantum technology", International Journal of Quantum Information **7**, 125 (2009).

[150] H. M. Wiseman and G. J. Milburn, *Quantum measurement and control* (Cambridge university press, 2009).

[151] J. P. Dowling and K. P. Seshadreesan, "Quantum optical technologies for metrology, sensing, and imaging", Journal of Lightwave Technology **33**, 2359 (2014).

[152] D. Petz and C. Ghinea, "Introduction to quantum Fisher information", in *Quantum probability and related topics* (World Scientific, 2011), pp. 261–281.

[153] A. Luis, "Fisher information as a generalized measure of coherence in classical and quantum optics", Optics Express **20**, 24686 (2012).

[154] J. Chao, E. S. Ward, and R. J. Ober, "Fisher information theory for parameter estimation in single molecule microscopy: tutorial", JOSA A **33**, B36 (2016).

[155] D. Šafránek, "Simple expression for the quantum Fisher information matrix", Phys. Rev. A **97**, 042322 (2018).

[156] J. Liu, H. Yuan, X.-M. Lu, and X. Wang, "Quantum Fisher information matrix and multiparameter estimation", Journal of Physics A: Mathematical and Theoretical **53**, 023001 (2020).

[157] A. Vivas-Viaña and C. Sánchez Muñoz, "Two-photon resonance fluorescence of two interacting nonidentical quantum emitters", Phys. Rev. Res. **3**, 033136 (2021).

[158] L. Allen and J. H. Eberly, *Optical resonance and two-level atoms*, Vol. 28 (Courier Corporation, 1987).

[159] P. Borri, W. Langbein, S. Schneider, U. Woggon, R. L. Sellin, D. Ouyang, and D. Bimberg, "Ultralong Dephasing Time in InGaAs Quantum Dots", Phys. Rev. Lett. **87**, 157401 (2001).

[160] P. Borri, W. Langbein, U. Woggon, M. Schwab, M. Bayer, S. Fafard, Z. Wasilewski, and P. Hawrylak, "Exciton Dephasing in Quantum Dot Molecules", Phys. Rev. Lett. **91**, 267401 (2003).

[161] E. A. Muljarov, T. Takagahara, and R. Zimmermann, "Phonon-Induced Exciton Dephasing in Quantum Dot Molecules", Phys. Rev. Lett. **95**, 177405 (2005).

[162] M. R. Delbecq, T. Nakajima, P. Stano, T. Otsuka, S. Amaha, J. Yoneda, K. Takeda, G. Allison, A. Ludwig, A. D. Wieck, and S. Tarucha, "Quantum Dephasing in a Gated GaAs Triple Quantum Dot due to Nonergodic Noise", Phys. Rev. Lett. **116**, 046802 (2016).

[163] I. Kilen, M. Kolesik, J. Hader, J. V. Moloney, U. Huttner, M. K. Hagen, and S. W. Koch, "Propagation Induced Dephasing in Semiconductor High-Harmonic Generation", Phys. Rev. Lett. **125**, 083901 (2020).

[164] F. Katsch, M. Selig, and A. Knorr, "Exciton-Scattering-Induced Dephasing in Two-Dimensional Semiconductors", Phys. Rev. Lett. **124**, 257402 (2020).

[165] T. Yu and J. H. Eberly, "Qubit disentanglement and decoherence via dephasing", Phys. Rev. B **68**, 165322 (2003).

[166] S. Haroche, "Nobel Lecture: Controlling photons in a box and exploring the quantum to classical boundary", Rev. Mod. Phys. **85**, 1083 (2013).

[167] W. H. Zurek, "Decoherence, einselection, and the quantum origins of the classical", Rev. Mod. Phys. **75**, 715 (2003).

[168] S. Habib, K. Shizume, and W. H. Zurek, "Decoherence, Chaos, and the Correspondence Principle", Phys. Rev. Lett. **80**, 4361 (1998).

[169] D. P. DiVincenzo, "Quantum computation", Science **270**, 255 (1995).

[170] S. I. Bogdanov, A. Boltasseva, and V. M. Shalaev, "Overcoming quantum decoherence with plasmonics", Science **364**, 532 (2019).

[171] D. A. Lidar, I. L. Chuang, and K. B. Whaley, "Decoherence-Free Subspaces for Quantum Computation", Phys. Rev. Lett. **81**, 2594 (1998).

[172] A. Grodecka and P. Machnikowski, "Partly noiseless encoding of quantum information in quantum dot arrays against phonon-induced pure dephasing", Phys. Rev. B **73**, 125306 (2006).

[173] M. Ban, S. Kitajima, and F. Shibata, "Decoherence of quantum information of qubits by stochastic dephasing", Physics Letters A **349**, 415 (2006).

[174] Q. Guo, S.-B. Zheng, J. Wang, C. Song, P. Zhang, K. Li, W. Liu, H. Deng, K. Huang, D. Zheng, X. Zhu, H. Wang, C.-Y. Lu, and J.-W. Pan, "Dephasing-Insensitive Quantum Information Storage and Processing with Superconducting Qubits", Phys. Rev. Lett. **121**, 130501 (2018).

[175] G. Kurizki, P. Bertet, Y. Kubo, K. Mølmer, D. Petrosyan, P. Rabl, and J. Schmiedmayer, "Quantum technologies with hybrid systems", Proceedings of the National Academy of Sciences **112**, 3866 (2015).

[176] A. Clerk, K. Lehnert, P. Bertet, J. Petta, and Y. Nakamura, "Hybrid quantum systems with circuit quantum electrodynamics", Nature Physics **16**, 257 (2020).

[177] B. Lounis and M. Orrit, "Single-photon sources", Reports on Progress in Physics **68**, 1129 (2005).

[178] J. M. Gambetta, J. M. Chow, and M. Steffen, "Building logical qubits in a superconducting quantum computing system", npj quantum information **3**, 2 (2017).

[179] M. Ganzhorn, D. Egger, P. Barkoutsos, P. Ollitrault, G. Salis, N. Moll, M. Roth, A. Fuhrer, P. Mueller, S. Woerner, I. Tavernelli, and S. Filipp, "Gate-Efficient Simulation of Molecular Eigenstates on a Quantum Computer", Phys. Rev. Appl. **11**, 044092 (2019).

[180] R. Uppu, F. T. Pedersen, Y. Wang, C. T. Olesen, C. Papon, X. Zhou, L. Midolo, S. Scholz, A. D. Wieck, A. Ludwig, et al., "Scalable integrated single-photon source", Science advances **6**, eabc8268 (2020).

[181] A. Auffèves, D. Gerace, J.-M. Gérard, M. F. ç. Santos, L. C. Andreani, and J.-P. Poizat, "Controlling the dynamics of a coupled atom-cavity system by pure dephasing", Phys. Rev. B **81**, 245419 (2010).

[182] J. J. Hopfield, "Theory of the Contribution of Excitons to the Complex Dielectric Constant of Crystals", Phys. Rev. **112**, 1555 (1958).

[183] M. Gross and S. Haroche, "Superradiance: An essay on the theory of collective spontaneous emission", Physics reports **93**, 301 (1982).

[184] K. Cong, Q. Zhang, Y. Wang, G. T. Noe, A. Belyanin, and J. Kono, "Dicke superradiance in solids", JOSA B **33**, C80 (2016).

[185] P. Kirton, M. M. Roses, J. Keeling, and E. G. Dalla Torre, "Introduction to the Dicke Model: From Equilibrium to Nonequilibrium, and Vice Versa (Adv. Quantum Technol. 1-2/2019)", Advanced Quantum Technologies **2**, 1970013 (2019).

[186] K. Hepp and E. H. Lieb, "On the superradiant phase transition for molecules in a quantized radiation field: the Dicke maser model", Annals of Physics **76**, 360 (1973).

[187] Y. K. Wang and F. T. Hioe, "Phase Transition in the Dicke Model of Superradiance", Phys. Rev. A **7**, 831 (1973).

[188] C. Emary and T. Brandes, "Quantum Chaos Triggered by Precursors of a Quantum Phase Transition: The Dicke Model", Phys. Rev. Lett. **90**, 044101 (2003).

[189] C. Emary and T. Brandes, "Chaos and the quantum phase transition in the Dicke model", Phys. Rev. E **67**, 066203 (2003).

[190] N. Lambert, C. Emary, and T. Brandes, "Entanglement and the Phase Transition in Single-Mode Superradiance", Phys. Rev. Lett. **92**, 073602 (2004).

[191] V. Bu žek, M. Orszag, and M. Ro ško, "Instability and Entanglement of the Ground State of the Dicke Model", Phys. Rev. Lett. **94**, 163601 (2005).

[192] G. M. Andolina, F. M. D. Pellegrino, V. Giovannetti, A. H. MacDonald, and M. Polini, "Cavity quantum electrodynamics of strongly correlated electron systems: A no-go theorem for photon condensation", Phys. Rev. B **100**, 121109 (2019).

[193] G. M. Andolina, F. M. D. Pellegrino, V. Giovannetti, A. H. MacDonald, and M. Polini, "Theory of photon condensation in a spatially varying electromagnetic field", Phys. Rev. B **102**, 125137 (2020).

[194] K. Rza żewski, K. Wódkiewicz, and W. Żakowicz, "Phase Transitions, Two-Level Atoms, and the A^2 Term", Phys. Rev. Lett. **35**, 432 (1975).

[195] J. M. Knight, Y. Aharonov, and G. T. C. Hsieh, "Are super-radiant phase transitions possible?", Phys. Rev. A **17**, 1454 (1978).

[196] I. Bialynicki-Birula and K. Rza c żewski, "No-go theorem concerning the superradiant phase transition in atomic systems", Phys. Rev. A **19**, 301 (1979).

[197] T. Tufarelli, K. R. McEnery, S. A. Maier, and M. S. Kim, "Signatures of the A^2 term in ultrastrongly coupled oscillators", Phys. Rev. A **91**, 063840 (2015).

[198] K. Rzą żewski and K. Wódkiewicz, "Comment on "Instability and Entanglement of the Ground State of the Dicke Model"", Phys. Rev. Lett. **96**, 089301 (2006).

[199] P. Nataf and C. Ciuti, "No-go theorem for superradiant quantum phase transitions in cavity QED and counter-example in circuit QED", Nature communications **1**, 72 (2010).

[200] M. Hayn, C. Emary, and T. Brandes, "Phase transitions and dark-state physics in two-color superradiance", Phys. Rev. A **84**, 053856 (2011).

Bibliography

[201] A. Baksic, P. Nataf, and C. Ciuti, "Superradiant phase transitions with three-level systems", Phys. Rev. A **87**, 023813 (2013).

[202] D. Hagenmüller and C. Ciuti, "Cavity QED of the Graphene Cyclotron Transition", Phys. Rev. Lett. **109**, 267403 (2012).

[203] J. Keeling, "Coulomb interactions, gauge invariance, and phase transitions of the Dicke model", Journal of Physics: Condensed Matter **19**, 295213 (2007).

[204] C. Ciuti and P. Nataf, "Comment on "Superradiant Phase Transitions and the Standard Description of Circuit QED"", Phys. Rev. Lett. **109**, 179301 (2012).

[205] T. Jaako, Z.-L. Xiang, J. J. Garcia-Ripoll, and P. Rabl, "Ultrastrong-coupling phenomena beyond the Dicke model", Phys. Rev. A **94**, 033850 (2016).

[206] M. Bamba, K. Inomata, and Y. Nakamura, "Superradiant Phase Transition in a Superconducting Circuit in Thermal Equilibrium", Phys. Rev. Lett. **117**, 173601 (2016).

[207] G. Mazza and A. Georges, "Superradiant Quantum Materials", Phys. Rev. Lett. **122**, 017401 (2019).

[208] K. Gaw cedzki and K. Rza c źewski, "No-go theorem for the superradiant phase transition without dipole approximation", Phys. Rev. A **23**, 2134 (1981).

[209] O. Viehmann, J. von Delft, and F. Marquardt, "Superradiant Phase Transitions and the Standard Description of Circuit QED", Phys. Rev. Lett. **107**, 113602 (2011).

[210] L. Chirolli, M. Polini, V. Giovannetti, and A. H. MacDonald, "Drude Weight, Cyclotron Resonance, and the Dicke Model of Graphene Cavity QED", Phys. Rev. Lett. **109**, 267404 (2012).

[211] M. Bamba and T. Ogawa, "Stability of polarizable materials against superradiant phase transition", Phys. Rev. A **90**, 063825 (2014).

[212] F. M. D. Pellegrino, L. Chirolli, R. Fazio, V. Giovannetti, and M. Polini, "Theory of integer quantum Hall polaritons in graphene", Phys. Rev. B **89**, 165406 (2014).

[213] A. Vukics and P. Domokos, "Adequacy of the Dicke model in cavity QED: A counter-no-go statement", Phys. Rev. A **86**, 053807 (2012).

[214] A. Stokes and A. Nazir, "Uniqueness of the Phase Transition in Many-Dipole Cavity Quantum Electrodynamical Systems", Phys. Rev. Lett. **125**, 143603 (2020).

[215] D. Guerci, P. Simon, and C. Mora, "Superradiant Phase Transition in Electronic Systems and Emergent Topological Phases", Phys. Rev. Lett. **125**, 257604 (2020).

[216] P. Nataf, T. Champel, G. Blatter, and D. M. Basko, "Rashba Cavity QED: A Route Towards the Superradiant Quantum Phase Transition", Phys. Rev. Lett. **123**, 207402 (2019).

[217] J. Román-Roche, F. Luis, and D. Zueco, "Photon Condensation and Enhanced Magnetism in Cavity QED", Phys. Rev. Lett. **127**, 167201 (2021).

[218] O. Viehmann, J. von Delft, and F. Marquardt, "Reply to comment on" superradiant phase transitions and the standard description of circuit qed"", arXiv preprint arXiv:1202.2916 (2012).

[219] O. Dmytruk and M. Schiró, "Gauge fixing for strongly correlated electrons coupled to quantum light", Phys. Rev. B **103**, 075131 (2021).

[220] K. Cho, ""ABC"-Free Theory of Polariton: From Semi-Infinite Medium to Quantum Well", Journal of the Physical Society of Japan **55**, 4113 (1986).

[221] S. Savasta and R. Girlanda, "Quantum description of the input and output electromagnetic fields in a polarizable confined system", Phys. Rev. A **53**, 2716 (1996).

[222] S. Sachdev and J. Ye, "Gapless spin-fluid ground state in a random quantum Heisenberg magnet", Phys. Rev. Lett. **70**, 3339 (1993).

[223] Y. Gu, A. Kitaev, S. Sachdev, and G. Tarnopolsky, "Notes on the complex Sachdev-Ye-Kitaev model", Journal of High Energy Physics **2020**, 1 (2020).

[224] R. Peierls, "Zur theorie des diamagnetismus von leitungselektronen", Zeitschrift für Physik **80**, 763 (1933).

[225] K. G. Wilson, "Confinement of quarks", Phys. Rev. D **10**, 2445 (1974).

[226] U.-J. Wiese, "Ultracold quantum gases and lattice systems: quantum simulation of lattice gauge theories", Annalen der Physik **525**, 777 (2013).

Bibliography

[227]   P. Pirro, V. I. Vasyuchka, A. A. Serga, and B. Hillebrands, "Advances in coherent magnonics", Nature Reviews Materials **6**, 1114 (2021).

[228]   D. Lachance-Quirion, Y. Tabuchi, A. Gloppe, K. Usami, and Y. Nakamura, "Hybrid quantum systems based on magnonics", Applied Physics Express **12**, 070101 (2019).

[229]   B. Z. Rameshti, S. V. Kusminskiy, J. A. Haigh, K. Usami, D. Lachance-Quirion, Y. Nakamura, C.-M. Hu, H. X. Tang, G. E. Bauer, and Y. M. Blanter, "Cavity magnonics", Physics Reports **979**, 1 (2022).

[230]   Y. Li, W. Zhang, V. Tyberkevych, W.-K. Kwok, A. Hoffmann, and V. Novosad, "Hybrid magnonics: Physics, circuits, and applications for coherent information processing", Journal of Applied Physics **128**, https://doi.org/10.1063/5.0020277 (2020).

[231]   X. Zhang, C.-L. Zou, N. Zhu, F. Marquardt, L. Jiang, and H. X. Tang, "Magnon dark modes and gradient memory", Nature communications **6**, 8914 (2015).

[232]   L. Bai, M. Harder, P. Hyde, Z. Zhang, C.-M. Hu, Y. P. Chen, and J. Q. Xiao, "Cavity Mediated Manipulation of Distant Spin Currents Using a Cavity-Magnon-Polariton", Phys. Rev. Lett. **118**, 217201 (2017).

[233]   N. Crescini, D. Alesini, C. Braggio, G. Carugno, D. Di Gioacchino, C. Gallo, U. Gambardella, C. Gatti, G. Iannone, G. Lamanna, et al., "Operation of a ferromagnetic axion haloscope at $m_a = 58$ μeV", The European Physical Journal C **78**, 1 (2018).

[234]   R. Hisatomi, A. Osada, Y. Tabuchi, T. Ishikawa, A. Noguchi, R. Yamazaki, K. Usami, and Y. Nakamura, "Bidirectional conversion between microwave and light via ferromagnetic magnons", Phys. Rev. B **93**, 174427 (2016).

[235]   B. Yao, Y. S. Gui, J. W. Rao, Y. H. Zhang, W. Lu, and C.-M. Hu, "Coherent Microwave Emission of Gain-Driven Polaritons", Phys. Rev. Lett. **130**, 146702 (2023).

[236]   R. W. Roberts, B. A. Auld, and R. R. Schell, "Magnetodynamic Mode Ferrite Amplifier", Journal of Applied Physics **33**, 1267 (1962).

[237]   B. Auld, "Coupling of electromagnetic and magnetostatic modes in ferrite-loaded cavity resonators", Journal of Applied Physics **34**, 1629 (1963).

[238] A. G. Gurevich and G. A. Melkov, *Magnetization oscillations and waves* (CRC press, 1996).

[239] H. Maier-Flaig, S. Klingler, C. Dubs, O. Surzhenko, R. Gross, M. Weiler, H. Huebl, and S. T. B. Goennenwein, "Temperature-dependent magnetic damping of yttrium iron garnet spheres", Phys. Rev. B **95**, 214423 (2017).

[240] A. Imamo ğlu, "Cavity QED Based on Collective Magnetic Dipole Coupling: Spin Ensembles as Hybrid Two-Level Systems", Phys. Rev. Lett. **102**, 083602 (2009).

[241] Ö. O. Soykal and M. E. Flatté, "Strong Field Interactions between a Nanomagnet and a Photonic Cavity", Phys. Rev. Lett. **104**, 077202 (2010).

[242] J. Bourhill, N. Kostylev, M. Goryachev, D. L. Creedon, and M. E. Tobar, "Ultrahigh cooperativity interactions between magnons and resonant photons in a YIG sphere", Phys. Rev. B **93**, 144420 (2016).

[243] N. Kostylev, M. Goryachev, and M. E. Tobar, "Superstrong coupling of a microwave cavity to yttrium iron garnet magnons", Applied Physics Letters **108**, `https://doi.org/10.1063/1.4941730` (2016).

[244] B. Zare Rameshti, Y. Cao, and G. E. W. Bauer, "Magnetic spheres in microwave cavities", Phys. Rev. B **91**, 214430 (2015).

[245] G. Bourcin, J. Bourhill, V. Vlaminck, and V. Castel, "Strong to ultrastrong coherent coupling measurements in a YIG/cavity system at room temperature", Phys. Rev. B **107**, 214423 (2023).

[246] L. Liensberger, A. Kamra, H. Maier-Flaig, S. Geprägs, A. Erb, S. T. B. Goennenwein, R. Gross, W. Belzig, H. Huebl, and M. Weiler, "Exchange-Enhanced Ultrastrong Magnon-Magnon Coupling in a Compensated Ferrimagnet", Phys. Rev. Lett. **123**, 117204 (2019).

[247] M. Białek, J. Zhang, H. Yu, and J.-P. Ansermet, "Strong Coupling of Antiferromagnetic Resonance with Subterahertz Cavity Fields", Phys. Rev. Appl. **15**, 044018 (2021).

[248] J. R. Everts, G. G. G. King, N. J. Lambert, S. Kocsis, S. Rogge, and J. J. Longdell, "Ultrastrong coupling between a microwave resonator and antiferromagnetic resonances of rare-earth ion spins", Phys. Rev. B **101**, 214414 (2020).

[249] H. Huebl, C. W. Zollitsch, J. Lotze, F. Hocke, M. Greifenstein, A. Marx, R. Gross, and S. T. B. Goennenwein, "High Cooperativity in Coupled Microwave Resonator Ferrimagnetic Insulator Hybrids", Phys. Rev. Lett. **111**, 127003 (2013).

[250] R. Morris, A. Van Loo, S. Kosen, and A. Karenowska, "Strong coupling of magnons in a YIG sphere to photons in a planar superconducting resonator in the quantum limit", Scientific Reports **7**, 11511 (2017).

[251] J. T. Hou and L. Liu, "Strong Coupling between Microwave Photons and Nanomagnet Magnons", Phys. Rev. Lett. **123**, 107702 (2019).

[252] I. A. Golovchanskiy, N. N. Abramov, V. S. Stolyarov, M. Weides, V. V. Ryazanov, A. A. Golubov, A. V. Ustinov, and M. Y. Kupriyanov, "Ultrastrong photon-to-magnon coupling in multilayered heterostructures involving superconducting coherence via ferromagnetic layers", Science advances **7**, eabe8638 (2021).

[253] Y. Li, V. G. Yefremenko, M. Lisovenko, C. Trevillian, T. Polakovic, T. W. Cecil, P. S. Barry, J. Pearson, R. Divan, V. Tyberkevych, C. L. Chang, U. Welp, W.-K. Kwok, and V. Novosad, "Coherent Coupling of Two Remote Magnonic Resonators Mediated by Superconducting Circuits", Phys. Rev. Lett. **128**, 047701 (2022).

[254] I. Golovchanskiy, N. Abramov, V. Stolyarov, A. Golubov, M. Y. Kupriyanov, V. Ryazanov, and A. Ustinov, "Approaching Deep-Strong On-Chip Photon-To-Magnon Coupling", Phys. Rev. Appl. **16**, 034029 (2021).

[255] R. Macêdo, R. C. Holland, P. G. Baity, L. J. McLellan, K. L. Livesey, R. L. Stamps, M. P. Weides, and D. A. Bozhko, "Electromagnetic Approach to Cavity Spintronics", Phys. Rev. Appl. **15**, 024065 (2021).

[256] S. Martínez-Losa del Rincón, I. Gimeno, J. Pérez-Bailón, V. Rollano, F. Luis, D. Zueco, and M. J. Martínez-Pérez, "Measuring the Magnon-Photon Coupling in Shaped Ferromagnets: Tuning of the Resonance Frequency", Phys. Rev. Appl. **19**, 014002 (2023).

[257] T. Holstein and H. Primakoff, "Field Dependence of the Intrinsic Domain Magnetization of a Ferromagnet", Phys. Rev. **58**, 1098 (1940).